THE UNIVERSITY OF HULL
FACULTY OF SCIENCES AND ENGINEERING
SCHOOL OF ENGINEERING

PhD Thesis

# PROCESS MODELLING, SIMULATION AND OPTIMISATION OF NATURAL GAS COMBINED CYCLE POWER PLANT INTEGRATED WITH CARBON CAPTURE, COMPRESSION AND TRANSPORT

**Xiaobo Luo**

Supervisor: Professor Meihong Wang

May 2016

This thesis is submitted in fulfilment of the requirements for the degree of Doctor of Philosophy (PhD)

The candidate confirms that the work submitted is his/her own, except where work which has formed part of co-authored publications has been included. The contribution of the candidate and the other authors to this work has been explicitly indicated below. The candidate confirms that appropriate credit has been given within the thesis where reference has been made to the work of others.

The work in Chapter 5 of the thesis has appeared in publication as follows:

Luo, X., Wang, M., Chen, J., 2015. Heat integration of natural gas combined cycle power plant integrated with post-combustion $CO_2$ capture and compression. *Fuel*, 151, 110-117.

> *Prof M. Wang is my supervisor who provided suggestions regarding the research direction, analysis methods and commented the paper writing. Prof J. Chen provided suggestions on the research direction.*

The work in Chapter 6 of the thesis has appeared in publication as follows:

Luo, X., Wang, M., Oko, E., Okezue, C., 2014. Simulation-based techno-economic evaluation for optimal design of $CO_2$ transport pipeline network. *Applied Energy*, 132, 610-620.

> *Prof M. Wang is my supervisor who provided suggestions regarding the research direction, analysis methods and commented the paper writing. Dr E.Oko and Mr. C.Okezue discussed and commented on this research topic.*

The work in Chapter 7 of the thesis has appeared in publication as follows:

Luo, X., Wang, M., 2016. Optimal operation of MEA-based post-combustion carbon capture for natural gas combined cycle power plants under different market conditions. *International Journal of Greenhouse Gas Control*, 48, Part 2**,** 312-320.

> *Prof M. Wang is my supervisor who provided suggestions regarding the research direction, analysis methods and commented the paper writing.*

This copy has been supplied on the understanding that it is copyright material and that no quotation from the thesis may be published without proper acknowledgement.

The right of Xiaobo Luo to be identified as Author of this work has been asserted by him in accordance with the Copyright, Designs and Patents Act 1988.

© 2016 University of Hull and Xiaobo Luo

# Acknowledgements

I wish to express my gratitude to all who have supported me throughout my PhD study.

Firstly, I would like to thank Prof Meihong Wang for supervising me through this project. With his guidance, I enjoyed this research work and was able to publish several journal and conference papers in different stages of this project. Moreover, his diligence and being responsible encourage me to overcome the challenges from both the research work and the life. I am also thankful to all the members of the Thesis Advisory Panel (TAP) meetings, including Prof Ron Patton, Dr Ming Hou, Dr Chunfei Wu and Dr Dipesh Patel, for their support and suggestions for this project.

Secondly, I am very grateful to my wife Hongling Sui. She has made great contribution to take care of the family during this period. With her sacrifice and support, I was able to focus on the research work and finished this project. I am also glad to see the growing of my son Junhao Luo and his great understanding about my being busy for this project. I am also thankful to my parents for their support and forgiving me being far away from them to pursue my dreams.

Thirdly, I would like to thank all friends around me for your love and supports. We shared the experience and the joys of our life, which is very precious for me during this period and in the future.

Finally, I would like to thank the funding bodies involved this project. They are: (1) Natural Environment Research Council (NERC Ref: NE/H013865/2); (2) EU FP7 Marie Curie (Ref: FP7-PEOPLE-2013-IRSES); (3) 2013 China-Europe small-and medium sized enterprises energy saving and carbon reduction research project (No.: SQ2013ZOA100002), and (4) Department of Energy and Climate Change (DECC) for the project *Process intensification for carbon capture with new solvents*.

# Abstract

Reducing $CO_2$ emissions from fossil fuel-fired power plants is a significant challenge, technically and economically. Post-combustion carbon capture (PCC) using amine solvents is widely regarded as the most promising technology that can be commercially deployed for carbon capture from fossil fuel-fired power plants. However, for its application at full commercial scale, the main barrier is high cost increment of the electricity due to high capital costs and significant energy penalty. This thesis presents the studies on optimal design and operation of Monoethanolamine (MEA)-based PCC process and the integrated system with natural gas combined cycle (NGCC) power plant through modelling, simulation and optimisation, with the aim to reduce the cost of PCC commercial deployment for NGCC power plants.

The accuracy of optimisation depends on good predictions of both process model and economic model. For the process modelling, the philosophy with its framework was analysed for this reactive absorption (RA) process. Then the model was developed and validated at three stages. In the first stage, the predictions of thermodynamic modelling were compared with experimental data of $CO_2$ solubility in aqueous MEA solutions. The results show the combination of correlations used in this study has higher accuracy than other three key published contributions. Then key physical properties of MEA-$H_2O$-$CO_2$ system were also validated with experimental data from different publications. Lastly, a steady state process model was developed in Aspen Plus® with rate-based mass transfer and kinetic-controlled reactions. The process model was validated against comprehensive pilot plant experiment data, in terms of absorption efficiency and thermal performance of the integrated system.

The cost model was developed based on the major equipment costs provided by vendors after detailed engineering design in a benchmark report. The uncertainty of this method could be in the range of from −15% to 20%, instead of other empirical methods with uncertainty of from −30% to 50%. The cost model was integrated into the process model by coding Fortran subroutine in Aspen Plus®. Using this integrated model, the optimisation studies were carried out for the PCC process only. The impact of key variables variation was also analysed.

Subsequently, the scope of this study was extended to cover different sections of the integrated system including a 453$MW_e$ NGCC power plant, PCC process, $CO_2$ compression trains and $CO_2$ transport pipeline network. For the integration of NGCC power plant with PCC process and $CO_2$ compression, exhaust gas recirculation (EGR) technology was investigated and showed significant economic benefit. A specific supersonic shock wave compressor was adopted for the $CO_2$ compression and its heat integration options with power plant and PCC process were studied.

For the study on the $CO_2$ transport pipeline network planned in the Humber region of the UK, a steady state process model was developed using Aspen HYSYS®. The process model was integrated with Aspen Process Economic Analyzer® (APEA), to carry out techno-economic evaluations for different options of the $CO_2$ compression trains and the trunk onshore\offshore pipelines respectively. The results show the optimal case has an annual saving of 22.7 M€ compared with the base case.

In the end, optimal operations of NGCC power plant integrated with whole carbon capture and storage (CCS) chain under different market conditions were studied. Levelised cost of electricity (LCOE) is formulated as the objective function. The optimal operations were investigated for different carbon capture level under different carbon price, fuel price and $CO_2$ transport and storage (T&S) price. The results show that carbon price needs to be over €100/ton $CO_2$ to justify the total cost of carbon capture from the NGCC power plant and needs to be €120/ton $CO_2$ to drive carbon capture level at 90%. The results outline the economic profile of operating an NGCC power plant integrated with CCS chain. It could help power plants operators and relevant government organizations for decision makings on the commercial deployment of solvent-based PCC process for power plans.

*Keywords: Process modelling, Process simulation, Process optimisation, Post-combustion carbon capture, Gas-fired power plant, NGCC, $CO_2$ pipeline transport, CCS*

# Table of Contents

# List of Figures

# List of Tables

# Nomenclature

| Symbols | Unit | Description |
|---|---|---|
| Letters | | |
| $A$ | $m^2$ | Area |
| $b$ | | Parameter of bypass air calculation for gas turbine cooling |
| $c$ | | Correlations for property calculations |
| $d$ | | The vector of the coefficients |
| $D$ | m | Column diameter |
| $e$ | | The vector of the design variables |
| $E$ | kJ/mol | Activation energy |
| $f$ | | The objective function |
| $F_P$ | | Packing factor |
| $G$ | kg/s | Total vapour flow rate in mass |
| $\Delta G_j^0$ | J/kmol | Reference state Gibbs energy change for reaction |
| $H$ | | Henry's constant |
| $HP$ | m | Packing height of a column |
| $i$ | | The interest rate |
| $I$ | | Cost index |
| $k^o$ | | The pre–exponential factor |
| $K$ | | Parameter of bypass air calculation for gas turbine cooling |
| $K_4$ | | Parameter for size calculation of column |
| $K_{Rj}$ | | Chemical equilibrium constants of reaction *j* |
| $L$ | kg/s | Total liquid flow rate in mass |
| $m$ | | Specific factor for different type of equipment |
| $\dot{m}$ | | Bypass air mass flow rate for gas turbine cooling |
| $M$ | | Mass fraction in a mixture |
| $n$ | | The economic life of plant |
| $o$ | | The vector of operational variables |
| $P$ | bar | Pressure |
| $PC_k$ | cost | Direct material cost |
| $R$ | | Ideal gas constant |
| $r_j$ | mol/(min.$m^3$) | Reaction rate of reaction *j* |
| $s$ | | Parameter of bypass air calculation for gas turbine cooling |
| $T$ | K | Temperature |
| $V_i^\infty$ | $m^3$/mole | Partial molar volume of molecular solute *i* at infinite dilution in solvent |
| $w$ | | Weight factor for the calculation of Henry's constant |

| | | |
|---|---|---|
| $x$ | | Mole fraction in a mixture |
| $X$ | | Selected scaling factor |
| Greek | | |
| $\alpha$ | | $CO_2$ loading in lean solvent or rich solvent |
| $\alpha_{ij}$ | | the reaction order of component $i$ in reaction $j$ |
| $\gamma_i^{\infty}$ | | the infinite dilution activity coefficient of molecular solute $i$ in solvent |
| $\lambda$ | | Lagrange multipliers |
| $\rho$ | kg/m$^3$ | density |
| $\sigma$ | | Lagrange multipliers |
| $\Psi_{CO_2}$ | | $CO_2$ capture level |
| $\omega_{MEA}$ | | MEA concentration in solvent |
| Superscript | | |
| o | | Standard state |
| T | | Vector transpose |
| Subscript | | |
| $ABS$ | | Absorber |
| $c$ | | Cooling |
| $CO_2$ | | $CO_2$ component |
| EG | | Exhaust gas |
| FG | | Flue gas |
| $g$ | | Gas |
| $lean$ | | Lean solvent |
| L | | Liquid phase |
| $MEA$ | | MEA |
| $STR$ | | Stripper |
| $rich$ | | Rich solvent |
| V | | Vapour phase |

# Abbreviations

| | |
|---|---|
| AAD | Average absolute deviations |
| APE | Absolute percentage error |
| ACAPEX | Annualised capital expenditure |
| APEA | Aspen Process Economic Analyser® |
| ASNI | American National Standards Institute |
| BBC | British Broadcasting Corporation |
| BP | British Petroleum |
| CAPEX | Capital expenditure |
| CCA | The cost of $CO_2$ avoidance |
| CCGT | Combined cycle gas turbine |
| CCS | Carbon capture and storage |
| CL | Capture level |
| $CO_2$ FOLU | $CO_2$ from forestry and other land use |
| CRF | Capital recovery factor |
| DCC | Direct contact cooler |
| DECC | Department of Energy and Climate Change (of the UK) |
| DOE | Department of Energy (of the USA) |
| EGR | Exhaust cas recirculation |
| EIA | Energy Information Administration (of the USA) |
| EU | The European Union |
| eNRTL | Electrolyte Non-Random Two Liquid |
| EOR | Enhanced oil recovery |
| EOS | Equation of state |
| ETP | Energy Technology Perspective |
| ETS | Emission Trading System |
| F-Gases | Fluorinated gases covered under the Kyoto Protocol |
| FOPEX | Fixed operational expenditure |
| GHG | Greenhouse gas |
| GCCSI | The Global CCS Institute |
| HICP | The Harmonised Consumer Price Index |
| HP-ST | High pressure steam turbine |
| HRSG | Heat recovery steam generator |
| IEA | International Energy Agency |
| IEAGHG | International Energy Agency Greenhouse Gas Team |
| IGCC | Integrated gasification combined cycle |
| IGHAT | Integrated gasification humid turbines |
| IPCC | Intergovernmental Panel on Climate Change |
| IP-ST | Intermediate pressure steam turbine |
| LCOE | Levelised cost of electricity |
| LHV | Low heat value |

| | |
|---|---|
| LP-ST | Low pressure steam turbine |
| L/G | Liquid gas ratio |
| NASA | National Aeronautics and Space Administration |
| NERC | Natural Environment Research Council |
| NG | Natural gas |
| NGCC | Natural gas combined cycle |
| NOAA | National Oceanic and Atmospheric Administration (of the USA) |
| MAPE | Mean absolute percentage error |
| MEA | Monoethanolamine |
| O&M | Operating and maintenance cost |
| OEM | Original equipment manufacturers |
| OPEX | Operational expenditure |
| PCC | Post-combustion carbon capture |
| PR | Peng-Robinson |
| QP | Quadratic Programming |
| SAFT | Statistical Associating Fluid Theory |
| SCCS | Scottish Carbon Capture and Storage Research Group |
| SQP | Sequential Quadratic Programming |
| SW | Span and Wagner |
| TAC | Total annualised cost |
| T&S | Transport and storage |
| UNFCCC | The United Nations Framework Convention on Climate Change |
| VLE | Vapour-liquid equilibrium |
| VOPEX | Variable operational expenditure |
| WEO | World Energy Outlook |

# Chapter 1: Introduction

This chapter introduces the background of this research. Section 1.1 updated current status of global warming, $CO_2$ emissions and CCS technologies. Section 1.2 stated the motivations for of this study. Section 1.3 summarized the aim and objectives and Section 1.4 justified the novel contributions. Section 1.5 outlined the study scope of each chapter. In Section 0, the selections of tools used in this study were explained.

## 1.1 Background

### *1.1.1 Global warming and greenhouse gases emissions*

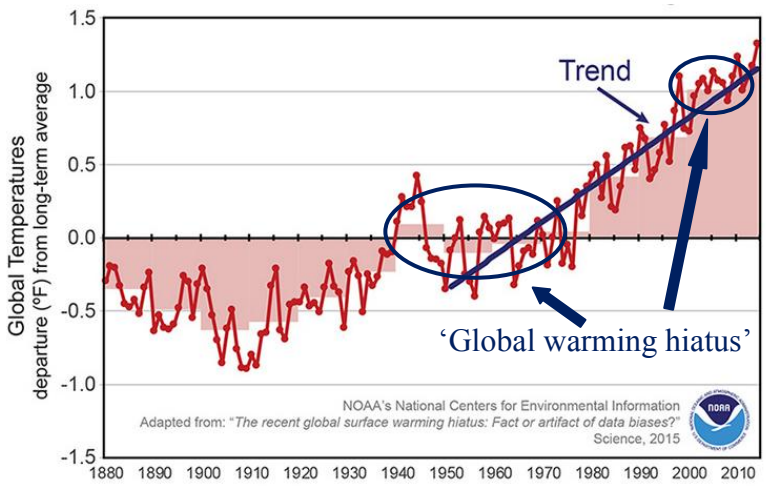


Figure 1.1 Global temperature departure from long-term average (NOAA, 2015)

Global warming including its anthropogenic causes is one of the most contentious scientific issues in the last two decades (Easterling and Wehner, 2009). The evidence of a warming world including changes in surface, atmospheric and oceanic temperatures; glaciers; snow cover; sea ice; sea level and atmospheric water vapour comes from multiple independent climate indicators and have been independently verified many times by scientists all over the world (Hartmann et al., 2013). Although the hiatus of global warming has been widely discussed, one recent research (Lin and Franzke, 2015) suggested that the hiatus is due to natural fluctuations imposing a decreasing temperature trend and, thus, temporally overshadowing the global warming trend. Another study by Karl et al. (2015) pointed out global warming does not slow down at all (see Figure 1.1). Therefore, anthropogenic global warming still exerts a strong signal and is worth world-wide concern.

The scientific understandings of the causes of global warming are the changes of external forcing including increased concentrations of greenhouse gases, more intensive solar luminosity, more volcanic eruptions, and variations in Earth's orbit around the Sun (Hegerl et al., 2007). Among these factors, increasing concentrations of greenhouse gases (GHGs) caused by anthropogenic activities are responsible for most of global warming and this is more than 95% proven by scientists (Pachauri et al., 2014). The main GHGs include water vapour, carbon dioxide ($CO_2$), methane ($CH_4$) and ozone ($O_3$). Figure 1.2 shows that total anthropogenic GHG emissions increased significantly in the last decade and $CO_2$ is the main anthropogenic GHG.

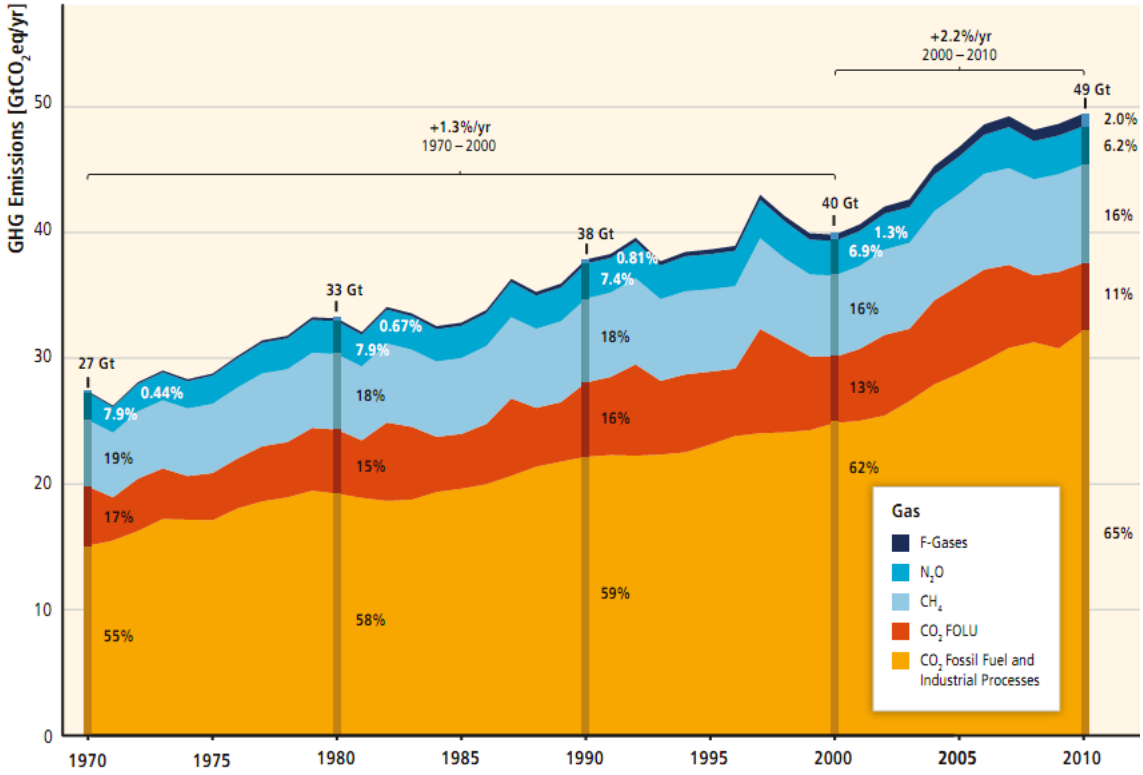


Figure 1.2 Total annual anthropogenic GHG emissions by groups of gases 1970–2010: $CO_2$ from fossil fuel combustion and industrial processes; $CO_2$ from Forestry and Other Land Use (FOLU); methane ($CH_4$); nitrous oxide ($N_2O$); fluorinated gases covered under the Kyoto Protocol (F-Gases) (IPCC, 2015)

### *1.1.2 $CO_2$ emission and its reduction*

Since the Industrial Revolution started in 1760s, atmospheric $CO_2$ concentration has increased more than 40%, from 280 ppm in 1760 to about 402 ppm in 2016 (Blasing,

2013; NASA, 2016). Recent researches (Buizert et al., 2014; Sime, 2014) into Greenland's ice sheets explained one of the mysteries of the climatic past, confirming the importance of carbon dioxide on global temperature changes. The indirect measurements by reconstruction analysis from ice cores show the $CO_2$ concentration in the atmosphere has increased rapidly in recent decades (refer to Figure 1.3(a)) and it has not slowed down (see Figure 1.3(b)).

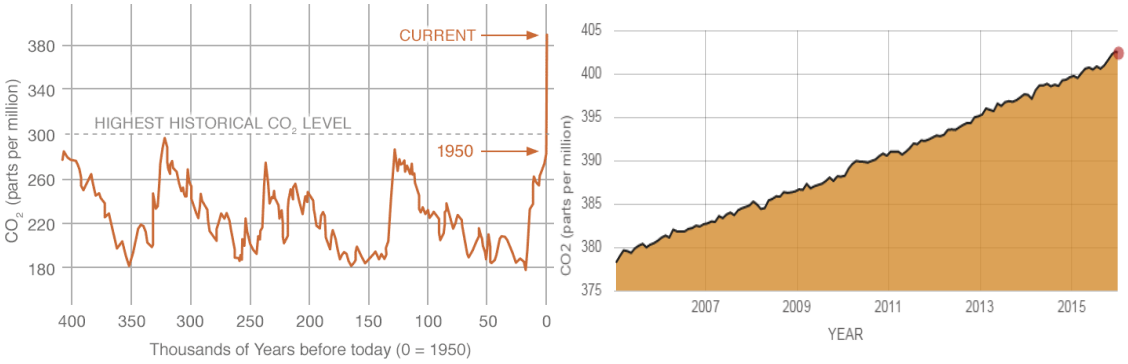


(a) (b)

Figure 1.3 $CO_2$ concentration in atmosphere, (a) indirect measurements for historical $CO_2$ level, (b) direct measurements from Jan 2005 to Feb 2016 (NASA, 2016)

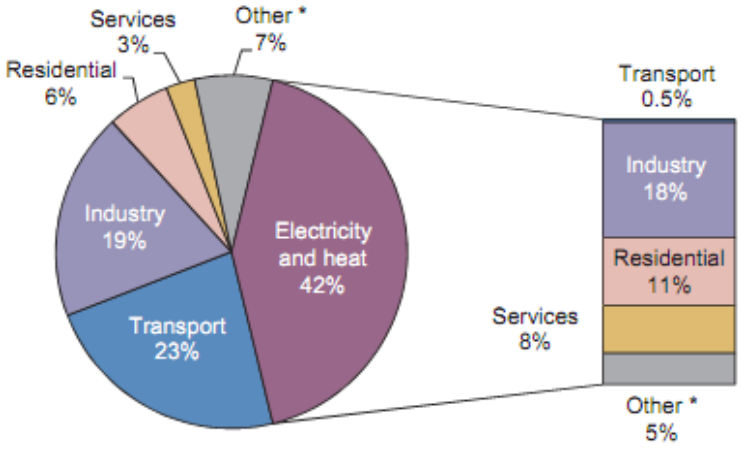


Figure 1.4 World $CO_2$ emissions by sector in 2013 (IEA, 2015)

In the successful UNFCCC 2015 Paris meeting, a common goal was agreed by all the 196 parties to keep global warming to less than 2°C compared to pre-industrial levels (UNFCCC, 2015). Anthropogenic $CO_2$ emission sources cover every aspects related with human activities, including electricity and heat generation, industrial

manufacturing, transport sector, residence, agriculture, forestry, fishing and so on (see Figure 1.4). Except for transport and residential emissions which are normally very small and distributed, industrial processes are major individual $CO_2$ sources. Table 1.1 lists worldwide large stationary $CO_2$ sources with emissions of more than 0.1 million tons of $CO_2$ per year (IPCC, 2005) which shows fossil-fired power generation is the biggest $CO_2$ emitter.

Table 1.1 $CO_2$ emissions from industry emitters (IPCC, 2005)

| Process | Number of emitters | Emission ($MtCO_2$/yr) |
|---|---|---|
| Fossil fuels | | |
| Power | 4,942 | 10,539 |
| Cement production | 1,175 | 932 |
| Refineries | 638 | 798 |
| Iron and steel industry | 269 | 646 |
| Petrochemical industry | 470 | 379 |
| Oil and gas processing | – | 50 |
| Other sources | 90 | 33 |
| Biomass | | |
| Bioethanol and bioenergy | 303 | 91 |
| Total | 7,887 | 13,468 |

Reducing $CO_2$ emission is a big challenge both technically and commercially because large amount of $CO_2$ emissions needs to be cut down to ensure global temperature rise remains below 2 degrees Celsius (UNFCCC, 2015). International Energy Agency (IEA) set up a BLUE Map scenario with 14 GT $CO_2$ emissions in 2050 compared with the 57 GT $CO_2$ emissions in Baseline scenario. In order to achieve this target, significant efforts are required to develop and improve the technologies related with energy efficiency and low-carbon energy supply (see Figure 1.5). CCS technology will play a vital role in delivering 19% of the cumulative carbon dioxide emissions reductions between 2015 and 2050 in the power sector.

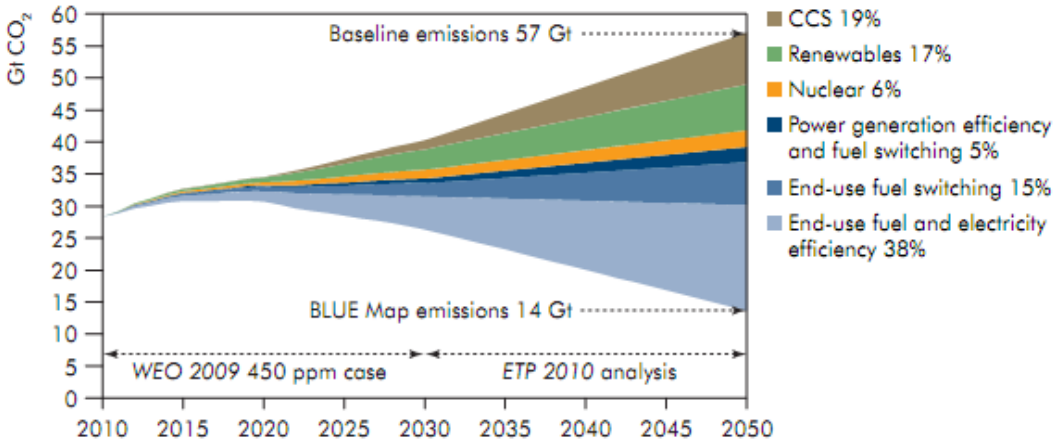


Note: WEO 2009 is World Energy Outlook 2009, ETP 2010 is Energy Technology Perspective 2010

Figure 1.5 Key technologies for reducing $CO_2$ emissions, (IEA, 2010)

### *1.1.3 CCS technology*

CCS is a process of capturing $CO_2$ from large industrial sources and transporting it to a storage site, to mitigate $CO_2$ emission to the atmosphere (see Figure 1.6). $CO_2$ in flue gases from industrial processes, such as fossil-fired power plants and refineries, is captured by physical adsorption or chemical absorption and then is compressed to a high pressure (over 100 bar) for transport. Except for a small part of $CO_2$ reutilized for other industry such as drink, food production and agriculture, concentrated $CO_2$ is finally injected into either a saline aquifer or depleted oil and gas reserves for storage.

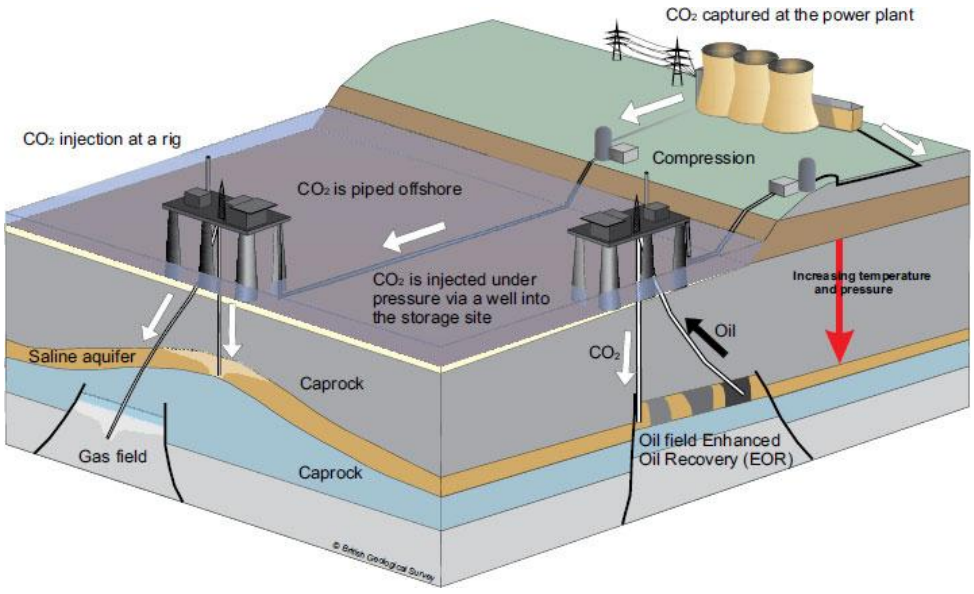


Figure 1.6 Schematic of whole CCS infrastructure (NERC, 2014)

### 1.1.3.1 $CO_2$ capture

Three main approaches can be envisaged for $CO_2$ capture from power plants: pre-combustion capture, post-combustion capture and oxy-fuel capture (Kanniche et al., 2010). Figure 1.7 illustrates the process diagram of main capture technologies. For post-combustion technology, $CO_2$ is separated from flue gas after combustion by using techniques such as chemical absorption (Wang et al., 2011), adsorption (Samanta et al., 2011), and membrane separation etc (Merkel et al., 2010). In pre-combustion technology, fuel reacts with steam and air or oxygen to produce syngas. In a shift reactor, CO component of syngas is converted to $CO_2$ which can then be separated by adsorption or physical absorption or membrane separation. Remaining $H_2$ component is then used to generate power and heat. Oxy-fuel combustion process employs an air separation unit to provide near pure oxygen for combustion (Buhre et al., 2005; Dillon et al., 2004), resulting in a high concentration of $CO_2$ around 80% in the flue gas. $CO_2$ can be enriched by cooling down the flue gases to condense the water vapour component. Among these technologies, solvent-based chemical absorption post-combustion capture is regarded as the preferred technology for carbon capture from fossil-fired power plants (Wang et al., 2011) because of its relatively low cost and easy implementation for existing power plant (POST, 2009).

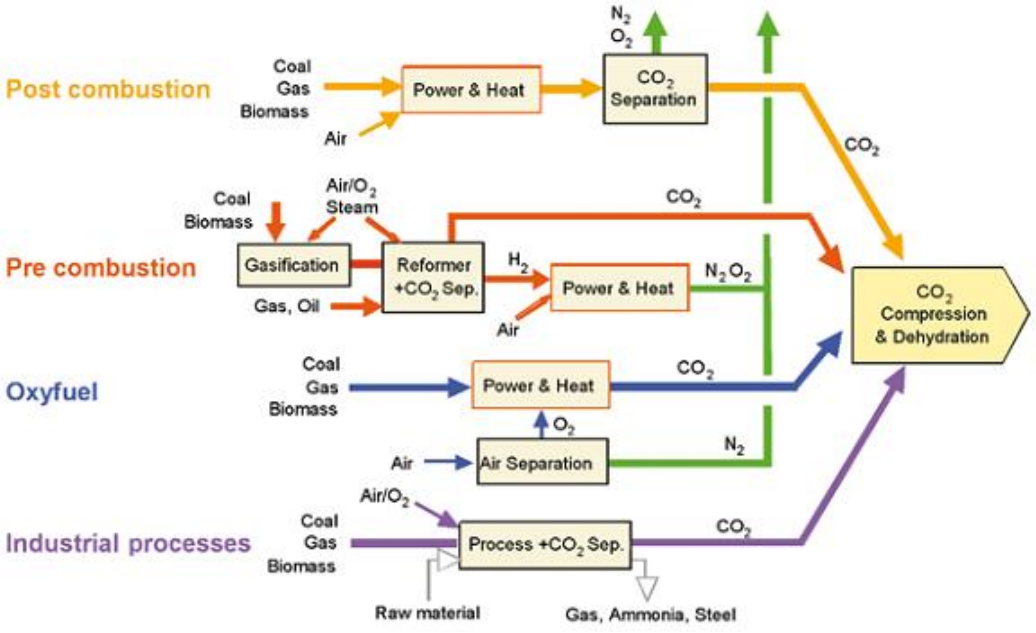


Figure 1.7 Processes of $CO_2$ capture technologies (IPCC, 2005)

#### 1.1.3.2 $CO_2$ transport

In the transport section of CCS, $CO_2$ is compressed and transported from capture plants to storage sites (or EOR sites) by pipeline, ship or tanker trucks mainly depending on the amount and the distance. Pipelines are the preferred method for onshore and offshore transport of large volumes of $CO_2$ (Svensson et al., 2004; IPCC, 2005). The $CO_2$ pipeline transport for enhanced oil recovery (EOR) is a mature technology. Several millions of tons of $CO_2$ are already transported for EOR purpose by pipelines in the USA and Canada. In 2050, to achieve the carbon emission target, the global $CO_2$ captured will be about 7Gt/y (IEA, 2012). This is a much larger amount than about 50 Mt/y transported in pipelines for EOR in the USA (USDOE, 2010b).

#### 1.1.3.3 $CO_2$ storage

Underground geological storage is a main method of $CO_2$ sequestration (Szulczewski et al., 2012) before major breakthroughs are achieved for $CO_2$ utilization (Aresta et al., 2013). Information and experience gained from $CO_2$ injection for EOR application indicates that $CO_2$ can be safely injected and stored in well-characterized and properly managed sites (IPCC, 2005). However, there is a great deal of uncertainty in the quantification of storage potential (Boot-Handford et al., 2014) and its costs.

## 1.2 Motivations

Although fossil-fired power generation is the biggest single $CO_2$ emitter, fossil energy is projected to remain a major source of energy in the near future with the advantages of high energy density and high reliability (Mac Dowell and Shah, 2013). Natural gas is a major source for electricity generation and it currently accounts for around 22% of global electricity generation capacity (BP, 2014). This number is expected to increase in the next coming decades because of the advent of cheap natural gas, high thermal efficiency and carbon emission mitigation policies (BBC, 2015). Natural gas can burn more cleanly than other fossil fuels such as coal and oil. Another remarkable advantage of natural gas power generation is its high net low heat value (LHV) efficiency (close to 60%) with the application of combined cycle gas turbine (CCGT) technology. Table 1.2 shows $CO_2$ emissions from different fuels in the world for 2015, reported by the US Energy Information Administration (EIA) (2016). To generate the same amount of electricity, burning natural gas emits about 42% less carbon dioxide than burning coal.

Table 1.2 $CO_2$ emissions from different fuels (EIA, 2016)

| Fuel | $CO_2$ content (kg/GJ) | Heat rate (kg/kWh) | $CO_2$ emission (kg/kWh) |
|---|---|---|---|
| Bituminous Coal | 98.25 | 10,644.50 | 0.94 |
| Sub-bituminous Coal | 101.79 | 10,644.50 | 0.98 |
| Lignite Coal | 103.08 | 10,644.50 | 0.98 |
| Natural gas | 56.03 | 10,924.09 | 0.55 |
| Distillate oil | 77.23 | 10,902.99 | 0.76 |
| Residual oil | 83.23 | 10,902.99 | 0.82 |

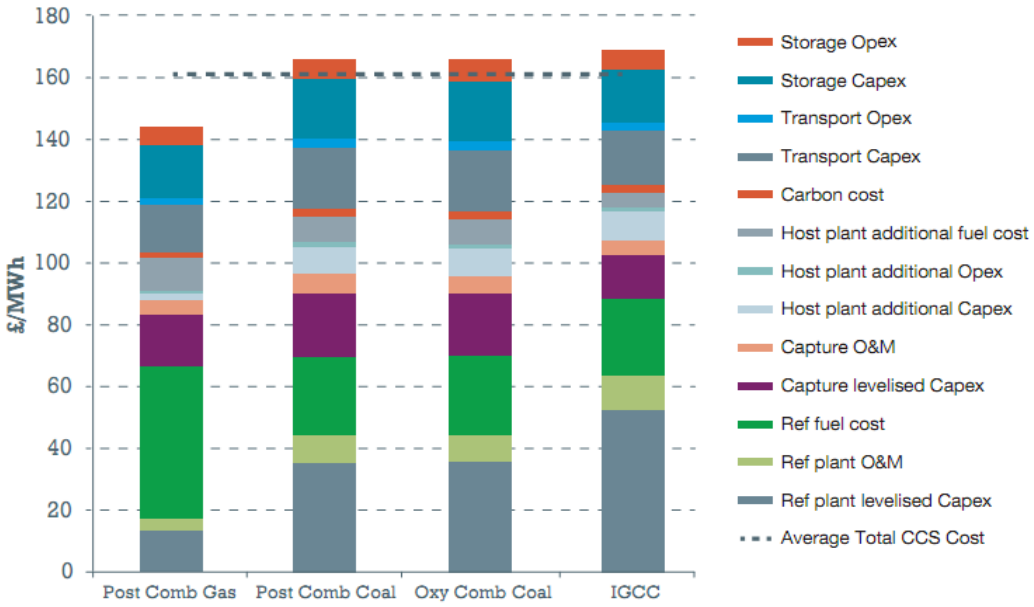


Note: IGCC is integrated gasification combined cycle power plant

Figure 1.8 Processes of $CO_2$ capture technologies (DECC, 2013)

Obviously, NGCC is not carbon neutral technology. In IEA BLUE map, 5% of NGCC power plants will be equipped with solvent-based PCC process to achieve the carbon reduction target (IEA, 2010). Using amine solvent such as MEA to absorb the $CO_2$ from the flue gases is mature technology (Rochelle, 2009). But for the full commercial scale application of this carbon capture technology, the main barrier is the high increment in electricity cost due to its massive capital costs and high thermal energy penalty (Rochelle, 2009; Marchioro Ystad et al., 2013). It is reported that the cost of electricity

from an NGCC power generation will increase to £144.1 from £66 per MWh (see Figure 1.8) when it is integrated with a PCC process (DECC, 2013). Considering the great amount of total electricity consumption, it's a great cost increment for both industry production and living expense. Therefore research efforts are required for potential improvements to reduce both the capital cost as well as the energy penalty to gain a better economic profile of commercial deployment of carbon capture.

## 1.3 Aim and objectives of this study

The research presented in this thesis is aimed to achieve optimal design and operation of NGCC power plant integrated with $CO_2$ capture and transport process to help reduce the CCS deployment cost. To achieve the stated aim, the following objectives have been identified:

i. To develop the process model for the optimisation studies, including (1) selecting and validating correlations for thermodynamic model and physical properties prediction of MEA-$H_2O$-$CO_2$ system, (2) developing a steady state rate-based process model of solvent-based PCC process in Aspen Plus® at the pilot scale and validating the model with experimental data, and (3) scaling up the model to match power plants at industry scale.
ii. To conduct optimal design of the solvent-based PCC process, including (1) developing the cost model of the PCC process, (2) integrating the cost model with the process model, and (3) conducting optimisation of the PCC process.
iii. To explore the integration of NGCC power plant with PCC process, including (1) developing a steady state process of NGCC power plant, (2) analysing the integration of NGCC power plant with PCC process and EGR, and (3) studying heat integration options based on a specific supersonic shock wave compression technology
iv. To carry out the study on optimal design of the $CO_2$ transport pipeline network consisting of the compression trains and onshore and offshore trunk pipelines, that was planned in the Humber region of the UK.
v. To carry out the study on optimal operation for an assumed existing NGCC power plant integrated with MEA-based PCC process based on whole CCS

chain consideration in response to different market conditions including different carbon price, fuel price and $CO_2$ T&S price.

## 1.4 Novel contributions

Compared with the literature on NGCC power plants integrated with solvent-based PCC process, novel contributions of the studies in this thesis are claimed as follows:

i. The model used for optimisation studies in this thesis is expected to have better accuracy than previous studies. It could be justified by (1) the correlations of the prediction for liquid density of mixture and effective vapour liquid interfacial area were improved by coding Fortan subroutines in Aspen Plus®; (2) different values were input to the kinetics of reverse reactions for bicarbonate formation in the absorber and the stripper respectively, which reflects the nature of different operating conditions of the absorber and the stripper; (3) the process model was validated at three different stages, including thermodynamic modelling, physical property calculation and a rate-based process model of the close-loop system; and (4) the cost model of PCC process was developed based on the major equipment costs provided by vendors after detailed engineering design in a benchmark report (IEAGHG, 2012). The uncertainty of this method could be in a range of from −15% to 20%, instead of empirical methods with uncertainty in a range of from −30% to 50%.

ii. In this thesis, non-linear optimisations were implemented in Aspen Plus® and solved by Sequential Quadratic Programming (SQP) method, which is a quasi-Newton nonlinear programming algorithm. In one recent similar study (Agbonghae et al., 2014) using Aspen Plus®, the optimal designs were obtained by comparing different options at the specified values of several key variables, which may exhibit local minimum solution.

iii. For study on the integration of NGCC power plant and solvent-based PCC process, a specific supersonic shock wave compression (Lawlor, 2009) technology was adopted for the $CO_2$ compression train. For conventional multi-stage compressors, the discharge temperature of each stage (around 90–110$^oC$) is lower than the lowest pinch temperature so that the compression heat cannot

be used directly (Gibbins et al., 2004). The discharge temperature of the compressed $CO_2$ is as high as 214.5–230.5$^{o}$C (Witkowski and Majkut, 2012), which provides opportunities for directly integrating compression heat with NGCC/PCC processes. Therefore, the study on heat integrations based on this compression technology with NGCC/PCC process is novel.

iv. For the study on optimal design of $CO_2$ transport pipeline network, simulation-based techno-economic evaluation method is used in this study, compared with empirical methods used in previous studies (IEAGHG, 2002; McCoy and Rubin, 2008; McCollum and Ogden, 2006). Detailed steady state model about the $CO_2$ transport pipeline network was developed including compression train and collecting system for multi-sources, onshore and offshore trunk pipelines with booster pump station. Most of previous process simulation models (Zhang et al., 2006; Nimtz et al., 2010; Liljemark et al., 2011; Chaczykowski and Osiadacz, 2012) for $CO_2$ pipeline network are about single emitter and pipelines without booster station.

v. The novelties of the study on optimal operation under different market conditions based on whole CCS chain consideration are (1) in the cost model, the total annual cost of $CO_2$ T&S was regarded as an operating expense charged by the operators of the $CO_2$ T&S infrastructure, which avoids heavy computationally demanding for the $CO_2$ T&S with many uncertainties. With this method, the cost model was developed to cover the cost of the whole integrated system. Thus the results and insights obtained from this study present the optimal operation for the NGCC power plant equipped with a whole integrated CCS chain, and (2) the optimisations were carried out for the optimal carbon capture level under different carbon price, natural gas (NG) price and $CO_2$ T&S price. It is found that the coactions of carbon price, NG price and $CO_2$ T&S price will significantly affect the decision making about the optimal carbon capture level for operating carbon capture process for an NGCC power plant.

## 1.5 Scope of the study

As can be seen in Figure 1.9, the integrated system in this thesis consists of 5 sections including the NGCC power plant, the solvent-based PCC process, the $CO_2$ compression process, the $CO_2$ transport pipeline network and the $CO_2$ storage section. However, this study focuses on solvent-based PCC process first and then extended to cover other sections and whole CCS chain.

Chapters 3 and 4 present model development and optimisation studies on solvent-based PCC process. In Chapter 3, different combinations of correlations were examined and validated for the thermodynamic model and physical property calculations of MEA-$H_2O$-$CO_2$ mixture. The steady state rate-based process model was developed in Aspen Plus® and validated with the pilot plant data. The model was then scaled up to match industrial power plant scale. In Chapter 4, the cost model is developed and is integrated into process model by coding Fortran subroutine. Optimal design was carried out for the solvent-based PCC process. These were illustrated in Figure 1.9 with red box.

Chapter 5 presents the study on the integration of a 453$MW_e$ NGCC power plant with solvent-based PCC process and $CO_2$ compression train. The process model inthis chapter includes the NGCC power plant, the solvent-based PCC process and the specific supersonic shock wave compressors. These were illustrated in Figure 1.9 with blue box.

Chapter 6 presents model-based techno-economic evaluations for optimal design the $CO_2$ transport pipeline network. The models developed in Aspen HYSYS® include compression trains and collecting system for multi-sources, onshore and offshore trunk pipelines with booster pump station. The process models were integrated with APEA for techno-economic evaluations. These were illustrated in Figure 1.9 with green box.

In Chapter 7, the optimal operation was studied for an assumed existing NGCC power plant integrated with whole CCS chain. The process models include the NGCC power plant, the solvent-based PCC process and the $CO_2$ compression train. The $CO_2$ transport and storage sections were considered as an operating expense ($CO_2$ T&S cost). These were illustrated in Figure 1.9 with purple box.

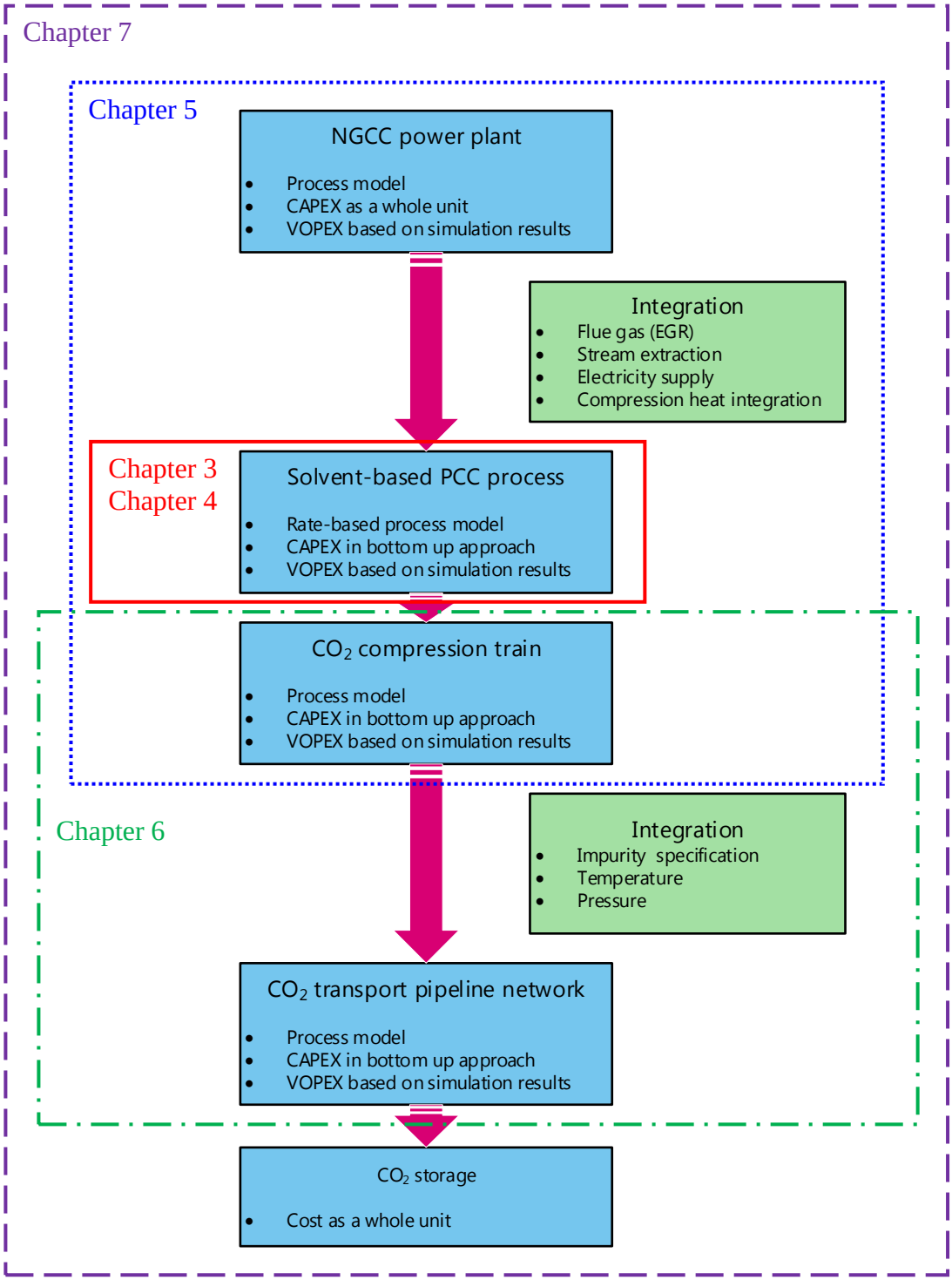


Figure 1.9 Study scope of each chapter

## 1.6 Tools to be used in this study

The study on solvent-based PCC process is a core part of this thesis. Aspen Plus® was chosen for model development and optimisation study of the PCC process. The reasons are: (1) Aspen Plus® has various physical property methods and comprehensive property databank, which makes it can well support thermodynamic modelling and process simulation involving complex electrolyte system. Different routes can be chosen by users for different physical properties. For example, in this study, PC-SAFT EOS was used to calculate major properties in vapour phase whilst eNRTL was used for liquid phase. (2) RateSep model in Aspen Plus® is proven to be capable to simulate the absorber and the stripper in solvent-based PCC process (Zhang et al., 2009; Zhang and Chen, 2013). It employs rate-based mass transfer and kinetic-controlled reactions to describe the chemical phenomenon happening in this reactive absorption process. The correlations and kinetics in the model could be adjusted by comparing model predictions against the experimental, to improve the model accuracy. (3) Aspen Plus® has optimisation function with SQP method, which has been one of the most successful general methods for solving large-scale nonlinear constrained optimization problems (Boggs and Tolle, 2000). (4) Aspen Plus® opens accesses of parameters and correlations of major equations to users and well support user defined model by coding Fortran subroutines. In this study, there are three Fortran subroutines linked into Aspen Plus®, including Han et al. (2012) correlations for density of liquid mixture, Tsai et al. (2011) correlations for interfacial area for packed column and the cost model. Aspen Plus® was also used for model development of NGCC power plant and $CO_2$ compression in Chapters 4, 5 and 7.

Although APEA has been embedded into Aspen Plus® for economic evaluation, the cost model used in Chapters 4, 5 and 7 was developed in Fortran and was integrated into the Aspen Plus® model. The reasons are: (1) APEA needs to re-map and re-size the equipment in the process for cost estimate in each case. Currently APEA cannot automatically run with iterating of optimisation in Aspen Plus®. (2) APEA uses a bottom-up approach for the cost estimate based on historic real project data but it hardly handle some special equipment. For example, the absorber is a rectangular column

constructed in concrete with epoxy lining inside surface. Its cost cannot be accurately estimated from historical cylindrical column with metal material.

In Chapter 6, Aspen HYSYS® was used for process model development for $CO_2$ pipelines network (including $CO_2$ compression) because its pipe model provides more detailed engineering specifications such as elevation changes and heat transfer between the pipeline and surroundings, which is important for this study involving $CO_2$ dense phase transport. As a comparison, the pipeline model in Aspen Plus® is relatively too simple for this study. It should also be noticed that, in this chapter, 'optimal design' is not strictly derived from optimisation study, just by comparing several specific options. In this way, APEA is capable for economic evaluation for pipelines and compressors.

# Chapter 2: Literature Review

This chapter presents literature review of previous experimental and model-based studies on NGCC power plant (Section 2.1), solvent-based PCC process(Section 2.2), NGCC integrated with capture process and $CO_2$ compression (Section 2.3), $CO_2$ transport pipeline network (Section 2.4) and whole CCS chain (Section 2.5). The research gaps were identified and discussed in Section 2.6.

## 2.1 NGCC power plant and its modelling

### *2.1.1 Combined cycle gas turbine (CCGT)*

For gas-fired power plant, CCGT is a prevailing technology because of its high thermal efficiency (IEA, 2008). The thermal efficiency of the CCGT power plant at the Irsching Power Station has reached a 60.75% net efficiency with a 578 megawatts SGT5-8000H gas turbine (SIEMENS, 2016).

CCGT uses a combination of Brayton cycle (gas turbine) and Rankine cycle (steam turbine) for electricity/heat generation. Figure 2.1 displays a typical schematic of a CCGT power plant which is a dual-cycle process. Air and fuel combust to generate heat and then gas mixture expands through gas turbine to generate a part of electricity. Exhaust gas enters heat recovery steam generator (HRSG) by which waste heat of the exhaust gas is recovered to create steam. In the steam cycle, steams at different pressure levels enter multi steam turbines to generate another part of electricity.

### *2.1.2 Modelling of gas turbine*

Although gas turbine is integrated equipment, it could be separated into three sections including air compression, combustion and gas expansion from process view (Refer to Figure 2.1). Analysis of gas turbine is complicated due to large number of parameters and their interactions. For modelling of gas turbines and power plants, some professional software package developed by the gas turbine manufacturers, such as GE Gate-cycle® and Thermoflow GT Pro®, are normally used to predict the performance. But accurate modelling of power plants in generic process software packages such as Aspen Plus® is also required in the case of the integration of power plant with chemical absorption PCC process in this study.

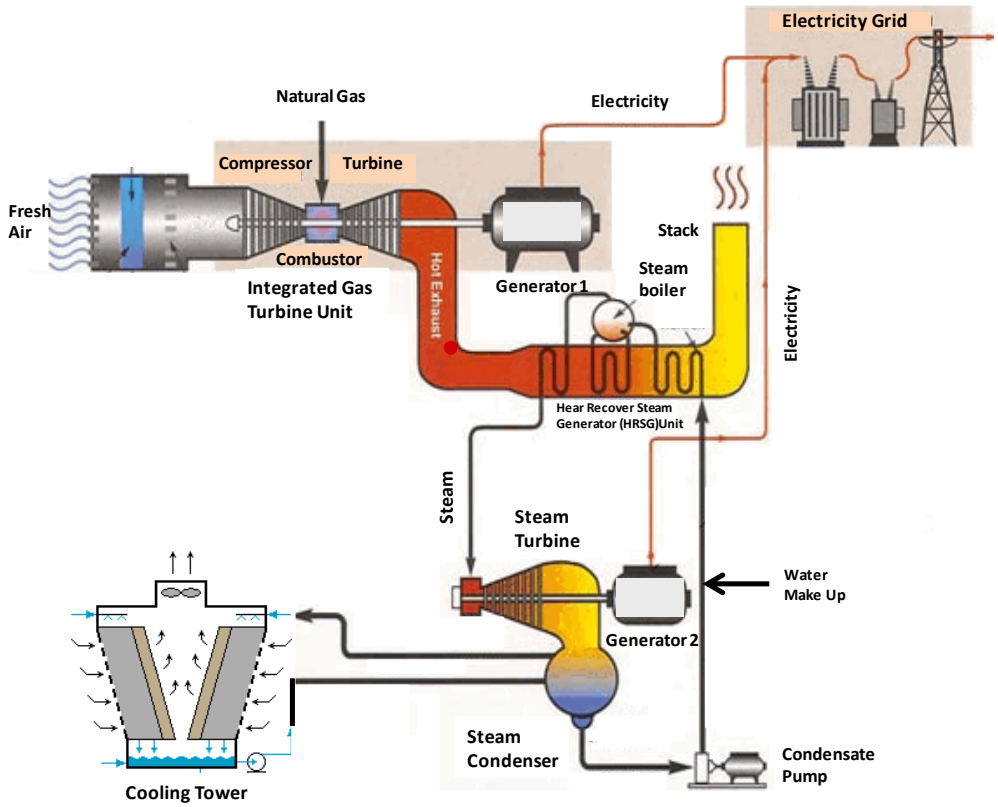


Figure 2.1 CCGT power plant schematic (Adapted from blog.gerbilnow.com (2012))

In the study by Ong'iro et al. (1995), the model in Aspen Plus® has been developed to analyse the performance of integrated gasification combined cycle (IGCC) and Integrated gasification humid turbines (IGHAT) power plants. COMPR block in Aspen Plus® was used to simulate the compressors, fans and turbines. COMPR calculates the power required for some certain pressure ratios and the accuracy depends on the efficiencies specified. The gas combustor was simulated with a Gibbs type reactor (RGIBBS) in Aspen Plus®, by which the equilibrium could be calculated by Gibbs free energy minimization method.

One important factor affecting the whole gas turbine performance is the modelling of cooling of gas turbine blades (Jonsson et al., 2005). Its calculation in the professional power plant software is very complex and requires rigorous heat transfer calculation for the blades stage by stage. Jonsson et al. (2005) proposed a generic cooling model for heavy-duty gas turbines in a joint-project with the gas turbine manufacturers. In their model, three adjustable parameters (i.e. $b, s, K$) could be tuned to represent a gas turbine by comparing the thermal performance (Canepa et al., 2013).

### 2.1.3 Simulation of NGCC power plants

Aside gas turbine, other two important parts of a whole NGCC power plant are HRSG and stream turbines. In order to achieve thermodynamic optimisation, there are many studies (Valdés and Rapún, 2001; Bassily, 2007; Vargas and Bejan, 2000; Godoy et al., 2010) on synthesis and design of different parts of NGCC power plants. For large scale power plants, a triple-pressure HRSG (see Figure 2.2) is employed to improve the overall efficiency (Bassily, 2007; Godoy et al., 2011), which is more complex than one pressure HRSG for small scale power plants.

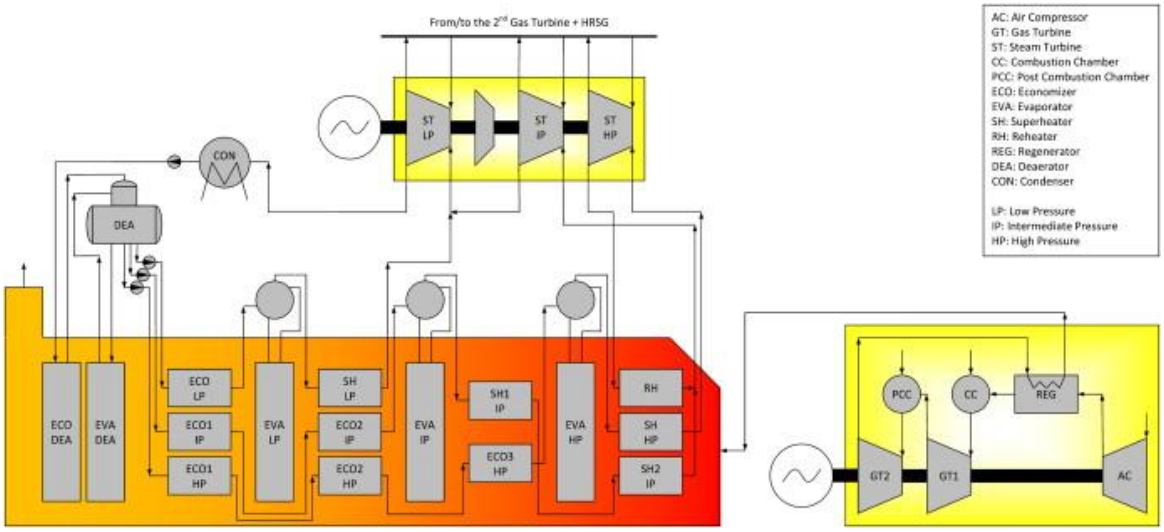


Figure 2.2 Diagram for a gas-fired power plant with a triple-pressure HRSG (Godoy et al., 2011)

For its simulation in Aspen Plus®, HRSG could be regarded as the combination of multiple heat exchangers including the economizer, evaporator, super-heater and water pre-heater, which reflects the functions of different sections in HRSG (Canepa et al., 2013). Those sections could be simulated using HeatX blocks in Aspen Plus® (Ong'iro et al., 1995; Canepa et al., 2013). Three kinds of steams at different pressures are produced from HRSG. The typical pressure and temperature are about 120 bar and 556 °C for high pressure steams, about 30 bar and 550 °C for intermediate pressure steams and 4.15 bar and 290°C for low pressure steams (Marchioro Ystad et al., 2013; Jordal et al., 2012). These steams are lined to the high pressure steam turbine (HP-ST), the intermediate pressure steam turbine (IP-ST) and the low pressure steam turbine (LP-ST) respectively to generate another part of electricity. The three steam turbine sections are simulated by Compr block in Aspen Plus® (Canepa et al., 2013).

For large scale power plants, there are few public data about design features, process and operating conditions because of security measures for intellectual properties. For model validation purpose, the simulation results from those professional software packages are used to validate the simulation results from generic process software tools (Canepa et al., 2013). In a benchmark report of IEAGHG (2012), the reference NGCC power plant with a net power output of 910.3$MW_e$ comprises two gas turbines, two HRSGs and one steam turbines generator. GT PRO® was used to implement thermal performance modelling for the design cases and GT MASTER® was used for the part-load cases. It is noticed that these steam conditions are higher in both temperature and pressure than what is currently typical, which are170 bar and 600 °C for the high pressure steam and 40 bar and 600 °C for the intermediate pressure steam. It was explained that original equipment manufacturers (OEMs) considered that utilizing these similar conditions in NGCC plant will be common practice by 2020 (IEAGHG, 2012).

## 2.2 PCC based on chemical absorption process

### *2.2.1 Experimental studies*

#### 2.2.1.1 Thermodynamic and physical properties

Using MEA solvent to absorb $CO_2$ is a mature technology (Rochelle, 2009). However, complex electrolyte aqueous solvent is involved in this reactive absorption process (Kenig et al., 2001), which requires accurate thermodynamic modelling and physical properties calculations for modelling this process. Generally, 30 wt% MEA solution is considered a benchmark solvent for this process. Thermodynamic data, especially about the $CO_2$ solubility in MEA aqueous solutions, around this condition have been reported (Jou et al., 1995; Harris et al., 2009; Tong et al., 2012). In addition, data covering wider MEA solution concentration range have also been reported (Mason and Dodge, 1936; Lee et al., 1974; Lee et al., 1976; Dang and Rochelle, 2003; Hilliard, 2008; Aronu et al., 2011; Xu and Rochelle, 2011; Wagner et al., 2013). Mason and Dodge (1936) presented $CO_2$ partial pressure of different $CO_2$ loaded MEA aqueous solutions with 0–100 wt% MEA with the temperature from 0°C to75°C under atmosphere pressure. Aronu et al. (2011) produced experimental data of vapour-liquid equilibrium (VLE) of $CO_2$ in MEA aqueous solutions with 15, 30, 45 and 60 wt% MEA and at temperatures from 40 to 120 °C. A low temperature equilibrium apparatus was first used to measure $CO_2$ partial

pressures over loaded MEA solutions with 1 bar, and then a high temperature equilibrium apparatus was operated to measure the total pressures from 1 bar to 10.5 bar. Wagner et al. (2013) published new experimental data for the $CO_2$ solubility of in aqueous 15 and 30 wt% MEA aqueous solutions at 313, 353, and 393K with a wider range of partial pressures of $CO_2$ between 0.001 and 8.6 MPa. With those data, it is possible to develop and validate a reliable thermodynamic model for MEA-$H_2O$-$CO_2$ system.

For parameterization and validation of properties calculation methods of MEA-$H_2O$-$CO_2$ mixture, the experimental data of aqueous MEA solution are valuable especially with $CO_2$ loaded. The correlations for the calculation of density and viscosity of MEA-$H_2O$-$CO_2$ mixture at different temperatures and MEA concentrations can be found in the literature (Cheng et al., 1996; Hartono et al., 2014; Littel et al., 1992; Weiland et al., 1998; Han et al., 2012). In the study of Han et al. (2012), liquid densities of $CO_2$ loaded aqueous MEA solutions were measured with 30, 40, 50, and 60 wt% MEA and at temperatures from 298.15 to 413.15 K. Surface tensions of unloaded MEA solutions were also measured at temperatures from 303.15 to 333.15K with MEA concentration ranged from 0 wt% (pure water) to 100 wt% (Pure MEA). Ying and Eimer (2012) measured the diffusivities of $N_2O$ in MEA aqueous solution and calculated the diffusivities of $CO_2$ in MEA aqueous solution by $N_2O$ analogy method. They found that the diffusivities of $CO_2$ in MEA aqueous solution decrease with increasing of MEA concentration and increase when solution temperature rises.

#### 2.2.1.2 Mass transfer and thermal performance

For the mass transfer and thermal performance of the integrated PCC based on chemical absorption process, there are many research projects having been implemented world-wide (CCP, 2000; CASTOR, 2004; CO2CRC, 2003; BIGCO2, 2007; CESAR, 2008). In most of these studies, MEA is chosen as a reference solvent for validation of the models and scale-up, sometimes also for comparison with new solvents investigations. The information about pilot plants experimental data obtained for the solvent MEA can be found in some reports (Chapel et al., 1999; Faber et al., 2011; Mangalapally and Hasse, 2011; Tobiesen et al., 2007; Dugas, 2006; Notz et al., 2012).

Dugas (2006) presented a great number of experimental data about separation performance and mass transfer of the absorber and the stripper respectively. Their pilot plant consists of the absorber and the stripper with same diameter of 0.427 m and same packing height of 6.1 m. But their study did not investigate the impact of process parameters on heat requirement for solvent regeneration of the closed-loop absorption and desorption process. Tobiesen et al. (2007) published various experimental data for validation purpose of rigorous modelling for the absorber and the stripper individually. In one recent contribution of Notz et al. (2012), the pilot plant with a closed-loop absorption/desorption process was continuously running. The diameter is 0.125m for both the absorber and the stripper and packing height (packing type: Sulzer® Mellapak 250Y™) is 4.2 and 2.25 m respectively. Comprehensive experimental studies were conducted about the impact of several key process conditions and operational variables such as $CO_2$ concentration in flue gases, $CO_2$ capture level, hydraulic parameter of the absorber, lean solvent flow rate, stripper pressure and MEA concentration in solvents on the process behaviour.

### *2.2.2 Model-based studies*

#### 2.2.2.1 Thermodynamic modelling of MEA-$H_2O$-$CO_2$ system

Accurate thermodynamic modelling and physical properties prediction of pure components and mixtures is one of the basic prerequisites for the process modelling and simulation (Lee et al. 1975). For highly non-linear electrolyte MEA-$H_2O$-$CO_2$ solution, the electrolyte Non-Random Two Liquid (eNRTL) model (Song et al., 1996; Chen and Evans, 1986) are the most widely adopted models. For example, Austgen et al. (1989) applied eNRTL to correlate $CO_2$ solubility in aqueous MEA solution. Hilliard (2008) impoved the model by regressing correlations of phase equlibrium, heat of absorption and heat capacity and predicted composition concentrations in MEA aqueous solutions loaded with $CO_2$ (Hilliard, 2008; Böttinger et al., 2008). Hessen et al. (2010) improved the eNRTL model from Bollas et al. (2008) to correlate $CO_2$ solubility in MEA aqueous solutions and to predict the composition in MEA-$H_2O$-$CO_2$ system. PC-SAFT EOS was used for vapour phase fugacity coefficients of $CO_2$ with system temperature up to 500 K and system pressure up to 150 MPa. The results was compared with REFPROP EOS

(Span and Wagner, 1996) developed specifically for the property prediction of pure $CO_2$.

The prediction of VLE of MEA-$H_2O$-$CO_2$ system largely depends on the accurate calculation of $CO_2$ solubility in MEA aqueous solutions, which is determined by both its physical solubility and chemical equilibrium in aqueous solutions (Zhang et al., 2011). Physical solubility is the equilibrium between $CO_2$ molecules in vapour phase and liquid phase and it can be calculated by Henry's law. The available binary Henry's constants are summarized in Table 2.1. In the system of MEA-$H_2O$-$CO_2$ mixture, early studies (Austgen et al., 1989; Yan and Chen, 2010) only considered Henry's constants for $CO_2$ with $H_2O$ and regressed its value from extensive amounts of experimental VLE data for the $CO_2$-$H_2O$ binary system. Some of them also considered binary Henry's constants for the $CO_2$-MEA. In one recent study (Wagner et al., 2013), MEA was regarded as a Henry component because they claimed MEA could evaporate in the column resulting in higher solvent make-up requirement.

Table 2.1 Correlations for the calculation of Henry's constants

| Henry constants | Unit | $C_1$ | $C_2$ | $C_3$ | $C_4$ | T (°C) | Source |
|---|---|---|---|---|---|---|---|
| $CO_2$ , $H_2O$ | Pa | 170.7126 | −8477.711 | −21.95743 | 0.005781 | 0–100 | Chen et al. (1979) |
| $CO_2$, $H_2O$ | Pa | −9624.4 | −28.749 | 0.01441 | 192.876 | 273–473 | Rumpf and Maurer (1992) |
| $CO_2$, $H_2O$ | Pa | 100.650 | −6147.7 | −10.191 | 0 | 273–473 | Yan and Chen (2010) |
| $CO_2$, MEA | Pa | 20.1759 | −1183.5 | 0 | 0 | | Aspen Databank (2012b) |
| MEA, $H_2O$ | MPa | −11803.5 | −10.617 | 0 | 84.599 | 288–408 | Wagner et al. (2013) |

The chemical equilibrium in aqueous solution of MEA-$H_2O$-$CO_2$ systems can be presented by a series of equilibrium reactions in an acid-base buffer mechanism (Austgen et al., 1989). The chemical equilibrium constants of those reactions can be

estimated in two ways. Most models (Austgen et al., 1989) used a polynomial correlation with parameters regressed using experimental data as in Equation (2.1).

$$lnK_j = C_1 + \frac{C_2}{T} + C_3 lnT + C_4 T \tag{2.1}$$

where $K_j$ is the chemical equilibrium constants for each equation $j$, $T$ is system temperature, $C_1, C_2, C_3, C_4$ are correlations for chemical equilibrium constants.

Another method is to calculate chemical equilibrium constants from the reference state Gibbs free energies of the participating components (Zhang et al., 2011), as in Equation (2.2).

$$-RTlnK_j = \Delta G_j^0 \tag{2.2}$$

where $K_j$ is the chemical equilibrium constant of reaction j , $\Delta G_j^0$ is the reference state Gibbs energy change for reaction j, $R$ is the universal gas constant, and $T$ is the system temperature.

#### 2.2.2.2 Rate-based model for solvent-based PCC Process

Using MEA solvent to absorb $CO_2$ is a reactive absorption process. A rate-based approach for both mass transfer and reactions (see Figure 2.3) offers a more accurate prediction than equilibrium-stage approach (Kenig et al., 2001; Lawal et al., 2009).

Gas absorption into liquid in the absorber and gas desorption from liquid in the stripper are fundamental for solvent-based PCC process. Various theories, including two-film theory (Whitman, 1962), penetration theory (Higbie, 1935), surface renewal theory (Danckwerts, 1951) and Eddy diffusivity theory (King, 1966) could be used to explain the phenomenon of mass transfer inside columns, Two-film theory (Whitman, 1962) is widely used to describe the mass transfer of components across the gas phase and the liquid phase in packed columns. In each phase, the thickness of the film is determined as the ratio of the average diffusivity to average mass transfer coefficient, the

calculation of film resistance is improved by discretizing the films (see Figure 2.4) and reactions are considered in the liquid phase (Austgen et al., 1989).

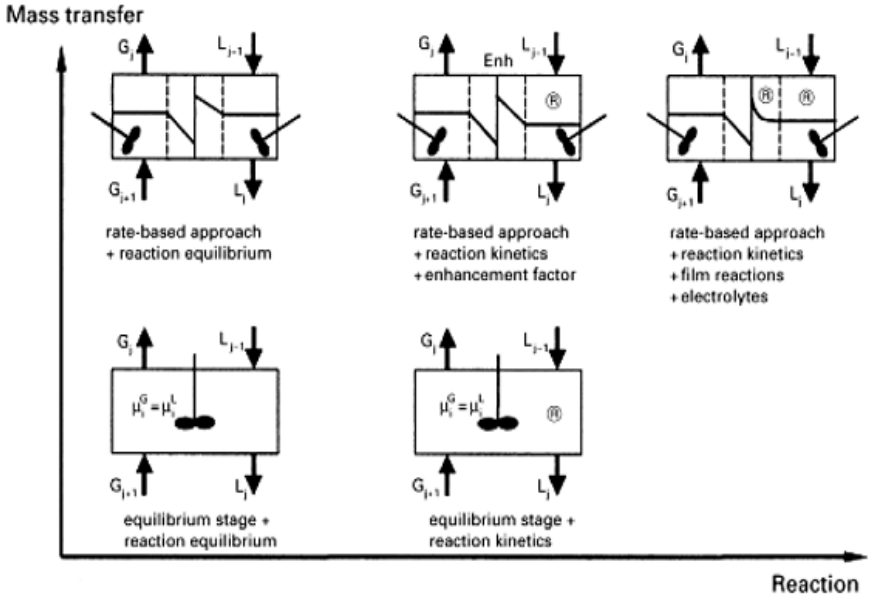


Note: G represents gas phase; L represents liquid phase; μ represents chemical potential; ® represents kinetic-controlled reaction model.

Figure 2.3 Model complexities for reactive absorption process (Kenig et al., 2001).

Zhang et al. (2009) published the details of a rate-based model development for the absorber in Aspen Plus®. The model was validated by comparing model predictions of lean solvent loading, rich solvent loading, capture level and the temperature profile with the experimental data from University of Texas at Austin (Dugas, 2006). The study showed that the rate-based model using Aspen Plus® was proven to be capable of providing acceptable accuracy for performance prediction of solvent-based PCC plant. In their recent study (Zhang and Chen, 2013), the kinetics of forward and reverse reactions for carbamate formation and bicarbonate formation were improved with new experimental data (Mangalapally and Hasse, 2011). The significant contribution is that the value of kinetic of reverse reactions for bicarbonate formation is different for the absorber and the stripper, which reflects the nature of different operating conditions of the absorber and the stripper.

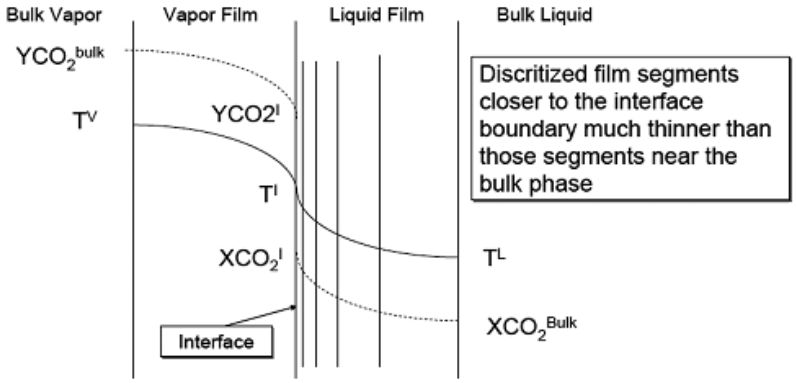


Note: V represents vapour phase; Y represents mole fraction in vapour phase; L represents liquid phase; X represents mole fraction in liquid phase; T represents chemical potential.

Figure 2.4 Discretized liquid film for counter current flow (Zhang et al., 2009)

The correlation selection for rate-based mass transfer also has large impact on the prediction accuracy (Kvamsdal et al., 2011a; Razi et al., 2012). It mainly includes mass transfer coefficients, interfacial area, liquid holdup and pressure drop inside packing beds. Razi et al. (2012) discovered large differences of the model prediction results for different correlations used in the model and they recommended that model validation using pilot plant or commercial data is required for accurate prediction.

#### 2.2.2.3 Model-based optimal design and operation of PCC processes

The process flow diagram can be seen in Figure 2.5. The flue gas is treated by a preconditioning process (desulfurizing and cooling) and then enters the absorber, in which, lean amine solvent reacts with the $CO_2$. The scrubbed flue gas is emitted to the atmosphere and the $CO_2$-rich solvent is discharged from the bottom of the absorber and enters the stripper. The $CO_2$-rich solvent is regenerated inside the stripper with heat input to the reboiler. The regenerated solvent is cooled and recirculated to the absorber for reuse.

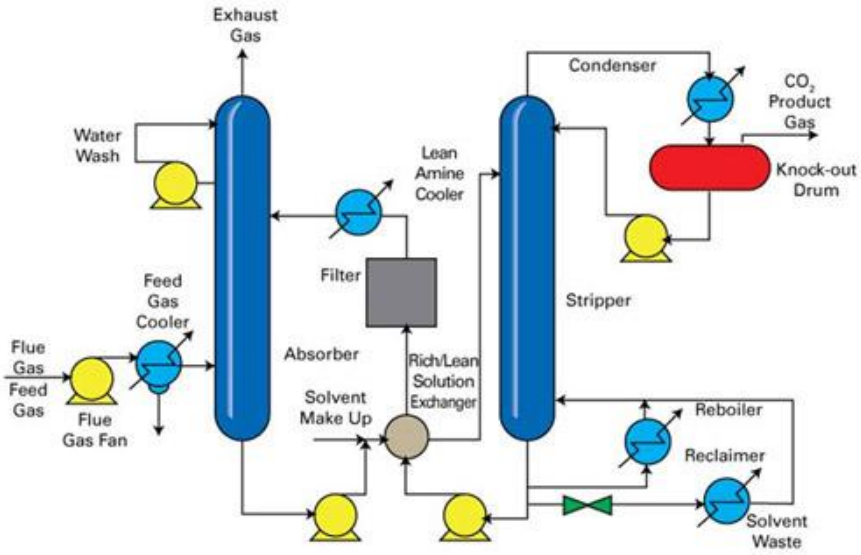


Figure 2.5 Process flow diagram of solvent-based PCC (IPCC, 2005)

In order to describe this process better, several technical items are defined as follows.

$CO_2$ capture level (CL) is defined in Equation (2.3).

$$CL(\%) = \left(\frac{y_{CO_2,FG}F_{FG} - y_{CO_2,EG}F_{EG}}{y_{CO_2,FG}F_{FG}}\right) \times 100 \tag{2.3}$$

where $F_{FG}$ and $F_{EG}$ are mass flow rates of flue gas and exhaust gas respectively, $y_{CO_2,\ FG}$ and $y_{CO_2,\ EG}$ are $CO_2$ mass fractions in the flue gas and exhaust gas respectively.

$CO_2$ loading in lean solvent (lean loading) and rich solvent (rich loading) in mole basis are defined in Equation (2.4).

$$CO_2\ loading\ (mol\ CO_2/molMEA) = \frac{[CO_2] + [HCO_3^-] + [CO_3^{2-}] + [MEACOO^-]}{[MEA] + [MEA^+] + [MEACOO^-]} \tag{2.4}$$

Specific duty is defined by Equation (2.5).

$$Q_{spe}\ (GJ/ton\ CO_2) = \frac{Q_{reb}}{F_{CO_2,cap}} \tag{2.5}$$

where $Q_{reb}$ is heat duty of the reboiler, $F_{CO_2,cap}$ is mass flow rate of $CO_2$ captured.

Because of significant energy requirement for solvent regeneration of the solvent-based PCC processes (Rochelle, 2009), the cost of carbon capture is high when PCC is

equipped to the emitters such as power plants, refineries and cement plants (DECC, 2013). One of the most important engineering tools for addressing these cost issues is optimisation (Edgar et al., 2001). Optimisation of a large process, such as NGCC power plant integrated with PCC process in this study, can involve several levels such as process configurations (Amrollahi et al., 2012; Oyenekan and Rochelle, 2007; Sipöcz and Tobiesen, 2012), equipment designs (Agbonghae et al., 2014; Mores et al., 2014; Canepa and Wang, 2015) (see Table 2.2), controlled variables of plant operations (Abu-Zahra et al., 2007a; Kvamsdal et al., 2011b; Mac Dowell and Shah, 2013) as well as control strategies (Panahi and Skogestad, 2011; Schach et al., 2013).

Most early studies were carried out for parametric studies of solvent-based PCC processes in the context of coal-fired power plants, which forms the base for later researches on PCC process in context of gas-fired power plants. Abu-Zahra (2007b) investigated carbon capture from the flue gas of a 600 $MW_e$ bituminous coal fired power plant using Aspen Plus®. The results proved that several key variables, such as $CO_2$ capture level, MEA concentration, $CO_2$ loading in lean solvent, stripper operating pressure and lean solvent temperature, have significant impact to energy requirement for solvent regeneration. A minimum specific duty of 3.0 GJ/ton $CO_2$ was achieve at lean loading of 0.3 mol $CO_2$/mol MEA, a 40 wt% MEA solvent and a 2.1 bar stripper operating pressure, compared to 3.9 GJ/ton $CO_2$ in the base case with 30 wt% MEA. However, in this study, equilibrium-based approach was used for modelling both the absorber and stripper and this adds big uncertainty to the results.

Temperature bulges in the absorber were demonstrated by Kvamsdal et al. (2008) with variations of L/G ratio, solvent type, height of packing, and flue gas $CO_2$ concentration. In their later publication (Kvamsdal et al., 2011b), they discovered that flue-gas cooling (30–50°C) has benefits for both coal-fired case and natural gas-fired case. Inter-cooling only has a positive effect for the coal case but a negative cost effect for the natural gas case.

Table 2.2 Literature review of key parameters of optimal PCC process for NGCC power plant at the industrial scale

| Description | | Kvamsdal et al. (2010) | Sipocz and Tobiesen (2012) | Biliyok and Yeung (2013) | Agbonghae et al. (2014) | Mores et al. (2014) | Canepa et al. (2015) |
|---|---|---|---|---|---|---|---|
| Power plant size ($MW_e$) | | 540 | 410.6 | 440 | 450 | 788 | 427 |
| Flue gas flow rate (kg/s) | | 1045.6 | 639.61 | 693.6 | 725 | – | 702 |
| $CO_2$ concentration (mol%) | | 3.5 | 4.2 | 3.996 | 4.00 | 3.99 | – |
| $CO_2$ capture level (%) | | 90 | 90 | 90 | 90 | 90 | 90 |
| MEA concentration (wt%) | | 30 | 30 | 30 | 30 | 30 | 32.5 |
| Liquid/Gas ratio (g/g) | | 0.87 | 0.68 | 1.04 | 0.96 | – | 0.97 |
| Lean loading (mol $CO_2$/mol MEA) | | 0.216 | 0.132 | 0.234 | 0.2 | 0.159 | 0.2 |
| Rich loading (mol $CO_2$/mol MEA) | | 0.47 | 0.473 | 0.495 | 0.483 | 0.451 | 0.477 |
| Specific duty (GJ/ton $CO_2$) | | 3.77 | 3.97 | 4.003 | 3.96 | 4.35 | 4.1 |
| Absorber | Number | 4 | 1 | 4 | 2 | 4 | 3 |
| | Dameter (m) | 9.6 | 9.13 | 10 | 12.88 | 11.9 | 10.3 |
| | Packing height (m) | 13.6 | 26.9 | 15 | 19.99 | 30.6 | 25 |
| | Packing type | Mellapak 250X | Mellapak 250[a] | Mellapak 250X | Mellapak 250Y | IMTP[a] | IMTP no. 40 |
| Stripper | Number | 1 | 1 | 1 | 1 | 1 | 1 |
| | Diameter (m) | 6.2 | 5.5 | 9 | 7.74 | 4.2 | 7.4 |
| | Packing height (m) | 7.6 | 23.5 | 15 | 28.15 | 8.2 | 15 |
| | Packing type | Mellapak 250X | Mellapak 250[a] | Mellapak 250X | Mellapak 250Y | IMTP[a] | Flexipack 1Y |
| | Pressure(bar) | 1.912 | 1.92 | 1.5 | 1.62 | 2 | 2.1 |
| Economics | LCOE(€/MWh) | – | 80.30 | 70.00 | 20.84 | 60.82 | 68.00 |
| | CCA (€/ton $CO_2$) | – | 99.67 | 51.00 | 63.79 | 63.38 | – |

a. The detailed size of the packing was not given in the publication.

The study by Mores et al. (2012) carried out different cost optimisations including both investments and operating costs for a typical chemical absorption PCC process. The cost model was developed based on empirical equation with correlations. Using the model, detailed investigations were performed about the impacts of different $CO_2$ capture level on the total annual cost, operating variables and equipment sizes. Later, they (Mores et al., 2014) developed an equations-oriented optimisation model for power plants coupled to $CO_2$ capture process. The electricity cost, $CO_2$ avoidance cost, energy penalties, as well as the optimal values of decision variables were investigated. In the context of a 731 $MW_e$ NGCC power plant with the PCC process, the optimal overall $CO_2$ capture level of 82.1% was achieved with three capture trains with 94.8% capture level of each train, whilst 13.4% of the flue gas stream is bypassed. The avoidance cost is €63.38 per ton of $CO_2$ captured.

Razi et al. (2013a) applied Aspen RateSep to study alternative absorber designs for a gas-fired power plant and a coal-fired power plant respectively, both with a power output of 400 $MW_e$ and a 90.0% of $CO_2$ capture level. Large electrical energy savings in the flue gas blower (decreasing from 4493 kW to 2223kW) was found following 52% decrease of the pressure drop when the diameter of the absorber increased from 16 m to 18m. However, the investment is slightly increased because of increase in the column cross sectional area. The optimal values of the flooding factor of the absorber in the two cases were 71.0 and 74.0% respectively.

In a recent study (Agbonghae et al., 2014), optimal designs have been carried out for two MEA-based carbon capture plants for gas-fired power plants of 400 $MW_e$ and 450 $MW_e$ respectively. Mellapak 250Y structured packing was used in the absorber and the stripper. The optimal lean $CO_2$ loading is about 0.2 mol $CO_2$/mol MEA. The optimal L/G ratio for a NGCC power plant with a flue gas with 4 mol % $CO_2$ is about 0.96, while it is from 2.68 to 2.93 for a flue gas.

Arias et al. (2016) conducted comprehensive sensitivity analyses of main parameters of a solvent-based PCC process. The results revealed that the temperature of flue gas feed, lean solvent, rich solvent have high sensitivities to the specific total cost.

## 2.3 NGCC integrated with solvent-based PCC

### *2.3.1 NGCC integrated with PCC*

For a typical NGCC power plant, the LHV efficiency approaches 60% while the $CO_2$ per kWh electricity generated is only about half of the coal-fired power plant of equivalent capacity. These advantages will promote more NGCC power plants to be built in the next decade, especially in developed countries. However NGCC is not a neutral carbon technology. The blue map of IEAGHG (2010) shows NGCC equipped with carbon capture will contribute 5% electricity supply in 2050 to achieve the target of $CO_2$ emission reduction (see Figure 2.6).

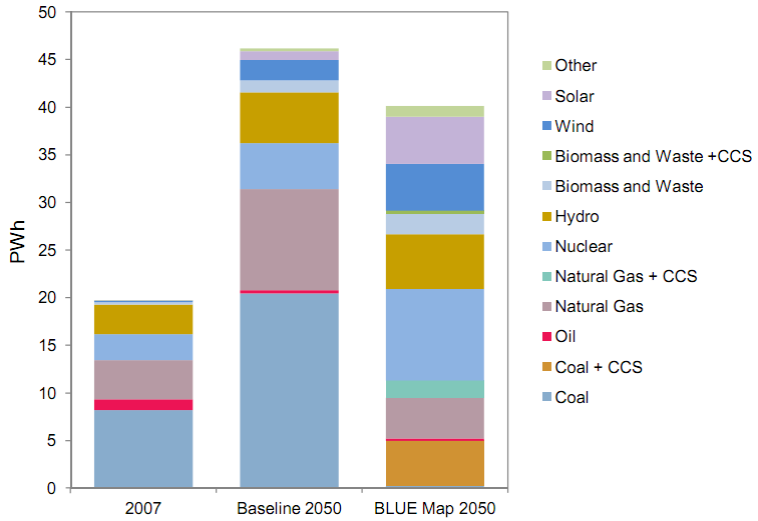


Figure 2.6 BLUE map emission reduction plant (IEAGHG, 2010)

MEA-based post-combustion chemical absorption is the most likely technology to be implemented for carbon capture from fossil fuel power plants (Wang et al., 2011; IEAGHG, 2012). This is because: (1) amine scrubbing, typically using MEA as a solvent, is a proven technology for $CO_2$ separation from flue gas (Rochelle, 2009); (2) they easily retrofits to existing power plants; and (3) it is easy to bypass the carbon capture process if need be.

### *2.3.2 Energy penalty*

In amine scrubbing, large amount of thermal energy is required for rich solvent regeneration in the stripper (Rochelle, 2009). When NGCC power plant is integrated with PCC capture plant, an efficiency penalty was reported with a reduction of net plant efficiency from 58.5% to 50.6% (Marchioro Ystad et al., 2013). This energy penalty

comprises: (1) steam extraction from power plant for solvent generation; (2) power consumption of $CO_2$ compression and (3) auxiliary power consumption for PCC capture plant.

For MEA-based PCC process, the typical thermal energy required to regenerate 1 ton of $CO_2$ is between 3.4 GJ and 4.2 GJ (Abu-Zahra et al., 2007b; Kvamsdal et al., 2007; Mac Dowell and Shah, 2013; Marchioro Ystad et al., 2013; Canepa and Wang, 2015). Recent research efforts focus on how to improve the capture plant efficiency to reduce the energy requirement for $CO_2$ captured. In the study of Abu-Zahra et al (2007b) several key parameters such as lean solvent loading, $CO_2$ capture level, MEA concentration in solvent and stripper operating pressure were examined. The lean solvent loading was found to have a major effect on the thermal energy requirement. The economic range of lean solvent loading is 0.29–0.32 mol $CO_2$/mol MEA for MEA concentration in solvent of 30–40 wt%. High operating pressure in the stripper would lead to a reduction of energy requirement of both solvent regeneration and $CO_2$ compression. Mac Dowell and Shah (2013) conducted a cost optimisation study of a capture plant. The results showed when the capture level increase from 85% to almost 100%, the optimal energy requirement of per ton of $CO_2$ decrease to 3.8 from 4.2 GJ with optimal lean loading 0.18–0.22 mol $CO_2$/mol MEA, which is obviously lower than the result of Abu-zahra et al. (2007). In a recent study by Canepa and Wang (2015), a sensitivity analysis was conducted for a capture plant scaled up to meet a 427$MW_e$ CCGT power plant. The optimal specific duty was approximately 4.1 GJ/ton $CO_2$ with a 0.2 lean loading, 0.97mol/mol L/G ratio (Table 2.2).

### *2.3.3 Exhaust gas recirculation (EGR) technology*

Compared with coal fired power plants, NGCC power plant emits only half $CO_2$ per unit power. Consequently, the $CO_2$ concentration in flue gas from an NGCC power plant is as low as 3.5–4.5 mol% whilst it is 11–13 mol% for flue gas from a coal fired power plant (Agbonghae et al., 2014). Low $CO_2$ concentration causes low absorption efficiency whilst large flow rate of inert gas requires big equipment size in PCC capture plant (Jonshagen et al., 2011). EGR is regarded as an effective solution (Biliyok and Yeung, 2013). The flue gas leaving the HRSG is split into two streams. One is lined to the PCC process and the other is cooled and recirculated to compressor inlet where it is

mixed with fresh air. Thus the flow rate of fresh air intake reduces greatly. Consequently, the flow rate of flue gas going to be treated by the PCC process would decrease largely whilst the $CO_2$ concentration in the flue gas increase obviously (Canepa et al., 2013). Sipöcz and Tobiesen (2012) presented thermodynamic and economic analyses of a 440 $MW_e$ NGCC plant integrated with an MEA-based PCC process, combining absorber intercooling, lean vapour recompression and EGR options together. The results showed that EGR adds significant benefits for reducing the operating and investment costs.

EGR ratio is defined as Equation (2.6):

$$EGR\ ratio = \frac{volume\ flow\ of\ recirculated\ exhaust\ gas}{volume\ flow\ of\ exhaust\ gas} \tag{2.6}$$

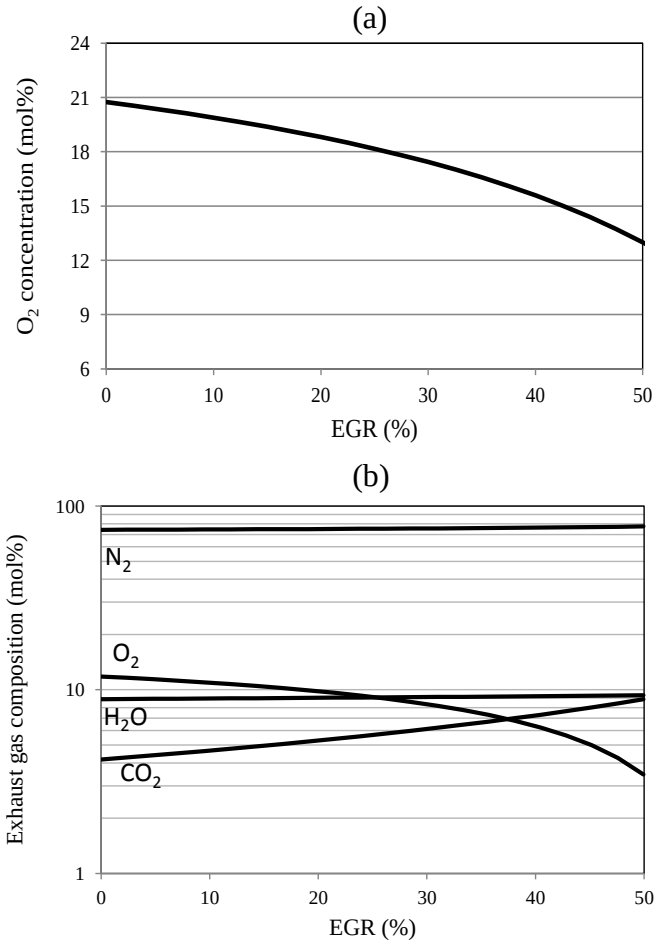


Figure 2.7 Impact of EGR, (a) on $O_2$ concentration in combustion air feed, and (b) on exhaust gas compositions (Canepa et al., 2013)

The impacts of EGR can be seen in Figure 2.7. Figure 2.7(a) illustrates the change of $O_2$ concentration in combustion air when EGR ratio varies. In Figure 2.7(b), exhaust gas composition is shown as a function of the EGR ratio. With the increase of EGR ratio, the concentrations of $N_2$, $H_2O$ and $CO_2$ increase. But $O_2$ concentration decreases because less oxygen is available in the recirculated stream.The maximum EGR ratio of flue gas recirculation is limited by combustion performance. It is believed that the changes in turbomachinery performance may be very small with an oxygen concentration in combustion air of minimum 16–18 mol % (Ulfsnes et al., 2003; Canepa et al., 2013).

## 2.4 $CO_2$ transport pipeline network

### *2.4.1 $CO_2$ transport pipeline*

$CO_2$ transportation is one important section of whole CCS chain. Captured and purified $CO_2$ is compressed and transported from the capture plant to other sites for storage or reutilization by pipeline, ship or tanker trucks mainly depending on the distance. Pipelines are the preferred method for onshore and offshore transport of large volumes of $CO_2$ (Svensson et al., 2004; IPCC, 2005). Pipelines have been used to transport $CO_2$ in gaseous and dense (i.e. sub-cooled liquid or supercritical) phases. The dense phase is regarded as the most energy-efficient condition due to its high density and low viscosity (Zhang et al., 2006; McCoy and Rubin, 2008). Consequently, current operating practice for $CO_2$ pipelines is to maintain the pressure well above the critical pressure.

### *2.4.2 EOS selection*

The cubic equation of state (EOS) such as Soave-Redlich-Kwong (SRK) (Soave, 1972) and Peng-Robinson (PR) (Peng and Robinson, 1976) has been widely used to calculate the physical properties of the $CO_2$ and impurities (Li and Yan, 2009). More complex EOS such as Lee-Kesler (Lee and Kesler, 1975), the Statistical Associating Fluid Theory (SAFT) (Wertheim, 1984; Wertheim, 1986), Span and Wagner (SW) (Span and Wagner, 1996) and GERG (Kunz and Wagner, 2012) were used in recent studies. SW is accurate for pure $CO_2$ as it was specially developed for pure $CO_2$. But it is difficult to generalize for multi-component mixture (Diamantonis et al., 2013) because it contains many terms,

some of which are complex exponential for computation (Kim, 2007). Molecular-based SAFT is an attractive EOS for $CO_2$ including impurities because of better performance than other models for predicting thermodynamic properties of several complex mixtures. SAFT-VR, one of modifications of original SAFT, is used for $CO_2$ capture process (Mac Dowell et al., 2009; Mac Dowell et al., 2011). But SAFT is not yet used in published literatures focusing on the dense phase pipeline transport of the $CO_2$ and impurities. GERG is the international reference equation of state for natural gas. The accuracy of GERG EOS claims to be very high covering a large part of the T/P range for CCS application. GERG was used in recent studies emphasizing the transient behaviours of the $CO_2$ and impurities in dense phase pipeline transport (Liljemark et al., 2011; Chaczykowski and Osiadacz, 2012). However the average absolute deviations (AAD) of the liquid volume of $CO_2$ mixtures could reach up to 18% (Li et al., 2011).

There is no consensus in literature regarding the best EOS for design of $CO_2$ transport pipeline. PR EOS was chosen in some studies (Zhang et al., 2006; Seevam et al., 2008; Mahgerefteh et al., 2008) giving reasonable results for properties of the $CO_2$ and impurities. Li et al. (Li and Yan, 2009; Li et al., 2009) concluded that calibrating the binary interaction parameters ($k_{ij}$) based on experimental data improves the accuracy of EOS after comparing results generated with the $k_{ij}$ from literature and $k_{ij}$ obtained through calibration. Their later study (Li et al., 2011) indicated that SAFT have better accuracy than PR for volume calculation, but PR is better for VLE calculations. (Diamantonis et al., 2013) compared the results of several EOS with experimental data and found that PR EOS is of reasonable accuracy, even when compared with more advanced EOS such as SAFT and PC-SAFT, when calibrated binary interaction parameters are used.

### *2.4.3 Modelling and simulation studies*

The impurities in $CO_2$ stream have great impacts on the design, operation and optimisation studies (Li et al., 2009; Li and Yan, 2006; Race et al., 2012). Seevam et al. (2008) studied the impact of the impurities on phase behaviour and density of $CO_2$. The presence of the impurities may result in the formation of gaseous $CO_2$ or two-phase $CO_2$ flow inside the pipelines. The water content in the $CO_2$ stream may cause hydrate formation, which results in flow assurance problems involving phase transient and

pipeline blockage (Race et al., 2012; Chapoy et al., 2011; Kvamme et al., 2014). Therefore, before the pipeline transport, the $CO_2$ stream has to be conditioned to remove impurities such as water vapour, $H_2S$, $N_2$, methane, $O_2$, hydrocarbons and free water (Aspelund and Jordal, 2007; Koornneef et al., 2010).

Steady state simulations and analysis were carried out to calculate pressure drop, temperature profile and mass flow in the pipelines. Zhang et al. (2006) studied the density and pressure profiles of $CO_2$ stream along the length of the pipeline with different inlet temperatures. Maximum length of pipeline, in which $CO_2$ stream stays in dense phase, is determined for different inlet temperatures. In the study of Nimtz et al. (2010), the model includes the pipeline and an injection well for pure $CO_2$ stream. The profiles of pressure, temperature, density and flow velocity were presented for several cases and the phase change was found and discussed. Regarding the dynamics of pipeline systems, there is little work reported in the literature. Liljemark et al. (2011) developed a pipeline transfer function model to evaluate phase transition of the transported $CO_2$ mixture. Operation scenarios of pipeline cooling, load change, start-up, shut-down and compressor trip were simulated. Chaczykowski and Osiadacz (2012) built a first principle single-phase compressible flow model, suitable for supercritical and dense-phase calculations, to examine the hydraulic parameters of the $CO_2$ pipeline. However, these simulations were performed for a single $CO_2$ emission source without intermediate boosters. This may not reflect realistic operating scenarios for a typical $CO_2$ pipeline network system.

### *2.4.4 The cost of $CO_2$ pipeline transport*

The cost of the $CO_2$ pipeline transport can become significant when the distances between the storage locations and the emission sources are more than a few hundred kilometres. Collecting $CO_2$ mixture from several emitters into trunk pipelines is more cost-effective than the use of separate pipelines (Chandel et al., 2010; IPCC, 2005). As a part of economic evaluation of CCS deployment, some research efforts were given on the cost estimate of $CO_2$ pipeline transport. Van den Broek et al. (2010), Heddle et al. (2003) and Pershad et al. (2010) used a linear cost related with diameter and length of the pipelines to calculate investment costs. Gao et al. (2011) developed a cost model based on the weight of the pipeline, which is specific for the Chinese market. In the

report of IEAGHG (2002), six different kinds of coefficients, for 600#, 900# and 1500# ASNI class and onshore/offshore pipelines, were used for the operating and maintenance costs calculation of $CO_2$ transport pipelines. McCoy and Rubin (2008) developed a cost equation for pipeline transport with different parameters for each cost category (material, labour, right of way and miscellaneous costs) for different regions of the USA. Dahowski et al. (2009) and McCollum and Ogden (2006) built their linear cost equations only based on the flow rate of $CO_2$ stream and the length of the pipelines.

The cost of transporting (without the compression) $CO_2$ by a 100 km onshore pipeline was estimated by the Global CCS Institute (GCCSI) at 0.46–1.55 €/t $CO_2$ (GCCSI, 2011). However, large ranges for capital and levelised costs of $CO_2$ transportation were found for a given diameter (Ogden et al., 2004; Wildenborg et al., 2004; McCollum and Ogden, 2006; Knoope et al., 2013). For example, Knoope et al. (2013) came up with a cost range of 0.6–11 M€/km for a 0.91 m diameter pipeline after comparing seven different models.

## 2.5 The studies on whole CCS chain

In terms of power plant integrated with whole CCS chain, like the schematic in Figure 2.8, most of studies focus on the overall performance combined with the cost performance of the power plants integrated with carbon capture process. Few of them considered the $CO_2$ transport section and geologic storage section.

In the study from Rao and Rubin (2002), $CO_2$ dense phase pipeline transport and geologic storage was taken into account in the integrate system of power plants and MEA-based PCC process. It is found that the design assumptions for all sections of whole CCS chain significantly affect the cost of $CO_2$ avoided. For the optimal operation of capture process with power plant, Rao and Rubin (2005) found that the relationship between the cost and carbon capture level is non-linear and venting a fraction of flue gas to keep low capture level less than 75% could achieve a significant cost saving.

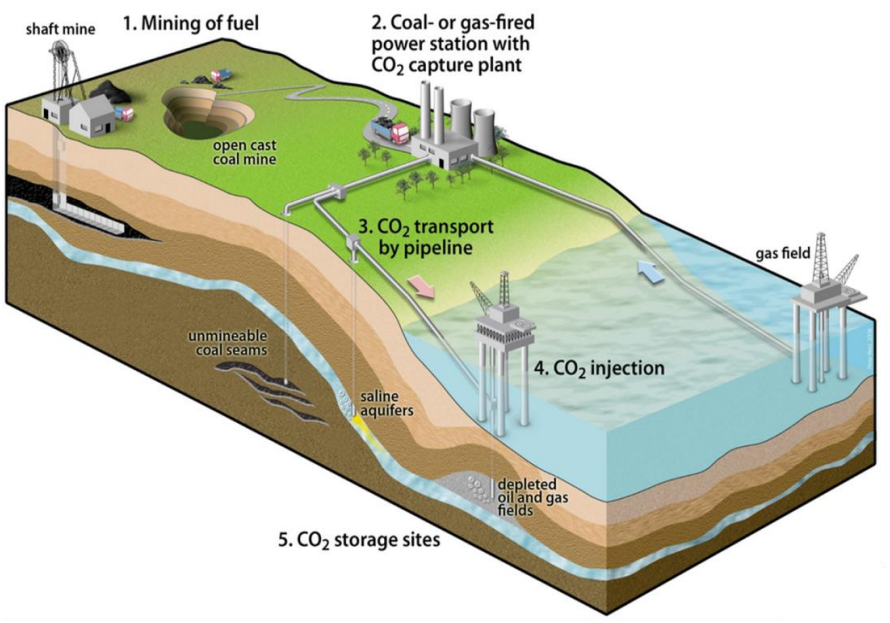


Figure 2.8 Schematic of a full CCS chain (SCCS, 2016)

Mores et al. (2012) found that the total annual cost of carbon capture plant varies linearly for carbon capture level within a range of 70–80% but it increases exponentially when carbon capture level increases from 80% to 95%. Cohen at al. (2012) investigated the economic benefits of a 500 $MW_e$ coal-fired power plant with $CO_2$ capture for a carbon pricing from 0 to 200 US$/ton $CO_2$ and concluded that $CO_2$ capture investment is unjustifiable at low $CO_2$ prices. In the study by Mac Dowell and Shah (2013), optimal $CO_2$ capture level is 95% for £30/ton $CO_2$ and £90/MWh scenario and is around 70% for £8/ton $CO_2$ and £55/MWh scenario for a 660 $MW_e$ coal fired power plant integrated with a capture plant. Their result shows that carbon price should be more than £40/ton $CO_2$ to justify the total cost of carbon capture for an objective of capture level greater than 90% without considering the costs of $CO_2$ compression, transport and storage.

## 2.6 Concluding remarks

From the above literature review, several research gaps have been identified towards the readiness of solvent-based PCC process for commercial deployment for power plants.

Firstly, most of the studies (Abu-Zahra et al., 2007b; Kvamsdal et al., 2011b; Lawal et al., 2012; Mac Dowell and Shah, 2013) on solvent-based PCC process were carried out in the context of coal-fired power plants and only a few papers (Kvamsdal et al., 2010;

Mores et al., 2014; Canepa et al., 2013) focus on its application for NGCC power plants. Compared to coal-fired power plants, $CO_2$ concentration in the flue gas is much lower for a gas fired power plant which causes some significantly different features in terms of the economic performance such as bigger equipment size and lower L/G ratio. Thus the research outputs of carbon capture for a coal-fired power plant may not be applied directly to NGCC power plant.

Secondly, in current studies on solvent-based PCC process for gas-fired power plants, the optimal ranges are very large for key equipment design features (such as diameters and packing heights of the absorber and the stripper) and key operational variables (such as lean loading and L/G ratio). For example, the packing height varies from 13.6 m (Kvamsdal et al., 2010) to 30.6 m (Mores et al., 2014) for the absorber and from 7.6 m (Kvamsdal et al., 2010) to 28.15m (Agbonghae et al., 2014) for the stripper for similar capture tasks, which has large impact to the capital cost. The optimal lean loading range is equally wide from 0.132 mol $CO_2$/mol MEA (Sipöcz and Tobiesen, 2012) to 0.234 mol $CO_2$/mol MEA (Biliyok et al., 2013) with corresponding specific duty at a range of 3.77–4.35GJ/ton $CO_2$. The significant inconsistencies in the literature cause confusions for future researches in this field. It also may cause some troubles for feasibility studies of industrial design of solvent-based PCC process.

Finally, most of current studies focused on the solvent-based PCC process itself, and some of them explored the integration of the power plants with PCC process. Few of them considered the optimal design and operation of the power plants integrated whole CCS chain. In fact, $CO_2$ transport and storage sections are strongly linked with carbon capture process via entry requirements of temperature, pressure and purities for $CO_2$ stream. Their capacity and costs significantly influence the optimal design and operation of carbon capture for power plants.

The main reasons for above gaps may be related to the conflicts between the complexity of the integrated system and the accuracy requirement for both technical and economic performance prediction of the modeling and simulation studies. It could be analysed as follows. (1) The models were relatively simple in some early publications. The papers published by Abu-Zahra et al. (Abu-Zahra et al., 2007b; Abu-Zahra et al., 2007a) are two of most cited papers in this field but the equilibrium models were used for both the

mass transfer and reaction in the absorber and the stripper. (2) Impropriate correlations were wrongly used in the models. Several publications (Agbonghae et al., 2014; Lawal et al., 2012; AspenTech, 2008b) were found that using Bravo et al. (1985) correlation for Mellapak 250 X/Y and Flexipak. Actually, Brava et al. (1985) correlation was obtained for wire gauze structured packing whilst Mellapak 250 X/Y and Flexipak$^{TM}$ are metal sheet structured packing. There are obvious differences between gauze structured packing and sheet structured packing in terms of the hydraulic performance such as effective wetted area, liquid hold-up and pressure drop (Sulzer, 2015; Koch-Glitsch, 2015). (3) Lacking of engineering experience caused some unrealistic designs, especially for the studies towards industrial applications. For large-diameter absorption column, structured packing is preferred considering serious maldistribution of both liquid and vapour phase inside random packing bed (Hoek, 1983; Harriott, 1989). But in some papers (Mores et al., 2014; Canepa and Wang, 2015), random packing was chosen for the absorber and the stripper with the diameters larger than 10 m. Low absorption efficiency of random packing required higher packing height which resulting higher CAPEX cost. Because of the above reasons, those designs may be suboptimal.

The new studies should be carried out by carefully checking most updated correlations for the models, such as new correlations (Yan and Chen, 2010) for Henry's constant of $CO_2$-$H_2O$ for thermodynamic model and new reaction kinetics (Zhang and Chen, 2013) in rate-based model. The models should be validated with updated experimental data (Aronu et al., 2011; Han et al., 2012; Notz et al., 2012) to ensure the predictions accuracy. On the other hand, detailed design with vender quotes for the solvent-based PCC process (IEAGHG, 2010; IEAGHG, 2012) provided a solid base for developing accurate cost model, rather than using empirical correlations developed on the basis of historical cost data. By implementing non-linear optimization programming based on the above process model and cost model, the study on optimal design and operation for solvent-based PCC process as well as the integrated system could be expected to be more realistic to support the decision making for the commercial deployment at the industrial scale.

# Chapter 3: Model Development of Solvent-based PCC Process

This chapter presents the model development and validation of PCC process. Section 3.1 analysed the framework of modelling of a PCC based on chemical absorption process. In Section 3.2, correlations of thermodynamic modelling were examined and validated against the experimental data of $CO_2$ solubility. In Section3.3 calculation methods of main physical properties were examined. In Section 3.4, a rate-based steady state process model was developed and validated with experimental data from a continual operation pilot plant. In Section 3.5 , the process model was scaled up to match the capacity requirement for carbon capture from a 453$MW_e$ NGCC power plant. The process model developed and validated in this chapter provides a solid base for the optimisation studies in Chapter 4, 5, 7.

## 3.1 Framework of modelling of solvent-based PCC process

Using amine solvent to absorb $CO_2$ from exhaust gases is a reactive absorption process involving electrolyte aqueous solvent (Rochelle, 2009). The numerical modelling of such a non-ideal multi-components system is a systematic work in different levels. Figure 3.1 outlines the framework of modelling of such a PCC process. Although the software package Aspen Plus® was used for the modelling and simulation of the process, it is important to check the calculation methods with their corrections in order to ensure the accuracy of process simulation and optimisation.

Accurate calculating of physical properties of pure components and mixtures is one of the basic prerequisites in process modelling and simulation. As the first step, the thermodynamic model should be developed to present vapour-liquid phase equilibrium (VLE) and to calculate the state parameters of the MEA-$H_2O$-$CO_2$ mixture, such as temperature, pressure and composition of the liquid and vapour phase. The solubility of $CO_2$ in MEA-$H_2O$-$CO_2$ mixture is one key parameter and is normally used for validation purpose for the correlations calibration or selection for VLE calculation. The acid gas solubility in aqueous amines solutions is determined by both its physical phase equilibrium and the chemical equilibrium for the aqueous phase reactions among acid gas, water and amines (Zhang et al., 2011).

For the simulation of solvent-based PCC process, the absorption and desorption in the packed columns are the key processes. Rate-based model offers better accuracy than equilibrium model for absorption efficiency and costs of the columns. This accuracy is a function of the appropriate correlations used for liquid and vapour phase mass transfer coefficients, the effective gas-liquid interfacial area and the pressure drop in rate-based model (Agbonghae et al., 2014).

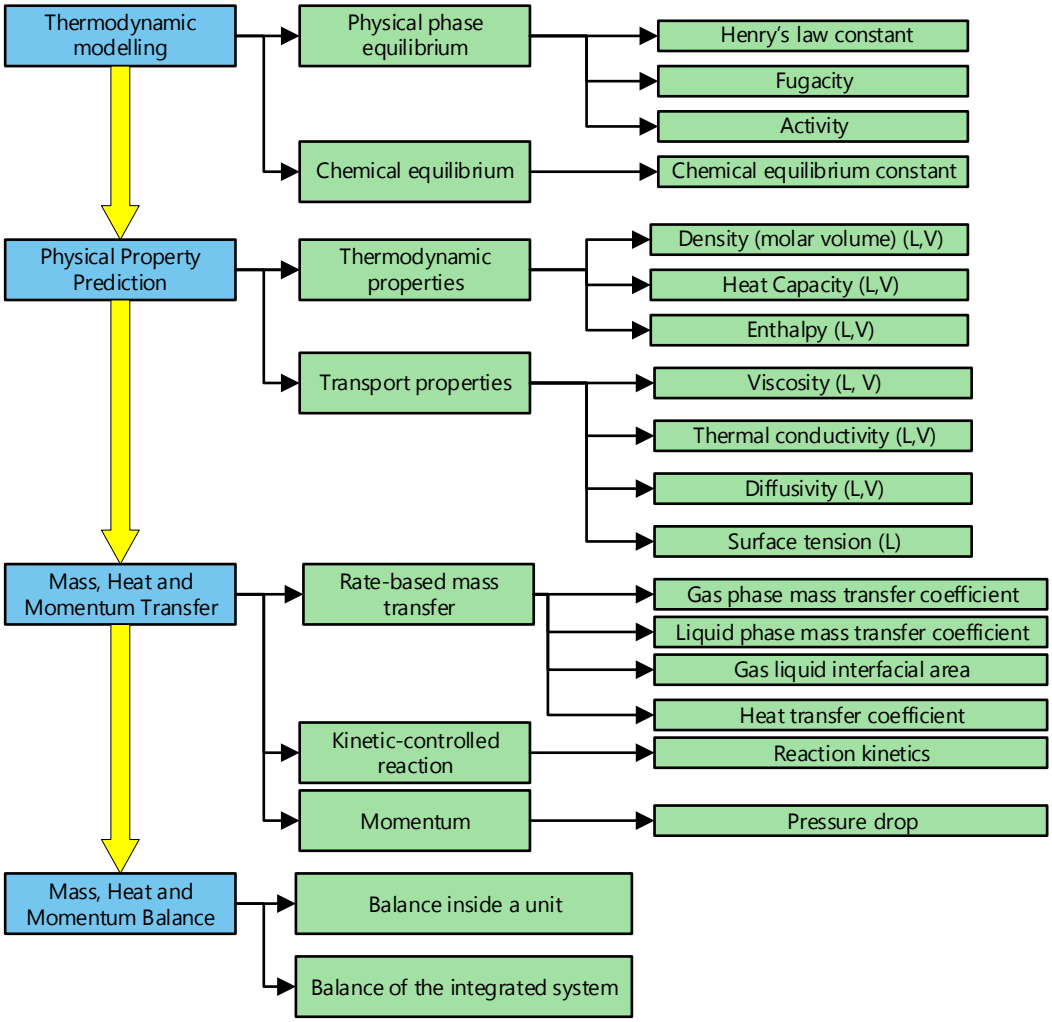


Figure 3.1 Framework of modelling of a solvent-based PCC process

## 3.2 Thermodynamic modelling of MEA-$H_2O$-$CO_2$ system

### *3.2.1 EOSs and relevant model parameters*

The selection of appropriate property methods is crucial to ensure the accuracy of the modelling and simulation. In this chapter, the eNRTL (Song and Chen, 2009; Chen and Evans, 1986; Chen et al., 1982) is used to model the electrolyte system of MEA-$H_2O$-

$CO_2$ mixture and the PC-SAFT EOS (Gross and Sadowski, 2001; Gross and Sadowski, 2002) is used to calculate the properties of vapour phase.

#### 3.2.1.1 PC-SAFT EOS for vapour phase

Compared with some typical cubic EOS such as PR and SRK, PC-SAFT EOS is able to accurately estimate vapour phase fugacity coefficients at high pressures(Zhang and Chen, 2011; Zhang et al., 2011), which is an important advantage for accurate performance predictions of $CO_2$ compression section. The PC-SAFT parameters of pure components were summarized in Table 3.1. The PC-SAFT pure component parameters for $H_2O$ and $CO_2$ are taken from Gross and Sadowski (2002) and Aspen Databank (AspenTech, 2012b). The parameters of MEA are obtained from Zhang's regression work (Zhang et al., 2011). Table 3.2 listed the PC-SAFT binary interaction parameters of the binary pairs.

Table 3.1 PC-SAFT parameters of pure components

| Component | $H_2O$ | $CO_2$ | MEA |
|---|---|---|---|
| Source | Gross and Sadowski (2002) | Aspen Databank (2012b) | Zhang et al. (2011) |
| segment number parameter, $m$ | 1.0656 | 2.5692 | 2.9029 |
| segment energy parameter, $\varepsilon$ | 366.51 | 152.1 | 306.2 |
| segment size parameter, $\sigma$ | 3.0007 | 2.5637 | 3.1067 |
| association energy parameter, $\varepsilon^{AB}$ | 2500.7 | 0 | 2369 |
| association energy parameter, $K^{AB}$ | 0.034868 | 0 | 0.01903 |

Table 3.2 Binary parameters for PC-SAFT EOS

| Component pair | MEA-$H_2O$ | $CO_2$-$H_2O$ |
|---|---|---|
| Source | Fakouri Baygi and Pahlavanzadeh (2015) | Yan and Chen (2010) |
| kij C | −0.052 | 0 |

#### 3.2.1.2 Electrolyte-NRTL for liquid phase

The liquid phase of MEA-$H_2O$-$CO_2$ mixture is a typical electrolyte solution (Austgen et al., 1989). The eNRTL method was validated and used for modelling of electrolyte solution in many publications (Austgen et al., 1989; Liu et al., 1999; Zhang et al., 2009; Zhang et al., 2011; Zhang and Chen, 2013).

Table 3.3 summarized the model parameters and their sources for this study. Most of the parameters were obtained from Aspen Databank (2012b). Some of them were updated by recent studies either by regression using new experimental data (Yan and Chen, 2010; Mangalapally and Hasse, 2011). Because of the large numbers, the values of the parameters were not listed in this thesis but can be obtained from the references.

Table 3.3 Model parameters for eNRTL

| Model parameters | Component | Source |
|---|---|---|
| Antoine equation parameters | $MEA$ | AspenTech (2012b) |
| $\Delta_{vap}H$ | $MEA$ | AspenTech (2012b) |
| Dielectric constant | $MEA$ | AspenTech (2012b) |
| NRTL binary parameters | $CO_2 - H_2O$ binary | Yan and Chen (2010) |
| | $MEA$ -$H_2O$ binary | Zhang et al. (2011) |
| | Molecule-electrolyte binaries | Zhang et al. (2011) |
| $\Delta_f G^{ig}_{298.15}$, $\Delta_f H^{ig}_{298.15}$, $C_p^{ig}$ | $H_2O$, $MEA$, $CO_2$ | AspenTech (2012b) |
| $\Delta_f G^{\infty,aq}_{298.15}$, $\Delta_f H^{\infty,aq}_{298.15}$ | $H_3O^+$, $HCO_3^-$, $CO_3^{2-}$, $OH^-$ | AspenTech (2012b) |
| | $MEAH^+$, $MEACOO^-$ | Zhang et al. (2011) |
| $C_p^{\infty,aq}$ | $H_3O^+$, $OH^-$ | AspenTech (2012b) |
| | $HCO_3^-$, $CO_3^{2-}$ | Zhang and Chen (2011) |
| | $MEAH^+$, $MEACOO^-$ | Zhang et al. (2011) |

### *3.2.2 Physical solubility and Henry's constant*

Physical solubility is the equilibrium between $CO_2$ molecules in vapour phase and in the liquid solutions, which is calculated by Henry's law, as Equation (3.1):

$$P \cdot y_{CO_2} \cdot \emptyset_{CO_2} = H_{CO_2} \cdot x_{CO_2} \cdot {y^*}_{CO_2} \qquad (3.1)$$

where P is the system pressure, $y_{CO_2}$ is the $CO_2$ mole fraction in vapour phase, $\emptyset_{CO_2}$ is the $CO_2$ fugacity coefficient in vapour phase which is calculated using the Redlich-

Kwong equation of state as modified by Soave (1972). $H_{CO_2}$ is the Henry's law constant of $CO_2$ in aqueous amine solution, $x_{CO_2}$ is the $CO_2$ mole fraction in liquid phase, $y^*_{CO_2}$ is the activity coefficient of $CO_2$ in aqueous amine solution.

The Henry's constant of the mixture ( $H_i$ ) can be calculated from the binary Henry's constants of pure solvents in Equation (3.2):

$$ln\left(\frac{H_i}{\gamma_i^{\infty}}\right) = \sum_A w_A \; ln\left(\frac{H_{iA}}{\gamma_{iA}^{\infty}}\right) \tag{3.2}$$

where $H_{iA}$ is the Henry's constant for binary pairs (i.e., $CO_2$-$H_2O$, $CO_2$-MEA), $\gamma_i^{\infty}$ is the infinite dilution activity coefficient of molecular solute $i$ in the mixed solvent, $\gamma_{iA}^{\infty}$ is the infinite dilution activity coefficient of molecular solute $i$ in pure solvent $A$. Weighting factor $w_A$ is calculated by Equation (3.3).

$$w_A = \frac{x_A (V_{iA}^{\infty})^{2/3}}{\sum_B x_B \, (V_{iB}^{\infty})^{2/3}} \tag{3.3}$$

where $x_A$ is the mole fraction of solvent $A$ on solute-free basis, $V_{iA}^{\infty}$ is the partial molar volume of molecular solute $i$ at infinite dilution in pure solvent $A$ and its detailed calculation method could refer to Brelvi-O'Connell model (1972).

The Henry's law constants for $CO_2$ with water and with MEA are required. They can be calculated by Equation (3.4).

$$ln(H_{i-j}) = C_1 + \frac{C_2}{T} + C_3 lnT + C_4 T \tag{3.4}$$

where $H_{i-s}$ is the binary Henry's constant between pure component $i$ and $j$, $T$ is system temperature, $C_1, C_2, C_3, C_4$ are correlations for Henry's constants. The available binary Henry's constants of MEA-$H_2O$-$CO_2$ mixture were summarized in Table 3.4. In the system of MEA-$H_2O$-$CO_2$ mixture, most of publications only take gases components such as $CO_2$, $N_2$ as Henry component. Most studies only considered Henry's constants for $CO_2$ with $H_2O$ in their study (Austgen et al., 1989). The Henry's law constants for $CO_2$ with $H_2O$ have been well studied by Yan and Chen (2010) by examining extensive amounts of experimental VLE data for the $CO_2$-$H_2O$ binary system. Recent studies (Liu

et al., 1999) considered Henry's constants for $CO_2$ with MEA. Normally, MEA is assumed to be mutual solution with $H_2O$ so MEA is not considered as a Henry component. One recent study (Wagner et al., 2013) regressed the Henry's constants correlations of MEA-$H_2O$ then MEA solvent loss in the process could be more accurately estimated. But their study used Pitzer equation for electrolyte system, not like eNRTL used in this thesis.

Table 3.4 Correlations for the calculation of Henry's constants (on the Molality Scale)

| Binary pairs | $CO_2$-$H_2O$ | $CO_2$-MEA |
|---|---|---|
| Unit | Pa | Pa |
| Source | Yan and Chen (2010) | Liu et al. (1999) |
| $C_1$ | 100.650 | 89.452 |
| $C_2$ | −6147.7 | −2934.6 |
| $C_3$ | −10.191 | −11.592 |
| $C_4$ | 0 | 0.01644 |
| T (°C) | 273 – 473 | 280 – 600 |

### *3.2.3 Chemical reaction equilibrium*

Aqueous phase chemical reactions involved in the MEA-$H_2O$-$CO_2$ system can be expressed as follows:

R1: water dissociation

$$2H_2O \leftrightarrow H_3O^+ + OH^- \tag{3.5}$$

R2: Dissociation of $CO_2$

$$CO_2 + 2H_2O \leftrightarrow H_3O^+ + HCO_3^- \tag{3.6}$$

R3: Dissociation of carbonate

$$HCO_3^- + H_2O \leftrightarrow H_3O^+ + CO_3^{2-} \tag{3.7}$$

R4: Dissociation of the protonated amine

$$MEAH^+ + H_2O \leftrightarrow H_3O^+ + \text{MEA} \tag{3.8}$$

R5: Carbonate formation

$$MEACOO^- + H_2O \leftrightarrow H\text{CO}_3^- + \text{MEA} \tag{3.9}$$

Chemical equilibrium constants of those reactions are calculated by Equation (2.1) and the related correlations can be seen in Table 3.5. Once the chemical equilibrium constants are determined, the chemical equilibrium of each reaction is determined by Equation (3.10) (Austgen et al., 1989).

$$K_{Rj} = \left[\frac{\prod_{reactant,i}(x_i\gamma_i)^{\nu^i}}{\prod_{product,j}(x_j\gamma_j)^{\nu^j}}\right] \tag{3.10}$$

Table 3.5 Correlations for chemical equilibrium constants (on the Molality Scale)

| Reaction | $C_1$ | $C_2$ | $C_3$ | $C_4$ | T (°C) | Source |
|---|---|---|---|---|---|---|
| R1 | 132.899 | −13445.90 | −22.4773 | 0 | 0–225 | Edwards et al. (1978) |
| R2 | 231.465 | −12092.10 | −36.7816 | 0 | 0–225 | Edwards et al. (1978) |
| R3 | 216.049 | −12431.70 | −35.4819 | 0 | 0–225 | Edwards et al. (1978) |
| R4 | −4.9074 | −6166.12 | 0 | −0.00098482 | 0–50 | Bates and Pinching (1951) |
| R5 | 2.8898 | −3635.09 | 0 | 0 | 25–120 | Austgen et al. (1989) |

### *3.2.4 Validation of $CO_2$ solubility prediction*

#### 3.2.4.1 Case setups

In order to compare and select out appropriate correlations for this study, several correlation combinations (Austgen et al., 1989; Liu et al., 1999; Zhang et al., 2011) were chosen for carrying out the validation against the experimental data. The model details can be seen in Table 3.6.

Table 3.6 Different combinations of correlations for validation

| Combinations of correlations | This study | Zhang et al. (2011) | Liu et al. (1999) | Austgen et al. (1989) |
|---|---|---|---|---|
| EOS for vapour | PC-SAFT | PC-SAFT | SRK | SRK |
| EOS for liquid | eNRTL | eNRTL | eNRTL | eNRTL |
| Dielectric Constants | Zhang et al. (2011) | Zhang et al. (2011) | – | Ikada et al. (1968) |
| NRTL binary | Zhang et al. (2011) | Zhang et al. (2011) | Liu et al. (1999) | Austgen et al. (1989) |
| Electronic–pair | Zhang et al. (2011) | Zhang et al. (2011) | Liu et al. (1999) | Austgen et al. (1989) |
| Henry's Constants $CO_2$ in $H_2O$ | Yan and Chen (2010) | Yan and Chen (2010) | Chen et al. (1979) | Chen et al. (1979) |
| Henry's Constants $CO_2$ in MEA | Liu et al. (1999) | Zhang et al.(2011) | Liu et al. (1999) | – |
| Chemical equilibrium constants | Liu et al. (1999) | Zhang et al. (2011) | Liu et al. (1999) | Austgen et al. (1989) |

#### 3.2.4.2 Experimental data

The experimental data of $CO_2$ solubility are normally used for validation of thermodynamic modelling. It is typical VLE validation. $CO_2$ partial pressure and/or total pressure of vapour phase at the different $CO_2$ loading in MEA aqueous solution were compared between model predictions and experimental data.

In this study, the experimental data from Aronu et al. (2011) were chosen for the validation purpose (see Table 3.7) because these data cover a wider range of the MEA concentration than other publications as well as system temperature and pressure.

Table 3.7 Chosen experimental data for solubility of $CO_2$ in MEA aqueous solution

| Source | Temperature ($^oC$) | Pressure (bar) | MEA concentration (wt%) | $CO_2$ loading (mol/mol) |
|---|---|---|---|---|
| Aronu et al. (2011) | 40–120 | 0.001–10.5 | 15, 30, 45, 60 | 0–saturated |

### 3.2.4.3 Validation results

The comparisons of partial pressure of $CO_2$ in the vapour phase of MEA-$H_2O$-$CO_2$ mixture between the model predictions and the experimental data for different concentration MEA could be seen in Figures 3.2–3.9, in which the lines present the model predictions whilst the blocks present the experimental data. The abbreviation representing experimental data in the legends in the figures of is 'Exp'.

Table 3.8 presents the mean absolute percentage error (MAPE) of validation results at the different MEA concentration. Generally, the deviations between experimental data and model predictions become bigger at the lower (15 wt%) and higher (45–60 wt%) MEA concentration, compared with 30 wt% MEA concentration. It also shows that model predictions of this study is more accurate than other three models for MEA concentration range of 15–45 wt% (20–40 wt% MEA concentration used in optimisation study in Chapter 4). It is notice that the model predictions of this study at 15wt% concentration are worse than Liu et al. (1999). The direct reason is that some correlations used in this study inherit from Zhang et al. (2011), which can be seen in Table 3.6. Further, none of these four combinations could have good predictions covering low to high MEA concentrations, which reflects one inherent limitation of correlation method, which is that correlation should not go beyond the conditions of the data for its regression. However, many correlations used for thermodynamic modelling of MEA-$H_2O$-$CO_2$ system were regressed based on the experimental data at the 30% MEA concentrations.

Table 3.8 MAPE of validation with $CO_2$ partial pressure of MEA-$H_2O$-$CO_2$ system

| MAPE (%) | This study | Zhang et al. (2011) | Liu et al. (1999) | Austgen et al. (1989) |
|---|---|---|---|---|
| Abbreviation in the legends in the figures | TS | Zhang | Liu | Austgen |
| 15wt% MEA | 23.86 | 43.33 | 7.97 | 11.06 |
| 30wt% MEA | 7.63 | 6.09 | 6.4 | 8.72 |
| 45wt% MEA | 10.62 | 11.57 | 38.76 | 36.47 |
| 60wt% MEA | 17.97 | 20.86 | 61.9 | 51.56 |
| **15–45wt%** MEA | 14.04 | 20.33 | 17.71 | 18.75 |

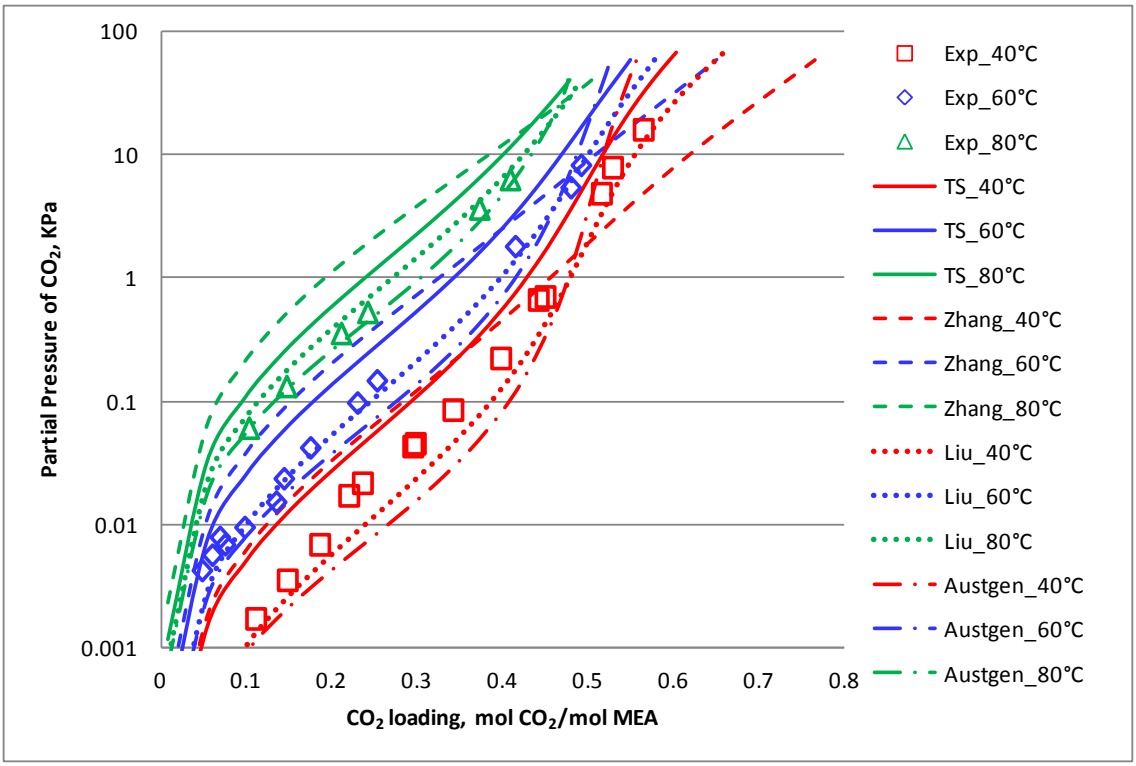


Figure 3.2 $CO_2$ partial pressure as function of $CO_2$ loading with 15 wt% MEA

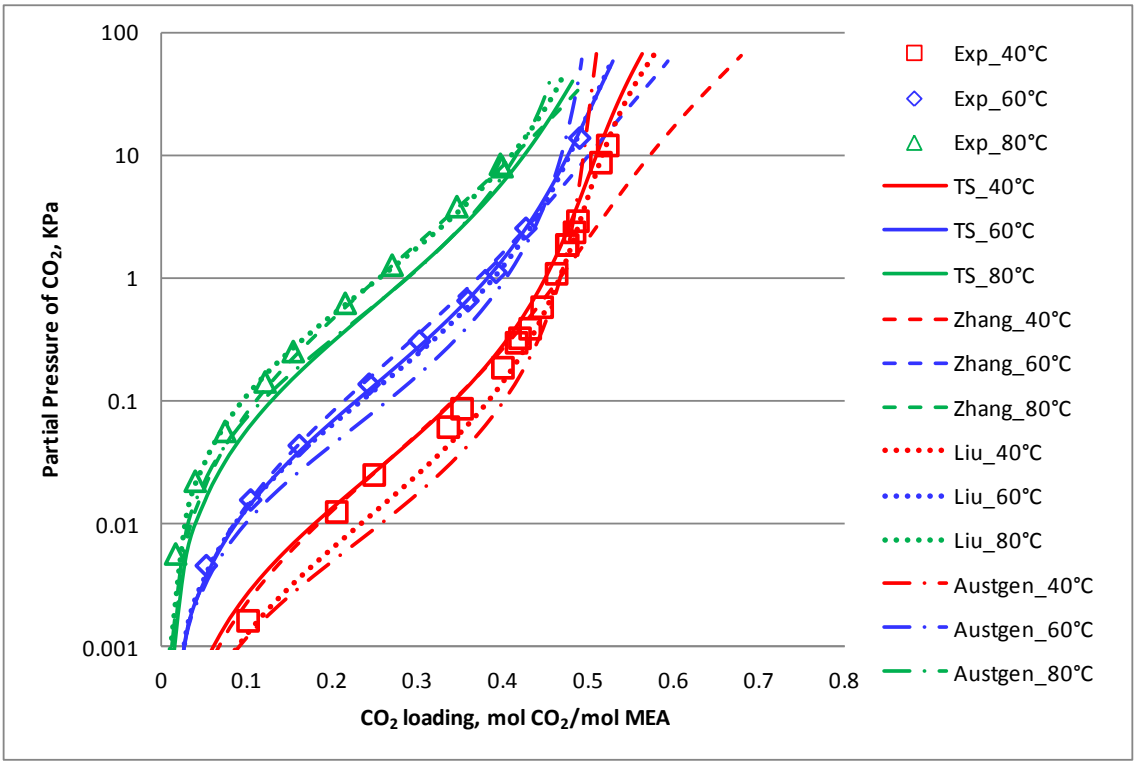


Figure 3.3 $CO_2$ partial pressure as function of $CO_2$ loading with 30 wt% MEA

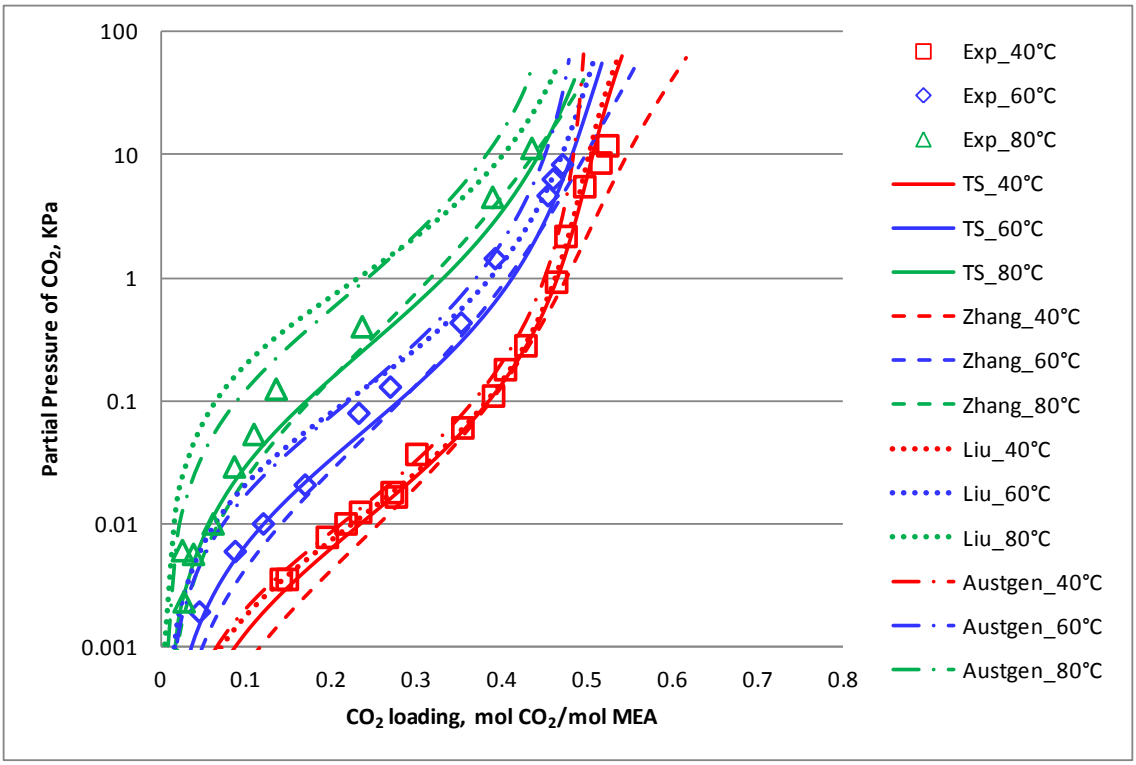


Figure 3.4 $CO_2$ partial pressure as function of $CO_2$ loading with 45 wt% MEA

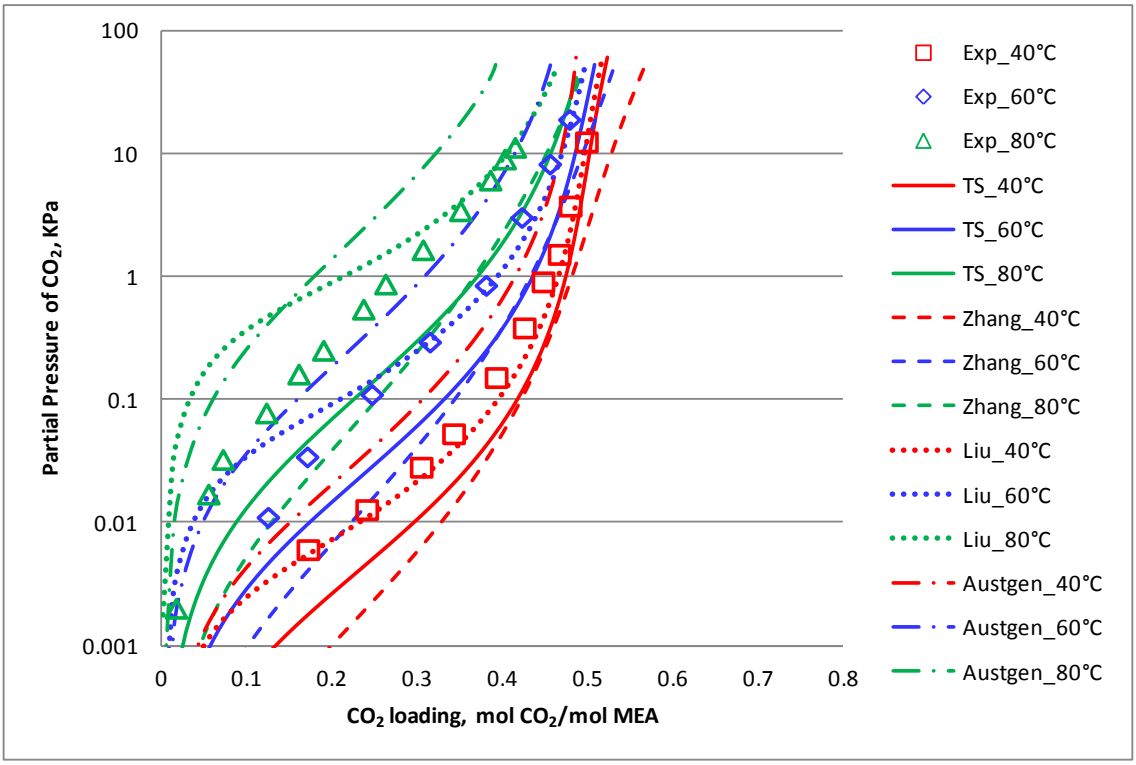


Figure 3.5 $CO_2$ partial pressure as function of $CO_2$ loading with 60 wt% MEA

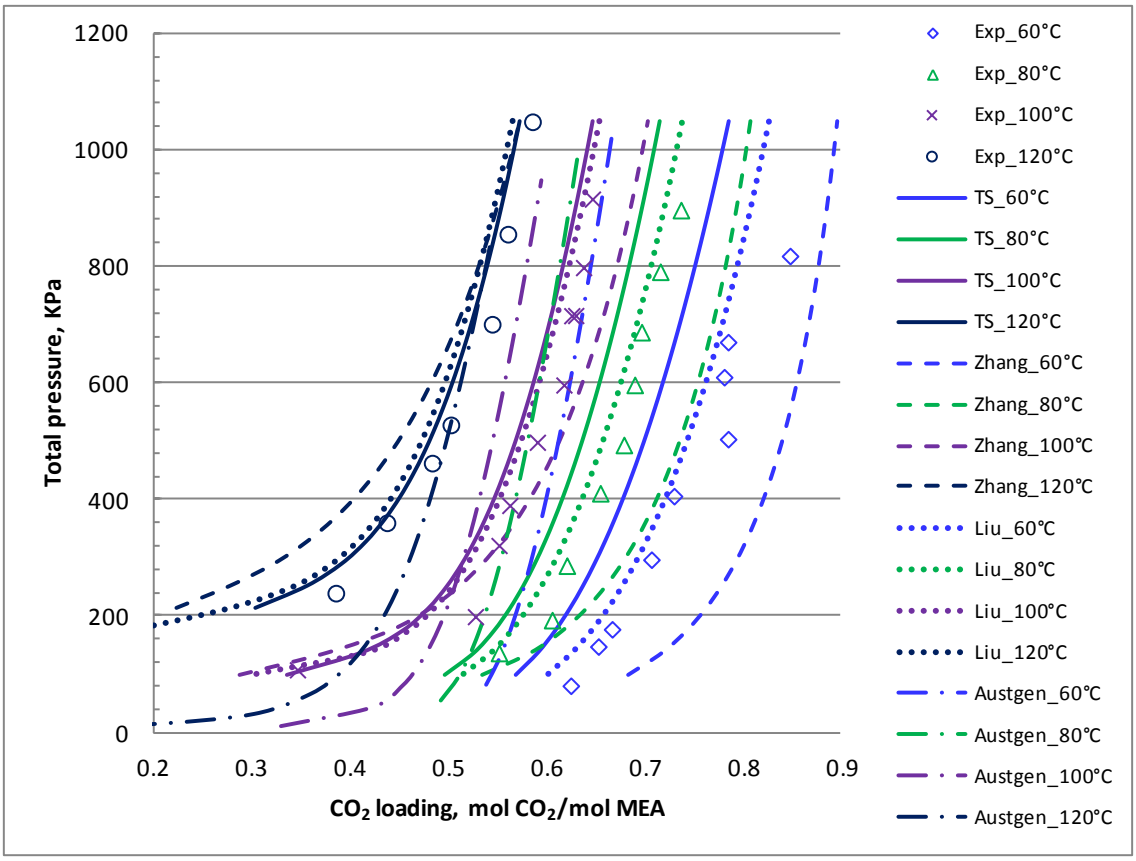


Figure 3.6 Total pressure as function of $CO_2$ loading with 15 wt% MEA solvent

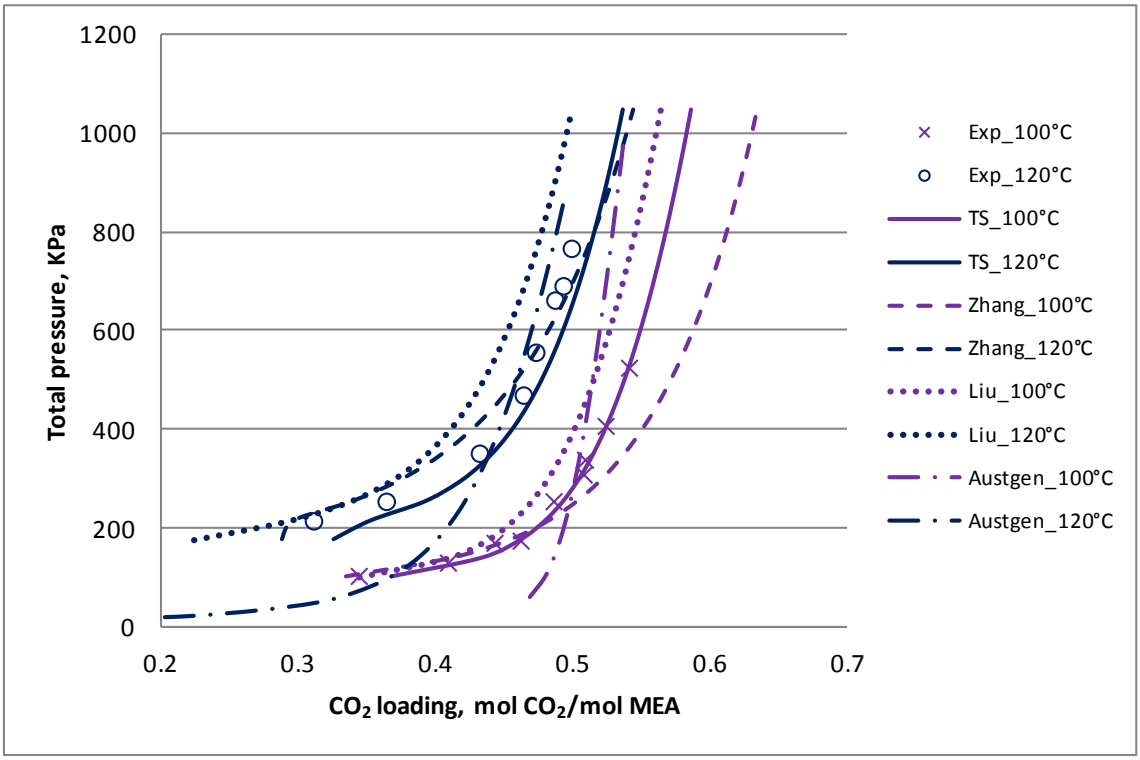


Figure 3.7 Total pressure as function of $CO_2$ loading with 30 wt% MEA solvent

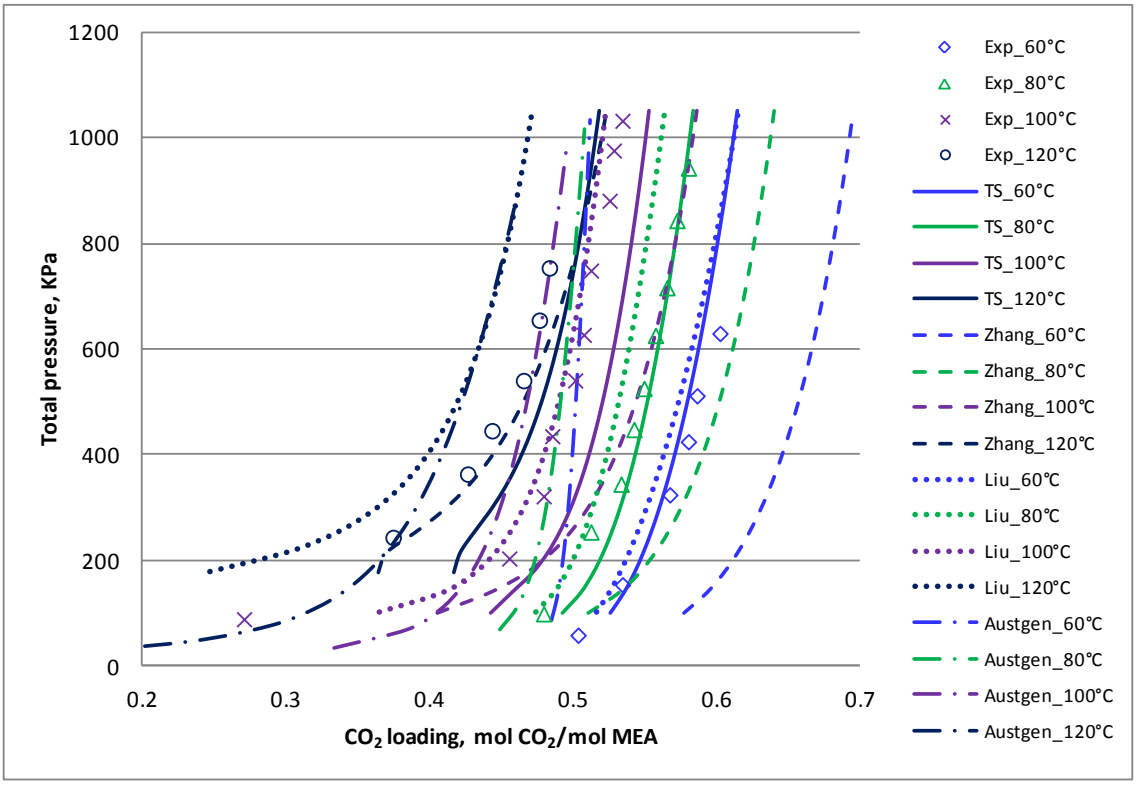


Figure 3.8 Total pressure as function of $CO_2$ loading with 45wt% MEA solvent

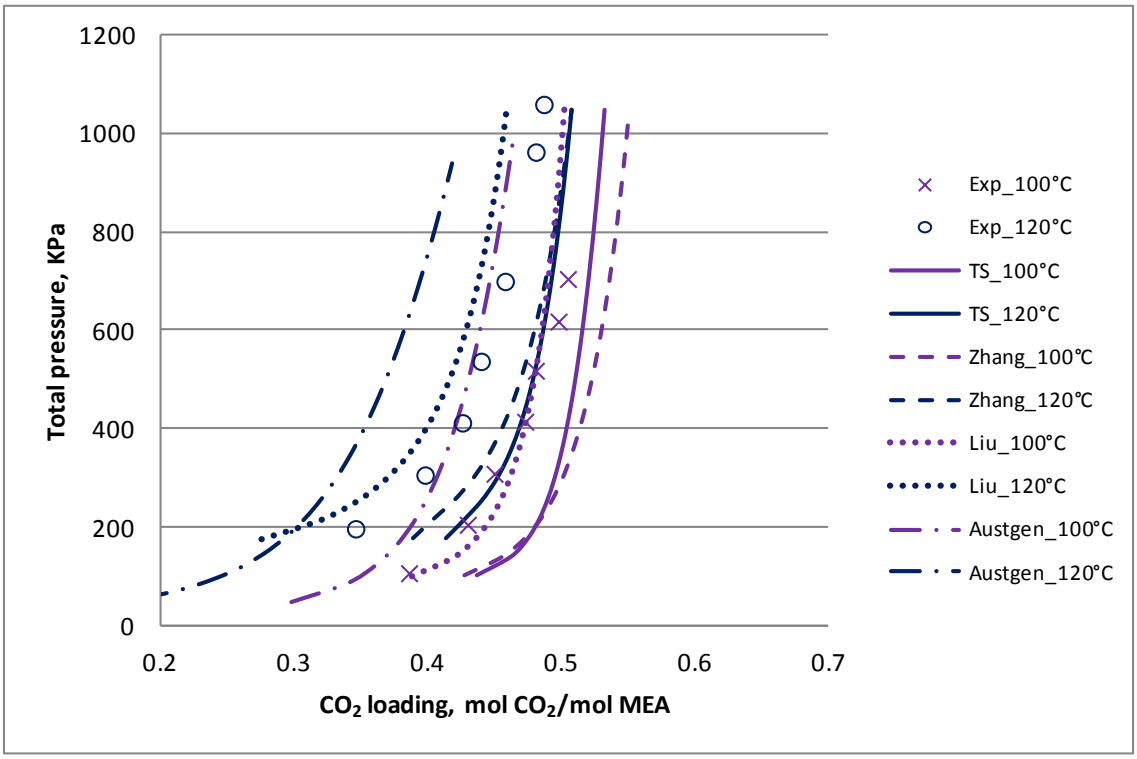


Figure 3.9 Total pressure as function of $CO_2$ loading with 60 wt% MEA solvent

## 3.3 Physical property of MEA-$H_2O$-$CO_2$ system

### *3.3.1 Physical property model*

This study will use rate-based model to simulate the MEA-$H_2O$-$CO_2$ system. Thus it is required to calculate quantitative values of physical properties. Those physical properties are part of the correlations for heat transfer, mass transfer, interfacial area, liquid holdup and pressure drop, etc. It is important to choose the right property models to ensure the success of process modelling and simulation.

The physical properties include (1) thermodynamic properties such as density and heat capacity, (2) transport properties such as viscosity, surface tension, thermal conductivity, and diffusivity. The chosen models for property calculation for mixture in this study were listed in Table 3.9. It should be noticed that the correlations of density of liquid mixture is from Han et al. (2012) by coding Fortran subroutine in Aspen Plus®.

Table 3.9 Correlations used for property calculation of the mixture

| | Property | Phase | Correlation |
|---|---|---|---|
| Thermodynamic Properties | Density | liquid | Han et al. (2012) |
| | | vapor | PC-SAFT |
| | Enthalpy | liquid | eNRTL |
| | | vapor | PC-SAFT |
| | Heat capacity | liquid | Calculated from Enthalpy |
| | | vapor | Calculated from Enthalpy |
| Transport Properties | Viscosity | liquid | Jones-Dole model |
| | | vapor | Chapman-Enskog-Brokaw |
| | Diffusivity | liquid (molecule) | Wilke-Chang |
| | | liquid (ion) | Nernst-Hartly |
| | | vapor | Dawsom-Khoury-Kobayashi |
| | Thermal conductivity | liquid | Sato-Reidel |
| | | vapor | Stiel-Thodos |
| | Surface tension | Liquid | Hakim-Steinberg-Stiel |

### 3.3.2 Available experimental data for validation

The available literature experimental data of physical properties validation of MEA-$H_2O$-$CO_2$ can be seen in Table 3.10. The vapour phase of MEA-$H_2O$-$CO_2$ mixture under operating temperature (20–150$^oC$) and pressure (1–2 bar) of the absorber and stripper is not an issue so there is no available experimental data for those properties of vapour phase. Available experimental data for the thermal conductivity of liquid phase were not found currently. Further, direct measurement of $CO_2$ diffusivity in MEA aqueous solution is impossible because $CO_2$ reacts with MEA. The $NO_2$ analogy method was used to produce the data of $CO_2$ diffusivity (Ying and Eimer, 2012).

Table 3.10 Available experimental data for physical properties of liquid phase

| Property | Temperature ($^oC$) | MEA concentration (wt%) | $CO_2$ loading (mol/mol) | Source |
|---|---|---|---|---|
| Density | 25–140 | 30,40,50,60 | 0.1–0.6 | Han and Eimer (2012) |
| Heat capacity | 25 | 10,20,30,40 | 0–0.5 | Weiland et al. (1997) |
| Viscosity | 25 | 10,20,30,40 | 0–0.5 | Weiland et al. (1998) |
| Surface tension | 25 | 10,20,30,40 | 0–0.5 | Weiland (1996) |

### 3.3.3 Validation results

The comparisons of different properties of MEA-$H_2O$-$CO_2$ mixture between the model predictions and experimental data for different concentration MEA could be seen in Figure 3.10 – Figure 3.16. In these figures, the lines present the modelling results whilst the blocks present the experimental data. The names for short representing experimental data and model predictions in the legends in the figures of are ‘Exp’ and ‘Model’ respectively.

Table 3.11 presents the deviations of validation results of physical properties. Both MAPE and maximum absolute percentage error (APE) are given. For liquid density (Figure 3.10–Figure 3.13), model predictions are in good agreement with the experimental data in full range of system conditions. For the heat capacity (see Figure 3.14), the deviations gradually increases when $CO_2$ loading rises up. For surface tension, the experimental data themselves have large deviations (see in Figure 3.16).

Table 3.11 MAPE of validation results of physical properties in liquid phase

| Property | Temperature ($^{o}$C) | MEA concentration (wt%) | $CO_2$ loading (mol/mol) | MAPE (%) | Max. APE (%) |
|---|---|---|---|---|---|
| Density | 25–140 | 30, 40, 50, 60 | 0.1–0.6 | 0.348 | 1.48 |
| Heat capacity | 25 | 20, 30, 40 | 0–0.5 | 3.74 | 10.74 |
| Viscosity | 25 | 20, 30, 40 | 0–0.5 | 5.46 | 9.7 |
| Surface tension | 25 | 20, 30, 40 | 0–0.5 | 8.58 | 18.29 |

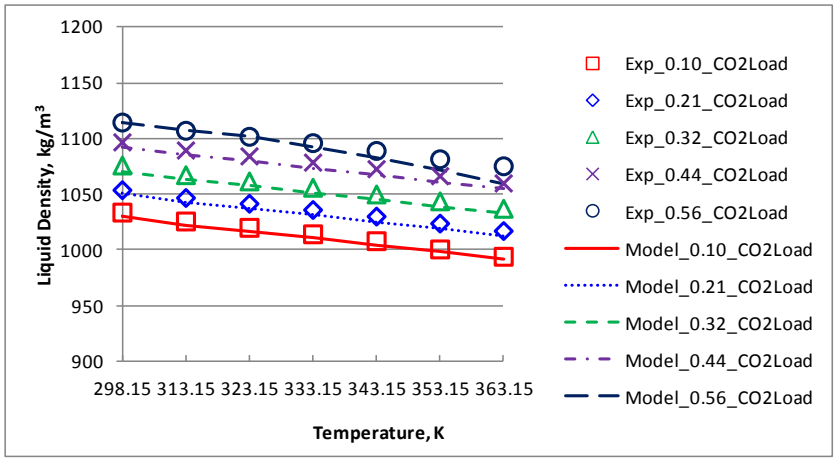


Figure 3.10 Liquid density of MEA-$H_2O$-$CO_2$ at 30 wt% MEA

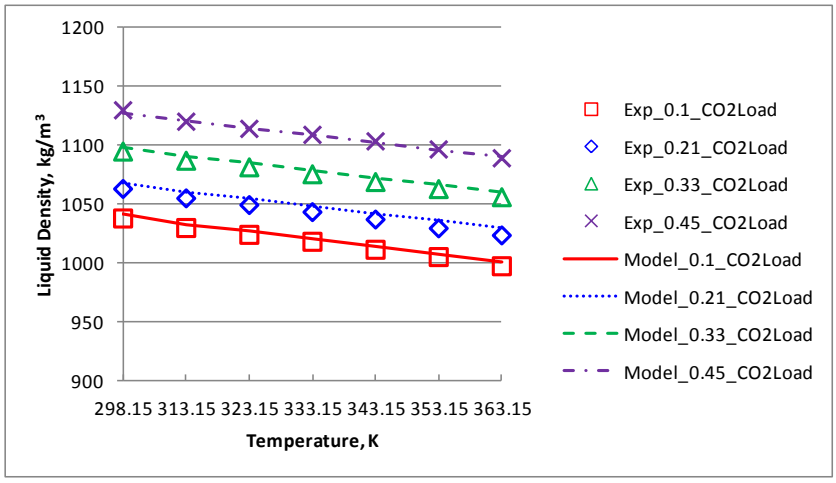


Figure 3.11 Liquid density of MEA-$H_2O$-$CO_2$ at 40 wt% MEA

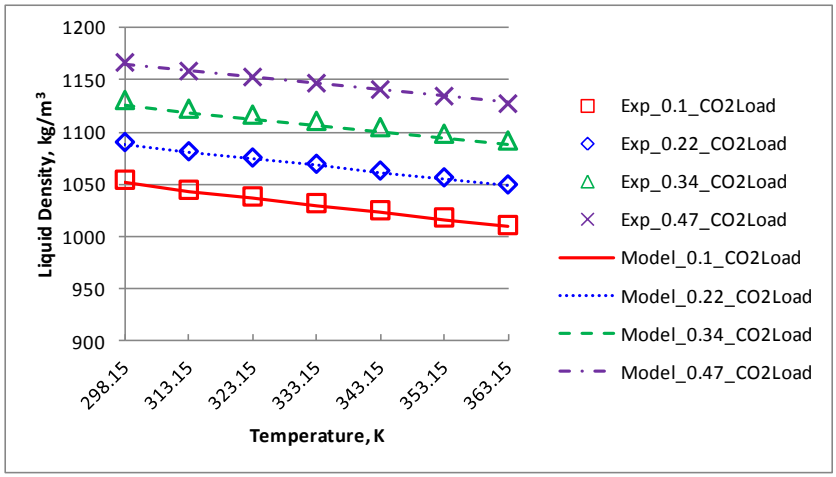


Figure 3.12 Liquid density of MEA-$H_2O$-$CO_2$ at 50 wt% MEA

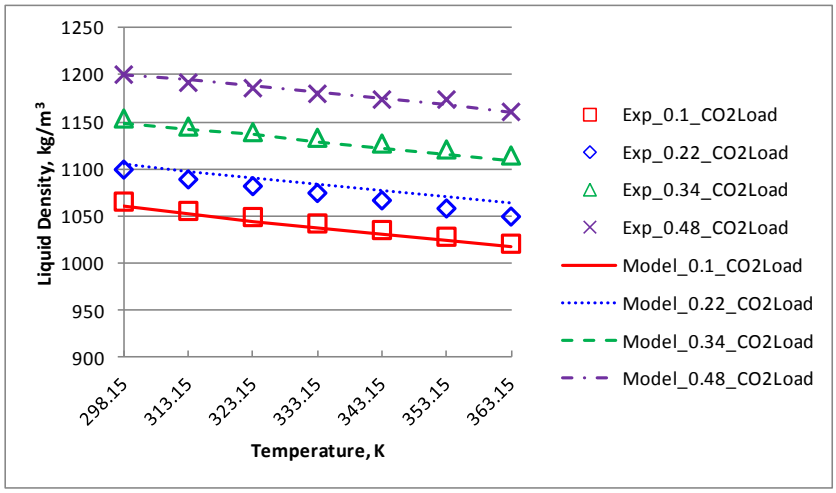


Figure 3.13 Liquid density of MEA-$H_2O$-$CO_2$ at 60wt% MEA

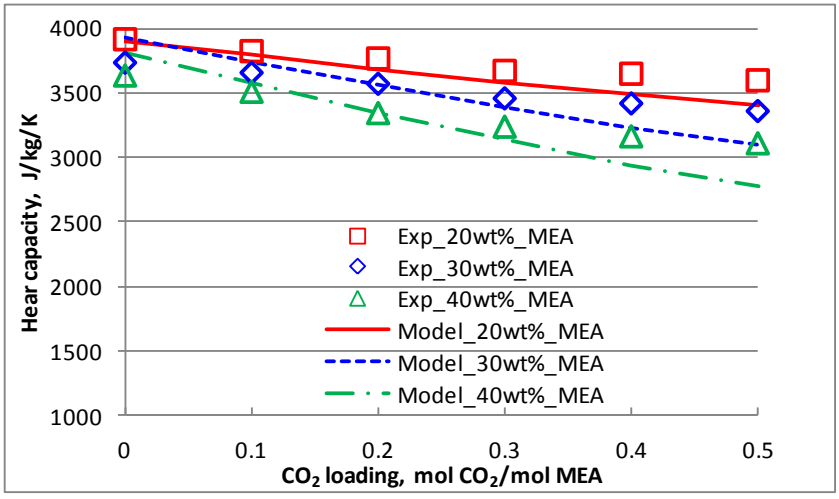


Figure 3.14 Liquid heat capacity of MEA-$H_2O$-$CO_2$ at 298.15K

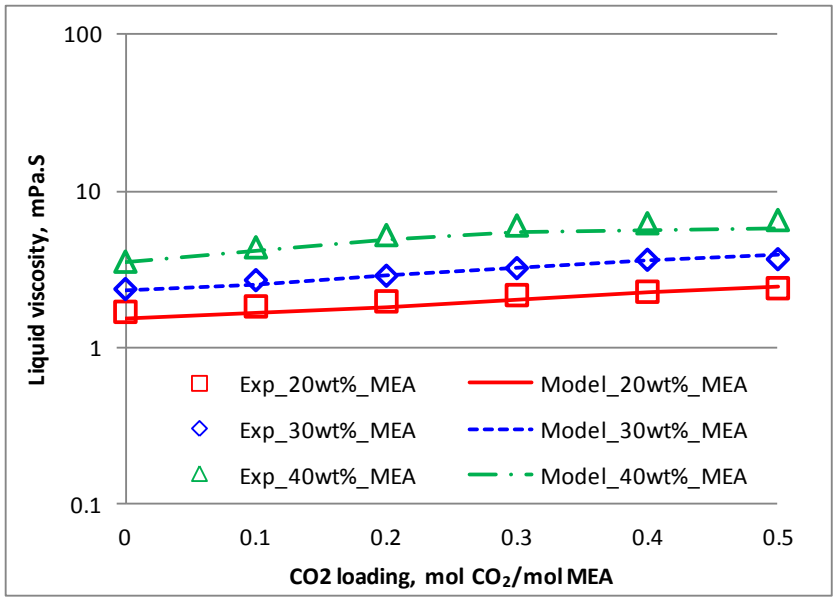


Figure 3.15 Liquid viscosity of MEA-$H_2O$-$CO_2$ at 298.15K

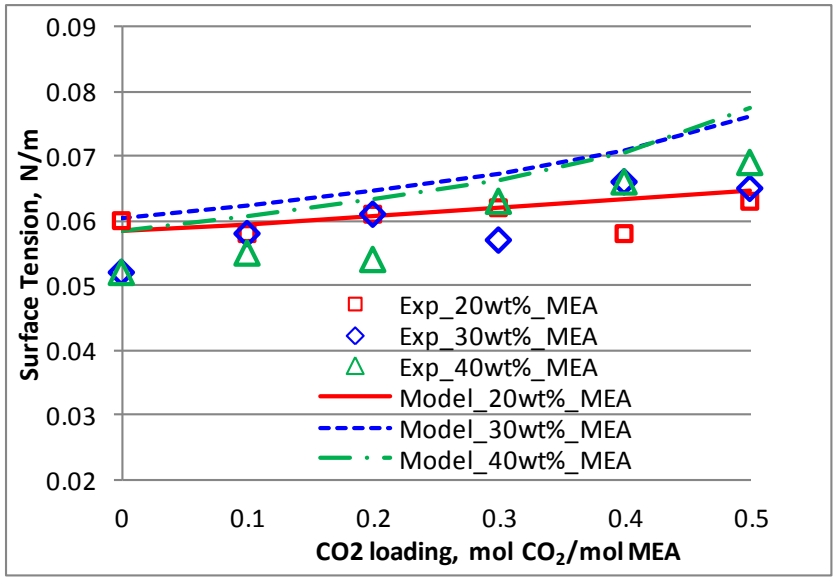


Figure 3.16 Surface tension of MEA-$H_2O$-$CO_2$ at 30 wt% MEA at 298.15K

## 3.4 Process model development and validation at the pilot scale

### *3.4.1 Introduction of the pilot plant*

In this thesis, the pilot plant located at the University of Kaiserslautern (Mangalapally and Hasse, 2011) was chosen for validating the process model. The reasons include (1) both the absorber and the stripper use Mellapak 250Y packing, which is regarded as appropriate structured packing type for industrial deployment (IEAGHG, 2012); (2) the experimental data are comprehensive and well presented in their publications (Notz et al., 2012), which helps the validation more comprehensive and could be compared with other studies (Agbonghae et al., 2014). The equipment features and the ranges of key operation variables are summarized in Table 3.12. More details about this pilot plant refer to the publication by Notz et al. (2012).

Table 3.12 Main specifications of the pilot plant

| | | |
|---|---|---|
| Flue gas source | | Natural gas burner |
| Flue gas flow rate (kg/h) | | 30–100 |
| $CO_2$ concentration in the flue gas (mol %) | | 3–14 |
| Solvent flow rate (kg/h) | | 50–350 |
| $CO_2$ loading in lean solvent (mol $CO_2$/mol MEA) | | 0.1 – 0.32 |
| Temperature of cooling water (°C) | | 5–10 |
| Absorber | Diameter (m) | 0.125 |
| | Height of packing (m) | 4.2 |
| | Packing type | Structured packing Mellapak 250Y |
| | Operating pressure (bar) | Atmospheric pressure |
| | Operating temperature (°C) | 40–70 |
| Stripper | Diameter (m) | 0.125 |
| | Height of packing (m) | 2.52 |
| | Packing type | Structured packing Mellapak 250Y |
| | Operating pressure (bar) | 1–2.5 |
| | Operating temperature (°C) | 100–130 |

### *3.4.2 Process model development*

#### 3.4.2.1 Model flowsheet and process description

Figure 3.17 shows a closed-loop process flowsheet of the model developed in Aspen Plus®. The flue gas leaving the power plant goes to a gas blower to increase its pressure slightly above atmospheric pressure, to balance the pressure losses in the downstream processes. Before entering the absorber, the flue gas has to be cooled down to between 40–50 °C in order to improve the absorption efficiency (Kvamsdal et al., 2011b). The cooling system consists of direct contact cooler (DCC) with a spray of water at 25 °C and with a packing bed also with Mellapak 250Y. The flue gas then enters the absorber, in which MEA aqueous solvent reacts with $CO_2$. The scrubbed flue gas is emitted to the atmosphere and the $CO_2$-rich solvent is discharged from the bottom of the absorber and enters the stripper. The $CO_2$-rich solvent is regenerated inside the stripper with heat input to the reboiler. The regenerated solvent is cooled and recirculated to the absorber for reuse.

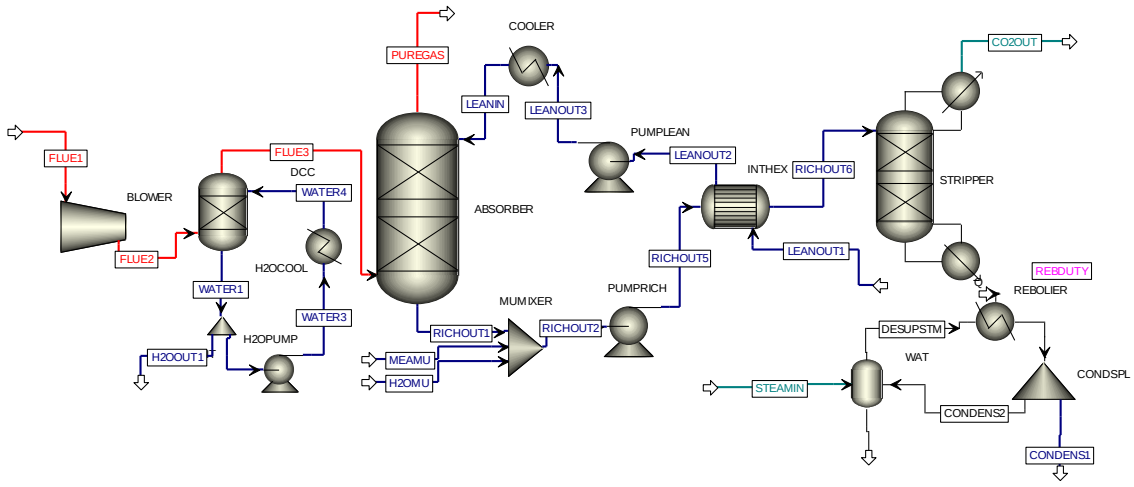


Figure 3.17 Process flowsheet in Aspen Plus®

#### 3.4.2.2 Kinetics-controlled reactions

In Section 3.3, the equilibrium reactions of MEA-$H_2O$-$CO_2$ mixture were described during the thermodynamic modelling. In the rate-based model, the reaction of dissociation of $CO_2$ and reaction of carbonate formation should be considered to be kinetics-controlled reactions (Zhang et al., 2009), presented as below:

R2*: Dissociation of $CO_2$

$$CO_2 + 2H_2O \rightarrow H_3O^+ + HCO_3^- \quad (3.11)$$

$$H_3O^+ + HCO_3^- \rightarrow CO_2 + 2H_2O \quad (3.12)$$

R5*: Carbonate formation

$$MEACOO^- + H_2O \rightarrow HCO_3^- + MEA \quad (3.13)$$

$$HCO_3^- + MEA \rightarrow MEACOO^- + H_2O \quad (3.14)$$

Power law expressions were used for the kinetic-controlled reactions. The kinetics in Equations (3.15) (Zhang et al., 2009) for Reactions R2* and R5* are in Table 3.13.

$$r_j = k_j^o T^n \exp\left(-\frac{E_j}{RT}\right) \prod_{i=1}^{N} C_i^{\alpha_{ij}} \quad (3.15)$$

where $r_j$ is the reaction rate for reaction $j$, $k_j^o$ is the pre-exponential factor, $T$ is the system temperature in K, $n$ is the temperature factor, $E_j$ is the activation energy, $R$ is the gas constant, $C_i$ is the concentration of species $i$, and $\alpha_{ij}$ is the reaction order of component $i$ in reaction $j$. $k_j^o$ and $E_j$ for the reactions were calculated using experimental data shown in Table 3.13.

Table 3.13 Parameters *k* and *E* in Equation (3.15) (Zhang and Chen, 2013)

| Related Species | Reaction direction | $k_j^o$ (kmol/m$^3$.s) | $E_j$ (kJ/mol) |
|---|---|---|---|
| $MEACOO^-$ | Forward | 3.02E+10 | 41.2 |
| | Reverse (absorber) | 5.52E+23 | 69.05 |
| | Reverse (stripper) | 6.56E+27 | 95.24 |
| $HCO^{3-}$ | Forward | 1.33E+17 | 55.38 |
| | Reverse | 6.63E+16 | 107.24 |

#### 3.4.2.3 Rate-based mass transfer

The absorber and the stripper were modelled based on two-film theory (Whitman, 1962), which is used to describe the mass transfer of components between the gas phase and the liquid phase. According to two-file theory, vapour film and liquid film with a phase equilibrium interface are assumed between the bulk gas and bulk liquid phase. Chemical reactions are assumed to occur in the liquid film only.

For the RateSep model in Aspen Plus®, Zhang et al (2009) had very detailed discussions about correlations and settings. In this study, the flow model "VPlug" was chosen to model the bulk properties with reasonable accuracy whilst "Countercurrent" model sometimes causes oscillations in the temperature profile although it is most closely approximates for the real situation (Razi et al., 2013b). It was also pointed out that the discretization points of the liquid film need to be over 10 to achieve accuracy, otherwise it results in an over-prediction of the rate of mass transfer.

For the correlations related with mass transfer, Razi et al. (2013b) validated 12 correlation combinations with the experimental data from CESAR Pilot Data and the results show that Billet and Schultes (1993) is one of accurate correlations provided by Aspen Plus®. The parameters and correlations related with mass transfer used in this study can be seen in Table 3.14. Here Fortran subroutine was used to implement correlation of Tsai et al. (2011) for liquid holdup calculation.

Table 3.14 Parameters and correlations selection for mass transfer in RateSep model

| Parameters | Correlations |
|---|---|
| Flow model | VPlug (Razi et al., 2013b) |
| Film discretization points | 20 (Razi et al., 2013b) |
| Mass transfer coefficients | Billet and Schultes (1993) |
| Interfacial area | Tsai et al. (2011) |
| Liquid holdup | Billet and Schultes (1993) |
| Heat transfer coefficient | Chilton and Colburn (1934) |
| Pressure drop | Sulzer correlation |

### 3.4.3 Model validation

For the PCC process, the key operational parameters affecting the performance are $CO_2$ concentration in the flue gas, MEA concentration in solvents, lean loading and L/G ratio. Thus, four sets of experiments from Notz et al. (2012) were chosen for the model validation purpose. These include (1) experiment 1–6 with different $CO_2$ concentrations in the flue gases; (2) experiment 24–27 with different MEA concentrations at two different $CO_2$ concentrations in the flue gases; (3) experiment 28–33 with different solvent flow rates at the high $CO_2$ concentrations in flue gases; (4) experiment 34–29 with different solvent flow rates at the low $CO_2$ concentrations in flue gases. Model validations were carried out based on the same feed conditions and targeted the $CO_2$ loading in lean solvent (lean loading) by varying the reboiler duty of the stripper. Then $CO_2$ loading in rich solvent (rich loading), $CO_2$ capture level and the stripper reboiler duty could be compared between the experimental data and model predictions.

Table 3.15 shows the overall validation results. MAPEs of the model predictions for the $CO_2$ capture level, the stripper reboiler duty, and the rich $CO_2$ loading, when compared with the experimental data from Notz et al. (2012), are 1.78, 1.54 and 7.49%, respectively. The MAPEs of the rich loading and the $CO_2$ capture level could be acceptable. The specific duty was calculated from the reboiler duty (see Equation (2.5)). However, in the experiments, reboiler duty was affected by the heat loss from the equipment and pipelines, which could not be measured directly. Although the values of specific duty in the publication (Notz et al., 2012) were corrected, the deviations of themselves could not be evaluated, which may be the reason for high APEs for the validation results of the specific duty.

Table 3.15 Validation results of model predictions against experimental data

| Case | Flue gas flow rate (kg/hr) | $CO_2$ content (mol/mol) | L/G (kg/kg) | MEA content (kg/kg) | Lean Loading (mol/mol) | Rich loading(mol $CO_2$/mol MEA) | | | $CO_2$ capture level (%) | | | Specific duty (GJ/ton $CO_2$) | | |
|---|---|---|---|---|---|---|---|---|---|---|---|---|---|---|
| | Exp. | Exp. | Exp. | Exp. | Exp. | Exp. | Model | APE (%) | Exp. | Model | APE (%) | Exp. | Model | APE (%) |
| 1 | 72.0 | 0.085 | 2.8 | 0.275 | 0.265 | 0.386 | 0.379 | 1.81 | 75.91 | 74.02 | 2.49 | 5.01 | 5.24 | 4.59 |
| 2 | 72.4 | 0.165 | 2.8 | 0.284 | 0.308 | 0.464 | 0.458 | 1.29 | 51.32 | 51.23 | 0.18 | 3.98 | 4.25 | 6.78 |
| 3 | 72.1 | 0.055 | 2.8 | 0.287 | 0.230 | 0.308 | 0.313 | 1.62 | 84.93 | 86.89 | 2.31 | 7.18 | 8.25 | 14.90 |
| 4 | 71.8 | 0.088 | 2.8 | 0.278 | 0.268 | 0.397 | 0.392 | 1.26 | 76.45 | 78.41 | 2.56 | 5.05 | 5.45 | 7.92 |
| 5 | 71.8 | 0.130 | 2.8 | 0.284 | 0.306 | 0.446 | 0.446 | 0.00 | 60.67 | 61.48 | 1.34 | 4.19 | 4.43 | 5.73 |
| 6 | 72.1 | 0.198 | 2.8 | 0.286 | 0.317 | 0.464 | 0.471 | 1.51 | 43.67 | 44.43 | 1.74 | 3.85 | 4.01 | 4.16 |
| 24 | 71.8 | 0.085 | 2.8 | 0.221 | 0.251 | 0.392 | 0.399 | 1.79 | 74.63 | 75.24 | 0.82 | 5.11 | 5.36 | 4.89 |
| 25 | 71.8 | 0.085 | 2.8 | 0.104 | 0.166 | 0.435 | 0.440 | 1.15 | 68.61 | 68.92 | 0.45 | 5.46 | 5.72 | 4.76 |
| 26 | 72.8 | 0.164 | 2.7 | 0.217 | 0.288 | 0.474 | 0.475 | 0.21 | 49.29 | 50.32 | 2.09 | 4.13 | 4.51 | 9.20 |
| 27 | 72.4 | 0.165 | 2.8 | 0.104 | 0.169 | 0.501 | 0.500 | 0.20 | 42.13 | 44.01 | 4.46 | 4.77 | 5.11 | 7.13 |
| 28 | 75.6 | 0.164 | 2.0 | 0.298 | 0.266 | 0.470 | 0.477 | 1.49 | 53.42 | 52.30 | 2.10 | 3.68 | 4.05 | 10.05 |
| 29 | 76.0 | 0.163 | 2.6 | 0.297 | 0.306 | 0.465 | 0.472 | 1.51 | 53.65 | 53.52 | 0.24 | 3.92 | 4.21 | 7.40 |
| 30 | 75.1 | 0.159 | 3.3 | 0.264 | 0.316 | 0.459 | 0.463 | 0.87 | 55.91 | 56.50 | 1.06 | 4.38 | 4.62 | 5.48 |
| 31 | 75.7 | 0.159 | 3.6 | 0.267 | 0.338 | 0.454 | 0.462 | 1.76 | 55.57 | 56.41 | 1.51 | 4.30 | 4.29 | 0.23 |
| 32 | 76.6 | 0.156 | 3.9 | 0.259 | 0.335 | 0.449 | 0.460 | 2.45 | 55.39 | 56.12 | 1.32 | 4.57 | 4.56 | 0.22 |
| 33 | 77.1 | 0.157 | 4.5 | 0.256 | 0.360 | 0.441 | 0.468 | 6.12 | 54.59 | 55.71 | 2.05 | 4.35 | 4.2 | 3.45 |
| 34 | 70.3 | 0.083 | 1.1 | 0.300 | 0.146 | 0.417 | 0.425 | 1.92 | 75.87 | 77.42 | 2.04 | 4.85 | 5.58 | 15.05 |
| 35 | 70.1 | 0.085 | 1.4 | 0.291 | 0.208 | 0.411 | 0.421 | 2.43 | 76.57 | 76.98 | 0.54 | 4.27 | 4.30 | 0.70 |
| 36 | 71.1 | 0.083 | 2.1 | 0.274 | 0.252 | 0.393 | 0.401 | 2.04 | 75.98 | 74.57 | 1.86 | 4.68 | 4.99 | 6.62 |
| 37 | 71.3 | 0.083 | 2.8 | 0.273 | 0.298 | 0.398 | 0.409 | 2.76 | 74.51 | 75.22 | 0.95 | 5.11 | 4.49 | 12.13 |
| 38 | 71.3 | 0.085 | 3.5 | 0.276 | 0.308 | 0.385 | 0.401 | 4.16 | 74.69 | 76.01 | 1.77 | 5.40 | 4.53 | 16.11 |
| 39 | 71.5 | 0.084 | 3.8 | 0.271 | 0.319 | 0.400 | 0.403 | 0.75 | 74.78 | 74.70 | 0.11 | 5.23 | 4.33 | 17.21 |
| MAPE(%) | | | | | | | | 1.78 | | | 1.54 | | | 7.49 |

The validations were also conducted to compare the temperature profiles and the $CO_2$ composition profiles inside the absorber and the stripper based on experiment A1, A2 and A3 (Notz et al., 2012). Figure 3.18 shows that the model predictions are in very good agreement with the experimental data. One statement is that the total packing height is 2.25m inside stripper, the 3m position of temperature profile and liquid phase $CO_2$ concentration profile is Figure 3.18 (b) and Figure 3.18 (d) is the reboiler. The comparison results show model predictions are in very good agreements with the experimental data.

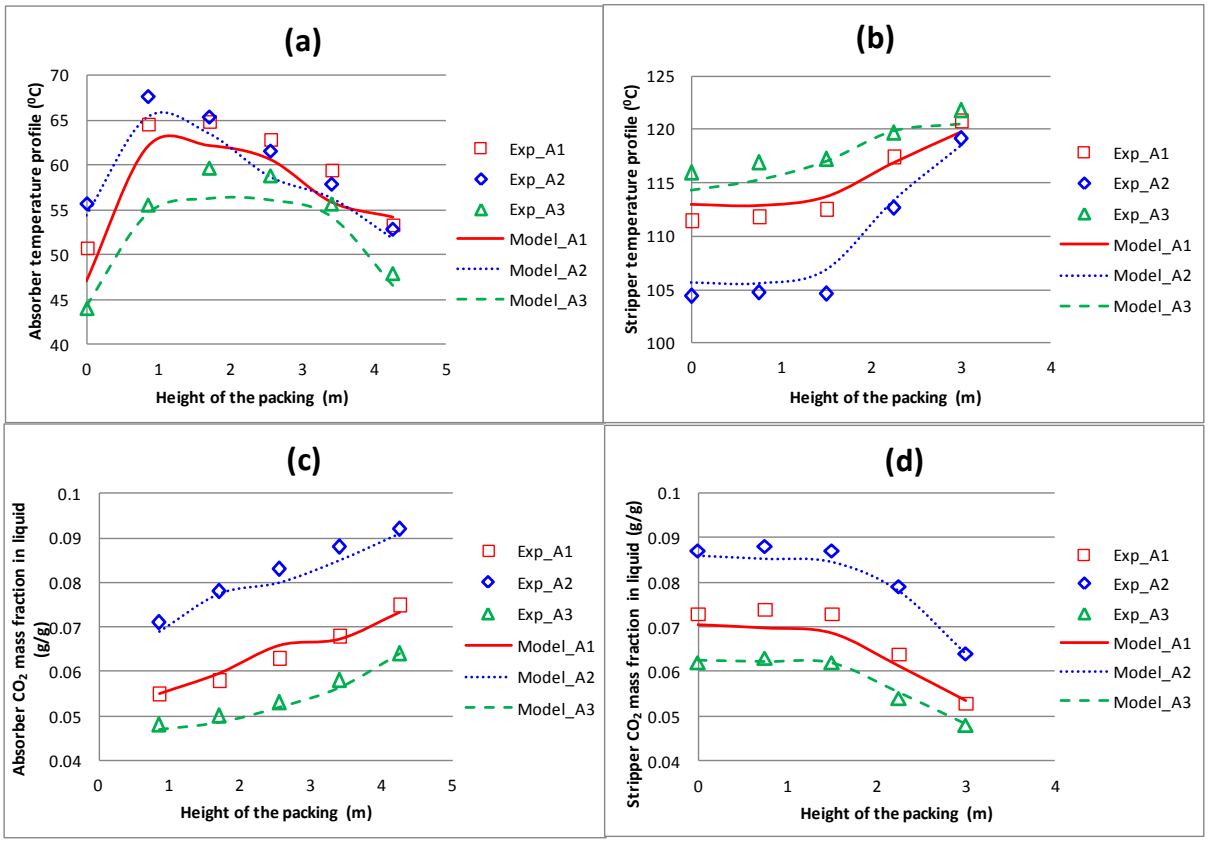


Note: Exp represents experimental data; Model represents model prediction; $CO_2$ concentrations in flue gases are 8.5mol% for A1, 16.5mol% for A2 and 5.5mol% for A3 respectively.

Figure 3.18 Validation results between model predictions and experimental data, (a) temperature profile of the absorber, (b) temperature profile of the stripper, (c) $CO_2$ composition profile inside the absorber, (d) $CO_2$ composition profile inside the absorber

## 3.5 Model scale-up

To match the capacity requirement of handling the flue gas from a 453 $MW_e$ NGCC power plant, the model of $CO_2$ capture process at pilot scale has been scaled up based on chemical engineering principles about estimating of column diameter and pressure drop (Towler and Sinnott, 2012).

The process conditions of the flue gas from the NGCC power plant and other requirements can be found in Table 3.16.

Table 3.16 Boundary conditions of solvent-based PCC process

| Description | Value |
|---|---|
| Flue gas flow rate (kg/s) | 660.54 |
| Flue gas $CO_2$ content (mol %) | 4.50 |
| Flue gas temperature ($^oC$) | 40 |
| Solvent MEA content (wt%) | 35 |
| Capture level (%) | 90 |
| Columns flooding (%) | 65 |

As initial inputs to the process model at the industrial scale in Aspen Plus®, first-guess diameters are required for both the absorber and the stripper. The column diameter can be calculated from the maximum flooding vapour. In this study, a generalised pressure drop correlation (GPDC) figure (see Figure 3.19) is used to estimate the maximum flooding vapour. The abscissa and ordinate are presented in Equation (3.16) and Equation (3.17) (Towler and Sinnott, 2012) respectively.

$$F_{LV} = \frac{L}{V}\sqrt{\frac{\rho_V}{\rho_L}} \tag{3.16}$$

$$K_4 = \frac{13(V_w^*)^2 \cdot F_P \cdot (\mu_L/\rho_L)^{0.1}}{\rho_V(\rho_L - \rho_V)} \tag{3.17}$$

In Equation (3.16), $F_{LV}$ is a flow parameter. For the absorber, the liquid feed is the lean solvent. Its flow rate can be estimated by Equation (3.18) (Agbonghae et al., 2014).

$$F_{Lean} = \frac{F_{Flue} x_{CO_2} \Psi_{CO_2}}{100(\alpha_{Rich} - \alpha_{Lean})}\left[\frac{M_{MEA}}{44.009}\left(1 + \frac{1 - \omega_{MEA}}{\omega_{MEA}}\right) + \alpha_{Lean}\right] \tag{3.18}$$

where $F_{Lean}$ is the mass flow rate of the lean solution, $F_{Flue}$ is the mass flow rate of the flue gas, $x_{CO_2}$ is the mass fraction of $CO_2$ in the flue gas, $\Psi_{CO_2}$ is required $CO_2$ capture level, $M_{MEA}$ is the molar weight of MEA, $\alpha_{Rich}$ and $\alpha_{Lean}$ are the $CO_2$ loading in rich solvent and lean solvent respectively, $\omega_{MEA}$ is the MEA concentration in solvent.

From Equation (3.18), $V_w^*$ (vapour mass flow rate per unit cross-sectional area) is calculated, and then the total cross-sectional area can be obtained given the flue gas flow rate. In this equation $K_4$ is a load parameter looked up from Figure 3.19, according to the value of $F_{LV}$ and specified pressure drop. $F_P$ is a packing factor.

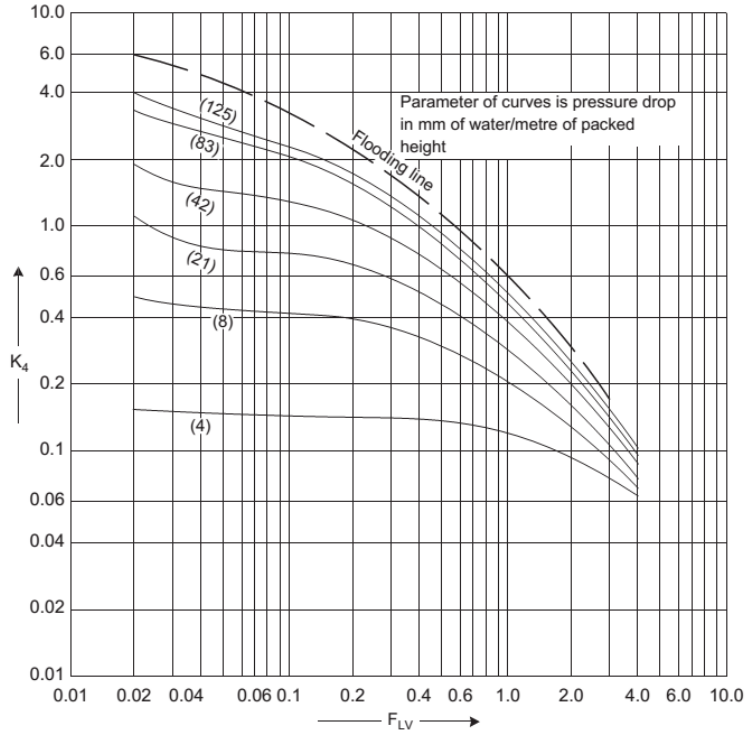


Figure 3.19 Generalized pressure drop correlation (Stichlmair and Fair, 1998)

In order to achieve good liquid and gas distribution and to avoid flooding inside packing beds, a pressure drop of 15–50 $mmH_2O$ per meter packing for absorber and stripper was recommended (Towler and Sinnott, 2012). In this study, a maximum pressure drop per unit height of 20.83 $mmH_2O$ (R.F., 1987) was used considering the forming of MEA solvent (Agbonghae et al., 2014). It should be noticed that the design of the column internals such as gas\liquid distributors and re-distributors is crucial to ensure good gas and liquid distribution inside the absorber and regenerator in such large diameters.

The first-guess diameters of the absorber and the stripper can be calculated using the above method. Starting from this, these parameters will be improved in the development of the

closed-loop $CO_2$ absorption model in Aspen Plus®. In order to directly use the detailed equipment costs in benchmark report of IEAGHG (2012) in Chapters 4, 5 and 7 for cost evaluation and optimisation, the design features of the equipment of the PCC process in this study were set to be consistent with Scenario 3 (NGCC integrated with PCC without EGR) in IEAGHG report. In this study, as one key operational variable, lean loading is set at 0.280 mol $CO_2$/mol MEA as an initial input for the base case by examining the experimental data (Notz et al., 2012). The overall process parameters of the capture plant is shown in Table 3.17 and Table 3.18.

Table 3.17 Design parameters of the absorber and the stripper at the base case

| Description | Absorber | Stripper |
|---|---|---|
| Cross sectional area ($m^2$) | 387.50 | 50.27 |
| Equivalent Column diameter (m) | 22.20 | 8.00 |
| Packing Type | Mellapak 250Y | Mellapak 250Y |
| Total Packing height (m) | 20.00 | 20.00 |
| Column pressure (bar) | 1.00 | 2.00 |
| Column pressure drop (bar) | 0.069 | 0.014 |

Table 3.18 Overall performance of PCC process at the base case

| Description | Value |
|---|---|
| $CO_2$ captured (kg/s) | 41.04 |
| L/G ratio (kg/kg) | 1.22 |
| Lean solvent temperature (℃) | 40.00 |
| Lean solvent flow rate (kg/s) | 807.84 |
| Lean loading (mol $CO_2$/ mol MEA) | 0.280 |
| Rich loading (mol $CO_2$/ mol MEA) | 0.461 |
| Lean Solvent MEA content (wt%) | 35 |
| Reboiler duty ($MW_{th}$) | 195.37 |
| Specific duty (GJ/ton $CO_2$) | 4.76 |
| Reboiler temperature (℃) | 120.16 |

## 3.6 Concluding remarks

This chapter presented the preparation of the process model. As the base of process model development, different correlations of the thermodynamic model were examined and validated with the experimental data of $CO_2$ solubility in aqueous MEA solutions in wide ranges of pressure, temperature and composition conditions. At the same time, the correlations combination in this study was compared with other three published studies (Austgen et al., 1989; Liu et al., 1999; Zhang et al., 2011). The results show the better prediction performance of this study. To improve prediction accuracy of liquid mixture density, Han and Eimer (2012) model was used by coding Fortran subroutine. Then several key physical properties, such as liquid density, liquid heat capacity, liquid viscosity and liquid surface tension of MEA-$H_2O$-$CO_2$ system were validated with the experimental data.

A steady state rate-based process model was developed in Aspen Plus® at the pilot plant scale referring to the pilot plant in the University of Kaiserslautern (Mangalapally and Hasse, 2011). For kinetics-controlled reactions, different values were set for kinetics of the reverse carbonate formation reactions happening in the absorber and the stripper respectively, which improves the accuracy of the process model. Another improvement work is that the correlation of effective gas liquid interfacial area was updated to Tsai et al. (2011) by coding Fortran subroutine. The process model was then validated with series of comprehensive pilot plant data, in terms of its absorption efficiency and thermal performance of the integrated system. The comparison results show that model predictions are in very good agreement with the experimental data from pilot plant, which ensure that the process model has good accuracy for the optimisation studies in next chapters.

# Chapter 4: Optimal Design of Solvent-based PCC Process

In this Chapter, the cost model of PCC process is developed first. The cost breakdowns including CAPEX, fixed OPEX and variable OPEX were analysed. The cost model was developed in Fortran subroutine and was dynamically linked with Aspen Plus®. Therefore it is equivalent as a new model. Optimisation method is then explained. Cost of $CO_2$ avoided (CCA) is formulated as the objective function. The key design parameters and operational variables have been analysed to get their reasonable variation range. The optimisation is conducted and the performance of optimal case was compared with the base case. In order to get comprehensive understanding, case studies were carried out about the impact of variations of the key variables.

## 4.1 Development of cost model

### *4.1.1 Cost breakdown*

For operating an industrial process plant, the total cost includes capital expenditure (CAPEX) and operational expenditure (OPEX). OPEX can be split into fixed OPEX (FOPEX) and variable OPEX (VOPEX) (IEAGHG, 2012). For a carbon capture plant, the costs could be detailed as follows: (1) CAPEX includes equipment material and installation, labour cost, engineering and management cost and other costs happened during the project contracture and commissioning, (2) FOPEX includes overhead cost, operating and maintenance cost (O&M) and other costs fixed for the plant no matter running at partial or full load or shutdown, and (3) VOPEX mainly includes energy and utilities costs and solvent make-up cost. It is noticed that in this chapter VOPEX does not include the emission cost of $CO_2$ discharged into atmosphere. In Chapter 8, it will be involved when the optimal operation was analysed for the power plants integrated with whole CCS chain.

To harmonize the results for comparison with future new studies, the following assumptions were made: (1) all costs are corrected to €2015 using the harmonised consumer price index (HICP) in Europe zone (Inflation, 2015), (2) the captured $CO_2$ mixture has no economic value, and (3) cooling water is sourced from a nearby body of water at the cost of pumping and operation of a cooling tower.

### *4.1.2 CAPEX*

#### 4.1.2.1 Equipment type and material

Because of the corrosivity of the solvent at operating conditions of carbon capture plant, the material selection is important to ensure the integrity of the plant design. Table 4.1 lists the type and material selection of main equipment based on IEAGHG reports (IEAGHG, 2010; IEAGHG, 2012), which is the base for the cost estimation of equipment.

Table 4.1 Equipment type and material selection of PCC process

| Category | Name of equipment | Type | Material |
|---|---|---|---|
| Separation equipment | DCC | Rectangular tank | Concrete with epoxy lining |
| | DCC packing | Mellapak 250Y | SS316 |
| | Absorber | Rectangular column | Concrete with polyproylene lining |
| | Absorber packing | Mellapak 250Y | SS316L |
| | Stripper | Vertical cylinder | SS316L |
| | Stripper packing | Mellapak 250Y | SS316L |
| Heat exchanger | Stripper reboiler | Vertical shell & tube thermosyphon | SS316L |
| | Stripper condenser | Shell and tubes | SS 304 |
| | Cross heat exchanger | Plate and frame | SS316L |
| | Lean cooler | Plate and frame | SS304 |
| | DCC water cooler | Plate and frame | CS |
| Pressure Change | Flue gas blower | Axial | CS |
| | Rich solvent pump | Centrifuge | SS316L |
| | Lean solvent pump | Centrifuge | SS304 |
| | DCC water pump | Centrifuge | CS |
| Compression train | Compressor | Multi-stage Integrally geared Type | Cr Ni alloy casing/impeller |
| | Knock out drum | Vertical tank | SS304 |
| | Inter-stage cooler | Shell and tubes | SS304 |

#### 4.1.2.2 Direct cost of equipment

The accuracy of the equipment cost estimation depends on the available design details at different project phase. The major equipment costs of PCC process in IEAGHG report were estimated by contacting the vendors after detailed engineering design (IEAGHG, 2012). The method could be regarded as Class 2 detailed estimates whose accuracy could be in the range from -15% to 20% (Feng and Rangaiah, 2011). The direct material costs and other fixed costs in the report could be trusted although the process simulation may not be accurate enough. In this study, the base case was set up with same equipment design features and process boundary conditions of Scenario 3 (NGCC integrated with PCC without EGR) in IEAGHG report. Thus, the direct material costs can be derived from IEAGHG report. For the absorber and the stripper, the costs of the packing with internals can be directly calculated by the volumes of the packing beds. For the other cases, the direct material cost could be calculated based on their reference value in the base case and the specific scaling factor for different types of equipment, by Equation (4.1) (Mores et al., 2012).

$$PC = PC^o \left(\frac{X}{X^o}\right)^m \left(\frac{I}{I^o}\right) \tag{4.1}$$

where $X$ is the value of selected scaling factor related to equipment capacity, $I$ is cost index for different year and area, $m$ is the specific factor and the value is 1.0 for structured packing inside the columns and 0.6 for other equipment according to six-tenths rule (Sweeting, 1997). $PC^o$ is the direct material cost of the base case. Table 4.2 lists the main investment items considered including the construction material of each one of them. The flue gas cooling system includes flue gas blower, DCC, DCC pump and DCC cooler.

#### 4.1.2.3 Annualized CAPEX

For a PCC plant, the major equipment costs include the costs of the absorbers, strippers, pumps and all other plant items which are listed in Table 4.2. The other direct and indirect costs were estimated using factors of the overall major equipment cost. Those factors are listed in Table 4.3.

Table 4.2 Direct material costs and the scaling factor of equipment

| Name of equipment | X, Selected scaling factor | $PC^o$, Base cost* (€@2011) |
|---|---|---|
| Flue gas cooling system | flue gas flow rate | 8,768,110 |
| Absorber column shell | shell surface area | 995,908 |
| Stripper column shell | shell surface area | 18,095,040 |
| Unit price of packing | volume of packing | 4,565 (€/$m^3$) * |
| Stripper reboiler | heat duty | 25,539,000 |
| Stripper condenser | heat duty | 9,287,000 |
| Inter Heat Exchanger | heat duty | 1,963,000 |
| Lean cooler | heat duty | 557,000 |
| Rich solvent pump | electricity consumption | 51,000 |
| Lean solvent pump | electricity consumption | 51,000 |
| Compression train | electricity consumption | 8,256,245 |

*The values were derived from IEAGHG (2012)

Table 4.3 Factors for total project cost calculation

| | Description | Percentage of major equipment cost * |
|---|---|---|
| Direct material | Major equipment | 1 |
| | Piping | 0.1500 |
| | Control and instrumentation | 0.0200 |
| | Electrical | 0.0400 |
| | Catalysts and other chemicals | 0.0085 |
| | Civil/steelwork/buildings | 0.2803 |
| Labour only contracts | Mechanical | 0.1097 |
| | Electrical/instrumentation | 0.0366 |
| | Scaffolding/lagging/rigging | 0.0305 |
| Other cost | Engineering service/construction management | 0.0457 |
| | Commissioning | 0.0101 |
| | Soft costs contractor (inc contingency & profit) | 0.5026 |
| | Soft costs owner | 0.2011 |
| CAPEX | | 2.4349 |

*The values were derived from IEAGHG (2012)

The annualized CAPEX is the total CAPEX multiplying by capital recovery factor (CRF) (McCollum and Ogden, 2006), which is calculated by Equation (4.2) (Mores et al., 2012).

$$CRF = \frac{i(i+1)^n}{(i+1)^n + 1} \tag{4.2}$$

where $n$ is the economic life of plant and $i$ is the interest rate. It is assumed a project life of 25 years and 12% of interest rate (McCoy and Rubin, 2008).

### 4.1.3 Fixed OPEX

Fixed OPEX (FOPEX) includes long term service agreement costs, overhead cost, operating and maintenance cost (O&M) and other costs fixed for the plant no matter if it is running at partial or full load or shutdown. FOPEX can be simply calculated by Equation (4.3)

$$FOPEX = 0.03 \times CAPEX \tag{4.3}$$

### 4.1.4 Variable OPEX

For operating a carbon capture process integrated with a power plant, the power plant could supply electricity and lower pressure steam to the capture plant. Other utilities could also be provided from the power plant accessory facilities. However, in this chapter, the study scope only includes the PCC process with $CO_2$ compression. Each utility cost will be calculated by multiplying the market unit price with its amount obtained from the simulation results. Furthermore, for heat input required for solvent regeneration, the low pressure steam consumption is converted into equivalent power electricity consumption. The utility unit prices can be seen in Table 4.4 with the costs given in Euro. VOPEX includes the cost of power electricity consumption for pumps/blower/compressor, the cost of power electricity for solvent regeneration, the cost of cooling utilities and the cost of MEA solvent make-up. The water make-up is neglected because Kvamsdal et al. (2010) proven the water in a solvent-based PCC process could be in a neutral balance without make-up.

Table 4.4 Key economic evaluation cost inputs

| Description | Unit | Value | Source |
|---|---|---|---|
| Electricity price | €/kW | 0.0775 | 1st quarter of 2012 of APEA |
| Cooling water price | €/$m^3$ | 0.0317 | 1st quarter of 2012 of APEA |
| MEA price | €/t | 1,452 | Alibaba (2016) |
| Operating hours | hr/year | 8,000 | |
| Project economic life | year | 25 | |
| Interest rate | /year | 0.12 | |

### *4.1.5 The costs of the base case*

The case of PCC process after scale-up in Section 3.5 (process parameters can be seen in Tables 3.16 – 3.18) was defined as the base case in this chapter. With all the basic costs and relevant correlations in above sections, the costs of the base case (process parameters can be seen in Tables 3.16 – 3.18) were calculated. Table 4.5 shows the costs of the base case of PCC standalone. In the base case, the annualized CAPEX, FOPEX and VOPEX account for 38.46%, 8.87% and 52.67% of the total annual cost respectively. For the variable OPEX, power electricity cost is the biggest part and solvent make-up cost is the second largest part. The CCA is 86.85 €/ton $CO_2$.

Table 4.5 Costs of the base case

| Description | | Base case |
|---|---|---|
| $CO_2$ captured rate (ton/year) | | 1,179,064 |
| CAPEX (M€) | | 302.85 |
| Annualized CAPEX (M€/year) | | 39.37 |
| Fixed OPEX (M€/year) | | 9.09 |
| Variable OPEX | Power electricity (M€/year) | 49.72 |
| | Cooling water (M€/year) | 1.46 |
| | Solvent make-up cost (M€/year) | 2.75 |
| Total annual cost (M€/year) | | 102.38 |
| CCA (€/ton $CO_2$) | | 86.85 |

## 4.2 Optimisation methodology

### *4.2.1 Sequential quadratic programming (SQP)*

The SQP method has been one of the most successful general methods for solving large-scale nonlinear constrained optimization problems (Boggs and Tolle, 2000). A typical optimisation model consists of an objective function supplemented with equality and inequality constraints. This optimisation problem can be formulated as follows:

$$\text{Minimize } f(d,e,o) \tag{4.4}$$

Subject to the process constrains and operation constrains:

$$h(d,e,o) = 0 \tag{4.5}$$

$$g(d,e,o) \leq 0 \tag{4.6}$$

where $f$ is the objective function; $b$ is the vector of the coefficients in the objective function and constrains; $d$ is the vector of the design variables (e.g. diameters and packing heights of the absorber and stripper, the operating pressure and operating temperature of the towers). And $o$ is the vector of operational variables (i.e. $CL$, capture level, $\alpha_{lean}$, lean loading, $L/G_{ratio}$, solvent and flue gas ratio and $Q_{reb}$ , reboiler duty).

The Lagrangian for this problem is:

$$L(d,e,o,\lambda,\sigma) = f(d,e,o) - \lambda^T\, h(d,e,o) - \sigma^T\, g(d,e,o) \tag{4.7}$$

where λ and σ are Lagrange multipliers; $^T$ denotes the vector transpose.

The SQP method converges fast with a few iterations but it needs numerical derivatives for all decision and tear variables at each iteration. At an iterate $k$, a basic SQP algorithm defines an appropriate search direction $z_k$ as a solution to the quadratic programming (QP) subproblem, in which a quadratic objective function is minimized subject to inequality or equality constraints.

Minimize:

$$f(d_k, e_k, o_k) + \nabla f(d_k, e_k, o_k)^{\mathrm{T}} z_k + \frac{1}{2} z_k{}^T \nabla^2 L(d_k, e_k, o_k\ \lambda_k, \sigma_k) z_k \quad (4.8)$$

Subject to:

$$h(d_k, e_k, o_k) + \nabla h(d_k, e_k, o_k)^{\mathrm{T}} z_k = 0 \quad (4.9)$$

$$g(d_k, e_k, o_k) + \nabla g(d_k, e_k, o_k)^{\mathrm{T}} z_k \leq 0 \quad (4.10)$$

where $\nabla f$ , $\nabla h$ , $\nabla g$ are the gradients.

The SQP method used in Aspen Plus® has a novel feature which is that tear streams can be partially converged using Wegstein for each optimization iteration (AspenTech, 2008a). Then the solving can start with only a single point and does not need to calculate the derivatives (Wegstein, 1958), which normally stabilizes convergences and reduces the total number of iterations.

### *4.2.2 Objective function*

For techno-economic evaluation or cost optimisation of a power plant integrated with carbon capture process, different economic indexes have been used in different studies, including (a) total annual operating profits; (b) total annualized cost; (c) levelised cost of electricity (LCOE); (d) cost of $CO_2$ avoided. In this Chapter, the study scope only includes PCC process and compression train so that the cost of $CO_2$ avoided (CCA) was formulated to be the objective function of the optimisation.

CCA was calculated through dividing total annual cost by annual numbers of $CO_2$ captured as in Equation (4.11). The total annual cost is a sum of annualized CAPAX, FOPEX and VOPEX as in Equation (4.12).

$$CCA = \frac{TAC}{F_{co_2,cap}} \quad (4.11)$$

$$TAC = ACAPEX + FOPEX + VOPEX \quad (4.12)$$

$$ACAPEX = CAPEX \times CRF \quad (4.13)$$

### 4.2.3 Optimisation constraints

#### 4.2.3.1 Equality constraints

Equality constraints related to the mass balances, reactions and phase balance were embedded in the first principle process model built in Aspen Plus® described in Chapter 3.

#### 4.2.3.2 Inequality constraints

The consideration of the first constraint is that current perspective studies predict 90% capture level from the fossil-power plants is required to reach the target of $CO_2$ emission control (IPCC, 2005; DECC, 2013). For operating the column, the constraints about the flooding and pressure drop are strict considering MEA solvent easily cause foaming inside packing beds (Agbonghae et al., 2014) at this context.

$$CL \geq 90\% \tag{4.14}$$

$$0 \leq F_{flood} \leq 0.65 \tag{4.15}$$

$$0 \leq \Delta P_{pack} \leq 20.00\ (mmH_2O/m) \tag{4.16}$$

### 4.2.4 Optimisation variables

#### 4.2.4.1 Key design variables

##### 4.2.4.1.1 Diameter of the absorber and the stripper

Previously, a maximum column diameter of 12.6 m for carbon capture process was suggested by Chapel et al. (1999). In recent years, with different column internal technologies developed by different equipment manufacturers (Carbon Capture Journal, 2013; Sulzer, 2014; Koch-Glitsch, 2014), the upper limit of column diameter is increasing. For Fluor's $CO_2$ capture demonstration plant using Econamine FG PlusSM Technology, Reddy et al. (2013) reported that a maximum diameter of 18.0 m was used as the criterion for deciding the numbers of the column required. It is also noticed that concrete rectangular tower with appropriate lining rather than cylindrical metal material tower could be used for the absorber (IEAGHG, 2012; SASKPOWER, 2015) in a power plant to get a better economic profile because the operating pressure of the absorber is near the atmosphere pressure. In line with the IEAGHG report, the absorber is a rectangular column with a size of 15.5m x 25m (equivalent to a cylindrical column with 22.2 m diameter) and the stripper is a cylindrical column with 8.0 m diameter. However, for model input format in Aspen Plus®, the diameter

of the absorber was given by calculating same from the cross-section area of the rectangular column. This could also give a generic sizing of the absorber for comparison with other publications. Then the variation ranges of the diameters of the absorber and the stripper in the optimisation are presented as:

$$8.00 \leq D_{ABS} \leq 30.00\ (m) \tag{4.17}$$

$$3.00 \leq D_{STR} \leq 20.00\ (m) \tag{4.18}$$

#### 4.2.4.1.2 Packing height of the absorber and the stripper

In the pilot plant at the University of Texas at Austin (Dugas, 2006), the packing heights of absorber and stripper are 6.1m and $CO_2$ capture level could be over 95% in some scenarios (Zhang et al., 2009). Notz et al (2012) reported the capture level could reach 90% and lean loading could reach 0.1 mol $CO_2$/mol MEA with the packing height of 4.2 m for the absorber and of 2.25 m for the stripper in the pilot plant at the University of Kaiserslautern (Mangalapally and Hasse, 2011). In the studies (IEAGHG, 2012; Sipöcz and Tobiesen, 2012; Kvamsdal et al., 2010; Mores et al., 2014; Biliyok and Yeung, 2013; Agbonghae et al., 2014) on industrial scale PCC process, the packing height of the columns varies from 6 m to 30 m. In this optimisation, the variation ranges of the packing height of the absorber and the stripper are presented as:

$$4.5 \leq HP_{ABS} \leq 40\ (m) \tag{4.19}$$

$$2.25 \leq HP_{STR} \leq 40\ (m) \tag{4.20}$$

### 4.2.4.2 Operating pressure and temperature

*Operating pressure and temperature of the columns*

Generally, low operating temperature and high operating pressure is beneficial in chemical absorption efficiency (Sinnott and Towler, 2009). However, the operating pressure of the absorber of PCC process is normally set at near atmosphere pressure because it is very costly to compress the flue gas with a huge volumetric flow rate (599.195 $m^3$/s in the base case in this study).

For the stripper, Abu-Zahra et al. (2007b) investigated that increasing the operating pressure from 90 kPa to 210 kPa leads to an 8.5% reduction in heat requirement in the reboiler and lower electricity consumption of the $CO_2$ compression train. One limitation of the trade-off is that MEA solvent degradation increases sharply if the temperature increases over 125 °C (Davis and Rochelle, 2009; Rochelle, 2012). Correspondingly, the operating pressure for stripper is then set up to 2.0 bar.

For both the absorber and the stripper, the operating temperature is a dependant variable once the operating pressure is specified. It is affected by the feeding conditions and the reaction heat released or heat input for solvent generation.

*Temperature of flue gas*

Kvamsdal et al. (2011b) found the specific duty decreases from 2.87 to 2.71 GJ/ton $CO_2$ when flue gas temperature changes from 50°C to 30°C. So the benefit of low flue gas temperature is not significant, especially considering the extra cooling cost.

*Temperature of lean solvent*

In the study by Abu-Zahra (2007b), when the lean solvent temperature decreased from 50 °C to 25 °C, the specific duty decreased from 4.15 to 3.75 GJ/ton $CO_2$. However, more cooling energy is required in the lean solvent cooler.

Then the variation ranges of the operating pressure of the columns and the temperature of the feeding streams in the optimisation are presented as below:

$$P_{ABS} = 1.00\ (bar) \tag{4.21}$$

$$1.50 \leq P_{STR} \leq 2.00\ (bar) \tag{4.22}$$

$$30.00 \leq T_{flue} \leq 50.00\ (°C) \tag{4.23}$$

$$30.00 \leq T_{lean} \leq 50.00\ (°C) \tag{4.24}$$

#### 4.2.4.3 Key operational variables

*MEA concentration*

In the study of Abu-Zahra et al (2007b), it was found that thermal energy requirement decreases by about 5–8% when MEA concentration in the lean solvent increase from 20 wt%

to 40 wt%. However, higher MEA concentration leads to pronounced corrosive effects to the equipment and cause higher solvent degradation loss (Davis and Rochelle, 2009; Rochelle, 2012).

*Lean Loading*

Lean loading has large impact for operating the absorber in terms of both the absorption efficiency and hydraulic performance. Abu-Zahra et al. (2007b) examined the lean loading with a range of 0.18–0.38 mol $CO_2$/mol MEA while Agbonghae et al. (2014) investigated the range of 0.10–0.30 mol $CO_2$/mol MEA. Lean loading can be controlled by adjusting the heat input to the reboiler of the stripper.

*Liquid/Gas ratio*

In the contribution of Agbonghae et al. (2014), the range of L/G (kg/kg) ratio is from 0.70 to 2.75 for gas fired power plant and is from 2.00 to 5.50 for coal-fired power plant. It is noticed that the interactions between these key operational variables are complex and nonlinear. For a certain capture task (fixed flue gas flow rate and capture level requirement), amongst MEA concentration, lean loading and L/G ratio, when two of them are specified, the other one is then independent. The variation ranges of these three key operational variables in this optimisation are presented as below:

$$20 \leq M_{MEA} \leq 40 \ \ (wt\%) \tag{4.25}$$

$$0.100 \leq \alpha_{lean} \leq 0.380 \ (mol\ CO_2/mol\ \ MEA) \tag{4.26}$$

$$0.50 \leq \frac{L}{G} \leq 6.00 \ (\frac{kg}{kg}) \tag{4.27}$$

## 4.3 Optimisation results

Table 4.6 shows optimisation results compared with the base case. The CCA of the optimal case decreased by 18.7% compared with the base case. The main contribution is the saving from the CAPEX. Both the diameter and packing height of the columns in the optimal case are less than the base case. VOPEX in the optimal case is also lower than the base case as the

reboiler duty is less with optimal lean loading although higher L/G ratio means high operating cost for the solvent circulations.

Table 4.6 Comparison of the optimal case and the base case

| Input conditions | | |
|---|---|---|
| Parameter | Values | |
| Flue gas flow rate (kg/s) | 660.05 | |
| $CO_2$ concentration in flue gas (mol%) | 4.50 | |
| $CO_2$ capture level (%) | 90.00 | |
| MEA concentration in solvents (wt%) | 35.00 | |
| Technical performance comparison | | |
| Parameter | Base case | Optimal case |
| Lean loading (mol $CO_2$/mol MEA) | 0.280 | 0.294 |
| L/G (kg/kg) | 1.22 | 1.37 |
| Reboiler duty ($MW_{th}$) | 195.37 | 166.21 |
| Specific duty (GJ/ton $CO_2$) | 4.76 | 4.05 |
| Absorber column diameter (m) | 22.20 | 18.93 |
| Absorber column packing height (m) | 20.00 | 10.43 |
| Stripper column diameter (m) | 8.00 | 7.72 |
| Stripper column packing height (m) | 20.00 | 7.67 |
| Economic performance comparison | | |
| Parameter | Base case | Optimal case |
| ACAPEX (M€/year) | 39.37 | 29.79 |
| FOPEX (M€/year) | 9.09 | 6.41 |
| VOPEX(M€/year) | 53.93 | 47.51 |
| TAC (M€/year) | 102.38 | 81.71 |
| CCA (€/ton $CO_2$) | 86.85 | 69.13 |

## 4.4 Optimisations in response to variations of key variables

As can be seen in Table 4.6, the optimisation result is a series of the values of each parameter in the optimal case and it could not reflect the impact of the variables on the objective function and the interactions between different variables. In order to obtain more comprehensive understanding of the influence of important process parameters, systematic

case studies about variation of MEA concentration in solvents, $CO_2$ concentration in flue gas and flow rate of flue gas are carried out in this section

In the case studies, the selected variables were specified with discrete values to see that how the objective function and related variables change, driven by the optimisations. It should be pointed out that, in all the figures in this section, each point on lines is concerned with a steady state solution for one discrete optimisation running. The lines present the trends of the changes instead of continual changes of the variables.

### *4.4.1 Variation of MEA concentration in solvent*

The MEA concentration in solvent affects both the $CO_2$ physical solubility and chemical reactions, thus it influences on the energy requirement of solvent regeneration. In the study of Abu-Zahra et al (2007b), it was found that thermal energy requirement decrease about 5–8% when MEA concentration in the lean solvent increase from 20 wt% to 40 wt%. However, higher MEA concentration leads to pronounced corrosive effects to the equipment and cause higher solvent degradation loss (Davis and Rochelle, 2009; Rochelle, 2012). In this case study, the MEA concentration in solvent was specified at 20, 25, 30, 35, 40 wt% respectively. The results could be seen in Table 4.7 and Figure 4.1.

With increasing MEA concentration, the $CO_2$ solubility increases because there are more MEA molecules available to react with $CO_2$ molecules. The $CO_2$ loading in rich solvent is also increasing (see Figure 4.1(a)).The results show the required L/G ratio decreases because of increasing of absorption capacity of the solvent (the difference of $CO_2$ loading between rich and lean solvent).

Lower L/G ratio (Figure 4.1(b)) results in column cross sectional area decreases by 17.74% for the absorber and by 29.49 % for the stripper (Figure 4.1(d)). The reason is that the flow rate of the flue gas entering the absorber remains same in the case study. With higher MEA concentration in solvent, the optimal packing height of the absorber slightly decreases (Figure 4.1(e)) because of lower solvent flow rate. The optimal packing height of the stripper increases significantly in Case M5 because the absorption capacity of solvent increases largely which means the required solvent regeneration degree increases in the stripper.

The economic results (see Figure 4.1 (f)) shows CCA decreases 14.54%, from 80.34 €/ton $CO_2$ to 68.66 €/ton $CO_2$. The cost breakdown shows ACAPEX decreases by 15.88% and VOPEX decrease by 13.47 %. It is also noticed that the CCA in Case M5 is just slightly

lower than in Case M4 (see Table 4.7). However at 40 wt% concentration, MEA degradation in the system will cause significant solvent loss.

Table 4.7 Optimisation results with variation of MEA concentration

| Case tag | M1 | M2 | M3 | M4 | M5 |
|---|---|---|---|---|---|
| MEA concentration (wt%) | 20 | 25 | 30 | 35 | 40 |
| Flow rate of flue gas(kg/s) | 660.05 | 660.05 | 660.05 | 660.05 | 660.05 |
| $CO_2$ concentration in flue gas (mol%) | 4.50 | 4.50 | 4.50 | 4.50 | 4.50 |
| $CO_2$ capture level (%) | 90 | 90 | 90 | 90 | 90 |
| $CO_2$ captured (kg/s) | 41.04 | 41.04 | 41.04 | 41.04 | 41.04 |
| Lean Loading (mol $CO_2$/ mol MEA) | 0.324 | 0.317 | 0.299 | 0.294 | 0.310 |
| Rich Loading (mol $CO_2$/ mol MEA) | 0.428 | 0.439 | 0.456 | 0.462 | 0.477 |
| Flow rate of lean solvent (kg/s) | 2856.68 | 1933.54 | 1274.52 | 905.60 | 894.17 |
| L/G ratio (kg/kg) | 4.32 | 2.93 | 1.93 | 1.37 | 1.35 |
| Reboiler duty ($MW_{th}$) | 177.90 | 179.17 | 172.66 | 166.21 | 157.13 |
| Specific duty (GJ/ton $CO_2$) | 4.33 | 4.37 | 4.21 | 4.05 | 3.83 |
| Diameter of absorber (m) | 20.65 | 20.18 | 19.44 | 18.93 | 18.63 |
| Packing height of absorber (m) | 11.89 | 11.38 | 11.21 | 10.42 | 10.84 |
| Diameter of stripper (m) | 9.17 | 8.43 | 7.54 | 7.72 | 7.70 |
| Packing height of stripper (m) | 3.23 | 4.44 | 6.26 | 7.68 | 12.67 |
| ACAPEX (M€/year) | 34.26 | 32.29 | 29.72 | 27.79 | 28.82 |
| FOPEX (M€/year) | 7.91 | 7.45 | 6.86 | 6.41 | 6.65 |
| VOPEX (M€/year) | 52.79 | 51.52 | 49.27 | 47.51 | 45.68 |
| TAC (M€/year) | 94.96 | 91.26 | 85.84 | 81.71 | 81.15 |
| CCA (€/ton $CO_2$) | 80.34 | 77.21 | 72.62 | 69.13 | 68.66 |

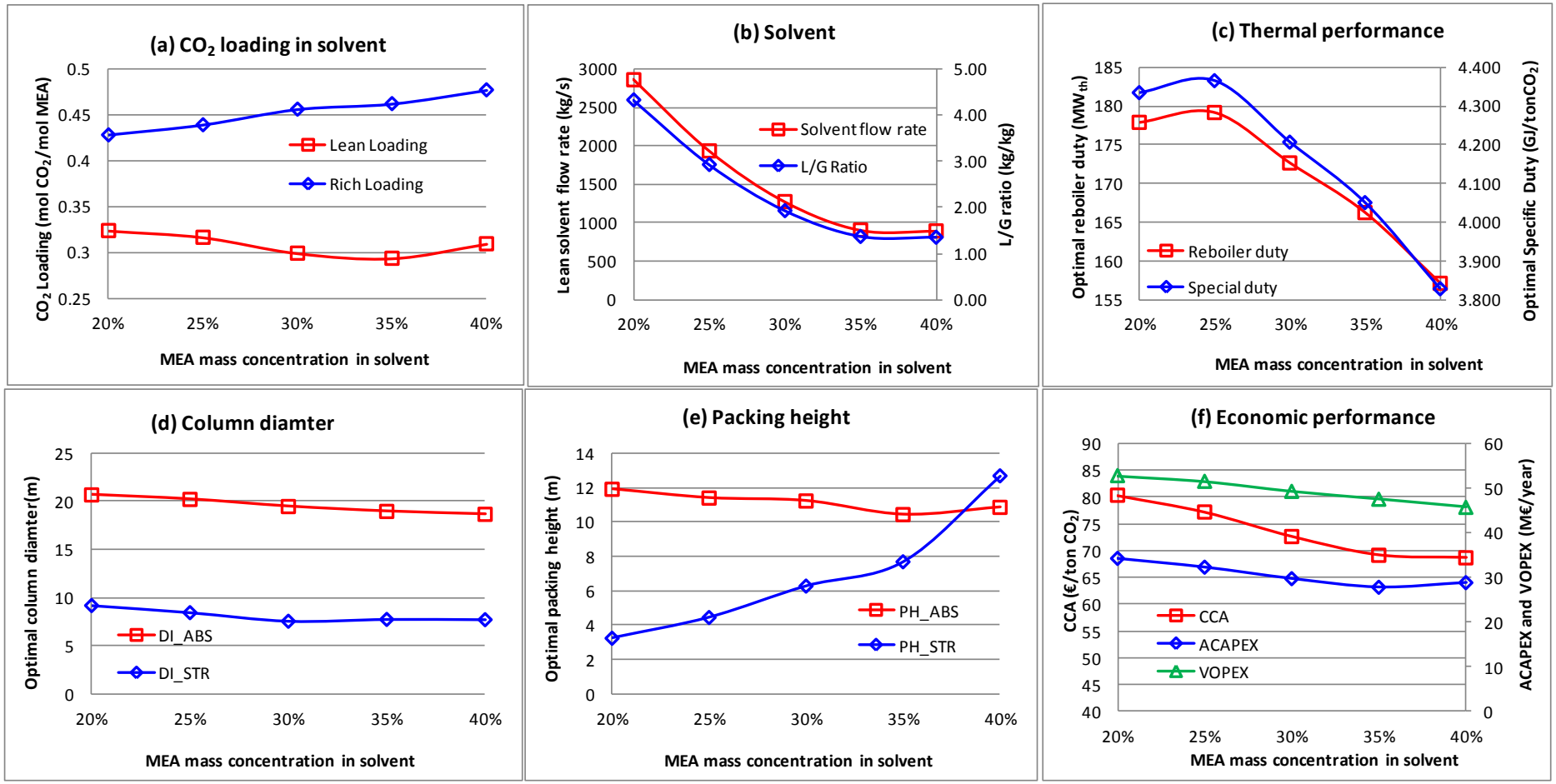


Figure 4.1 Optimisation results with variation of MEA concentration in solvent

### 4.4.2 Variation of $CO_2$ concentration in flue gas

The $CO_2$ concentration differs in the flue gases produced by different type of emitters. For example, $CO_2$ concentration in flue gas is around 4.4 mol% for a NGCC power plant without EGR (Biliyok et al., 2013) while it is around 13.5 mol% for coal-fired power plant (Agbonghae et al., 2014). The $CO_2$ concentration in flue gases from refinery and cement are around 20–33 mol% (IPCC, 2005). The changes of $CO_2$ concentration in flue gases do significantly affect key equipment design features as well as the economic range of the key operational variables because it not only changes the required capacity of the capture plant but also impacts the absorption efficiency. In this case study, the $CO_2$ concentration was specified at 4.5, 7.5, 13.5, 20, 30 mol% respectively. The optimisation results could be seen in Table 4.8 and Figure 4.2.

With the increase of the $CO_2$ concentration but fixing the capture level, the amount of $CO_2$ captured increases from 41.04 kg/s to 243.85 kg/s (see Table 4.8). The optimal $CO_2$ rich loadings (Figure 4.2(a)) have been pushed high towards the saturated loading (could be roughly estimated with the $CO_2$ solubility data in Figure 3.2–Figure 3.4) for $CO_2$ concentrations from 7.5 mol% to 30 mol%. At the same time, optimal $CO_2$ lean loading gradually increases which means the solvent regeneration degree becomes low. This helps to keep the increase of reboiler duty (Figure 4.2(c)) not such sharp.

The solvent flow rate increases sharply to meet the capture capacity, resulting in big increasing of L/G ratio from 1.37 kg/kg to 9.60 kg/kg (Figure 4.2(b)). The optimal diameters of the columns also increase significantly (Figure 4.2(d)). The optimal packing height (Figure 4.2(e)) of the absorber does not show clear change trend. The optimal packing height of the stripper decreases slightly because lean loading increases which means lower solvent regeneration degree.

From Case C1 to Case C5, ACAPEX increases by 192.39% and VOPEX increases by 358.83%, which indicate that the operating cost is more sensitive to the change of $CO_2$ concentration. However, CCA decreases by 34.5%, from 69.13 €/ton $CO_2$ to 45.28 €/ton $CO_2$, because the captured $CO_2$ increases 494.16%. It reflects that high $CO_2$ concentration in the flue gas benefits low CCA, which is consistent with the result of EGR study in Chapter 5.

Table 4.8 Optimisation results with variation of $CO_2$ concentration in flue gas

| Case tag | C1 | C2 | C3 | C4 | C5 |
|---|---|---|---|---|---|
| $CO_2$ concentration in flue gas (mol%) | 4.40 | 7.50 | 13.50 | 20.00 | 30.00 |
| MEA concentration (wt%) | 35 | 35 | 35 | 35 | 35 |
| Flow rate of flue gas(kg/s) | 660.05 | 660.05 | 660.05 | 660.05 | 660.05 |
| $CO_2$ capture level (%) | 90.00 | 90.00 | 90.00 | 90.00 | 90.00 |
| $CO_2$ captured (kg/s) | 41.04 | 68.64 | 119.54 | 174.89 | 243.85 |
| Lean Loading (mol $CO_2$/ mol MEA) | 0.294 | 0.298 | 0.308 | 0.315 | 0.331 |
| Rich Loading (mol $CO_2$/ mol MEA) | 0.462 | 0.476 | 0.474 | 0.474 | 0.475 |
| Flow rate of lean solvent (kg/s) | 905.60 | 1542.67 | 2973.22 | 4565.87 | 6338.98 |
| L/G ration (kg/kg) | 1.37 | 2.34 | 4.50 | 6.91 | 9.60 |
| Reboiler duty ($MW_{th}$) | 166.21 | 265.84 | 463.44 | 676.94 | 943.83 |
| Specific duty (GJ/ton $CO_2$) | 4.05 | 3.87 | 3.88 | 3.87 | 3.87 |
| Diameter of absorber (m) | 18.93 | 19.71 | 21.54 | 23.22 | 24.58 |
| Packing height of absorber (m) | 10.42 | 12.50 | 11.54 | 11.19 | 10.60 |
| Diameter of stripper (m) | 7.72 | 10.30 | 12.91 | 15.55 | 18.09 |
| Packing height of stripper (m) | 7.68 | 6.50 | 6.29 | 5.93 | 5.77 |
| ACAPEX (M€/year) | 27.79 | 36.63 | 50.30 | 64.89 | 81.26 |
| FOPEX (M€/year) | 6.41 | 8.45 | 11.61 | 14.97 | 18.75 |
| VOPEX (M€/year) | 47.51 | 69.87 | 113.56 | 160.54 | 217.98 |
| TAC (M€/year) | 81.71 | 114.95 | 175.46 | 240.40 | 317.99 |
| CCA (€/ton $CO_2$) | 69.13 | 58.15 | 50.97 | 47.73 | 45.28 |

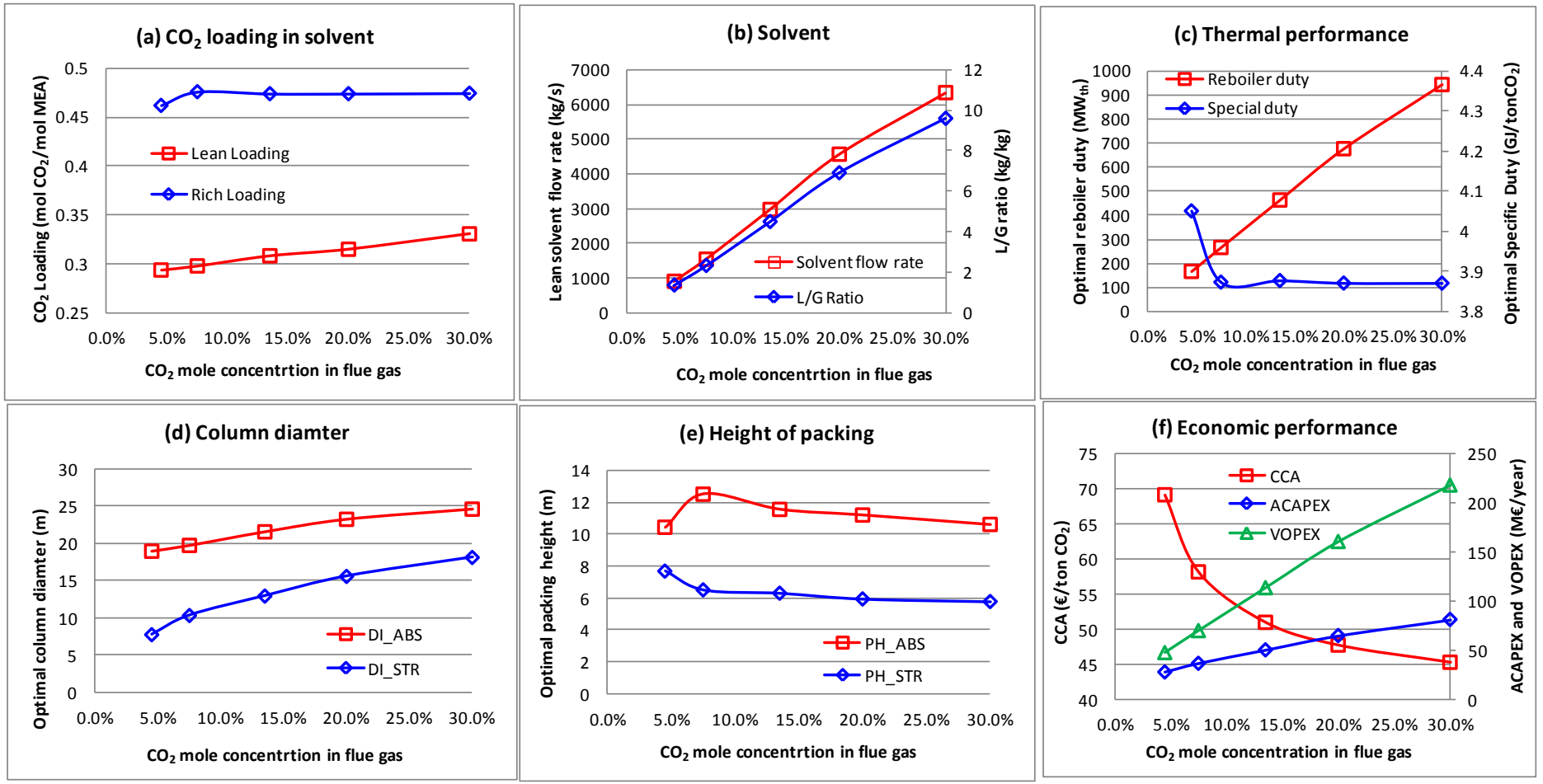


Figure 4.2 Optimisation results with variation of $CO_2$ concentration in flue gas

### 4.4.3 Variation of flue gas flow rate

Another major change is the flow rate of the flue gas, which reflects different sizes of NGCC power plants, or if a part of flue gas is designed to bypass the capture process (Mores et al., 2014) or if operating at part load condition. In this case study, the flow rate of flue gas was specified at 50, 75, 100, 125, 150 % of its value in the base case in Table 4.9. The optimisation results could be found in Table 4.9 and Figure 4.3.

The flow rate change of flue gas (with same $CO_2$ concentration in the flue gas and same capture level) just means simple scale-up or scale-down. With only technical considerations, it is expected that the equipment size should change in proportion with the flow rate change of flue gas and the optimal values for key operational variables should be kept same. However the optimisation results give different answers. The optimal $CO_2$ rich loading keeps high towards its saturated loading. The optimal $CO_2$ lean loading (Figure 4.3 (a)) is stable at around 0.294 in Case F2, F3 and F4 with flue gas flow rate change range of 75–125%. But it rises to 0.315 in Case F1 (50% of flow rate of flue gas) and down to 0.275 in Case F5 (150% of flow rate of flue gas). The optimal reboiler duty is roughly in proportion with the flue gas flow rate which results in a relatively stable specific duty at range of 3.99–4.04 GJ/ton $CO_2$ (Figure 4.3(c)).

It is easy to understand that the diameters of both the absorber and the stripper increase with the increase of flue gas flow rate (Figure 4.3(d)). The optimal packing heights (Figure 4.3(e)) of the absorber are relatively stable in a range of 10.43–11.92 m while the optimal packing heights of the stripper significantly increase from 5.44 m to 9.425 m because of higher solvent regeneration degree (difference between lean loading and rich loading).

The economic results (Figure 4.3(f)) shows that from Case F1 to Case F5, CCA decreases by 26.97%, from 86.538 €/ton $CO_2$ to 63.2 €/ton $CO_2$, although ACAPEX increases by 119.13% and VOPEX increases by 137.11% because the capture $CO_2$ increases by 200%. The results reflect scales effect here. It indicates that, if the capacity meets the requirement, a single train design would be more cost-effective than a multi-train design for a capture plant.

Table 4.9 Optimisation results with variation of flue gas flow rate

| Case tag | F1 | F2 | F3 | F4 | F5 |
|---|---|---|---|---|---|
| Flue gas flow rate (% of the base case) | 50 | 75 | 100 | 125 | 150 |
| $CO_2$ concentration in flue gas (mol%) | 4.50 | 4.50 | 4.50 | 4.50 | 4.50 |
| MEA concentration (wt%) | 35 | 35 | 35 | 35 | 35 |
| $CO_2$ capture level (%) | 90.00 | 90.00 | 90.00 | 90.00 | 90.00 |
| $CO_2$ captured (kg/s) | 20.52 | 30.78 | 41.04 | 51.30 | 61.56 |
| Lean Loading (mol $CO_2$/ mol MEA) | 0.315 | 0.294 | 0.294 | 0.293 | 0.275 |
| Rich Loading (mol $CO_2$/ mol MEA) | 0.463 | 0.465 | 0.462 | 0.464 | 0.467 |
| Flow rate of lean solvent (kg/s) | 542.41 | 701.25 | 905.60 | 1257.06 | 1337.10 |
| L/G ration (kg/kg) | 1.64 | 1.42 | 1.37 | 1.52 | 1.35 |
| Reboiler duty ($MW_{th}$) | 82.92 | 123.70 | 166.21 | 207.37 | 245.67 |
| Specific duty (GJ/ton $CO_2$) | 4.04 | 4.02 | 4.05 | 4.04 | 3.99 |
| Diameter of absorber (m) | 13.37 | 16.17 | 18.93 | 20.65 | 22.75 |
| Packing height of absorber (m) | 11.29 | 11.51 | 10.42 | 11.10 | 11.92 |
| Diameter of stripper (m) | 5.44 | 6.67 | 7.72 | 7.92 | 9.42 |
| Packing height of stripper (m) | 5.35 | 6.84 | 7.68 | 8.87 | 9.48 |
| ACAPEX (M€/year) | 18.74 | 23.41 | 27.79 | 31.92 | 36.97 |
| FOPEX (M€/year) | 4.32 | 5.40 | 6.41 | 7.37 | 8.53 |
| VOPEX (M€/year) | 28.07 | 37.48 | 47.51 | 57.83 | 66.56 |
| TAC (M€/year) | 51.14 | 66.29 | 87.71 | 97.11 | 112.05 |
| CCA (€/ton $CO_2$) | 86.54 | 74.78 | 69.13 | 65.73 | 63.20 |

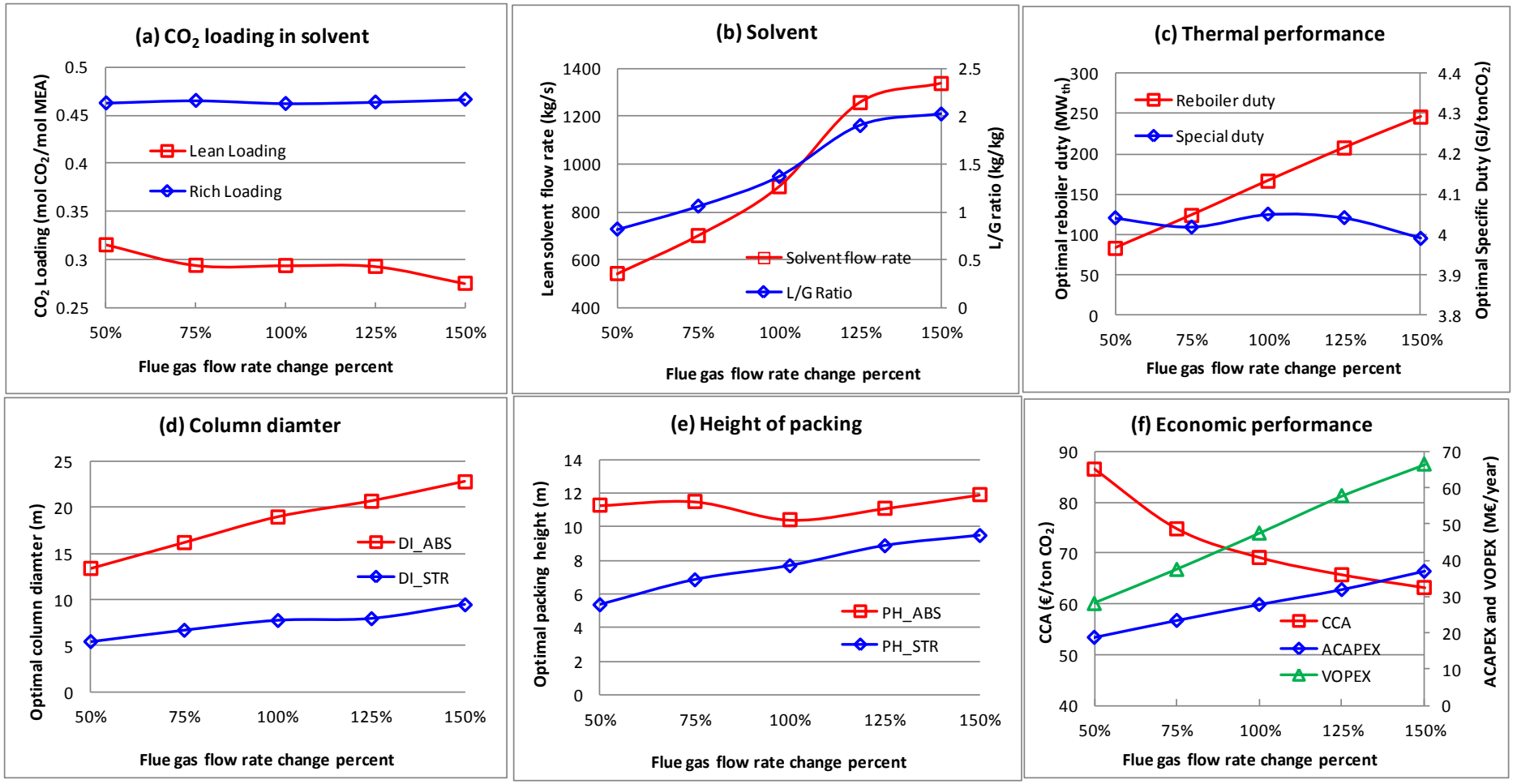


Figure 4.3 Optimisation results with variation of flue gas flow rate

## 4.5 Concluding remarks

In this chapter, the cost model of solvent-based PCC process was developed based on the major equipment costs provided by vendors after detailed engineering design in IEAGHG (2012). The uncertainty of this method could be in the range of from −15% to 20%, instead of other correlation-based methods with uncertainty in the range of from −30% to 50%. The cost model was then integrated into the process model by coding Fortran subroutine in Aspen Plus®. Using this model, the optimisation studies were carried out for the carbon capture process and on the impacts of variations of the key variables.

Compared to the base case, the optimal case has smaller diameter and lower packing height for both the absorber and the stripper. This leads to significant savings in CAPEX. There are also slight savings of VOPEX because of optimal values obtained for key operational variables such as lean loading and L/G ratio. As a result, the cost of $CO_2$ avoided of the optimal case is 69.13€/ton $CO_2$, which is about 18.4% lower than the base case of 86.83€/ton $CO_2$.

Findings from case studies on cost optimisation in response to variations in several key variables include:

- In the optimisations in all cases, the rich solvent reaches its upper loading limit in all the cases at the temperature, pressure and composition conditions.
- The range of optimal lean loading in these three case studies is 0.275–0.331 mol $CO_2$/mol MEA compared with 0.132–0.234 mol $CO_2$/mol MEA from the literature.
- The optimal packing height of the stripper significantly depends on the solvent regeneration degree (difference between $CO_2$ loading in lean solvent and rich solvent).
- The reduction of CCA is more significant when MEA concentration in solvents increases from 20 wt% to 30 wt% than increasing from 35 wt% to 40 wt%.
- For scale-up of the optimal design, scale effect impacts not only economic terms but also process variables. New optimisation could be carried out for each single case to obtain optimal values of both the equipment sizes and key operational variables. It should be aware that optimal values of process variables may drift off recommended ranges by experimental studies. In this case, the optimisation model should be carefully checked to see whether it includes relevant process constraints discovered by experimental studies.

# Chapter 5: Integration of NGCC Power Plant and Solvent-based PCC Process and $CO_2$ Compression Train

This chapter aims to explore the integration between the NGCC power plant and the PCC process and the $CO_2$ compression train. The steady state model of a $453MW_e$ NGCC power plant was developed, including the gas turbine, HRSG and steam turbine. The general interfaces between NGCC and PCC were discussed. Exhaust gas recirculation (EGR) was investigated. The supersonic shock wave compressor was adopted for the $CO_2$ compression and its heat integration options were explored.

## 5.1 NGCC power plant model

### *5.1.1 Modelling of gas turbine*

In the model of a $453MW_e$ of NGCC power plant, GE PG9371FB gas turbine from General Electric was employed. The modelling of gas turbine in Aspen Plus® was performed by combining three process sections including air compressor, combustion reactor and gas expander (Ong'iro et al., 1995). The compressor and expander sections were simulated as isentropic compressors or turbines using *Compr* block in Aspen Plus®, in which, isentropic efficiency and mechanical efficiency could be specified to improve the prediction accuracy (Canepa et al., 2013). The combustor section was simulated with an *RGibbs* reactor block (Ong'iro et al., 1995). The vent oxygen is controlled to a certain value to ensure complete (equilibrium) combustion. It calculates the equilibriums by the Gibbs free energy minimization thus the complicated calculations of reaction stoichiometry and kinetics are avoided with only required inputs of the temperature and the pressure of the reactor. PR-BM (Peng-Robinson equation of state with Boston-Mathias modifications) was used for the property calculations for this gas turbine (Canepa et al., 2013).

One key factor affecting the accuracy of modelling of the gas turbine is the modelling of the turbine cooling. This relatively large cooling flow (approximately 20% of the inlet air flow) has two negative effects: firstly it reduces the temperature of the gas expanding through the turbine, and therefore its power output, secondly it adds losses connected with the mixing of the cooling air with the turbine working fluid. Here a simple and generic method proposed by Jonsson et al. (2005) was used, compared with very detailed and complex modelling in some specific software packages such as Thermoflex®. In this model, a part of fresh air is split from

the exit of the air compressor and bypasses the combustor to mix with the hot combustion gas before entering the gas expander (see Figure 5.1).

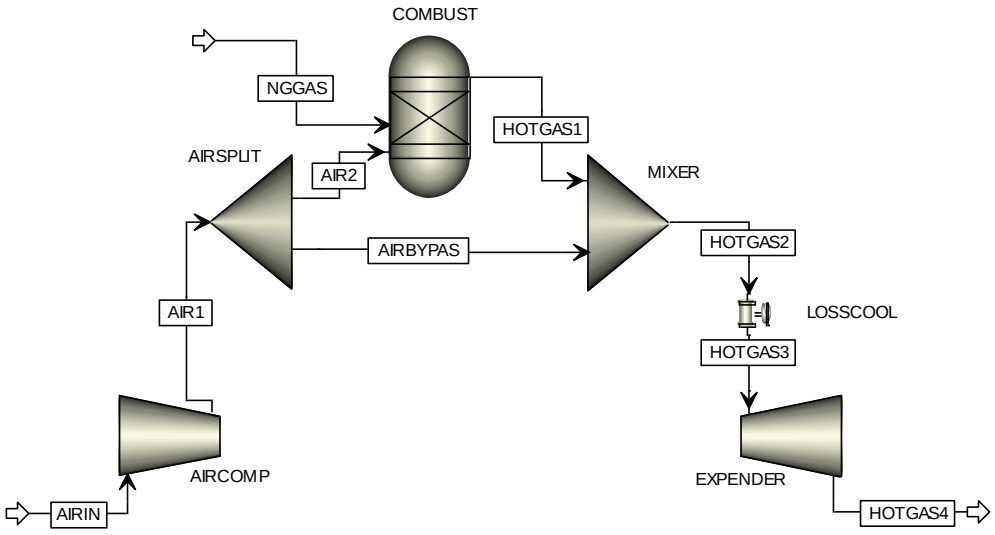


Figure 5.1 Schematic of gas turbine developed in Aspen Plus®

The mass flow rate $\dot{m}_c$ of this bypass air for turbine blade cooling is calculated by Equation (5.1) (Jonsson et al., 2005).

$$\frac{\dot{m}_c c_{p,c}}{\dot{m}_g c_{p,g}} = b\left(\frac{T_{g,cmb\ exit} - T_b}{T_b - T_{c,cmpr\ exit}}\right)^s \tag{5.1}$$

where $b$ and $s$ are tunable parameters; $\dot{m}_g$ is the mass flow rate of the hot combustion gas; $T_b$ represents the maximum blade surface temperature, $c_{p,c}$ and $c_{p,g}$ is the average specific heat capacity of bypass air and hot gas between combustion exit and gas expander.

This pressure drop across the hot gas-cooling air mixer $\Delta P_g$ is calculated using by Equation (5.2) (Jonsson et al., 2005), which is derived from momentum balance.

$$\frac{\Delta P_g}{P_{tbn,inlet}} = -\frac{\dot{m}_c}{\dot{m}_g} K \tag{5.2}$$

where, $K$ is a tunable parameter; $P_{tbn,inlet}$ is the pressure of hot gas entering the gas expander.

During the thermal performance analysis of gas turbine, these three model parameters (b, K and s) can be tuned to represent different type of the gas turbines. The main model inputs and

the results of the model in this study are summarized in Table 5.1, while model performance and validation results are shown in Table 5.2.

Table 5.1 GT modelling assumptions and tuning parameters

| Process conditions | |
|---|---|
| Ambient temperature (°C) | 15 |
| Atmospheric pressure (bar) | 1.00 |
| Air mass flow rate (ton/h) | 2,365 |
| Compressor pressure ratio | 18.3 |
| Compressor isentropic efficiency | 0.915 |
| Expander isentropic efficiency | 0.915 |
| Combustor exit temperature (°C) | 1,425 |
| Tb (°C) | 860 |
| Tuned parameters | |
| S | 1 |
| *B* | 0.1668 |
| *K* | 1.1927 |

Table 5.2 Model validation with manufactory product data sheet

| | This study | GE Product Data (GE Power, 2016) |
|---|---|---|
| Cooling mass flow rate (kg/hr) | 28,700 | – |
| Cooling loss (bar) | −2.45 | – |
| Compressor discharge pressure (bar) | 18.3 | 18.3 |
| Exhaust temperature (°C) | 641.8 | 642.0 |
| Net power output ($MW_e$) | 299.1 | 299.0 |
| Net Efficiency (%, LHV) | 38.7 | 38.7 |
| Exhaust Energy (MJ/h) | 1,704.3 | 1681.0 |

### *5.1.2 Model development for NGCC power plant*

Another part of electricity is generated from the steam cycle. PR-BM method is used for the gas cycle and STEAMNBS (AspenTech, 2012b) property method is used for steam cycle.

Figure 5.2 show the flow diagram of the model. At the ambient conditions (ambient temperature is 9 °C and ambient pressure is 1.01 bar), fresh air is compressed and mixed with natural gas before entering the combustion chamber. The hot gas leaves the combustion chamber at a temperature of 1,427 °C. The hot gas expands in the gas turbine and consequently generates a part of the total electricity output of the NGCC power plant. Exhaust gases from the gas turbine is used to generate steam in the HRSG. Steams from different stages of the HRSG go to the high pressure steam turbine (HP-ST), the intermediate pressure steam turbine (IP-ST) and the low pressure steam turbine (LP-ST) to generate another part of the total electricity output of the NGCC power plant. The main model parameters are given in Table 5.3.

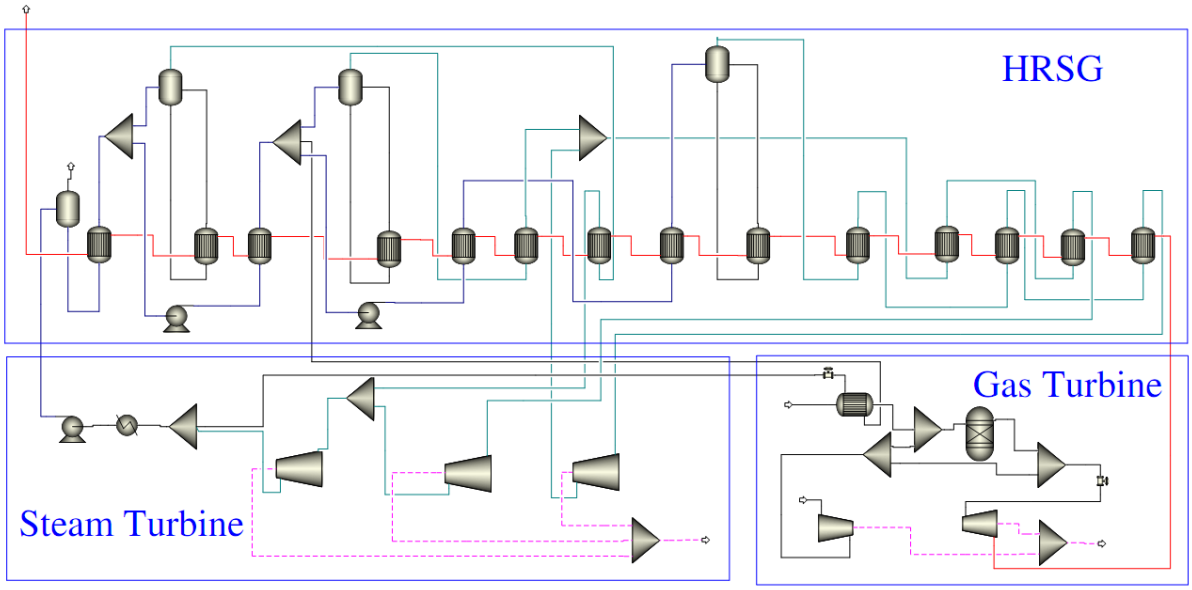


Figure 5.2 The flowsheet of NGCC power plant standalone

One feature of this model is that the steam conditions of HRSG are higher in both temperature and pressure than what is currently obtainable. The pressure and temperature of high pressure steam are 170 bar and 600 °C compared to about 120 bar and 556°C in existing cases. The pressure and temperature of intermediate pressure steam are 40 bar and 600 °C compared to about 30 bar and 550°C in existing cases. An explanation is described in the referred benchmark report (IEAGHG, 2012) as the original equipment manufacturers are already considering similar steam conditions and it is considered that utilizing these conditions in NGCC power plant will be proven and typical by 2020.

Table 5.3 Model parameters of NGCC power plant

| Parameters | | Value |
|---|---|---|
| Natural gas composition | $CH_4$ (vol%) | 89 |
| | $C_2H_6$ (vol%) | 7 |
| | C3–C5 (vol%) | 1.11 |
| | $CO_2$ (vol%) | 2 |
| | $N_2$ (vol%) | 0.89 |
| Steam turbine | Steam inlet of HP turbine (bar/°C) | 172.6/601.7 |
| | Steam inlet of IP turbine (bar/°C) | 41.5/601 |
| | Steam inlet of LP turbine (bar/°C) | 5.8/293.1 |
| | HP/IP/LP turbine efficiencies (%) | 92/94/90 |
| Minimum temperature approach of HRSG | Steam and gas (°C) | 25 |
| | Gas and boiling liquid (°C) | 10 |
| | Liquid and gas (°C) | 10 |
| | Approach of economizer (°C) | 5 |
| Condenser pressure and temperature (bar/°C) | | 0.039/29.0 |

### *5.1.3 Model validation*

For large scale NGCC power plant simulations, operational or experimental data for model validation purpose is not available. In this study, the simulation results using Aspen Plus® were compared with the simulation results using another software package, GT Pro®, in order to make a brief validation. Table 5.4 shows the comparison results of Aspen Plus® and GT Pro®, which appear to be in good agreement.

Table 5.4 Comparison of the simulation results for model validation

| Input | | |
|---|---|---|
| Fuel flow rate (kg/s) | 16.62 | |
| Air flow rate(kg/s) | 656.94 | |
| Validation results | | |
| | IEAGHG, (2012) | This study |
| Temperature of flue gas to HRSG (°C) | 638.4 | 638.4 |
| Flow rate of flue gas to HRSG (kg/s) | 114.97 | 114.97 |
| HP turbine inlet pressure, temperature (bar/°C) | 172.5/601.7 | 172.6/601.7 |
| IP turbine inlet pressure, temperature (bar/°C) | 41.4/601.5 | 41.5/601.0 |
| LP turbine inlet pressure, temperature (bar/°C) | 5.81/293.3 | 5.8/293.1 |
| Condenser pressure and temperature (mbar/°C) | 0.04/29.2 | 0.039/29.0 |
| Gas turbine power output ($MW_e$) | 295.24 | 295.03 |
| Steam turbine power output ($MW_e$) | 171.78 | 170.71 |
| Net plant power output ($MW_e$) | 455.15 | 453.872 |
| Net plant efficiency (%,LHV) | 58.87 | 58.74 |

## 5.2 Integration of NGCC with PCC process and $CO_2$ compression

### *5.2.1 General interfaces of the integration*

When an NGCC power plant is designed or retrofitted with a PCC and compression processes, some structural modifications are required for basic interfaces. These include: (1) connecting flue gas from exit of HRSG of the power plant to the PCC process, (2) extracting low pressure steam from the steam cycle of the power plant to provide heat for solvent regeneration in the PCC process, (3) connecting steam condensate outlet in the PCC process to the steam cycle of power plant, and (4) electrical power connection from the power plant to service electrical power consumption in the PCC and $CO_2$ compression processes.

The process flow diagram can be seen in Figure 5.3. Flue gas leaves the HRSG at a temperature of around 80 °C and enters a gas conditioning unit which consists of a direct contact column (DCC), a water recirculating pump and a blower. The flue gas is then cooled down to 40–50 °C (Kvamsdal et al., 2011b) by a spray of water at 25 °C, in order to improve the absorption efficiency and to reduce solvent evaporation losses in the absorber (Wang et

al., 2011). At the same time, a part of water is removed from the flue gas due to the condensation. The flue gas is pressurized by the blower before it feeds into the absorber.

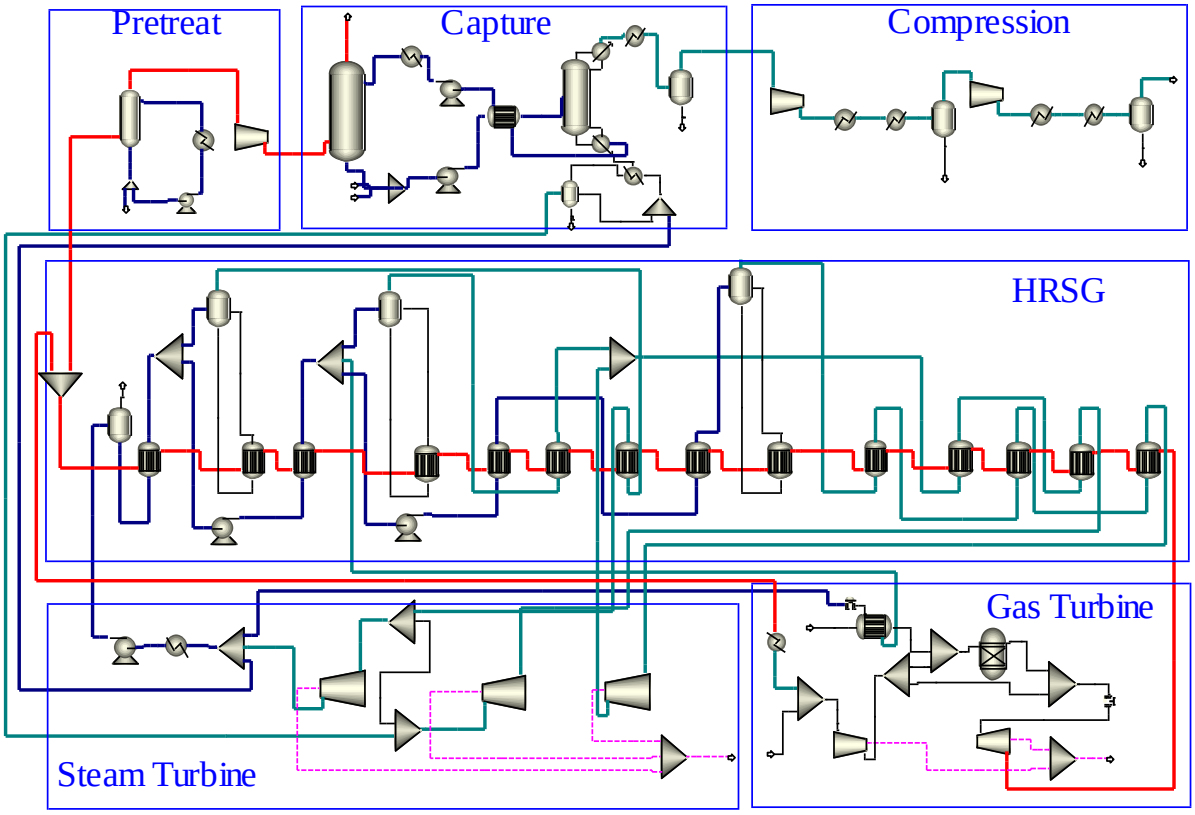


Figure 5.3 The flowsheet of NGCC power plant with EGR integrated with PCC process and compression

Heat input for the solvent regeneration process is provided by extracting low pressure steam from the steam cycle of the NGCC power plant into the stripper reboiler of the PCC process. The flow rate of the steam extraction is decided by the operating conditions of PCC process and has a large impact on the output of the power plant. Considering that high temperature would result in thermal degradation of the solvent in the reboiler and the stripper, normally, the temperature of the reboiler is maintained between 110 °C to 130 °C at an operating pressure of 1.6–2.0 bar. There are three potential configurations, clutched turbine, throttled turbine and floating crossover pressure, in the NGCC power plant process for steam extraction (Kang et al., 2011). In this study, the steam is extracted off from the floating IP/LP crossover, the most feasible solutions for steam extraction (Lucquiaud and Gibbins, 2009), at 5.8 bar and 303 °C. Before the steam enters the reboiler, it is cooled down just above saturation temperature with a spray of the condensate circulated from the reboiler, which helps to reduce the requirement of steam to be extracted from the power plant. After heat

exchange inside the reboiler, the steam is cooled down to condensate, which then is returned to the deaerator in the HRSG of the power plant for cycling.

### 5.2.2 EGR technology

One disadvantage of using PCC process to NGCC power plant is that the $CO_2$ concentration in flue gas is as low as 3–4 mol% whilst it is 11–13 mol% for a coal fired power plant, resulting in lower absorption efficiency and larger equipment size in PCC capture plant (Jonshagen et al., 2011; Biliyok et al., 2013). EGR is regarded as an effective solution. The underpinning of EGR is that the $O_2$ concentration in the flue gas leaving from the HRSG is still high (11.41 mol% in this study). Even though EGR is applied, a relatively high oxygen concentration in the combustion air can be ensured with an appropriate recirculation ratio. However, in order to ensure the combustion efficiency in the burner, the minimum oxygen concentration in combustion air should be 16 – 18 mol % (Ulfsnes et al., 2003; Canepa et al., 2013).

In this study, EGR ratio of 0.38 is selected to ensure the minimum oxygen content of 16 mol%. Table 5.5 presents the comparison results of the integration without EGR and with EGR. With EGR, 4.73 kg/s less steam is extracted for solvent regeneration. So the net power generated from the gas turbine section decreases by 0.39 $MW_e$ but steam turbines section generates more by 4.13 $MW_e$. At the same time, significant equipment size reductions are achieved for both absorber and stripper in the case with EGR. In this case, the flow rate of the flue gas feed reduces by 38% which results in 37.39% and 9.36% reduction of the cross-section area of the absorber and stripper respectively. The reason for the difference between these values is that the required cross-section area of a column is decided by both gas phase and liquid phase loadings inside the column. Although the flow rate of flue gas reduces 38%, the flow rate of lean solvent only decreases by 8.1% because higher liquid gas ratio (L/G ratio) is needed for higher $CO_2$ concentration in the flue gas (it increases from 4.5 mole% to 7.32 mol%). The economic results shows CCA in the case with EGR decreases 5.12%, from 69.713 €/ton $CO_2$ to 66.142 €/ton $CO_2$ while CAPEX decreases by 6.81% and VOPEX decrease by 2.93%.

Table 5.5 Optimal design of the integration without EGR and with EGR

| Category | Parameter | without EGR | with EGR |
|---|---|---|---|
| Power plant performance | Flow rate of fresh air intake (kg/s) | 656.94 | 407.45 |
| | $O_2$ concentration in combustion air (mol %) | 20.74 | 16.0 |
| | $O_2$ concentration in gas turbine vent gas (mol%) | 11.4 | 6.45 |
| | Gas turbine power output ($MW_e$) | 295.03 | 294.64 |
| | Steam turbine power output ($MW_e$) | 113.56 | 117.69 |
| | Steam extracted for reboiler (kg/s) | 76.39 | 71.06 |
| | Flow rate of flue gas to PCC (kg/s) | 660.54 | 408.75 |
| | $CO_2$ concentration in flue gas (mol%) | 4.5 | 7.32 |
| PCC technical performance | $CO_2$ captured (kg/s) | 41.04 | 40.94 |
| | Lean loading (mol $CO_2$ /mol MEA) | 0.294 | 0.299 |
| | Rich loading (mol $CO_2$ /mol MEA) | 0.462 | 0.472 |
| | Flow rate of lean solvent (kg/s) | 905.60 | 987.65 |
| | L/G (kg/kg) | 1.37 | 1.495 |
| | Reboiler duty (kW) | 166.26 | 164.003 |
| | Specific duty (GJ/ton $CO_2$) | 4.05 | 4.01 |
| | Absorber pressure loss (bar) | 0.048 | 0.036 |
| | Absorber diameter (m) | 18.93 | 16.13 |
| | Packing height of absorber (m) | 10.43 | 10.37 |
| | Stripper pressure loss (bar) | 0.012 | 0.011 |
| | Stripper diameter (m) | 7.72 | 7.35 |
| | Packing height of stripper (m) | 7.68 | 6.87 |
| PCC economic performance | CAPEX (M€) | 213.78 | 199.21 |
| | FOPEX (M€/year) | 6.41 | 5.89 |
| | VOPEX(M€/year) | 47.51 | 46.11 |
| | TAC (M€/year) | 81.71 | 77.99 |
| | CCA (€/ton $CO_2$) | 69.13 | 66.14 |

## 5.3 Heat integration options based on supersonic shock wave compression

### *5.3.1 $CO_2$ compression technology*

After the $CO_2$ leaves the capture plant, it will be transfered for geologic sequestration. In the transport section of CCS, pipelines are the preferred method for onshore and offshore transport of large volumes of $CO_2$. The dense phase is regarded as the most energy-efficient condition due to its high density and low viscosity. Consequently, current operating practice for $CO_2$ pipelines is to maintain the pressure well above the critical pressure. Considering the pressure drop along the length of the pipeline and the impact of the elevation change and impurities, the entry pressure of the $CO_2$ pipeline network is as high as 110–150 bar. Thus a compression train is required to pressurize the $CO_2$ stream from PCC captured plant to reach a so high entry pressure.

One limitation of conventional compressor is that the pressure ratio per stage is normally less than 3, otherwise the efficiency would decrease drastically as the temperature rises with the pressure during the adiabatic compression process. Thus 6 – 16 stage compressor is normally required. Witkowski et al. (2013) performed a thermodynamic evaluation of various $CO_2$ compression configurations with 6 – 12 stages compressor based on conventional centrifugal compressor and integrally geared compressor. In Section 6.4 in this study, a comprehensive techno-economic evaluation was conducted for different configuration of compression train. The optimal option was selected to get a minimum annual cost including annualized capital cost, operating and maintenance cost and energy cost. The optimal configuration of the compression train compromises 6 stages integrally geared following pumping and intercoolers with an exit temperature of 20 $^{o}$C. The multi-stage compression means a great capital investment in terms of the equipment material cost, construction and installation cost.

With the aim to address the challenge of the high investment cost, supersonic shock wave compression technology was developed by RAMGEN Power System (Lawlor, 2009) for $CO_2$ compression. The shock wave compression only needs two stages of compression (compared with 6 to 16 stages for the conventional multi-stage approach), and the potential capital cost saving for compression chain is up to 50% (Ciferno et al., 2009) in addition to reduced footprint requirement. The discharge temperature of compressed $CO_2$ is as high as 246–285$^{o}$C (Witkowski et al., 2013) due to higher pressure ratio of each stage, providing an opportunity for compression heat integration.

In this study, supersonic shock wave compression technology was adopted for the $CO_2$ compression. The compression model was developed also in Aspen Plus® and was validated with published data from RAMGEN Power System (Lawlor, 2009). After that, the inlet and outlet pressure of the compression train were modified to adopt for the boundary conditions in this study. The model parameters are seen in Table 5.6. In terms of reliability, there is no report about the comparison between this new compression technology and conventional compressors. However, it should be aware that reliability of compressors is an important performance for real industrial applications.

Table 5.6 Process boundary conditions and parameters of $CO_2$ compression

| Parameters | Value |
|---|---|
| Flow rate of $CO_2$ stream (kg/s) | 41.04 |
| Inlet pressure (bar) | 1.9 |
| Inlet temperature ($^oC$) | 20 |
| Outlet pressure (bar) | 136 |
| Stage number | 2 |
| Exit temperature of stage 1($^oC$) | 214.5 |
| Exit temperature of stage 2 ($^oC$) | 230.5 |
| pressure ratio per stage | 8.65 |
| Isentropic efficiency (%) | 85 |
| Intercooler exit temperature ($^oC$) | 20 |
| Last stage exit temperature ($^oC$) | 20 |
| Pressure drop of intercooler (%) | 3 |
| Power consumption ($MW_e$) | 14.8 |

### *5.3.2 Heat integration case setups*

Table 5.6 shows that the exit temperature of the $CO_2$ stream is as high as 214.5–230.5 °C for the supersonic shock wave compressors. At this temperature, the compression heat could be recovered by integrating the pressurized streams with low temperature streams in the NGCC power plant and the PCC process. Two options could be justified as below.

1) The compression heat is integrated into the steam generation cycle of HRSG to generate more steam.

In the NGCC power plant, the steam coming out of the LP-ST is cooled down to condensate with a temperature of 29.0 °C at a pressure of 0.039 bar before it is pressurized to a high pressure by a pump. Then the subcooled water enters the economizer section of HRSG, in which, it is heated to around 158°C by the hot flue gas in normal case. Applying this heat integration option, this subcooled water could be lined to the compression train first as a refrigerant of the intercoolers. With this additional heat recovered from compression process, more LP steam generation is expected to go to the LP-ST to generate more electricity.

2) The compression heat is integrated into the stripper reboiler of the PCC process for solvent regeneration.

In the PCC process, the operating temperature range of the stripper reboiler is from 110°C to 125°C, which is much lower than the exit temperature of each stage of the compressor. So the compression heat could be transferred to provide heat to the reboiler. However, the reboiler duty is so high that the compression exhaust heat cannot satisfy the reboiler duty requirement. Thus, the steam from the power plant is still required at the same time using a multiple shell kettle reboiler (Shah and Sekulic, 2003).

In previous sections, different process integration options were discussed when NGCC power plant is integrated with a PCC process and the $CO_2$ compression. A case study was conducted for the evaluation of power consumptions and heat requirement of different options for comparison purposes. For the case setup, five scenarios were summarized as below:

1) Reference case: NGCC power plant without integration with PCC and compression
2) Case 1: NGCC power plant without EGR integrated with PCC and compression without compression heat integration
3) Case 2: NGCC power plant with EGR integrated with PCC and compression without compression heat integration
4) Case 3: NGCC power plant with EGR integrated with PCC and compression with compression heat integration into the steam cycle of HRSG
5) Case 4: NGCC power plant with EGR integrated with PCC and compression with compression heat integration into the reboiler of the stripper

### 5.3.3 Results and discussion

Table 5.7 shows the results of energy and electricity consumptions of each case. By comparing the reference case (NGCC standalone) and Case 1, a total 9.58%-points net power efficiency decrease is observed when the NGCC power plant integrated with the PCC process. This obvious reduction is caused by three main factors: 1) the steam through the LP-ST decreases hugely to lead to a power output reduction because of steam extraction, which contributes 7.40%-points net efficiency decrease; 2) the electricity consumption of $CO_2$ compression contributes 1.92%-points net efficiency decrease; 3) auxiliary electricity consumption of the blower and solvent circulation pumpers accounts for 0.55%-points net efficiency decrease.

The results of Case 2 shows EGR help to achieve a 0.77% efficiency improvement compared with Case 1. The reason is dissected as follows. Firstly, the specific reboiler duty decreases to 4.31 $MJ_{th}$/kg $CO_2$ from 4.54 $MJ_{th}$/kg $CO_2$. The absorption efficiency is improved because of increase in the $CO_2$ concentration in the flue gas (from 4.5 mol% to 7.32 mol% in Table 5.5), which leads to a higher rich solvent loading and then a lower recirculating solvent flow rate. The above results in a lower reboiler duty for the solvent regeneration. Secondly, the power consumption of the PCC process reduces to 2.04 $MW_e$ from 4.24 $MW_e$. With EGR at a ratio of 0.38, the flue gas flow rate decreases significantly, which causes a great reduction of the power consumption of the blower at the upstream of the absorber. Meanwhile, the simulation results show the discharge pressure of the blower also decreases because of the decrease of the whole tower pressure drop of the absorber (see Table 5.5).

Applying compression heat integrations into the main process of NGCC and PCC, Case 3 and Case 4 improves the net LHV efficiency of the power plant to 50.25% and 50.47% respectively. In Case 3, the subcooled water from the feed water pump of the HRSG is lined to the compression train and is heated to around 65°C before entering the economizer of the HRSG. One limitation of this option is that the temperature of the water leaving the economizer should be lower than its boiling temperature, otherwise there would be vapour phase exiting in its downstream pump. In Case 4, the temperature of the stream from compression train is 135 °C, which is still higher than expected recoverable temperature of 90 °C, after it exchanges heat the stripper reboiler. Thus more efficiency improvement could be achieved by combining other low-temperature heat recover technology.

Table 5.7 Performance comparison results of different cases

| Description | Reference | Case 1 | Case 2 | Case 3 | Case 4 |
|---|---|---|---|---|---|
| Major process components | NGCC | NGCC +PCC | NGCC +PCC | NGCC +PCC | NGCC +PCC |
| The application of EGR | without EGR | without EGR | with EGR | with EGR | with EGR |
| Compression heat integration | without | without | Without | with HRSG | With reboiler |
| Gas turbine power output ($MW_e$) | 295.03 | 295.03 | 294.64 | 294.64 | 294.64 |
| Steam turbine power output ($MW_e$) | 170.71 | 113.56 | 117.69 | 120.14 | 121.85 |
| Power island power consumption ($MW_e$) | 11.69 | 9.7 | 9.7 | 9.7 | 9.7 |
| $CO_2$ compression power consumption ($MW_e$) | – | 14.8 | 14.8 | 14.8 | 14.8 |
| Power consumption in PCC ($MW_e$) | – | 4.24 | 2.04 | 2.04 | 2.04 |
| Stripper reboiler duty ($MW_{th}$) | – | 186.8 | 176.2 | 176.2 | 176.2 |
| Steam extracted for reboiler (kg/s) | – | 76.39 | 71.06 | 71.06 | 65.50 |
| $CO_2$ captured (kg/s) | – | 41.11 | 40.92 | 40.92 | 40.92 |
| Specific reboiler duty ($MJ_{th}$/kg $CO_2$) | – | 4.54 | 4.31 | 4.31 | 4.31 |
| Net plant power output ($MW_e$) | 453.87 | 379.85 | 385.80 | 388.25 | 389.96 |
| Net plant efficiency (%, lower heating value) | 58.74 | 49.16 | 49.93 | 50.25 | 50.47 |
| Efficiency decrease (%-points) compared with reference case | – | 9.58 | 8.81 | 8.49 | 8.27 |
| Efficiency increase (%-points) compared with Case 1 | – | – | 0.77 | 1.09 | 1.31 |

As a comparison of these two options, Marchioro Ystad et al. (2013) reported that employing a $CO_2$ Rankine cycle with an additional turbine improves the thermal efficiency by 1.63%-points. In this study, there is no major capital cost required for the integration options in both Case 3 and Case 4. These efficiency improvements are meaningful especially considering great amount of the total electricity output from the gas-fired power plants. Taking the total number of gas-fired electricity consumption in EU (2016b) in 2015 as the calculation base, the annual saving could be around 100 M€, assuming that this heat integration is applied to even only 5% of the gas-fired power plants in Europe.

## 5.4 Concluding remarks

This chapter presents the investigation on thermal performances of different the integration options of a 453$MW_e$ NGCC equipping with a PCC process and a $CO_2$ compression train. The process models of each process were developed using Aspen Plus® and were validated with published data or experimental data. The effect of EGR to the performance of the integration was investigated first. Significant savings was achieved with the contributions from both the CAPEX and VOPEX. The CCA of the case with EGR decreases 5.12% compared with the case without EGR, from 69.13 €/ton $CO_2$ to 66.14 €/ton $CO_2$.

Integrated with the PCC process and the compression train, the thermal efficiency (LHV) of the NGCC power plant deceases from 58.74% to 49.16%. This reduction includes 7.40%-points decrease due to steam extraction, 0.55%-points reduction due to PCC power consumption and 1.92%-points reduction due to compression train power consumption. With the application of EGR in the NGCC power plant at a recirculation ratio of 0.38, the net efficiency increases 0.77%-points while the cross-section areas of the absorber and stripper in the carbon capture process reduced by 37.39% and 9.36% respectively. The compression heat integration options have been analysed by applying supersonic shock wave compression technology. Compression heat integration into the steam cycle of HRSG and stripper reboiler achieves 0.32%-points and 0.54%-points net efficiency improvement separately without major capital investment required. The study indicates that EGR technology, supersonic shock wave compression technology and compression heat integrations could be future directions for commercial PCC deployment in NGCC power plants.

# Chapter 6: Optimal Design of $CO_2$ Transport Pipeline Network

This chapter presented the study on optimal design of the pipeline network planned in the Humber region of the UK. Steady state process simulation models of the $CO_2$ transport pipeline network were developed using Aspen HYSYS®. The simulation models were integrated with Aspen Process Economic Analyser® (APEA). Techno-economic evaluations for different options were conducted for the $CO_2$ compression train and the trunk pipelines respectively. The evaluation results were compared with other published cost models. Optimal options of compression train and trunk pipelines were applied for the whole pipeline network. The overall cost of $CO_2$ transport pipeline network was analysed and compared between the base case and the optimal case.

## 6.1 Pipeline network system

In the UK, the Humber region offers good opportunities for CCS deployment as it is not only the biggest $CO_2$ emission area in the UK, but also the area with easy reach to $CO_2$ offshore storage sites in the North Sea (Lazic et al., 2013). There are two advanced proposals for CCS power station developments that utilise the trunk pipelines: The Don Valley Power Project (DVPP) and the White Rose CCS Project (even though cancelled very recently). DVPP will use pre-combustion carbon capture technology at a new-build integrated gasification combined cycle (IGCC) power plant of 920 $MW_e$ gross output (CCSA, 2014). The White Rose CCS project is a demonstration project of an oxy-fuel power plant of 450 $MW_e$ gross output (CPL, 2013).

Figure 6.1 shows the proposed route corridor of the pipeline network. $CO_2$ captured from DVPP will be transported in gaseous phase at a maximum allowable operating pressure (MAOP) of 35 bar, and would then be boosted to dense phase by a compressor near the multi-junction site, before joining the dense phase $CO_2$-rich stream from the White Rose CCS plant. The combined $CO_2$-rich stream will then be transported in dense phase via an onshore trunk pipeline with a MAOP of 136 bar. The onshore pipelines are buried under ground 1.2 m. A booster pumping station located near the coast will boost the pressure of the $CO_2$-rich stream before it is transported in the offshore trunk pipeline with a MAOP of 186 bar to a saline aquifer storage site more than 1 km beneath the bed of the North Sea. Table 6.1 presents the key parameters of the pipelines. The material of pipelines is carbon steel and the size of pipelines follows ANSI standard.

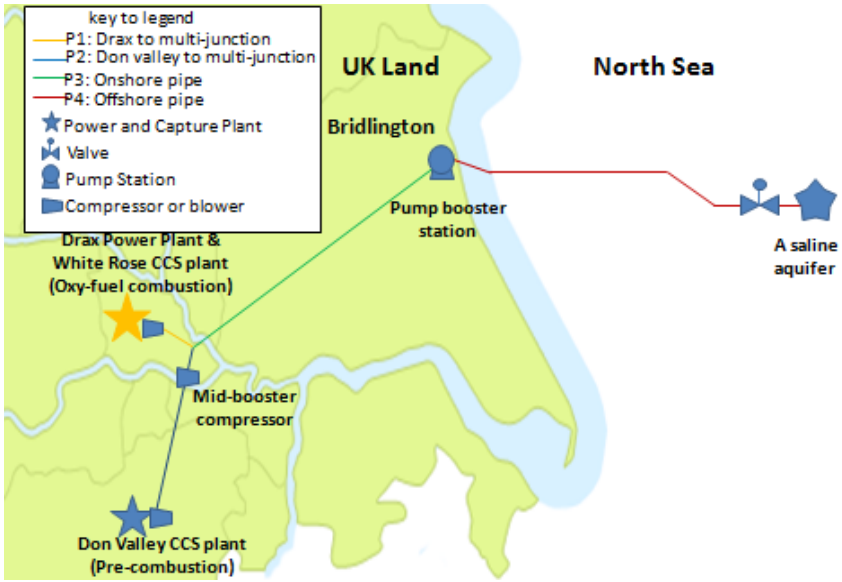


Figure 6.1 The pipeline sketch for the Humber case study

Table 6.1 Parameters of the pipelines

| Emitter | Flow rate range | Collecting pipelines | | Onshore trunk pipeline | | Offshore trunk pipeline | |
|---|---|---|---|---|---|---|---|
| | | Length | Internal diameter | Length | Internal diameter | Length | Internal diameter |
| | Mt/a | km | mm | km | mm | km | mm |
| Don Valley | 0.91–6.27 | 15 | 738.2 | 71 | 571.8 | 91 | 559.2 |
| White Rose | 0.61–2.65 | 5 | 295.5 | | | | |

An entry specification for the $CO_2$-rich stream is needed to define the acceptable range of composition, taking into account safety, impact on pipeline integrity and hydraulic efficiency (Race et al., 2012). In this case study, the entry specification was defined to be 96 mol% $CO_2$ and a mixture of nitrogen, oxygen, hydrogen, argon and methane with hydrogen limited to 2.0 mol% and oxygen limited to 10 ppmv.

## 6.2 Process model development and economics evaluation methodology

For a real $CO_2$ pipeline network project described in Section 6.1, the techno-economic evaluation should be more detailed and realistic. In this study, process simulation models were developed in Aspen HYSYS®. Then the simulation results were exported into APEA for economic evaluation.

### *6.2.1 Process simulation model development for the base case*

#### 6.2.1.1 Physical property method

The cubic equation of state (EOS) has been widely used to calculate the physical properties of $CO_2$ for pipeline transport modelling (Li and Yan, 2009). Peng-Robinson EOS (Peng and Robinson, 1976) is most frequently used. More complex EOS such as Lee Kesler (Lee and Kesler, 1975), SAFT (Wertheim, 1984; Wertheim, 1986), Span and Wagner (Span and Wagner, 1996) and GERG (Kunz and Wagner, 2012) were used in recent studies. There is no consensus in the literature regarding the best EOS for the design of $CO_2$ pipelines. (Diamantonis et al., 2013) compared the results of several EOS with experimental data and found that PR EOS is of reasonable accuracy, even when compared with more advanced EOS, when binary interaction parameters are used. In this study, PR EOS has been selected considering both the accuracy and the simplicity.

In this study, PR EOS with calibrated binary interaction parameters has been used considering both the accuracy and the simplicity. Table 6.2 lists the calibrated binary interaction parameters for PR-EOS used in this study. The APEs between the calculations of PR EOS and the experimental data were listed for corresponding $k_{ij}$ values. For calibration of $k_{ij}$ of $CO_2$-$H_2$, there is no good agreement among the available experimental data and there is no liquid volume experimental data.

One weakness of PR EOS reported by E.ON's report (E.ON, 2010) is that it is very accurate in the near-critical region. This study focuses on the techno-economic evaluations based on steady state simulations. For the trunk pipeline transport section, $CO_2$-rich stream is in the subcooled liquid phase. The temperature range is from 4$^{o}$C to 20$^{o}$C and the pressure range is from 101 bar to 150 bar, which is far away from the critical region of the $CO_2$. In this T/P range, the deviation of pure $CO_2$ density is from -4.8% to 0.1% for the calculations of PR compared to the calculations of SW according to the comparison results from E.ON's report.

Table 6.2 APE between experimental data and PR-EOS for corresponding $k_{ij}$ values

| Binary | $k_{ij}$ | Bubble pressure | | | Liquid volume | | | Reference |
|---|---|---|---|---|---|---|---|---|
| | | Temp. (K) | Pressure (MPa) | APE (%) | Temp. (K) | Pressure (MPa) | APE (%) | |
| $CO_2$- $N_2$ | −0.007 | 220–301 | 1.4–16.7 | 3.73 | 209–320 | 1.4–16.7 | 1.54 | Li and Yan (2009) Diamantonis et al. (2013) |
| $CO_2$- Ar | 0.141 | 288 | 7.5–9.8 | 2.32 | 288 | 2.4–14.5 | 1.83 | Diamantonis et al. (2013) |
| $CO_2$- $H_2$ | 0.147 | 290.2 | 5.0–20.0 | 5.6% | – | – | – | Foster et al. (2010) |

### 6.2.1.2 Assumptions, constraints and inputs

The maximum entry flow rates from both the White Rose plant and the Don Valley plant and the highest ambient temperature were chosen as the base case. This is considered as the worst case scenario with respect to the energy requirement since it would require the highest entry pressure and the greatest boosting pressure at the pump station. Figure 6.2 shows the flowsheet of pipeline network developed in this study.

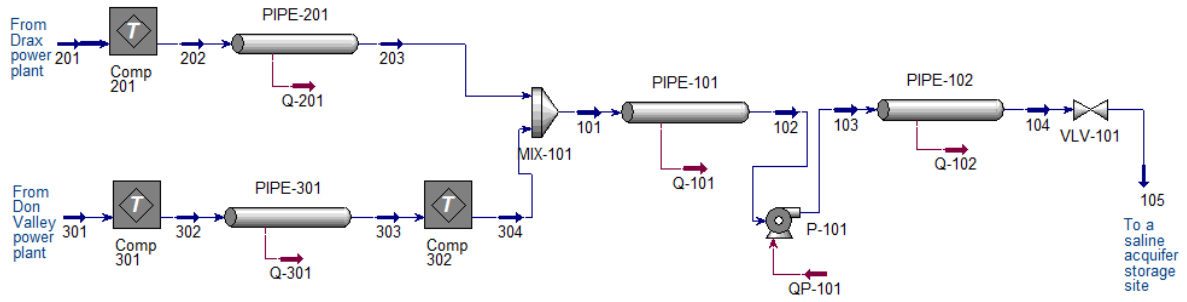


Figure 6.2 The flowsheet of pipeline network in Aspen HYSYS®

The assumptions made for the pipeline network model are as follows: (1) the pressure drops across valves and other fittings are negligible; (2) the adiabatic efficiencies of compressors and pumps used in this model are fixed at 75%.

The pressure settings of key sections are based on two operational constraints: (1) the entry pressure (i.e. the outlet pressure of the compressor at each capture plant) should be high enough to maintain a minimum pipeline operating pressure of 101barg to avoid two phase flow in the common pipeline; (2) a constant injection pressure of 126 bar is specified to satisfy the injection rate. In reality, the required injection pressure at the offshore storage site will rise over the lifetime of the operation with injection pressures below 126 bar being

sufficient in the initial phase. The input and boundary conditions for the base case are specified in Table 6.3.

Table 6.3 Input and boundary conditions of the base case

| | unit | White Rose | Don Valley |
|---|---|---|---|
| Capture technology | – | oxy-fuel | IGCC |
| Composition of $CO_2$ -rich stream | mol% | 96%$CO_2$, 2%$N_2$, 2%Ar | 96%$CO_2$, 2%$N_2$, 2%$H_2$ |
| Flow rate | t/h | 334.596 | 791.667 |
| Suction pressure of compression | bar | 1 | 1 |
| Suction temp. of compression | $^oC$ | 20 | 20 |
| Number of compression stages | – | 5 | 4 |
| Exit pressure of compression | bar | 112.5 | 35 |
| Exit temp. of compression | $^oC$ | 20 | 20 |
| Number of mid-compressor stages | – | – | 2 |
| Exit pressure of mid-compression | bar | – | 121.23 |
| Trunk pipelines entry temperature | $^oC$ | 20 | 20.0 |
| Differential pressure of pump station | bar | 43 | |
| Offshore platform arrival pressure | bar | 126 | |

#### 6.2.1.3 Model validation

For large scale $CO_2$ pipeline network simulations, operational or experimental data for model validation purpose is not available as the projects considered are currently only in the planning stage. In this study, the results of the Aspen HYSYS® base case model were compared with the results from another software package, PIPE-FLO® from industrial collaborator National Grid. Table 6.4 shows the results of Aspen HYSYS® and PIPE-FLO®, which appear to be in good agreement.

Table 6.4 Comparison of the simulation results

| | Entry pressure at White Rose | Entry pressure at Don Valley | DP of mid-booster for Don Valley | DP of pump station | Arrival pressure |
|---|---|---|---|---|---|
| | bar | bar | bar | bar | bar |
| Aspen HYSYS® | 120.5 | 35 | 86.92 | 43 | 126 |
| PIPEFLO® | 120.2 | 35 | 86.70 | 42.4 | 126 |
| APE (%) | 0.25 | – | 0.25 | 1.40 | – |

### *6.2.2 Economic evaluation methodology*

Economic evaluations were conducted using APEA V8.0 using data from the 1st quarter of 2012. APEA becomes an industry-standard tool known to be far more accurate than correlation-based economic approaches and is used for engineering design of many projects. APEA includes design procedures and costs data for hundreds of types of materials of projects. A bottom-up approach is used in APEA. When the simulation models are exported into APEA, the unit operations are mapped and sized according to relevant design codes. Then the cost was estimated for single piece of equipment.

The total cost includes capital expenditure (CAPEX) and operational expenditure (OPEX). OPEX can be split into fixed OPEX (operating and maintenance (O&M) cost) and variable OPEX (mainly the energy and utilities cost). In this study, for a clearer comparison, the annual cost and the levelised cost (per ton of $CO_2$) were used. The total annual cost was split into annualized capital investment cost (capital return factor is 0.15), annual O&M cost and annual energy and utilities cost. In consistency with that, the levelised cost was split into levelised capital cost, levelised O&M cost and levelised energy and utilities cost.

To harmonize results for comparison with other studies, the following assumptions are made: 1) the project begins in January 2012; 2) all costs are corrected to €2012 using the average inflation index; 3) the captured $CO_2$ mixture has neither economic value nor disposal cost; 4) cooling water is sourced from a nearby body of water at the cost of pumping and operation of a cooling tower. Other important cost inputs are provided in Table 6.5, with the costs given in Euro.

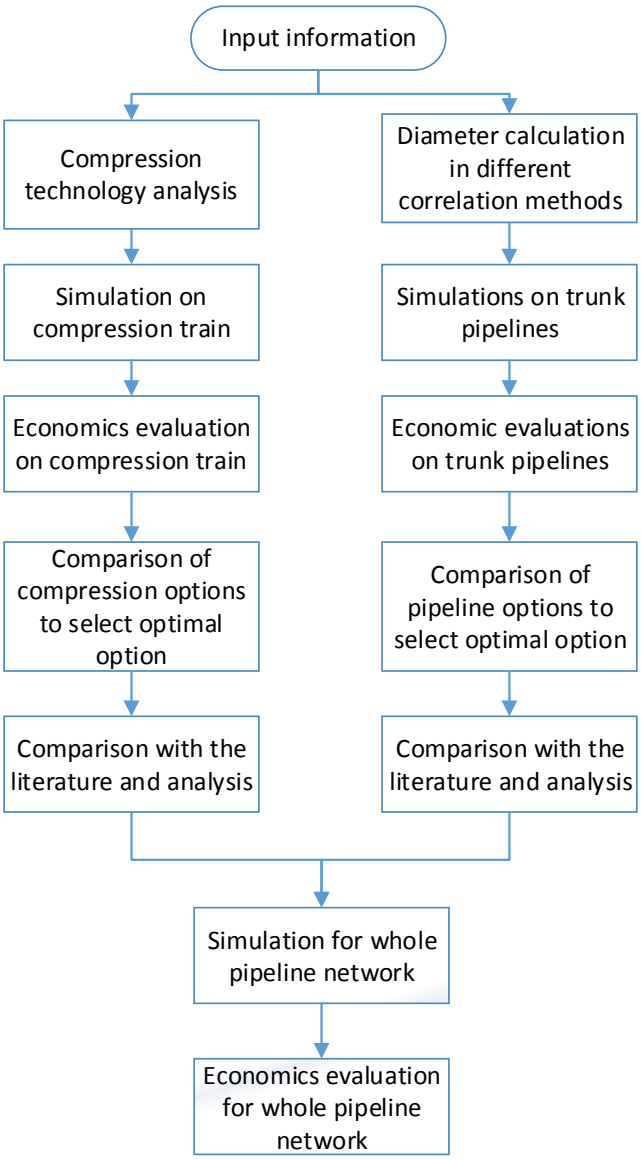


Figure 6.3 The work flow of the techno-economic evaluation

Table 6.5 Economic evaluation cost inputs

| Description | Unit | Value |
|---|---|---|
| Electricity price | €/kW | 0.0775 |
| Cooling water price | €/$m^3$ | 0.0317 |
| The price of refrigerant-Freon 12 | €/t | 0.17 |
| Carbon steel price | €/kg | 500 |
| Interest rate | % | 15 |
| Contingency | % | 5 |
| Project economic life | a | 25 |

For a given base case, the simulation model of whole pipeline network was developed first to check its accuracy and to gain basic data of streams and processes. The evaluations for different technical options go forward for compression train and trunk pipelines respectively, in order to confirm whether the designs of base case are optimal. Otherwise, optimal options would be applied for an optimal case. Finally, the overall costs of the whole pipeline network in the base case and the optimal case are summarized and compared. Figure 6.3 shows the work flow of the techno-economic evaluation in this study.

## 6.3 Techno-economic evaluation of $CO_2$ compression

Various types of compression configurations for $CO_2$ pipeline transport were found in literature. In the study of Zhang et al. (2006), 5 stage centrifugal compression was applied for pressurization power consumption analysis. McCollum and Ogden (2006) evaluated the energy cost, CAPEX and O&M cost of the compression achieved with 5 stage centrifugal compression followed by pumping. Witkowski et al. (2013) performed a thermodynamic evaluation of various $CO_2$ compression configurations and only the power requirements of those options were compared. In this section, the case studies about the compression train at the White Rose plant was conducted to get optimal configuration. The results were compared with other published studies in literature.

### *6.3.1 Compression configuration options*

After the conditioning process, the $CO_2$ captured in the White Rose plant will be pressurized from 1bar to 136 bar for dense phase transport by a compression train. Four compression configurations were selected (see Table 6.6) for techno-economic evaluation and compared with the base case. For options C3 and C4, the $CO_2$ mixture is initially pressurized to supercritical pressure (80 bar considering the impurities content in this study) and then further pressurized to the final exit pressure 136 bar by pumping. The difference between option C3 and C4 is the exit temperature of the intercoolers.

Table 6.6 Compression technology options and their process definition

| Option | Unit | Base Case | C1 | C2 | C3 | C4 |
|---|---|---|---|---|---|---|
| Description | | Centrifugal 5 stages with 4 intercoolers | Centrifugal 16 stages 4 intercoolers | 8 stages centrifugal geared with 7 intercoolers | 6 stages integrally geared with 5 intercoolers to 20 $^{o}$C +pumping | 6 stages integrally geared with 5 intercoolers to 38 $^{o}$C +pumping |
| Capacity | t/h | 334.60 | 334.60 | 334.60 | 334.60 | 334.60 |
| Suction pressure | bar | 1 | 1 | 1 | 1 | 1 |
| Suction temp. | $^{o}$C | 20 | 20 | 20 | 20 | 20 |
| Pumping suction pressure | bar | – | – | – | 80.0 | 80.0 |
| Pumping suction temp. | $^{o}$C | – | – | – | 20 | 20 |
| Exit pressure | bar | 136.0 | 136.0 | 136.0 | 136.0 | 136.0 |
| Stage | – | 5 | 16 | 8 | 6 | 6 |
| Isentropic efficiency | % | 75 | 75 | 75 | 75 | 75 |
| Interstage cooler exit temperature | $^{o}$C | 20 | 38 | 38 | 20 | 38 |
| Last stage exit temp. | $^{o}$C | 20 | 20 | 20 | 20 | 20 |

### 6.3.2 Results and analysis

The comparison of energy and utilities requirement for the five compression configurations can be seen in Table 6.7. Option C3 has the lowest annual energy and utilities cost. The intercooling performance is one of the key factors related with the energy consumption of the compressor. Option C2 has less compressor stages but more intercoolers than option C1. Option C2 has 12.78% annual saving of energy and utilities cost, compared to option C1. Compared to option C4, the lower intercooler exit temperature in option C3 results in 3.10% energy saving, resulting in 4.59% saving in annual energy and utilities cost. Option C3 has 5.44% energy saving but only 2.07% annual energy cost saving compared with option C2. The reason is that, in option C3, a suction temperature of 20 $^{o}$C is specified to cool down the $CO_2$ mixture with suction pressure at 80 bar, to avoid any gas formation for the pumping, which cause higher refrigerant cost.

Table 6.7 Energy and utilities requirements of compression technologies

| Cases | Energy requirements (kWh) | Cooling duty ($m^3$/h) | Refrigerant (t/h) | Energy and utilities cost (M€/a) |
|---|---|---|---|---|
| Base case | 34546 | – | 1257 | 23.13 |
| C1 | 39921 | 2540 | 656 | 26.29 |
| C2 | 34832 | 2977 | 423 | 22.93 |
| C3 | 31921 | – | 1197 | 21.42 |
| C4 | 32972 | 2304 | 592 | 22.45 |

Figure 6.4 shows the comparison of levelised cost in breakdown of these five compression technologies. The range of total levelised costs is from 11.81 €/ton $CO_2$ to 14.99 €/ton $CO_2$. Energy and utilities cost is the biggest part with a proportion of 65.6–71.3%. Option C3 has the lowest total levelised cost of 11.81 €/ton $CO_2$ although levelised capital cost of option C3 is 0.25 €/ton $CO_2$ higher than the base case. The reason is that lower pressure ratio of each stage compression benefits a big saving of energy and utilities consumption. Compared with the base case, option C3 has an annual saving of 1.13 M€.

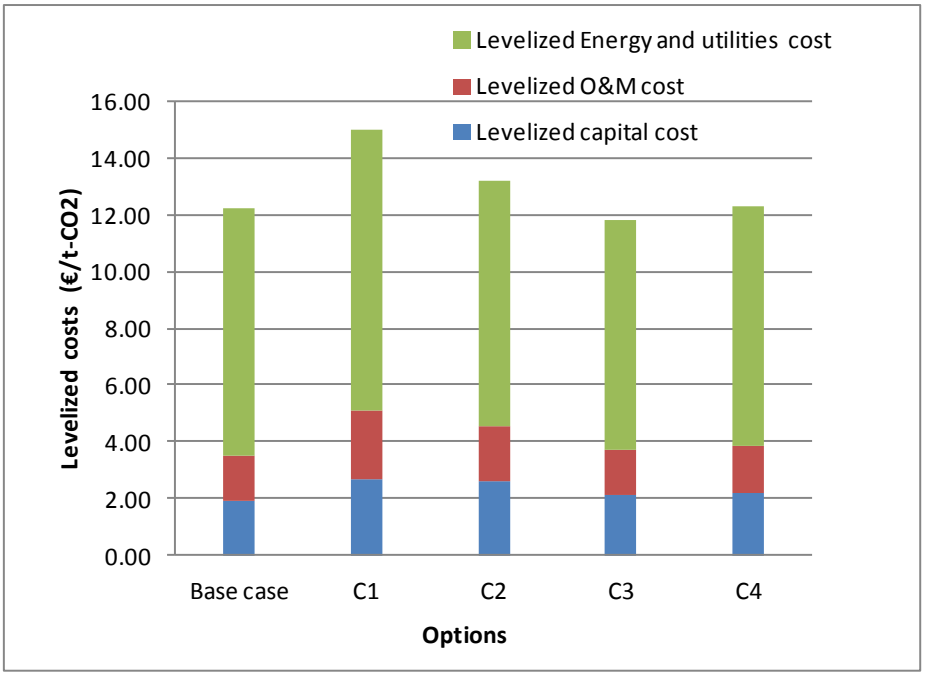


Figure 6.4 Comparison of levelised costs of different compression options

### 6.3.3 Comparison with other studies in the literature

There is a little published literature about the cost estimate of $CO_2$ compression. IEAGHG (2002) proposed an equation for the calculation of capital cost of compression based on the power required. Ogden et al. (2004) developed a correlation summarizing the data from Carbon Capture Project (CCP). The annual O&M cost was calculated by applying a factor of 0.04 to the total capital cost. Wong (2005) reported that the typical levelised cost of $CO_2$ compression varies from 5.5 € to 7.4 € per ton of $CO_2$ with an estimated capital cost of 4.12 M€ per 3000HP in average. The method for O&M calculation was not mentioned in the paper. McCollum and Ogden (2006) studied the cost of the compression train with 5-stage compression followed by pumping and the O&M factor is also 0.04.

For the energy and utilities cost, it is generally accepted that it can be accurately calculated based on the consumption data of process simulation results. So it was not included in the comparison. Figure 6.5 shows the comparison of levelised capital cost and O&M cost of different cost models used in IEAGHG (2002), McCollum and Ogden (2006) and this study. The method used by McCollum and Ogden (2006) failed to distinguish the costs of different options as a flow-based equation was applied for the capital cost calculation. The comparison shows the O&M cost in this study is much higher than in other two methods.

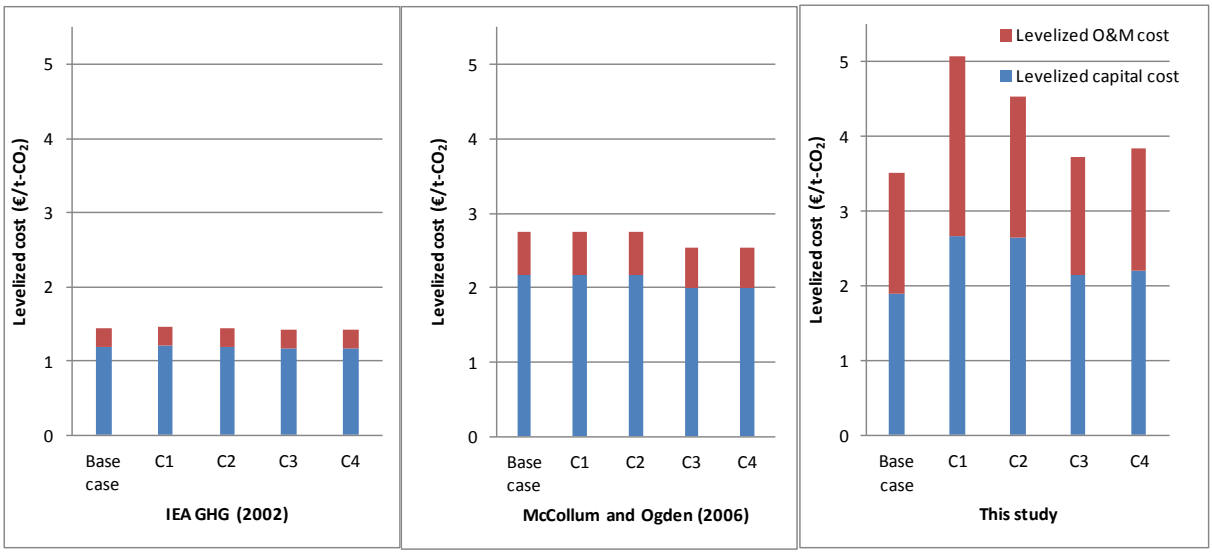


Figure 6.5 The comparison of levelised cost of different cost model

## 6.4 Techno-economic evaluation of trunk pipelines

In Section 6.1, the diameters of the onshore and offshore trunk pipelines were selected with a velocity-based equation for the base case. In this section, different published pipeline diameter models were used for diameter calculation and different results were obtained. Steady-state simulations were conducted to do a rating calculation for different diameters in order to compare process performance and economic evaluation. The model used in this section only includes the trunk pipelines and the booster pump station. The same entry conditions were used for each simulation model (see Table 6.8). The results of different models were compared and the optimal diameter was chosen for the optimal design.

Table 6.8 Input and boundary conditions

| Condition | unit | Value |
|---|---|---|
| Composition of $CO_2$ mixture stream | mole% | 96%$CO_2$, 2%$N_2$, 1.41%$H_2$, 0.59%Ar |
| Flow rate | t/h | 1126.263 |
| Entry pressure | bar | 136 |
| Entry temperature | $^oC$ | 20 |
| Minimum arrival pressure at offshore platform | bar | 126 |

### 6.4.1 Calculation of pipeline diameter

The diameter is a key factor for both technical and economical assessments in designing a pipeline system. For a given $CO_2$ pipeline transport task, several published models can be used to calculate the diameter of the pipelines. Table 6.9 shows an overview about the equations of several models. The velocity based equation is often used to do an initial estimation by setting input velocity in an experienced economical range. The (extensive) hydraulic equation is only capable for the fluid transport. McCoy and Rubin model can be used for both gaseous and liquid phase transport because it integrates the equation of state of real gas with the energy conservation and hydraulic equations.

For the diameter calculation, the parameters of the $CO_2$ mixture stream were obtained from the process simulation results and are substituted into each equation. Table 6.10 presents the results of calculated diameter of trunk pipelines. For the velocity based method, 1.0m/s, 1.5 m/s and 2.0m/s were selected for the diameter calculation. The results show the velocity range of other three methods is from 1.3 to1.8 m/s, which is close to the most effective velocity range of 1.5 to 2.0 m/s (Pershad et al., 2010). As only standard size pipeline diameters (ANSI standard) are specified in APEA, the calculated diameters were rounded off to the nearest whole number. With a diameter of 20 inches, the exit pressure of the onshore trunk pipeline is below 101 bar, which does not meet the operational constraint. The diameters of 22, 24 and 28 inches were then selected for the next techno-economic evaluations.

Table 6.9 Overview of the different diameter calculation methods in literature

| Name | Formula | Abbreviations | Limitation | Source |
|---|---|---|---|---|
| Velocity based equation | $D = \sqrt{\frac{4m}{v\pi\rho}}$ | $D$=diameter (m), $m$=mass flow (kg/s), $v$=velocity (m/s), $\rho$=density (kg/m$^3$) | | Wildenborg et al. (2004), Element Energy (2010), Chandel et al. (2010) |
| Hydraulic equation | $D = \left(\frac{32 f m^2 L}{\pi^2 \rho \Delta P}\right)^{1/5}$ | $f$=Fanning friction factor, $L$=length (m), $\Delta P$=overall pressure drop (Pa) | Re < 2000 or Re>4000 | Heddle et al. (2003), Van den Broek et al. (2010) |
| Extensive hydraulic equation | $D = \left(\frac{4^{10/3} n^2 m^2 L}{\pi^2 \rho^2 \left(\Delta h + (\Delta P/\rho\, g)\right)}\right)^{3/16}$ | $n$=Manning friction factor, $\Delta h$=height diffirence (m), $g$=gravity constant (9.81m/s$^2$) | originally developed for open channel flow | Piessens et al. (2008) |
| McCoy and Rubin model | $D = \left(\frac{-64 Z_{ave}^2 R^2 T_{ave}^2 m^2 f L}{\pi^2 [M Z_{ave} T_{ave} R (P_2^2 - P_1^2) + 2 g P_{ave}^2 M^2 \Delta h]}\right)^{1/5}$ | $Z_{ave}$=Average fluid compressibility, $R$=Gas constant (8.31Pa M$^3$/mol K), $T_{ave}$=average fluid temperature (K), $M$=molecular weight of flow (kg/kmol), $P_1$=Pressure at inlet (Pa), $P_2$=Pressure at outlet (Pa), $P_{ave}$= Average pressure in the pipeline= $\frac{2}{3}\left(P_2 + P_1 - \frac{P_2 \times P_1}{P_2 + P_1}\right)$ | Re < 2000 or Re>4000 | McCoy and Rubin (2008), Gao et al. (2011) |

Table 6.10 The calculation results of different diameter models

| Item | Calculated diameter (m) | Velocity (m/s) | Selected diameter in APEA (inch) |
|---|---|---|---|
| Velocity based equation | 0.699 | 1.0 | 28 |
| | 0.5713 | 1.5 | 24 |
| | 0.4948 | 2 | 20 |
| Hydraulic equation | 0.5262 | 1.77 | 22 |
| Extensive hydraulic equation | 0.6173 | 1.29 | 24 |
| McCoy and Rubin model | 0.5672 | 1.52 | 22 |

### *6.4.2 Results and analysis*

The selected diameters were used as the inputs in steady state models in order to simulate the hydraulic performance of the pipeline. The results of each simulation were exported into APEA to do the economic evaluations. Table 6.11 shows hydraulic results and power requirement of each simulation. Higher velocity results in a greater pressure drop of the $CO_2$-rich stream in the onshore and offshore trunk pipelines. Higher boosting pressure of the pump station is then needed to compensate the pressure loss to maintain a constant arrive pressure at the offshore storage platform.

Table 6.11 Technical performance of trunk pipelines system in different diameters

| Pipeline diameter (inch) | Actual initial velocity (m/s) | Pressure drop of onshore pipeline (bar) | Pressure drop of offshore pipeline (bar) | Boosting pressure of pump station (bar) | Energy required of pump station (kWh) |
|---|---|---|---|---|---|
| 28 | 1.08 | 5.9 | 10.0 | 5.9 | 301.5 |
| 24 | 1.49 | 13.5 | 20.6 | 24.1 | 1243 |
| 22 | 1.81 | 22.1 | 32.2 | 44.3 | 2305 |

Figure 6.6 illustrates the comparison of the levelised cost in breakdown of three options with different diameters. The comparison shows that the saving of capital cost is much bigger than the penalty of energy cost when the diameter of the pipelines decreases from 28 inches to 24 inches and then to 22 inches. The option with 22-inch diameter has the lowest total levelised

cost of 7.59 €/ton $CO_2$. Compared with the option of 24-inch diameter in the base case, the option with 22-inch diameter has an annual saving of 7.34 M€.

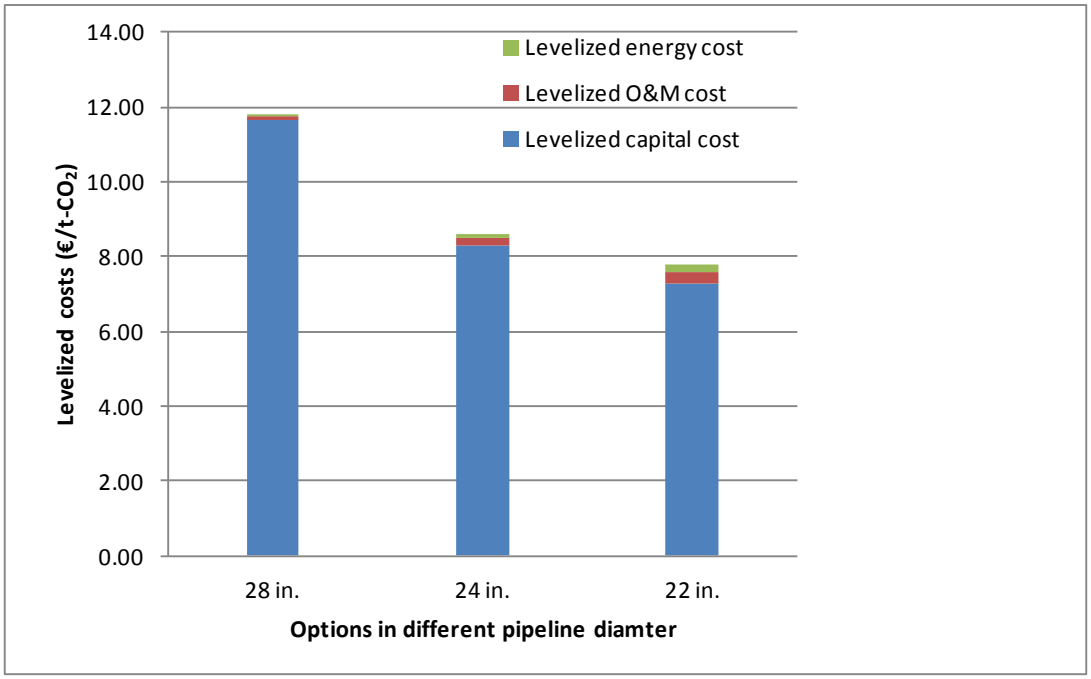


Figure 6.6 Annual cost comparison for different diameters of the pipelines

### *6.4.3 Comparison with other studies in the literature*

There are some models for cost evaluation of the $CO_2$ pipelines. Some of cost evaluation methods do not include a cost assessment of the booster pump. None of them can make an economic evaluation of the pipelines integrated with the energy cost of booster pump station. For the comparison, the capital costs of trunk pipelines were calculated respectively by different methods developed by IEAGHG (2002), McCollum and Ogden (2006), Piessens et al. (2008) and Van den Broek et al. (2010). Figure 6.7 shows a large range of the capital cost per kilometre of pipeline for different cost models. The total capital cost calculated in this study and Piessens et al. (2008) is much higher than those calculated with the other models. One main reason is that the method used by Piessens et al. (2008) is a weight-based model while the other methods are mainly based on the historical cost data of natural gas pipelines. Those correlation models, except for the weight-based models, do not consider the adaptation for the higher operation pressure of $CO_2$ pipeline transport. Normally, higher design pressure requires higher wall thickness of the pipelines, which results in a significant increase of the material cost.

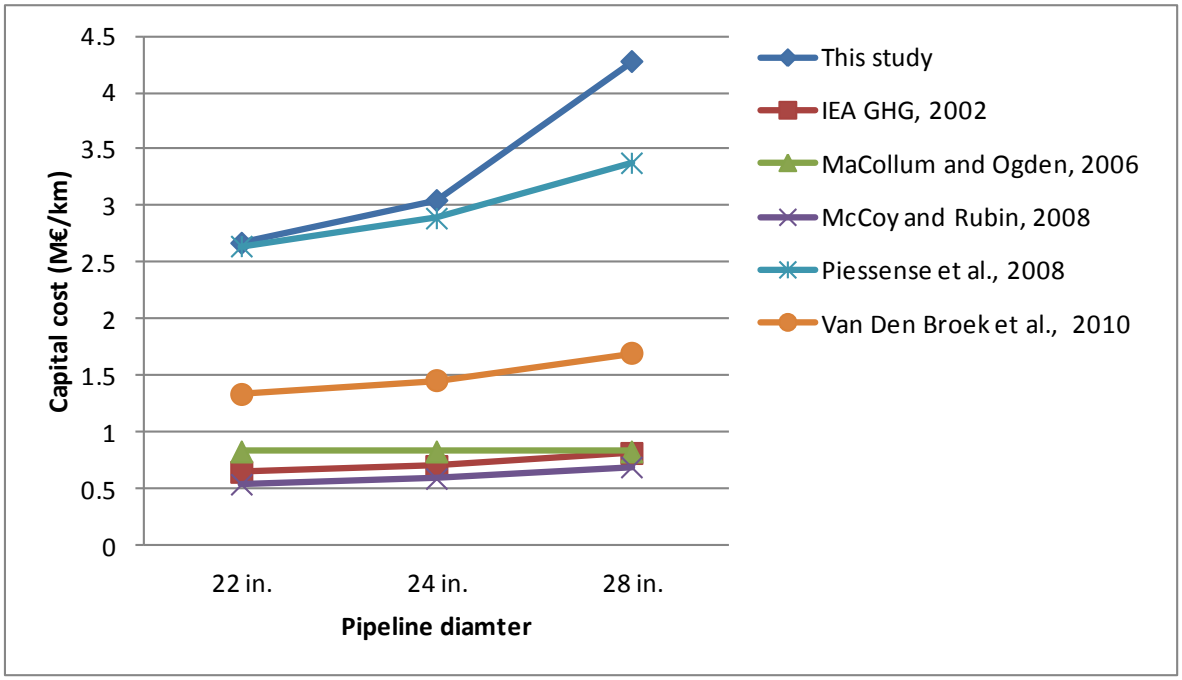


Figure 6.7 Comparison of capital cost of different cost models

## 6.5 Overall cost of $CO_2$ transportation pipeline network

### *6.5.1 Comparison of the base case and the optimal case*

In Sections 6.3 and 6.4, techno-economic evaluations were conducted for the compressors and trunk pipelines respectively. The options, which have the lowest annual costs, were used to optimise the design of the pipeline network in this study. For the compression train at the White Rose plant, 6-stage compression followed pumping and 5 intercoolers with 20 $^{o}$C exit temperature is the optimal option. The compression train for the Don Valley plant applied the similar configuration but it includes two parts, 5-stage compression and 1-stage compression as the $CO_2$ mixture will be transported in the gaseous phase at a pressure of 35 bar first and then boosted to dense phase at a pressure of 136 bar before entering the trunk pipelines. For the trunk onshore and offshore pipelines, 22-inch diameter is the optimal option. The overall cost of the base case (conceptual design provided by National Grid) and the optimal case were compared as shown in Figure 6.8. The total capital cost was split into the costs of trunk pipeline and collecting system for a better comparison. The collecting system includes the collecting pipelines and compression trains.

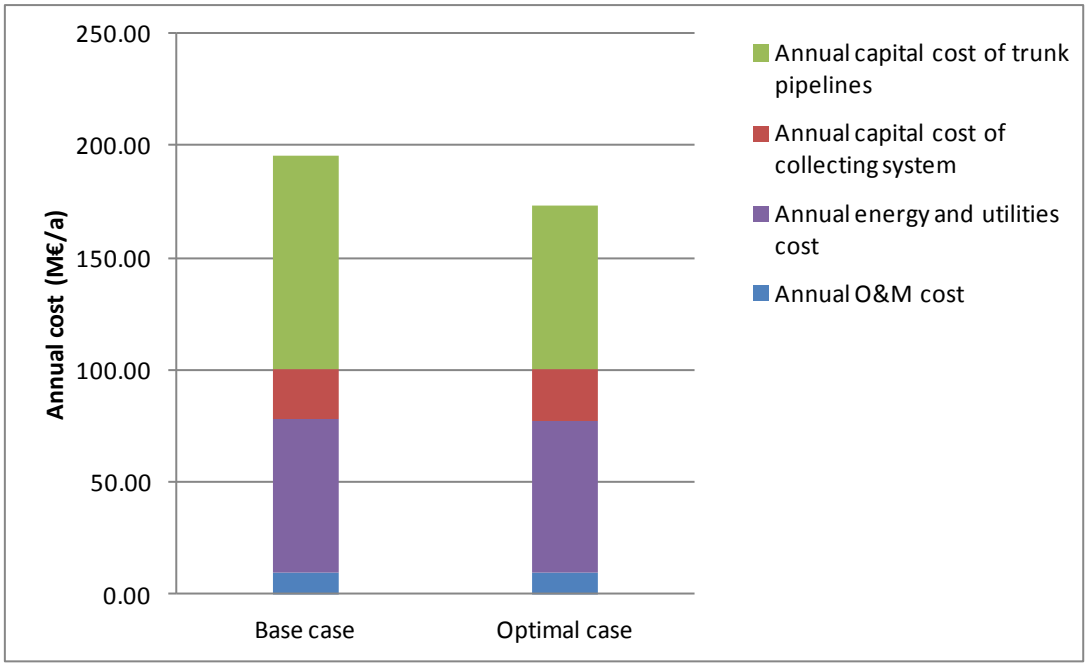


Figure 6.8 Comparison of annual costs of base case and optimal case

The comparison shows the annual O&M cost is almost same for two cases as there are similar processes. The annual energy and utilities cost is also very close to each other. Table 6.7 in Section 6.3 shows a significant compression energy saving for the optimal case compared to the base case. However the smaller diameter of trunk pipelines in optimal case increased the frictional pressure drop along the pipelines. This requires higher boosting pressure and therefore, higher energy consumption of the booster pump. The annual capital cost of trunk pipelines of the optimal case is obviously lower than the base case. Smaller diameter of pipelines has the advantage of incurring lower material cost and the construction cost may also be lower. Compared to the base case, optimal case has an annual total saving of 22.7 M€. It should be noticed that, having a larger diameter trunk pipelines, the base case provides the opportunities to transport extra $CO_2$ mixture from additional electricity generation capture plants or industrial capture plants in the future.

### *6.5.2 Comparison with other studies in the literature*

Public data are scarce for a cost comparison about the whole pipeline network for $CO_2$ transport. Most published studies present the costs evaluation for the pipelines without including a cost assessment of the compression train. The few studies that carried out an evaluation of the compression train failed to link it to the whole pipeline network system. In the study of Roussanaly et al. (2013), the economic evaluations were conducted to compare

different options for the COCATE project. The cost evaluation of the onshore pipelines option presented a typical pipeline network comprising a collecting pipeline system (including compression) around 40 km long and an onshore trunk pipelines around 620 km long.

The levelised costs per ton of $CO_2$ were summed up in each of the studies as shown in Figure 6.9. The levelised energy and utilities cost is close for these two studies. The levelised capital cost of trunk pipelines for the COCATE project is about 5.5 €/ton $CO_2$ , much lower than 8.1 €/ton $CO_2$ of the optimal case in this study, despite the fact that length of the COCATE pipeline is 620 km while the length of pipeline used in this study is 162 km. The evaluations of COCATE project used a specific pipeline cost model based on pipeline data of several published cost models. The reason for low capital costs predicted by most of the published models was analysed in Section 6.4. The levelised capital cost of collecting system in COCATE project is only 0.2 €/ton $CO_2$. The details of the evaluation method used for the collecting pipeline system in the COCATE project were not reported in the paper.

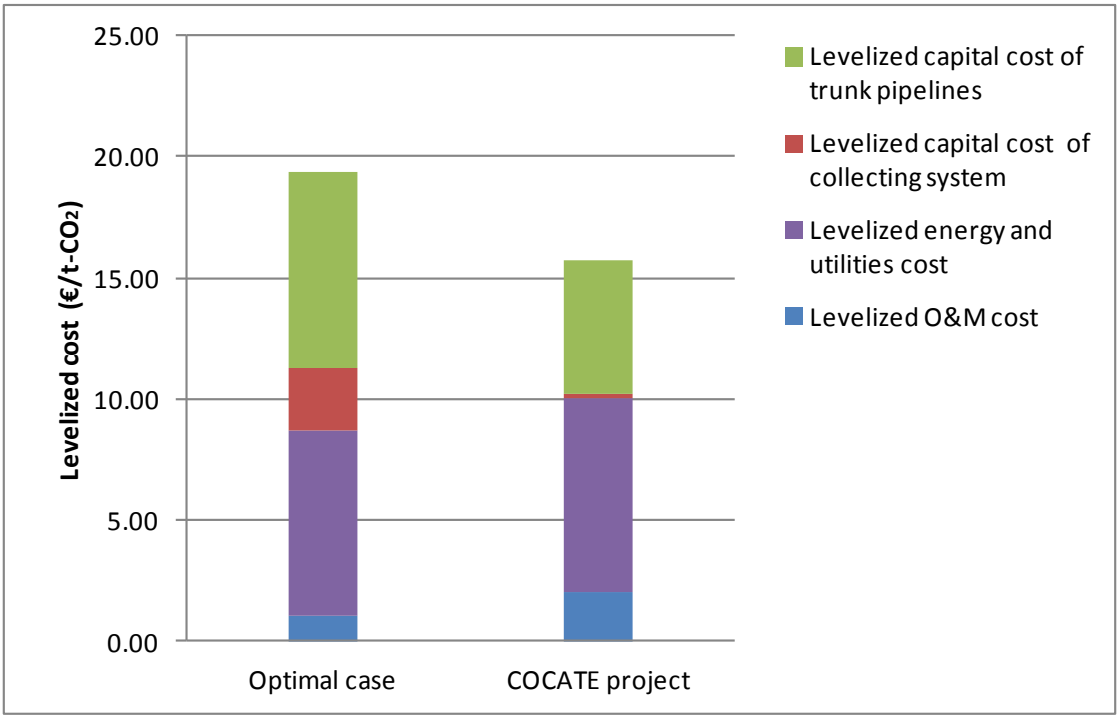


Figure 6.9 Comparison of levelised cost of the optimal case and COCATE project

## 6.6 Concluding remarks

The aim of this chapter is to conduct simulation-based techno-economic evaluations for the optimal design of the $CO_2$ transport pipeline network. A detailed steady state model was

developed, including $CO_2$ mixture streams from two emitters, the compression train, the onshore and offshore trunk pipelines and the booster pump station. The simulation results were exported into APEA for conducting the techno-economic evaluations. The optimal options with the lowest annual cost for compression train and trunk pipelines were selected after a comparative study of the different economic evaluation results. The overall costs of base case and optimal case were also compared. The optimal case has an annual total saving of 22.7 M€. For the optimal case, levelised energy and utilities cost is 7.62 €/ton $CO_2$, levelised capital cost of trunk pipeline is about 8.11 €/ton $CO_2$ and levelised capital cost of collecting system is 2.62 €/ton $CO_2$. The cost evaluation results of the compression train, trunk pipeline and whole pipeline network were compared with the cost evaluation results in the literature respectively to gain more insights, as follows.

- For $CO_2$ compression, the lower intercooler exit temperature (20 $^oC$ vs. 38 $^oC$ in this study) and lower pressure ratio per stage leads to lower energy and utilities consumption of compression train.

- The correlation cost models for $CO_2$ compression train cannot give good cost predictions for some different configuration options. The O&M factor of 0.04 in those models is very small comparing with the result of this study.

- The pipeline diameter models in the literature are generally reliable. Among these models, the hydraulic equation method gives the most accurate predictions. The initial velocity of $CO_2$ mixture is around 1.7m/s in the optimal case in this study.

- A large range of capital cost was obtained after applying different published cost models for the trunk pipelines. Most of the pipeline cost models in the literature predicted a much lower capital cost and the weight-based model in the study of Piessens et al. (2008) has the best prediction compared with the results in this study.

- Simulation-based techno-economics evaluation method offers a powerful tool for optimal designs for the projects, especially for the decision making support about the detailed technical options selection.

# Chapter 7: Optimal operation under different market conditions based on whole CCS chain consideration

This chapter aims to explore the optimal operation under different market conditions for an assumed existing NGCC power plant integrated with whole CCS chain including solvent-based PCC process, $CO_2$ compression, $CO_2$ transport and storage. Two major questions were answered: (1) what is the optimal carbon capture degree under different market situations? (2) what are the optimal values of key operational variables for an optimal capture level?

Compared with the optimisation model for solvent-based PCC process in Chapter 4, the model in this chapter was updated. Firstly, the objective function of optimisation is changed to levelised cost of electricity (LCOE), which could directly reflect the changes of electricity cost. Secondly, specific values were considered for two key operational variables, capture level (CL) and lean loading, although they are continuous in real process. Economic evaluation was carried out for the base case of the integrated system including $CO_2$ emission penalty cost and $CO_2$ T&S cost. The optimal operations were investigated for the carbon capture level under different carbon price (IPCC, 2007), fuel price and $CO_2$ T&S price.

## 7.1 Optimisation methodology update

The optimisation algorithm could also be represented by Equations (4.4–4.10) in Chapter 4. But several updates have been made to reflect the natures of optimal operation of the whole integrated system in this chapter, compared with optimal design for PPC process only in Chapter 4. The optimal operation study was conducted for an assumed existing plant whose design features such as the equipment sizes should be fixed during the study. Details are presented in the following sections.

### *7.1.1 Objective function*

In Chapter 4, several potential objective functions were discussed and CCA was finally chosen. However, in the optimisation studies in this chapter, LCOE was formulated to be the objective function of the optimisation. LCOE is one indicator normally used to directly present the electricity cost in the context of whole CCS chain consideration. LCOE was calculated by dividing total annual cost by annual net power output in Equation (7.1). The total annual cost is a sum of annualized CAPEX, FOPEX and VOPEX as in Equation (7.2).

$$LCOE = \frac{TAC}{Net\ power\ output} \tag{7.1}$$

$$TAC = ACAPEX + FOPEX + VOPEX \tag{7.2}$$

$$VOPEX = CFuel + CCO2EMI + CCOOLING + CT\&S + CSolvent \tag{7.3}$$

In this chapter, the integrated system in the study scope includes the NGCC power plant, PCC process and compression process. Correspondingly, CAPEX and FOPEX in this chapter present the cost for the above processes. At the same time, the electricity is supplied by the power plant and low pressure steam is also extracted from the power plant. Consequently, the costs of power electricity and LP steam are replaced by the cost of fuel. So VOPEX in this chapter includes the fuel cost, cooling utilities cost, solvent make-up cost, carbon emission cost and $CO_2$ T&S cost, as presented in Equation (7.3). It would be noticed that this study focuses on the optimal operation of NGCC power plant with the carbon capture process. Its CAPEX and FOPEX are assumed to be fixed neglecting the tax and labour cost changes. Only VOPEX was considered to vary in response to different market conditions.

### 7.1.2 $CO_2$ emission cost

In order to achieve the target of global climate control, carbon credit (EU, 2010) was set to drive the actions of reducing $CO_2$ emission. Under this policy, there is a $CO_2$ emission cost for plant operators if $CO_2$ emission is over the cap. The first part is the cost for buying carbon credits thought the The EU Emissions Trading System (ETS) at one floating carbon price determined by the market. If the $CO_2$ emission is still over the allowance, a non-compliance cost will be charged as a penalty at a much higher carbon price. Current carbon price in Europe is around €7/ton $CO_2$ (EEEAG, 2015). However future carbon price will increase with the time and could be highly uncertain (USDOE, 2010a).

### 7.1.3 $CO_2$ T&S cost

$CO_2$ transport and storage are two important sections of whole CCS chain and are also cost-intensive processes. Collecting $CO_2$ mixture from several emitters into trunk pipelines for geologic storage is more cost-effective than the use of separate pipelines (IPCC, 2005; Chandel et al., 2010). Other companies may operate $CO_2$ transport and storage infrastructure

and charge the emitters for the $CO_2$ stream entering the network. One example is that National Grid plc will construct and operate the $CO_2$ transport pipelines and the permanent $CO_2$ undersea storage facilities at a North Sea site in the Yorkshire and Humber CCS Project in the UK (National Grid, 2014).

The previous predictions of the costs of $CO_2$ transport and storage are in a wide range with high uncertainties. For the pipeline transport cost, IPCC predicted to be 9.9–14.9 €/ton $CO_2$ (IPCC, 2005). The study in Chapter 6 also estimated that transport cost is around €17/ton $CO_2$. For the $CO_2$ storage cost, IPCC predicted it to be 0–7.9 €/ton $CO_2$ for onshore storage and 6–30.8 €/ton $CO_2$ for ocean storage (IPCC, 2005). Department of Energy and Climate Change (DECC) (2013) reported that the transport and storage cost accounts for a big part of the increment of LCOE. Under FID 2013, 2020 and 2028 CCS technology scenarios, the $CO_2$ T&S cost is 49.7, 19.2 and 4.5 €/MWh, which correspond to equivalent prices of 102.5, 39.54 and 9.32 €/ton $CO_2$.

### *7.1.4 Equality constraints*

In this study, equality constraints such as the mass balances, reactions and phase balance were formulated in the first principle process models built in Aspen Plus® described in Chapter 3 and Chapter 5. For this optimal operation of an assumed existing plant, the design variables such as diameters and packing heights of the absorber and the stripper would not change. In this study, the values of key design variables can be seen in the tables for the base case in Chapter 3 and Chapter 5.

### *7.1.5 Inequality constraints*

The inequality constraints are imposed in the form of upper bounds for product flow rates for different cases. Those inequality constraints for controlled operational variables in this study are listed in Equations (7.4–7.7) considering the flexible operation range of packing towers and other equipment.

$$60\% \leq CL \leq 95\% \tag{7.4}$$

$$0.20 \leq \alpha_{lean} \leq 0.36\ (mol\ CO_2/mol\ \ MEA) \tag{7.5}$$

$$0.50 \leq L/G_{ratio} \leq 6.00 \text{ (kg/kg)} \tag{7.6}$$

$$0 \leq F_{flood} \leq 0.65 \tag{7.7}$$

For the optimisation of such a large scale model for rate-based first principle PCC process integrated with the NGCC power plant, high computational requirements and convergence problems often occur although commercial software package AspenPlus® was used. Compromising on those challenges, specific values were considered for two key operational variables although they are continuous in real process. Their value sets were presented in Equation (7.8) and (7.9) respectively.

$$CL = \{60\%, 70\%, 80\%, 85\%, 90\%, 95\%\} \tag{7.8}$$

$$\alpha_{lean} = \{0.20, 0.24, 0.26, 0.28, 0.30, 0.32, 0.36\} \ (mol\ CO_2/mol\ \ MEA) \tag{7.9}$$

## 7.2 Techno-economic evaluation of the base case

In this section, the technical performance was evaluated according to the process simulation results. Then the cost of whole chain for capturing carbon from NGCC power plant was evaluated for the base case by combining calculation results and the literature data, in order to give a basis for the optimal operation study in Section 7.5.

The base case was set up based on the PCC process described in Chapter 5 with 90% carbon capture level for the NGCC power plant with EGR. For the economic evaluation, CAPEX and fixed OPEX were referred to published benchmark report (IEAGHG, 2012). Variable OPEX was summarized from each subcost calculated based on the simulation results from process model. To harmonize results for comparison with other studies, following assumptions were made: 1) all costs are corrected to €2015 using the harmonised consumer price index (HICP) in Europe zone; 2) the captured $CO_2$ mixture has no economic value; 3) cooling water is sourced from a nearby body of water at the cost of pumping and operation of a cooling tower. Other important cost inputs are provided in Table 7.1 with the costs given in Euro.

Table 7.1 Key economic evaluation cost inputs

| Description | Value | Reference |
|---|---|---|
| Carbon price (€/kg) | 7.0 | EEEAG (2015) |
| NG price (€/GJ) | 6.58 | Ycharts (2015) |
| MEA solvent price (€/ton) | 1452 | Alibaba (2016) |
| $CO_2$ T&S cost (€/ton) | 39.54 | DECC (2013) |
| Project economic life (year) | 25 | |

Table 7.2 shows the comparison of the results between the reference case of NGCC standalone and the base case of NGCC integrated with whole CCS chain. In the base case, the annualized CAPEX of PCC process is close to the annualized CAPEX of NGCC power plant and the variable OPEX accounts for 65% of the total annual cost. For the variable OPEX of NGCC standalone, the fuel cost is the biggest part and carbon emission cost is the second largest part. However when NGCC is integrated with PCC process, the fixed OPEX increases significantly because of new expense items such as $CO_2$ T&S cost and MEA solvent make-up cost.

Table 7.2 Cost comparison

| Description | | Unit | NGCC standalone | Base case of NGCC integrated with CCS |
|---|---|---|---|---|
| ACAPEX of NGCC* | | M€/year | 44.23 | 41.26 |
| ACAPEX of PCC | | M€/year | – | 23.91 |
| FOPEX of NGCC* | | M€/year | 8.34 | 7.78 |
| FOPEX of PCC | | M€/year | – | 5.89 |
| VOPEX | Fuel cost | M€/year | 160.42 | 160.42 |
| | Carbon emission | M€/year | 9.70 | 0.970 |
| | $CO_2$ T&S cost | M€/year | – | 51.03 |
| | Solvent make-up cost | M€/year | – | 3.00 |
| | Refrigerant cost | M€/year | – | 0.67 |
| TAC | | M€/year | 222.69 | 294.93 |
| LCOE | | €/MWh | 56.00 | 87.26 |

Note: * the cost refers to a benchmark report from IEAGHG (2012).

## 7.3 Optimal operation

The economic evaluation of the base case in Section 7.2 shows high capital cost as well as wide ranging operating cost occurring for carbon capture from the NGCC power plant. In this section, optimisation study was carried to find the optimal carbon capture degree under different market situations and the optimal values of key operational variables for this optimal capture level, for an assumed existing NGCC power integrated with whole CCS chain.

### *7.3.1 Optimal capture level under different carbon price*

The economic performances with regard to LCOE were examined under different carbon prices of €7, €50, €100 and €150 per ton of $CO_2$ in this study.

The results were summarized in Figures 7.1–7.4. Under low carbon price of €7/ton $CO_2$ (Figure 7.1), LCOE gets the minimum value of €78.28/MWh with 60% CL at an optimal lean loading of 0.26 mol $CO_2$/mol MEA. Figure 7.1 also shows LCOE increase obviously with higher CL no matter what the lean loading would be. The trend indicates that the carbon emission cost cannot justify the high operating cost of the PCC process under low carbon price. The optimal operation in terms of minimum LCOE is to vent the flue gas to the atmosphere through bypassing the PCC process. With higher carbon price of €50/ton $CO_2$, the differences of LCOE of different CLs become smaller as indicated in Figure 7.2. For the scenario of carbon price of €100/ ton $CO_2$, the values of LCOE distribute in a very narrow range (Figure 7.3) which means the carbon emission penalty cost can just justify the extra VOPEX for carbon capture. With high carbon price of €150/ ton $CO_2$, the optimal value of LCOE of 90% CL and 95% is very close at a lean loading of 0.26–0.28 mol $CO_2$/mol MEA whilst LCOE is around €94.35/MWh (Figure 7.4).

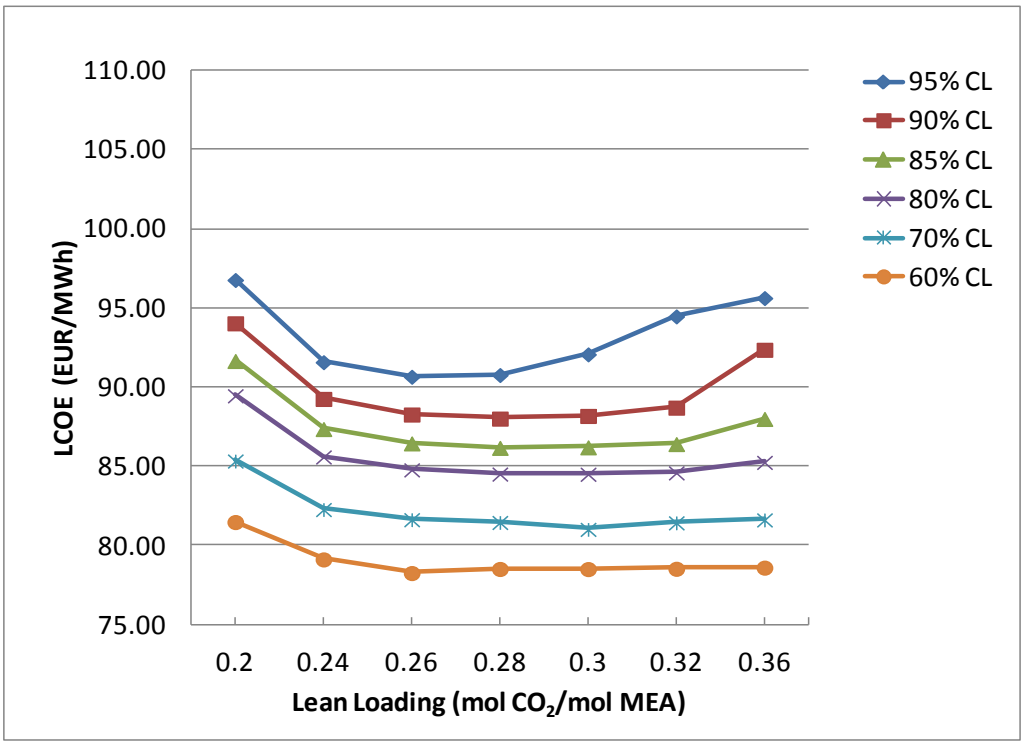


Figure 7.1 LCOE of different capture level with carbon price of 7 €/ton $CO_2$

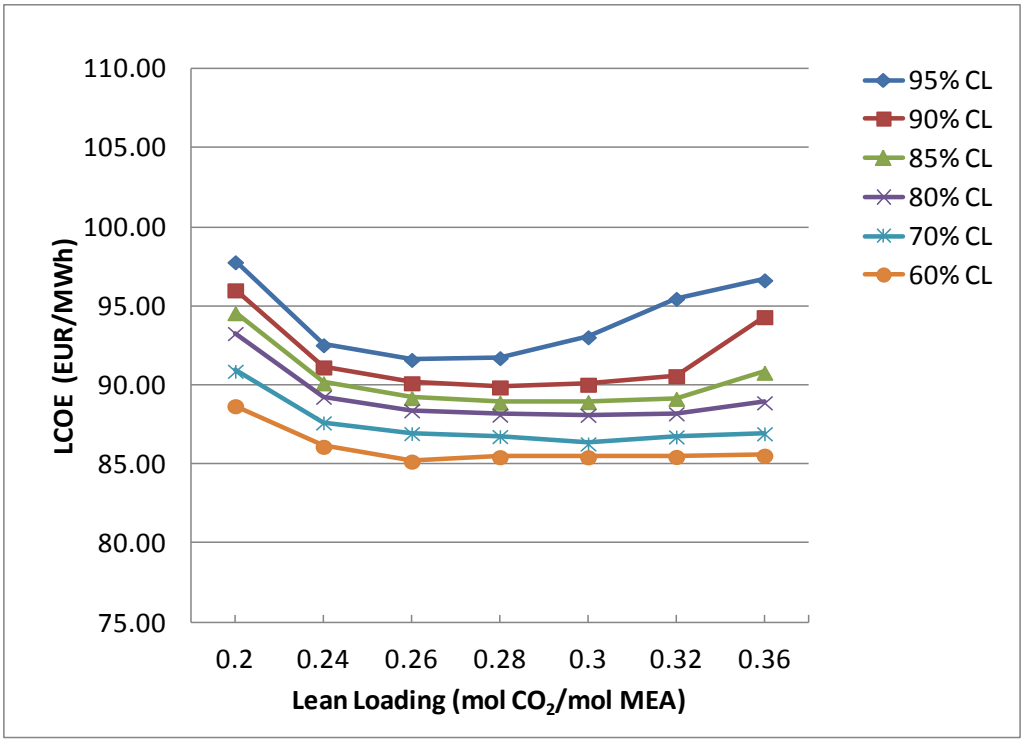


Figure 7.2 LCOE of different capture levels with carbon price of 50 €/ton $CO_2$

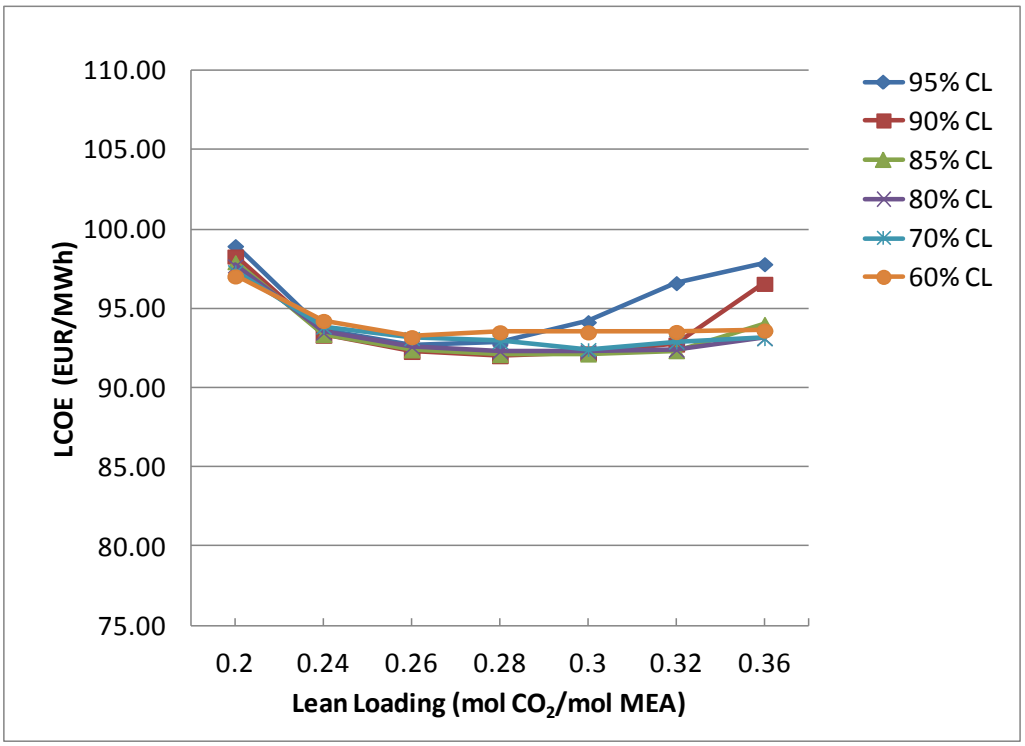


Figure 7.3 LCOE of different capture levels with carbon price of 100 €/ton $CO_2$

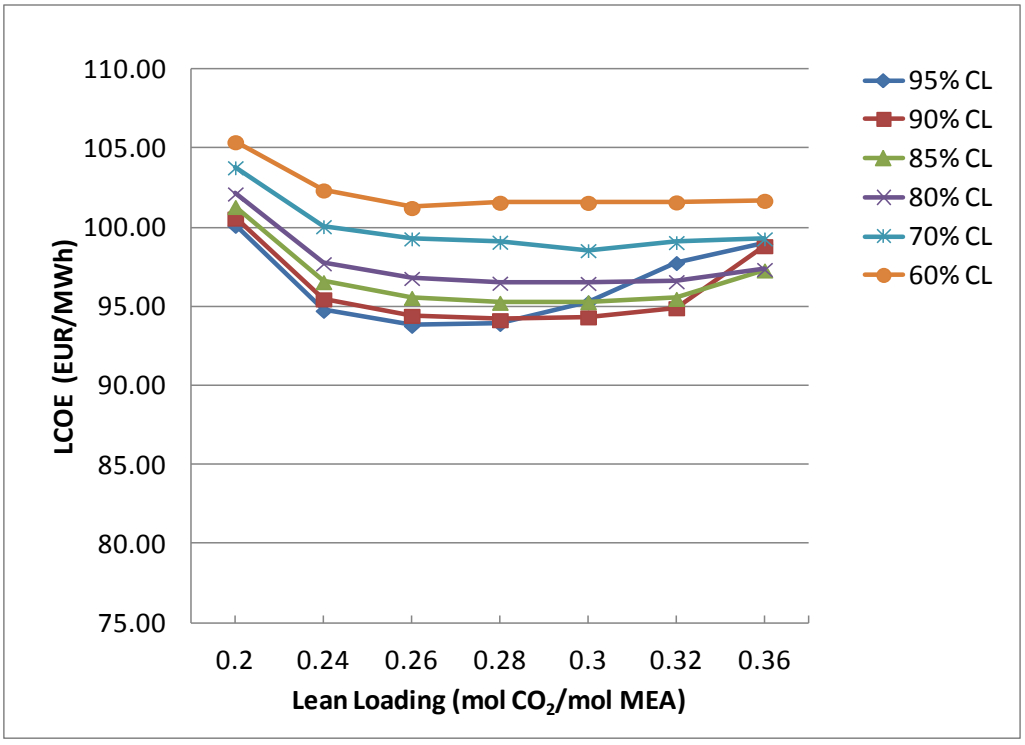


Figure 7.4 LCOE of different capture levels with carbon price of 150 €/ton $CO_2$

The optimal values for key operational variables at different capture levels were displayed in Figure 7.5. The economic range of the lean loading was found to be 0.26–0.3 mol $CO_2$/mol MEA for the capture level in a range from 60% to 95%. It is noticed that this result is different with the optimal values such as 0.158 mol $CO_2$/ mol MEA in the study of Mores et al. (2014) and 0.2 mol $CO_2$/ mol MEA in the study of Agbonghae et al. (2014). The reason is that the studies implemented optimisation studies for both design and operation. In this situation, lower lean loading required smaller L/G ratio (kg/kg) which results in a reduction of the required crossing sectional area of the absorber. However the diameter of the absorber was fixed in this study for optimal operation. Here, one practice could be obtained for the optimal operating of an existing PCC plant, which is that increasing the lean loading until reaching the maximum capacity of the absorber could reduce reboiler duty to achieve a lower energy cost.

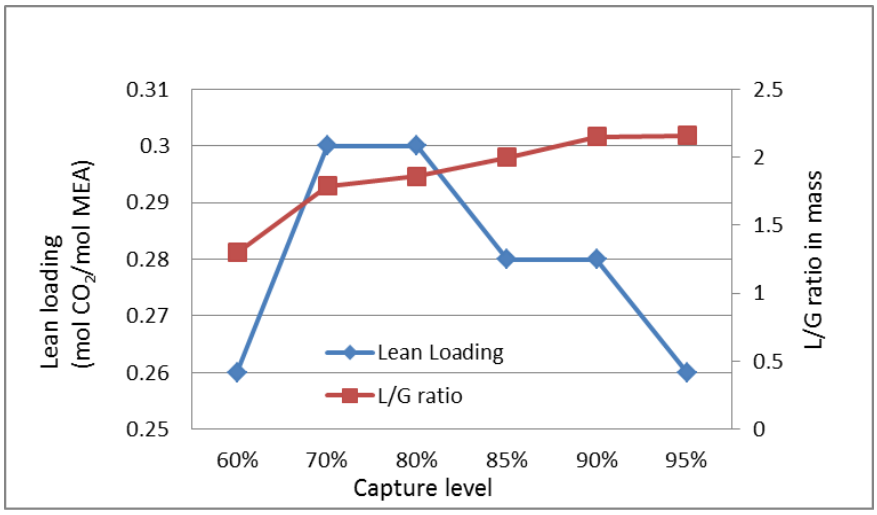


Figure 7.5 Optimal lean loading and L/G ratio for different capture levels

The trend of L/G ratio is different from the lean loading. Except for being relevant with the difference between lean loading and rich loading, L/G ratio relies more on the rate of $CO_2$ captured. As shown in Figure 7.5, L/G ratio increases as more solvent is required for absorbing more $CO_2$ at higher capture level. It is also noticed that the required L/G ratio for a same capture level varies for different $CO_2$ concentration in the flue gas. The range of L/G ratio in mass is from 0.5 to 1.5 for a NGCC power without EGR (4.04 mol% $CO_2$ content in the flue gas) and it is from 1.2 to 2.2 for a NGCC with EGR (7.32 mol% $CO_2$ content in the flue gas) in this study. As a comparison, it is from 2.0 to 5.0 for a subcritical coal-fired power plant with PCC process (13.5 mol% $CO_2$ content in flue gas) (Agbonghae et al., 2014).

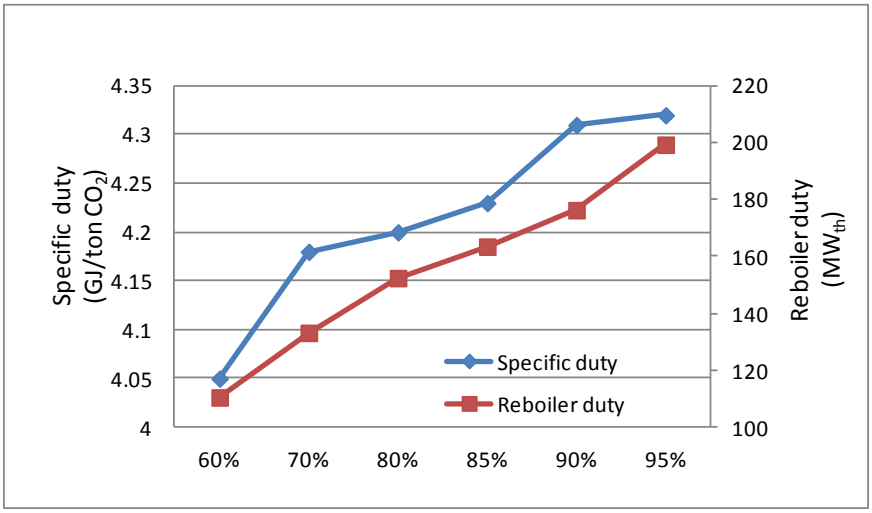


Figure 7.6 Optimal reboiler duty and specific duty for different capture levels

The specific duty was calculated from the reboiler duty divided by the mass flow rate of $CO_2$ captured. The range of specific duty is from 3.25 to 4.35 GJ/ton $CO_2$ for PCC process for gas-fired power plant in previous studies (Agbonghae et al., 2014; Canepa and Wang, 2015; Mores et al., 2014; Sipöcz and Tobiesen, 2012). Figure 7.6 presented the specific duty is from 4.05 to 4.32 GJ/ton $CO_2$ while the reboiler duty increases greatly when the capture level increase from 60% to 95%.

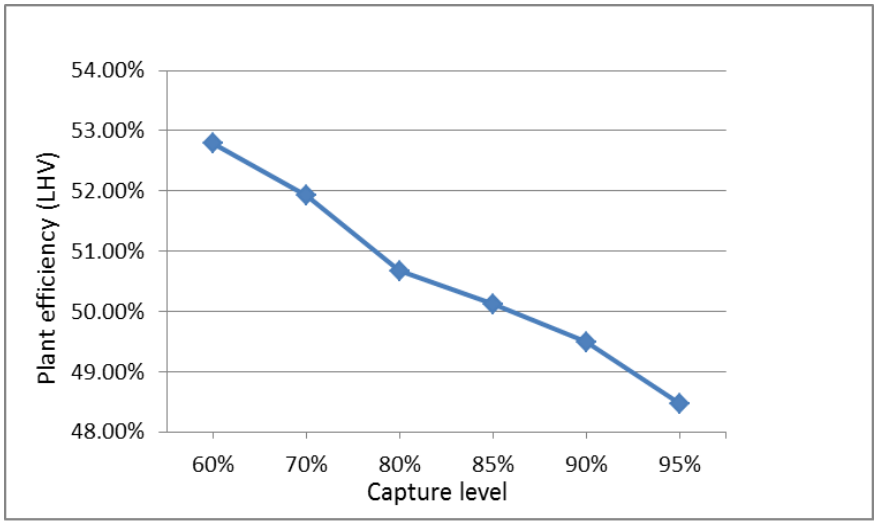


Figure 7.7 Thermal efficiency of the NGCC with PCC at different capture levels

Figure 7.7 gives the trend of thermal efficiency of the NGCC with PCC at different capture levels, which is easy to be justified because more steam would be extracted from the steam system of the NGCC power plant for providing heat to the stripper reboiler of the PCC process at the higher capture levels.

### 7.3.2 The effect of NG price

In Section 7.2, the economic evaluation results show fuel cost is the largest part of variable OPEX and is a huge expense even compared with annualized CAPEX. It is realized that the uncertain NG price would have big impact to decide the optimal operation strategy.

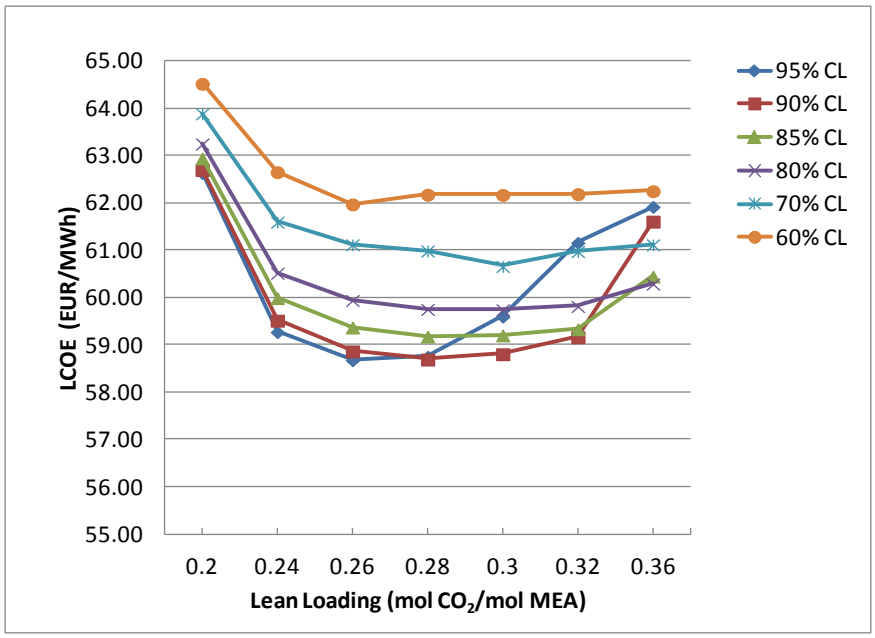


Figure 7.8 LCOE of different capture level with carbon price of €100/ton $CO_2$ and NG price of €2/GJ

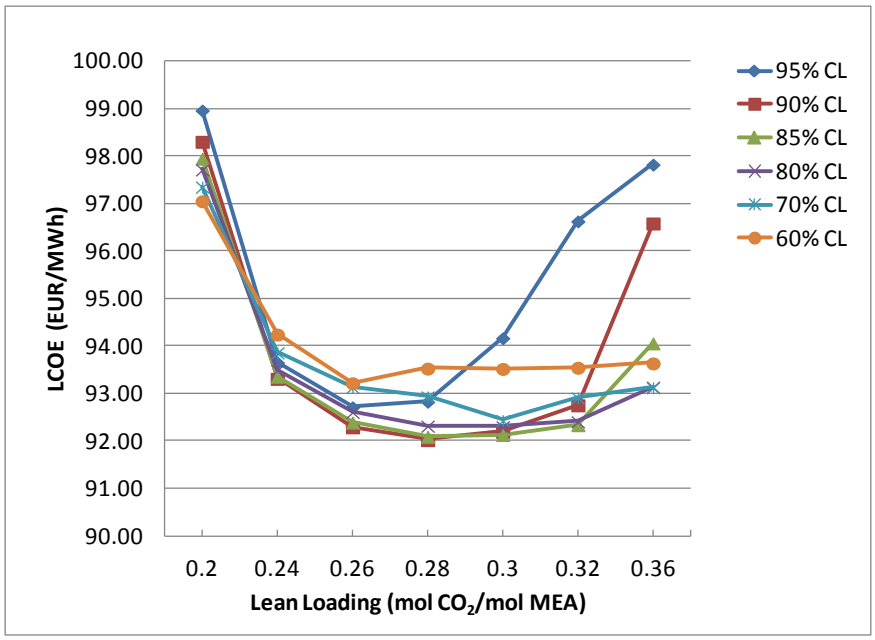


Figure 7.9 LCOE of different capture level with carbon price of €100/ton $CO_2$ and NG price of €6.58/GJ

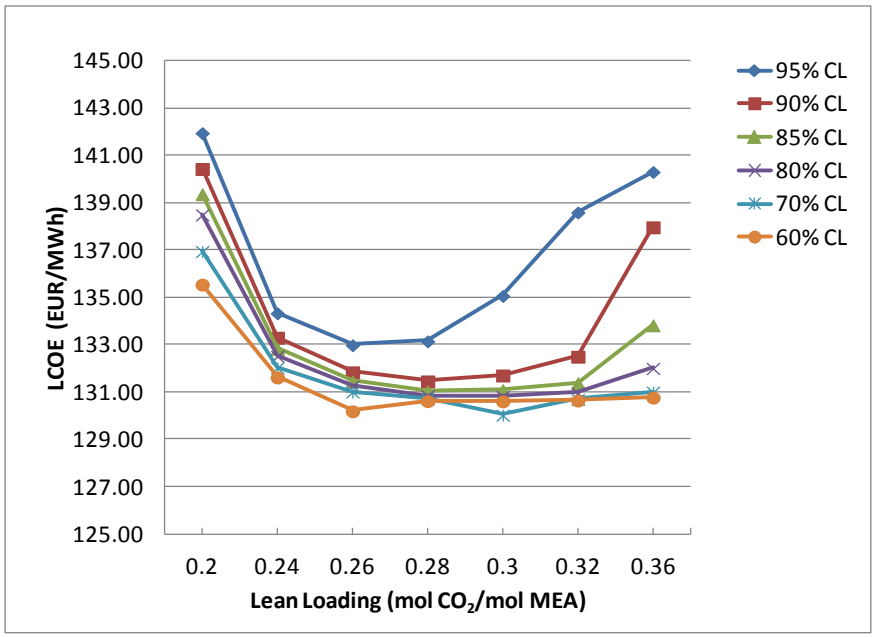


Figure 7.10 LCOE of different capture level with carbon price of €100/ton $CO_2$ and NG price of €12/GJ

Figures 7.8–7.10 shows the results of the optimal capture level under different fuel prices with fixed carbon price of €100/ton $CO_2$. At the scenario of low NG price at €2/GJ (Figure 7.8), the higher capture level shows a low LCOE because the $CO_2$ emission penalty can easily justify the fuel cost. The situation reverses when NG price rises up to €12/GJ (Figure 7.10). Thus a carbon price higher than €100/ton $CO_2$ is required to draw the balance back for carbon capture.

Figure 7.11 presents the required carbon price for driving the capture level to 90% in response to the changes of fuel price. The result shows a range of LCOE is 57.27–131.2 €/MWh when the NG price rises from €2/GJ to €12/GJ. For the based case in Section 7.2 with 90% capture level, the required carbon price is around €101.50/ton $CO_2$ with a LCOE of €92.09/MWh.

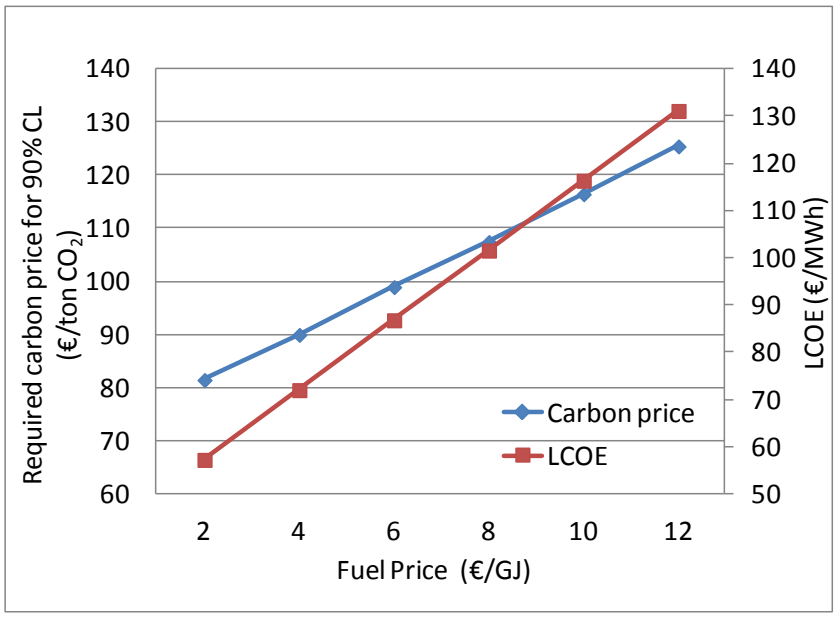


Figure 7.11 Required carbon price for driving 90% capture level in response to different fuel prices

### *7.3.3 The effect of $CO_2$ T&S price*

The change of the $CO_2$ T&S price may affect the optimal operation decision largely. In this section, the optimisations were carried out on three different $CO_2$ T&S equivalent prices of 102.5, 39.54 and 9.32 €/ton $CO_2$.

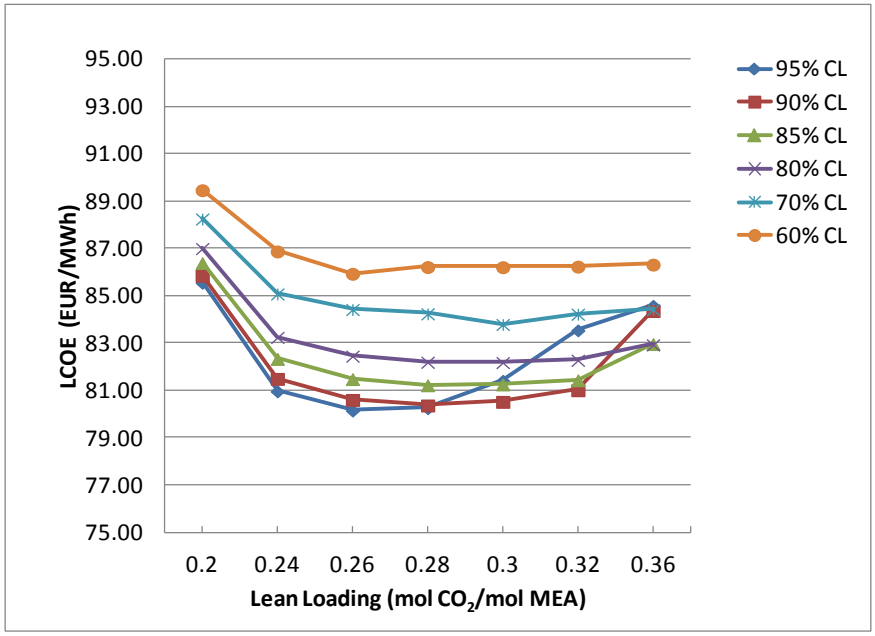


Figure 7.12 LCOE of different capture level with carbon price of €100/ton $CO_2$ and T&S price of €9.32/ton $CO_2$

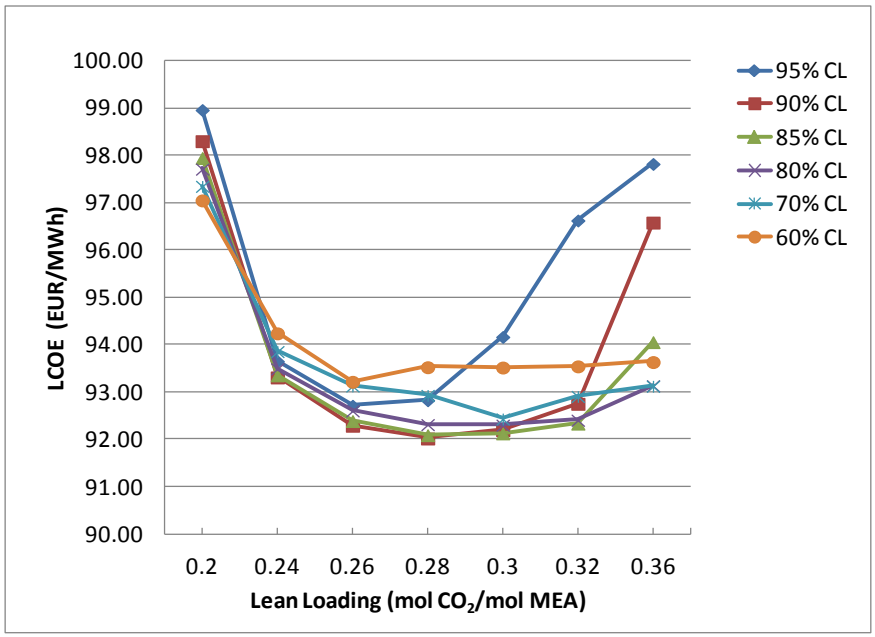


Figure 7.13 LCOE of different capture level with carbon price of €100/ton $CO_2$ and T&S price of €39.54/ton $CO_2$

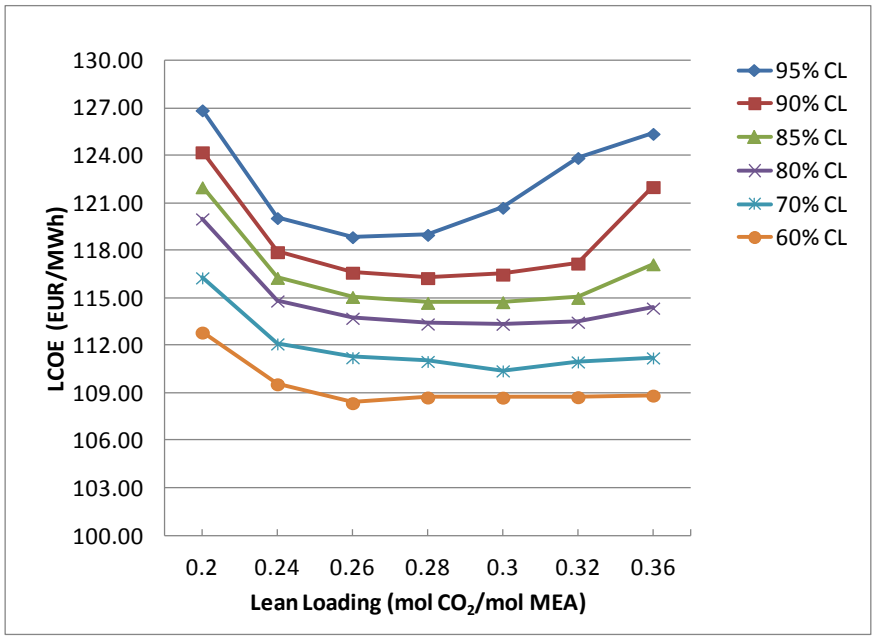


Figure 7.14 LCOE of different capture level with carbon price of €100/ton $CO_2$ and T&S price of €102.5/ton $CO_2$

The results were displayed in Figures 7.12–7.14. With low $CO_2$ T&S price of €9.32/ton $CO_2$, the optimal capture level is 90–95% compared to 80–90% at the intermediate price of €39.54/ton $CO_2$. At the high $CO_2$ T&S price of is €102.5/ton $CO_2$, the high cost of carbon capture cannot be justified (see Figure 7.14) and a carbon price higher than €100/ton $CO_2$ is

needed to provide driving force for carbon capture. Otherwise bypassing PCC process is the optimal choice.

Figure 7.15 presents the required carbon price for driving the capture level to 90% in response to changes of $CO_2$ T&S price. The result shows a range of LCOE is 73.99–117.33 €/MWh when the $CO_2$ T&S price rises from 0 to €100/ton $CO_2$. When the $CO_2$ T&S cost is 0, the carbon price is required to be €51.5/ton $CO_2$ for 90% capture level €54/ton $CO_2$ for the case without considering the $CO_2$ compression, transport and storage in the study by Mac Dowell and Shah (2013). Comparing the results of Figures 7.11 and 7.15, it is noticed that $CO_2$ T&S price has a lower sensitivity than fuel price to LCOE at 90% capture level.

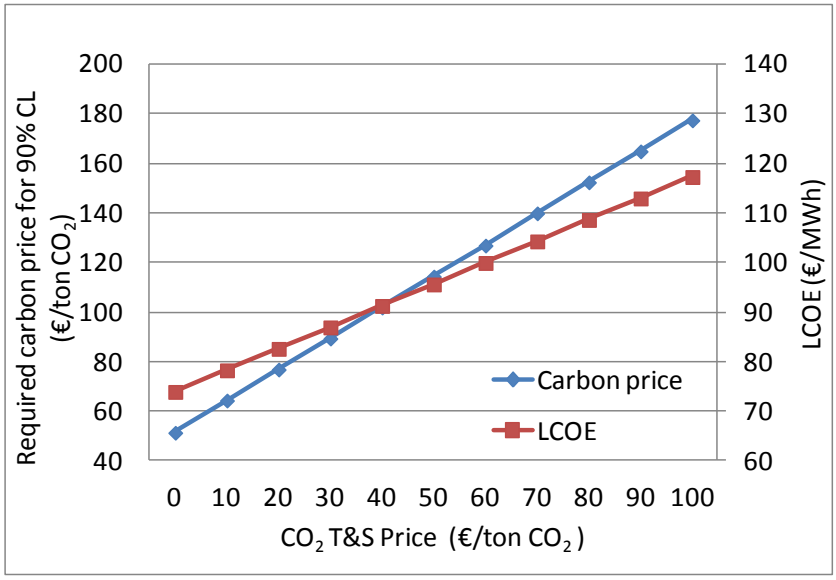


Figure 7.15 Carbon price for driving 90% capture level in response to different $CO_2$ T&S price

## 7.4 Concluding remarks

In this thesis, the optimal operation of NGCC power plant integrated with PCC process was investigated under different market conditions such as different carbon price, fuel price and $CO_2$ T&S cost. The objective function to be minimized in the optimisation is the LCOE obtained by dividing total annual cost by annual net power output. The economic estimate was carried out for the reference case of NGCC standalone and the base case of NGCC integrated with CCS chain. With the deployment of carbon capture at 90% capture level, LCOE increases from €56.00/MWh to €87.26/MWh. It is also found that fuel cost, carbon emission cost and $CO_2$ T&S cost are major parts of VOPEX.

For an assumed existing 453 $MW_e$ NGCC power plant with CCS whole system, current low carbon price of €7/ton $CO_2$ is not able to drive power generators to run carbon capture process because the carbon emission cost cannot is much lower than the operating cost of CCS based on the results from this study. During UNFCCC Paris Conference in 2015, EU stated a cut of at least 40% of greenhouse emission in its 2030 climate & energy framework and a further cut of 80% by 2050 (EU, 2016a). It could be predicted that the carbon price will increase when the cap of the total amount of $CO_2$ emission is reduced over time to achieve the GHG emission controlling target (EU, 2010). Predicted by this study, carbon price needs to be up to around €100–120/ton $CO_2$ to drive carbon capture level to 90%, which is similar with the penalty carbon price for non-compliance emission of €100/ton $CO_2$ in the phase 2 of EU ETS from 2008 to 2012 (EU, 2016c). From this study, it is also found that the required carbon price would be affected by the fuel price and $CO_2$ T&S price.

In a summary, this study indicates the coactions of carbon price, fuel price and $CO_2$ T&S price will significantly affect the decision making about the optimal capture level for operating carbon capture process for a NGCC power plant.

# Chapter 8: Conclusions and recommendations for future research

## 8.1 Conclusions

This thesis presents the studies on optimal design and operation of MEA-based PCC process and the integrated system with NGCC power plant through process modelling, simulation and optimisation, aiming to reduce the cost of PCC process commercial deployment. As the base of optimisation studies, both process model and cost model were developed with high accuracy.

In Chapter 3, the process model was developed and validated at different stages. The validation showed predictions of thermodynamic model developed in this study is better than other three correlation combinations (Austgen et al., 1989; Liu et al., 1999; Zhang et al., 2011). It also indicates that the uncertainties of those correlations should be carefully considered when they are used in process modelling and simulation. In order to improve the accuracy of the model predictions, two correlations were updated by coding Fortran subroutines, including Han and Eimer (2012) model for liquid mixture density and Tsai et al. (2011) effective gas liquid interfacial area. For kinetics-controlled reactions, different values were set for kinetics of the reverse carbonate formation reactions happening in the absorber and the stripper respectively, which improves the accuracy of the process model. The process model was then validated with comprehensive pilot plant experimental data, in terms of the absorption efficiency and thermal performance of the integrated system. The comparison results show that model predictions are in very good agreements with the experimental data, which ensures that the process model has good accuracy for the optimisation studies in the following chapters.

In Chapter 4, the cost model was developed in Fortran and then integrated into the process model by coding Fortran subroutine in Aspen Plus®. Using this newly developed model, the optimisation studies were carried out for the PCC process and on the impacts of variations of the key variables. The optimisation results show the cost of $CO_2$ avoided in the optimal case is 69.13 €/ton $CO_2$, which is about 18.4% lower than the base case which have a value of 86.85 €/ton $CO_2$. Findings from case studies on cost optimisation in response to variations in several key variables include:

- The optimal rich loadings should be saturated $CO_2$ loadings under the temperature, pressure and composition conditions.
- The range of optimal lean loading in these three case studies is 0.275–0.331 mol $CO_2$/mol MEA.
- The optimal packing height of the stripper significantly depends on the solvent regeneration degree.
- The reduction of CCA is more significant when MEA concentration in solvents increases from 20 wt% to 30 wt% than increasing from 35 wt% to 40 wt%.
- For scale-up of the optimal design, size effect impacts not only economic terms but also process parameters. New optimisation should be carried out for each single case to obtain optimal values of both the equipment sizes and key operational variables.

Chapter 5 presented the investigation on thermal performances of different integration options of a 453$MW_e$ NGCC equipped with a PCC process and $CO_2$ compression train. Employing EGR achieved significant saving with the contributions from both the CAPEX and VOPEX. The CCA of the case with EGR decreased from 69.13 €/ton $CO_2$ to 66.14 €/ton $CO_2$ about 5.12% compared with the case without EGR. The thermal efficiency (LHV) of the NGCC power plant deceases from 58.74% to 49.16% when integrated with the PCC process and the compression train. This reduction includes 7.40%-points decrease due to steam extraction, 0.55%-points reduction due to PCC power consumption and 1.92%-points reduction due to compression train power consumption. With the application of EGR in the NGCC power plant at a recirculation ratio of 0.38, the net thermal efficiency increases 0.77%-points while the cross-section areas of the absorber and stripper in the carbon capture process reduced by 37.39% and 9.36% respectively.

The compression heat integration options have been analysed by applying supersonic shock wave compression technology. Compression heat integration into the steam cycle of HRSG and stripper reboiler achieves 0.32%-points and 0.54%-points net efficiency improvement separately without major capital investment required. The study indicates that EGR technology, supersonic shock wave compression technology and compression heat integrations could be future directions for commercial PCC deployment in NGCC power plants.

In Chapter 6, a detailed steady state model was developed for transport system comprising $CO_2$ mixture streams from two emitters, the compression train, the onshore and offshore trunk

pipelines and the booster pump station. The overall costs of the base case and the optimal case were also compared. The optimal case has an annual total saving of 22.7 M€. The cost evaluation results of the compression train, trunk pipeline and whole pipeline network were compared with the cost evaluation results in open literature respectively to gain more insights.

- For $CO_2$ compression, lower intercooler exit temperature (20 $^oC$ vs. 38 $^oC$ in this study) and lower pressure ratio per stage leads to lower energy and utilities consumption of compression train.

- The correlation cost models for $CO_2$ compression train do not give good cost predictions for some configuration options. The O&M factor of 0.04 in those models is very small compared to the result of this study.

- The pipeline diameter models in literature are generally reliable. Among these models, the hydraulic equation method gives the most accurate prediction. The initial velocity of $CO_2$ mixture is around 1.7m/s in the optimal case in this study.

- Large range of capital cost was obtained after applying different published cost models for the trunk pipelines. Most of the pipeline cost models in literature predicted much lower capital cost and the weight-based model in the study of Piessens et al. (2008) has the best prediction compared to the results in this study.

- Simulation-based techno-economic evaluation method offers a powerful tool for optimal designs for the projects, especially for the decision making support on the detailed technical options selection.

In Chapter 7, the optimal operation of NGCC power plant integrated with whole CCS chain was investigated under different market conditions such as carbon price, fuel price and $CO_2$ T&S cost. The objective function to be minimized in the optimisation is the LCOE obtained by dividing total annual cost by annual net power output. The economic estimate was carried out for the reference case of NGCC standalone and the base case of NGCC integrated with CCS chain. With the deployment of carbon capture at 90% capture level, LCOE increases from €56.00/MWh to €87.26/MWh. It is also found that fuel cost, carbon emission cost and $CO_2$ T&S cost are major parts of VOPEX.

For an assumed existing 453 $MW_e$ NGCC power plant with CCS whole system, current low carbon price of €7/ton $CO_2$ is not able to drive power generators to run carbon capture

process because the carbon emission penalty do not justify the operating cost of CCS. Carbon price needs to increase to around €100/ton $CO_2$ to justify the cost of carbon capture and needs to increase to around €120/ton $CO_2$ to drive carbon capture level to 90%. An economic range of lean loading is 0.26–0.3 mol $CO_2$/mol MEA for the capture levels from 60% to 95%. The fuel price and the $CO_2$ T&S price have great impact on optimal operation results and the cost of electricity. In a summary, this study indicates the coactions of carbon price, fuel price and $CO_2$ T&S price will significantly affect the decision making about the optimal capture level for operating carbon capture process for an NGCC power plant.

## 8.2 Recommendations for future research

During the thermodynamic modelling in Chapter 3, it is found that, even for MEA, the most commonly used solvent, the experimental data are not available to cover the full range of temperature, pressure and composition conditions. Thus the correlations regressed from this data for some typical published models have some uncertainties. Thus two recommendations are (1) new experimental measurements of VLE and physical properties of MEA-$H_2O$-$CO_2$ to cover the full range of temperature, pressure and composition conditions, (2) the correlations in thermodynamic model and physical property calculation needs to be improved with new experimental data.

One challenge of the industrial deployment of solvent-based PCC process is the large sizes of the equipment. But there is a big gap in terms of the equipment sizes between the pilot plants and industrial scale plants. For example, the diameter of the absorber is around 20 m at the industrial scale and is only 0.427 m at the pilot plant. This gap would cause big uncertainty for the scale-up study of the process. As a result, comprehensive running data of existing demonstration plants (e.g. Boundary Dam CCS, Canada (SASKPOWER, 2015)) should be shared with the research communities to promote studies in this field. It is also important that the researchers at industrial scale should seek more collaboration with relevant stakeholders including power plant operators, key equipment suppliers such as column internals design companies and compressors manufactories.

In terms of the whole CCS chain, the costs of $CO_2$ transport and storage in the publications are found to be normally underestimated. One of the reasons is that most estimation models are empirical correlations developed on historical cost data of natural gas pipeline projects and do not reflect the process conditions of different $CO_2$ pipeline projects. Furthermore, current cost models (including this study) did not consider the costs related with safety issues,

such as monitoring and protection of facilities namely $CO_2$ pipelines located in dense population areas, the $CO_2$ geological storage sites etc. Therefore, more extensive studies in this field are required.

# Appendix A: Publications from this thesis

**Peer reviewed journal papers:**

**Luo, X.,** Wang, M., Oko, E., Okezue, C., 2014. Simulation–based techno–economic evaluation for optimal design of $CO_2$ transport pipeline network. *Applied Energy*, 132, 610–620.

**Luo, X.,** Wang, M., Chen, J., 2015. Heat integration of natural gas combined cycle power plant integrated with post–combustion $CO_2$ capture and compression. *Fuel*, 151, 110–117.

**Luo, X.**, Wang, M., 2016. Optimal operation of MEA-based post-combustion carbon capture for natural gas combined cycle power plants under different market conditions. *International Journal of Greenhouse Gas Control*, 48, Part 2**,** 312-320.

**Peer reviewed conference papers:**

**Luo, X.,** Mistry, K., Okezue, C., Wang, M., Cooper, R., Oko, E., Field, J., 2014. Process Simulation and Analysis for $CO_2$ Transport Pipeline Design and Operation – Case Study for the Humber Region in the UK, *Computer Aided Chemical Engineering*, pp. 1633–1638.

**Luo, X.,** Wang, M., 2015, Optimal operation of MEA–based post–combustion carbon capture process for gas–fired CCGT power plants, *In 7$^{th}$ International Exergy, Energy and Environment Symposium (IEEES7): University of Valenciennes et du Hainaut–Cambrésis – ENSIAME – Valenciennes – FRANCE*. April 27–30, 2015.

**Peer reviewed book chapter:**

**Luo, X.,** Wang, M.,. Process Simulation and Integration of Natural Gas Combined Cycle Power Plant Integrated with Chemical Absorption Carbon Capture and Compression, *In: The Water–Food–Energy Nexus: Processes, Technologies and Challenges*, Edited by I.M. Mujtaba, R. Srinivasan and N. O. Elbashir, In Press.

# Reference


Abu-Zahra, M. R. M., Niederer, J. P. M., Feron, P. H. M. & Versteeg, G. F. (2007a) $CO_2$ capture from power plants: Part II. A parametric study of the economical performance based on mono-ethanolamine. *International Journal of Greenhouse Gas Control*, 1(2), 135-142.

Abu-Zahra, M. R. M., Schneiders, L. H. J., Niederer, J. P. M., Feron, P. H. M. & Versteeg, G. F. (2007b) $CO_2$ capture from power plants Part I. A parametric study of the technical performance based on monoethanolamine. *International Journal of Greenhouse Gas Control*, 1(1), 37-46.

Agbonghae, E. O., Hughes, K. J., Ingham, D. B., Ma, L. & Pourkashanian, M. (2014) Optimal Process Design of Commercial-Scale Amine-Based $CO_2$ Capture Plants. *Industrial & Engineering Chemistry Research*, 53(38), 14815-14829.

Alibaba. (2016) *RE: Monoethanolamine (MEA) price.* Quotation to Luo, X.

Amrollahi, Z., Ystad, P. A. M., Ertesvåg, I. S. & Bolland, O. (2012) Optimized process configurations of post-combustion $CO_2$ capture for natural-gas-fired power plant – Power plant efficiency analysis. *International Journal of Greenhouse Gas Control*, 8(0), 1-11.

Aresta, M., Dibenedetto, A. & Angelini, A. (2013) The changing paradigm in $CO_2$ utilization. *Journal of $CO_2$ Utilization*, 3-4, 65-73.

Arias, A. M., Mores, P. L., Scenna, N. J. & Mussati, S. F. (2016) Optimal design and sensitivity analysis of post-combustion $CO_2$ capture process by chemical absorption with amines. *Journal of Cleaner Production*, 115, 315-331.

Aronu, U. E., Gondal, S., Hessen, E. T., Haug-Warberg, T., Hartono, A., Hoff, K. A. & Svendsen, H. F. (2011) Solubility of $CO_2$ in 15, 30, 45 and 60 mass% MEA from 40 to 120°C and model representation using the extended UNIQUAC framework. *Chemical Engineering Science*, 66(24), 6393-6406.

Aspelund, A. & Jordal, K. (2007) Gas conditioning—The interface between $CO_2$ capture and transport. *International Journal of Greenhouse Gas Control*, 1(3), 343-354.

AspenTech. (2008a) *Aspen Plus User Guide 10.2*. Burlington, MA: Aspen Technology, Lnc.

AspenTech. (2008b) *Rate-based Model of the $CO_2$ Capture Process by MEA using Aspen Plus*. Burlington, MA Aspen Technology, Inc.

AspenTech. (2012a) *Aspen Icarus Reference Guide: Icarus Evaluation Engine (IEE) V8.0*. Burlington, USA: Aspen Technology, Inc.

AspenTech. (2012b) *Aspen Physical Property System: Physical Property Methods*. Burlington, USA: Aspen Technology, Inc.

Austgen, D. M., Rochelle, G. T., Peng, X. & Chen, C. C. (1989) Model of vapor-liquid equilibria for aqueous acid gas-alkanolamine systems using the electrolyte-NRTL equation. *Industrial & Engineering Chemistry Research*, 28(7), 1060-1073.

Bassily, A. M. (2007) Modeling, numerical optimization, and irreversibility reduction of a triple-pressure reheat combined cycle. *Energy*, 32(5), 778-794.

Bates, R. G. & Pinching, G. D. (1951) Acidic dissociation constant and related thermodynamic quantities for monoethanolammonium ion in water from 0°C to 50°C. *J. Res. Natl. Bur. Stand.*, 46(5), 349-352.

BBC. (2015) *UK's coal plants to be phased out within 10 years* [Online]. Available: http://www.bbc.co.uk/news/business-34851718 [Accessed 6th June 2016].

BIGCO2. (2007) *$CO_2$ Management Technologies for Future Power Generation* [Online]. 2007–2011: BIGCO2 Research & Development Platform. Available: http://www.bigco2.com [Accessed 6th June 2016].

Biliyok, C., Canepa, R., Wang, M. & Yeung, H. (2013) Techno-Economic Analysis of a Natural Gas Combined Cycle Power Plant with $CO_2$ Capture. *In:* Andrzej, K. & Ilkka, T. (eds.) *Computer Aided Chemical Engineering.* Elsevier.

Biliyok, C. & Yeung, H. (2013) Evaluation of natural gas combined cycle power plant for post-combustion $CO_2$ capture integration. *International Journal of Greenhouse Gas Control*, 19(0), 396-405.

Billet, R. & Schultes, M. (1993) Predicting mass transfer in packed columns. *Chemical Engineering and Technology*, 16(1), 1-9.

Blasing, T. J. (2013) *Current Greenhouse Gas Concentrations* [Online]. CDIAC Web site. Available: http://cdiac.ornl.gov/pns/current_ghg.html [Accessed 6th June 2016].

Boggs, P. T. & Tolle, J. W. (2000) Sequential quadratic programming for large-scale nonlinear optimization. *Journal of Computational and Applied Mathematics*, 124(1–2), 123-137.

Bollas, G. M., Chen, C. C. & Barton, P. I. (2008) Refined electrolyte-NRTL model: Activity coefficient expressions for application to multi-electrolyte systems. *AIChE Journal*, 54(6), 1608-1624.

Boot-Handford, M. E., Abanades, J. C., Anthony, E. J., Blunt, M. J., Brandani, S., Mac Dowell, N., Fernandez, J. R., Ferrari, M.-C., Gross, R., Hallett, J. P., Haszeldine, R. S., Heptonstall, P., Lyngfelt, A., Makuch, Z., Mangano, E., Porter, R. T. J., Pourkashanian, M., Rochelle, G. T., Shah, N., Yao, J. G. & Fennell, P. S. (2014) Carbon capture and storage update. *Energy & Environmental Science*, 7(1), 130-189.

Böttinger, W., Maiwald, M. & Hasse, H. (2008) Online NMR spectroscopic study of species distribution in MEA-$H_2O$-$CO_2$ and DEA-$H_2O$-$CO_2$. *Fluid Phase Equilibria*, 263(2), 131-143.

BP. (2014) *BP Statistical Review of World Energy 2014* [Online]. Available: http://www.bp.com/content/dam/bp-country/de_de/PDFs/brochures/BP-statistical-review-of-world-energy-2014-full-report.pdf [Accessed 6th June 2016].

Bravo, J. L., Rocha, J. A. & Fair, J. R. (1985) Mass transfer in gauze packings. *Hydrocarbon Processing*, 64(1), 91-95.

Brelvi, S. W. & O'Connell, J. P. (1972) Corresponding states correlations for liquid compressibility and partial molal volumes of gases at infinite dilution in liquids. *AIChE Journal*, 18(6), 1239-1243.

Buhre, B., Elliott, L., Sheng, C., Gupta, R. & Wall, T. (2005) Oxy-fuel combustion technology for coal-fired power generation. *Progress in energy and combustion science*, 31(4), 283-307.

Buizert, C., Gkinis, V., Severinghaus, J. P., He, F., Lecavalier, B. S., Kindler, P., Leuenberger, M., Carlson, A. E., Vinther, B., Masson-Delmotte, V., White, J. W. C.,

Liu, Z., Otto-Bliesner, B. & Brook, E. J. (2014) Greenland temperature response to climate forcing during the last deglaciation. *Science*, 345(6201), 1177-1180.

Canepa, R. & Wang, M. (2015) Techno-economic analysis of a $CO_2$ capture plant integrated with a commercial scale combined cycle gas turbine (CCGT) power plant. *Applied Thermal Engineering*, 74(0), 10-19.

Canepa, R., Wang, M., Biliyok, C. & Satta, A. (2013) Thermodynamic analysis of combined cycle gas turbine power plant with post-combustion $CO_2$ capture and exhaust gas recirculation. *Proceedings of the Institution of Mechanical Engineers, Part E: Journal of Process Mechanical Engineering*, 227(2), 89-105.

Carbon Capture Journal. (2013) *Internals for carbon capture plants* [Online]. Available: http://www.carboncapturejournal.com/news/internals-for-carbon-capture-plants/3349.aspx?Category=featured [Accessed 6th June 2016].

CASTOR. (2004) EU-Project $CO_2$, from Capture to Storage (CASTOR): integrated research project under the 6th frame work programme of the European commission, . contract nr. ses6-ct-2004-502586: project duration from 01.02.2004 to 31.01.2008.

CCP. (2000) $CO_2$ Capture Project (CCP): CCP1, CCP2, and CCP3. project duration from 2000 to 2013.

CCSA. (2014) *Don Valley Power Plant and CCS Project* [Online]. Available: http://www.ccsassociation.org/about-us/our-members/sargas-power/ [Accessed 6th June 2016].

CESAR. (2008) EU-Project $CO_2$ Enhanced Separation and Recovery (CESAR): integrated research project under the 7th frame work programme of the European commission. project duration from 01.02.2008 to 31.01.2011: contract nr. 213569.

Chaczykowski, M. & Osiadacz, A. J. (2012) Dynamic simulation of pipelines containing dense phase/supercritical $CO_2$-rich mixtures for carbon capture and storage. *International Journal of Greenhouse Gas Control*, 9, 446-456.

Chandel, M. K., Pratson, L. F. & Williams, E. (2010) Potential economies of scale in $CO_2$ transport through use of a trunk pipeline. *Energy Conversion and Management*, 51(12), 2825-2834.

Chapel, D. G., Mariz, C. L. & Ernest, J. (Year) Recovery of $CO_2$ from flue gases: commercial trends. *In:* Canadian society of chemical engineers annual meeting, 1999.

Chapoy, A., Burgass, R., Tohidi, B., Michael Austell, J. & Eickhoff, C. (2011) Effect of common impurities on the phase behavior of carbon-dioxide-rich systems: Minimizing the risk of hydrate formation and two-phase flow. *SPE Journal*, 16(4), 921-930.

Chen, C.-C. & Evans, L. B. (1986) A local composition model for the excess Gibbs energy of aqueous electrolyte systems. *AIChE Journal*, 32(3), 444-454.

Chen, C. C., Boston, J. F., Evans, L. B. & Britt, H. I. (1982) Local composition model for excess Gibbs energy of electrolyte systems. Part I: Single solvent, single completely dissociated electrolyte systems. *AIChE Journal*, 28(4), 588-596.

Chen, C. C., Britt, H. I., Boston, J. F. & Evans, L. B. (1979) Extension and application of the pitzer equation for vapor - liquid equilibrium of aqueous electrolyte systems with molecular solutes. *AIChE Journal*, 25(5), 820-831.

Cheng, S., Meisen, A. & Chakma, A. (1996) Predict amine solution properties accurately. *Hydrocarbon Processing*, 75(2), 81-84.

Chilton, T. H. & Colburn, A. P. (1934) Mass transfer (absorption) coefficients prediction from data on heat transfer and fluid friction. *Industrial & engineering chemistry*, 26(11), 1183-1187.

Ciferno, J. P., Fout, T. E., Jones, A. P. & Murphy, J. T. (2009) Capturing carbon from existing coal-fired power plants. *Chemical Engineering Progress*, 105(4), 33-41.

CO2CRC. (2003) The Cooperative Research Centre for Greenhouse Gas Technologies (CO2CRC). project duration from 2003 to 2015.

Cohen, S. M., Rochelle, G. T. & Webber, M. E. (2012) Optimizing post-combustion $CO_2$ capture in response to volatile electricity prices. *International Journal of Greenhouse Gas Control*, 8(0), 180-195.

CPL. (2013) *About the White Rose CCS Project* [Online]. Capture Power Limited. Available: http://www.whiteroseccs.co.uk/about-white-rose [Accessed 6th June 2016].

Dahowski, R. T., Li, X., Davidson, C., Wei, N. & Dooley, J. (2009) *Regional opportunities for carbon dioxide capture and storage in China*. Richland, WA, USA: Pacific Northwest National Laboratory.

Danckwerts, P. (1951) Significance of liquid-film coefficients in gas absorption. *Industrial & Engineering Chemistry*, 43(6), 1460-1467.

Dang, H. & Rochelle, G. T. (2003) $CO_2$ absorption rate and solubility in monoethanolamine/piperazine/water. *Separation Science and Technology*, 38(2), 337-357.

Davis, J. & Rochelle, G. (2009) Thermal degradation of monoethanolamine at stripper conditions. *Energy Procedia*, 1(1), 327-333.

DECC. (2013) *CCS Cost Reduction Task Force: final report* [Online]. Available: https://www.gov.uk/government/publications/ccs-cost-reduction-task-force-final-report [Accessed 6th June 2016].

Diamantonis, N. I., Boulougouris, G. C., Mansoor, E., Tsangaris, D. M. & Economou, I. G. (2013) Evaluation of Cubic, SAFT, and PC-SAFT Equations of State for the Vapor–Liquid Equilibrium Modeling of CO2 Mixtures with Other Gases. *Industrial & Engineering Chemistry Research*, 52(10), 3933-3942.

Dillon, D., Panesar, R., Wall, R., Allam, R., White, V., Gibbins, J. & Haines, M. (Year) Oxy-combustion processes for $CO_2$ capture from advanced supercritical PF and NGCC power plant. *In:* 7 th International Conference on Greenhouse Gas Technologies, Vancouver, Canada, 2004.

Dugas, R. E. (2006) Pilot plant study of carbon dioxide capture by aqueous monoethanolamine. *MSE Thesis, University of Texas at Austin*.

E.ON. (2010) *Equation of State Prediction of Carbon Dioxide Properties* [Online]. Available: http://webarchive.nationalarchives.gov.uk/20111209170139/https:/www.decc.gov.uk/en/content/cms/emissions/ccs/demo_prog/feed/e_on_feed_/transport/transport.aspx [Accessed 6th June 2016].

Easterling, D. R. & Wehner, M. F. (2009) *Is the climate warming or cooling?* [Online]. Available: http://dx.doi.org/10.1029/2009GL037810 [Accessed 6th June 2016].

Edgar, T. F., Himmelblau, D. M. & Lasdon, L. S. (2001) *Optimization of Chemical Processes*: McGraw-Hill.

Edwards, T., Maurer, G., Newman, J. & Prausnitz, J. (1978) Vapor - liquid equilibria in multicomponent aqueous solutions of volatile weak electrolytes. *AIChE Journal*, 24(6), 966-976.

EEEAG. (2015) *EU Emission Allowances | Secondary Market* [Online]. European Energy Exchange AG. Available: https://www.eex.com/en/market-data/emission-allowances/spot-market/european-emission-allowances#!/2016/06/06 [Accessed 6th June 2016].

EIA. (2016) *How much carbon dioxide is produced per kilowatthour when generating electricity with fossil fuels?* [Online]. Available: https://www.eia.gov/tools/faqs/faq.cfm?id=74&t=11 [Accessed 6th June 2016].

EU. (2010) *EU ETS Handbook* [Online]. Available: http://ec.europa.eu/clima/publications/docs/ets_handbook_en.pdf [Accessed 6th June 2016].

EU. (2016a) *Climate strategies & targets* [Online]. EU. Available: http://ec.europa.eu/clima/policies/strategies/index_en.htm [Accessed 6th June 2016].

EU. (2016b) *Electricity production and supply statistics* [Online]. Available: http://ec.europa.eu/eurostat/statistics-explained/index.php/Electricity_production_and_supply_statistics#Further_Eurostat_information [Accessed 6th June 2016].

EU. (2016c) *Phases 1 and 2 (2005-2012) of The EU Emissions Trading System (ETS)* [Online]. Available: http://ec.europa.eu/clima/policies/ets/pre2013/index_en.htm [Accessed 6th June 2016].

Faber, R., Köpcke, M., Biede, O., Knudsen, J. N. & Andersen, J. (2011) Open-loop step responses for the MEA post-combustion capture process: Experimental results from the Esbjerg pilot plant. *Energy Procedia*, 4(0), 1427-1434.

Fakouri Baygi, S. & Pahlavanzadeh, H. (2015) Application of the perturbed chain-SAFT equation of state for modeling $CO_2$ solubility in aqueous monoethanolamine solutions. *Chemical Engineering Research and Design*, 93, 789-799.

Feng, Y. & Rangaiah, G. P. (2011) Evaluating capital cost estimation programs. *Chemical Engineering*, 118(8), 22-29.

Foster NR, B. K., Dehghani F. . (2010) *Modeling of Phase Equilibria for Binary and Ternary Mixture of Carbon Dioxide, Hydrogen and Methanol* [Online]. Available: http://webarchive.nationalarchives.gov.uk/20111209170139/https:/www.decc.gov.uk/en/content/cms/emissions/ccs/demo_prog/feed/e_on_feed_/transport/transport.aspx [Accessed 6th June 2016].

Gao, L., Fang, M., Li, H. & Hetland, J. (2011) Cost analysis of $CO_2$ transportation: Case study in China. *Energy Procedia*, 4, 5974-5981.

GCCSI. (2011) *Economic assessment of carbon capture and storage technologies* [Online]. GCCSI. Available: http://www.globalccsinstitute.com/publications/economic-assessment-carbon-capture-and-storage-technologies-2011-update [Accessed 2014-02-26].

GE Power. (2016) 9F.05 Gas Turbine (50 Hz). GE Power.

GerbilNow. (2012) *Why choose between solar and coal when you can use both?* [Online]. Available: http://blog.gerbilnow.com/2012/11/solar-coal-power.html [Accessed 6th June 2016].

Gibbins, J., Crane, R., Lambropoulos, D., Booth, C., Roberts, C. & Lord, M. (2004) Maximising the effectiveness of post-combustion $CO_2$ capture systems. *Proceedings of GHGT*, 7, 5-9.

Godoy, E., Benz, S. J. & Scenna, N. J. (2011) A strategy for the economic optimization of combined cycle gas turbine power plants by taking advantage of useful thermodynamic relationships. *Applied Thermal Engineering*, 31(5), 852-871.

Godoy, E., Scenna, N. J. & Benz, S. J. (2010) Families of optimal thermodynamic solutions for combined cycle gas turbine (CCGT) power plants. *Applied Thermal Engineering*, 30(6-7), 569-576.

Gross, J. & Sadowski, G. (2001) Perturbed-chain SAFT: An equation of state based on a perturbation theory for chain molecules. *Industrial and Engineering Chemistry Research*, 40(4), 1244-1260.

Gross, J. & Sadowski, G. (2002) Application of the Perturbed-Chain SAFT Equation of State to Associating Systems. *Industrial & Engineering Chemistry Research*, 41(22), 5510-5515.

Han, J., Jin, J., Eimer, D. A. & Melaaen, M. C. (2012) Density of Water (1) + Monoethanolamine (2) + $CO_2$ (3) from (298.15 to 413.15) K and Surface Tension of Water (1) + Monoethanolamine (2) from (303.15 to 333.15) K. *Journal of Chemical & Engineering Data*, 57(4), 1095-1103.

Harriott, P. (1989) Effect of liquid maldistribution on the performance of packed stripping columns. *Environmental Science & Technology*, 23(3), 309-314.

Harris, F., Kurnia, K. A., Mutalib, M. I. A. & Thanapalan, M. (2009) Solubilities of carbon dioxide and densities of aqueous sodium glycinate solutions before and after CO absorption. *Journal of Chemical and Engineering Data*, 54(1), 144-147.

Hartmann, D., Klein Tank, A., Rusicucci, M., Alexander, L., Broenniman, B., Charabi, Y., Dentener, F., Dlugokencky, E., Easterling, D. & Kaplan, A. (2013) *Observations: Atmosphere and Surface. In: Climate Change 2013: The Physical Science Basis. Contribution of Working Group I to the Fifth Assessment Report of the Intergovernmental Panel on Climate Change*. Cambridge, United Kingdom and New York, NY, USA: Cambridge University Press.

Hartono, A., Mba, E. O. & Svendsen, H. F. (2014) Physical Properties of Partially $CO_2$ Loaded Aqueous Monoethanolamine (MEA). *Journal of Chemical & Engineering Data*, 59(6), 1808-1816.

Heddle, G., Herzog, H. & Klett, M. (2003) The economics of $CO_2$ storage. *The economics of $CO_2$ storage.*

Hegerl, G., Zwiers, F., Braconnot, P., Gillet, N., Luo, Y., Marengo, J., Nicholls, N., Penner, J. & Stott, P. (2007) Understanding and attributing climate change. *In:* Solomon, S., Qin, D., Manning, M., Chen, Z., Marquis, M., Averyt, K. B., Tignor, M. & Miller, H.

L. (eds.) *Climate Change 2007: The Physical Science Basis. Contribution of Working Group I to the Fourth Assessment Report of the Intergovernmental Panel on Climate Change* Cambridge, United Kingdom and New York, NY, USA: Cambridge University Press.

Hessen, E. T., Haug-Warberg, T. & Svendsen, H. F. (2010) The refined e-NRTL model applied to $CO_2$-$H_2O$-alkanolamine systems. *Chemical Engineering Science*, 65(11), 3638-3648.

Higbie, R. (1935) The rate of absorption of a pure gas into a still liquid during short periods of exposure. *Transactions of the A.I.Ch.E.,*, (31), pp. 365–389.

Hilliard, M. D. (2008) *A Predictive Thermodynamic Model for an Aqueous Blend of Potassium Carbonate, Piperazine, and Monoethanolamine for Carbon Dioxide Capture from Flue Gas.* PhD, University of Texas at Austin.

Hoek, P. J. (1983) *Large and small scale liquid maldistribution in a packed column.* TU Delft, Delft University of Technology.

IEA. (2008) *Energy Technology Perspectives 2008 - In support of the G8 Plan of Action*. Paris: International Energy Agency.

IEA. (2010) *Energy Technology Perspectives 2010*. Paris: International Energy Agency.

IEA. (2012) *Energy Technology Perspectives 2012*. Paris: International Energy Agency.

IEA. (2015) *$CO_2$ emissions from fuel combustion-highlights 2015* [Online]. Paris: IEA. Available: https://www.iea.org/publications/freepublications/publication/co2-emissions-from-fuel-combustion-highlights-2015.html [Accessed 6th June 2016].

IEAGHG. (2002) Pipeline transmission of $CO_2$ and energy. Transmission study report. IEA GHG.

IEAGHG. (2010) *Corrosion and Materials Selection in CCS Systems*. Orchard, UK: International Energy Agency.

IEAGHG. (2012) $CO_2$ Capture at Gas Fired Power Plants. International Energy Agency.

Inflation. (2015) *Historic harmonised inflation Europe – HICP inflation* [Online]. Available: http://www.inflation.eu/inflation-rates/europe/historic-inflation/hicp-inflation-europe.aspx [Accessed 6th June 2016].

IPCC. (2005) *Carbon Dioxide Capture and Storage*. UK: Cambridge University Press.

IPCC. (2007) *Mitigation of climate change* [Online]. IPCC. Available: http://www.ipcc.ch/publications_and_data/publications_and_data_reports.shtml [Accessed 6th June 2016].

IPCC. (2015) *Climate Change 2014: Mitigation of Climate Change* (Vol. 3). UK: Cambridge University Press.

Jonshagen, K., Sipöcz, N. & Genrup, M. (2011) A Novel Approach of Retrofitting a Combined Cycle with Post Combustion $CO_2$ Capture. *Journal of Engineering for Gas Turbines and Power*, 133((1)), 011703.

Jonsson, M., Bolland, O., Bücker, D. & Rost, M. (2005) Gas turbine cooling model for evaluation of novel cycles. *Proceedings of ECOS*, 20-22.

Jordal, K., Ystad, P. A. M., Anantharaman, R., Chikukwa, A. & Bolland, O. (2012) Design-point and part-load considerations for natural gas combined cycle plants with post combustion capture. *International Journal of Greenhouse Gas Control*, 11(0), 271-282.

Jou, F.-Y., Mather, A. E. & Otto, F. D. (1995) Solubility of $CO_2$ in a 30 mass percent monoethanolamine solution. *Canadian Journal of Chemical Engineering*, 73(1), 140-147.

Kang, C. A., Brandt, A. R. & Durlofsky, L. J. (2011) Optimal operation of an integrated energy system including fossil fuel power generation, $CO_2$ capture and wind. *Energy*, 36(12), 6806-6820.

Kanniche, M., Gros-Bonnivard, R., Jaud, P., Valle-Marcos, J., Amann, J.-M. & Bouallou, C. (2010) Pre-combustion, post-combustion and oxy-combustion in thermal power plant for $CO_2$ capture. *Applied Thermal Engineering*, 30(1), 53-62.

Karl, T. R., Arguez, A., Huang, B., Lawrimore, J. H., McMahon, J. R., Menne, M. J., Peterson, T. C., Vose, R. S. & Zhang, H.-M. (2015) Possible artifacts of data biases in the recent global surface warming hiatus. *Science*, 348(6242), 1469-1472.

Kenig, E. Y., Schneider, R. & Górak, A. (2001) Reactive absorption: Optimal process design via optimal modelling. *Chemical Engineering Science*, 56(2), 343-350.

Kim, Y. (2007) Equation of state for carbon dioxide. *Journal of Mechanical Science and Technology*, 21(5), 799-803.

King, C. (1966) Turbulent liquid phase mass transfer at free gas-liquid interface. *Industrial & Engineering Chemistry Fundamentals*, 5(1), 1-8.

Knoope, M. M. J., Ramírez, A. & Faaij, A. P. C. (2013) A state-of-the-art review of techno-economic models predicting the costs of $CO_2$ pipeline transport. *International Journal of Greenhouse Gas Control*, 16, 241-270.

Koch-Glitsch. (2014) *Carbon capture* [Online]. Available: http://www.koch-glitsch.com/masstransfer/pages/carbon-capture.aspx [Accessed 6th June 2016].

Koch-Glitsch. (2015) *Structured Pakcing* [Online]. Available: http://www.koch-glitsch.com/Document%20Library/KGSP.pdf [Accessed 6th June 2016].

Koornneef, J., Ramirez, A., van Harmelen, T., van Horssen, A., Turkenburg, W. & Faaij, A. (2010) The impact of $CO_2$ capture in the power and heat sector on the emission of $SO_2$, $NO_x$, particulate matter, volatile organic compounds and $NH_3$ in the European Union. *Atmospheric Environment*, 44(11), 1369-1385.

Kunz, O. & Wagner, W. (2012) The GERG-2008 Wide-Range Equation of State for Natural Gases and Other Mixtures: An Expansion of GERG-2004. *Journal of Chemical & Engineering Data*, 57(11), 3032-3091.

Kvamme, B., Kuznetsova, T., Jensen, B., Stensholt, S., Bauman, J., Sjoblom, S. & Nes Lervik, K. (2014) Consequences of $CO_2$ solubility for hydrate formation from carbon dioxide containing water and other impurities. *Physical Chemistry Chemical Physics*, 16(18), 8623-8638.

Kvamsdal, H. M., Chikukwa, A., Hillestad, M., Zakeri, A. & Einbu, A. (2011a) A comparison of different parameter correlation models and the validation of an MEA-based absorber model. *Energy Procedia*, 4(0), 1526-1533.

Kvamsdal, H. M., Haugen, G. & Svendsen, H. F. (2011b) Flue-gas cooling in post-combustion capture plants. *Chemical Engineering Research and Design*, 89(9), 1544-1552.

Kvamsdal, H. M., Hetland, J., Haugen, G., Svendsen, H. F., Major, F., Kårstad, V. & Tjellander, G. (2010) Maintaining a neutral water balance in a 450 MWe NGCC-CCS power system with post-combustion carbon dioxide capture aimed at offshore operation. *International Journal of Greenhouse Gas Control*, 4(4), 613-622.

Kvamsdal, H. M., Jordal, K. & Bolland, O. (2007) A quantitative comparison of gas turbine cycles with $CO_2$ capture. *Energy*, 32(1), 10-24.

Kvamsdal, H. M. & Rochelle, G. T. (2008) Effects of the Temperature Bulge in CO2 Absorption from Flue Gas by Aqueous Monoethanolamine. *Industrial & Engineering Chemistry Research*, 47(3), 867-875.

Lawal, A., Wang, M., Stephenson, P. & Obi, O. (2012) Demonstrating full-scale post-combustion $CO_2$ capture for coal-fired power plants through dynamic modelling and simulation. *Fuel*, 101(0), 115-128.

Lawal, A., Wang, M., Stephenson, P. & Yeung, H. (2009) Dynamic modelling of $CO_2$ absorption for post combustion capture in coal-fired power plants. *Fuel*, 88(12), 2455-2462.

Lawlor, S. (2009) *$CO_2$ Compression Using Supersonic Shock Wave Technology* [Online]. Ramgen Power Systems. Available: http://www.netl.doe.gov/technologies/coalpower/ewr/co2/co2compression/supersonic.html [Accessed 6th June 2016].

Lazic, T., Oko, E. & Wang, M. (2013) Case study on $CO_2$ transport pipeline network design for Humber region in the UK. *Proceedings of the Institution of Mechanical Engineers, Part E: Journal of Process Mechanical Engineering*.

Lee, B. I. & Kesler, M. G. (1975) A generalized thermodynamic correlation based on three-parameter corresponding states. *AIChE Journal*, 21(3), 510-527.

Lee, J. I., Otto, F. D. & Mather, A. E. (1974) The solubility of $H_2S$ and $CO_2$ in aqueous monoethanolamine solutions. *Can. J. Chem. Eng.*, 52(6), 803-805.

Lee, J. I., Otto, F. D. & Mather, A. E. (1976) Equilibrium between carbon dioxide and aqueous monoethanolamine solutions. *J Appl Chem Biotechnol*, 26(10), 541-549.

Lepaumier, H., Grimstvedt, A., Vernstad, K., Zahlsen, K. & Svendsen, H. F. (2011) Degradation of MMEA at absorber and stripper conditions. *Chemical Engineering Science*, 66(15), 3491-3498.

Li, H., Jakobsen, J. P., Wilhelmsen, Ø. & Yan, J. (2011) PVTxy properties of $CO_2$ mixtures relevant for $CO_2$ capture, transport and storage: Review of available experimental data and theoretical models. *Applied Energy*, 88(11), 3567-3579.

Li, H. & Yan, J. (Year) Impact of Impurities in $CO_2$-Fluids on $CO_2$ Transport Process. *In:* ASME Turbo Expo 2006: Power for Land, Sea, and Air, May 8–11 2006 Barcelona, Spain. pp. 367-375.

Li, H. & Yan, J. (2009) Evaluating cubic equations of state for calculation of vapor–liquid equilibrium of $CO_2$ and $CO_2$-mixtures for $CO_2$ capture and storage processes. *Applied Energy*, 86(6), 826-836.

Li, H., Yan, J., Yan, J. & Anheden, M. (2009) Impurity impacts on the purification process in oxy-fuel combustion based $CO_2$ capture and storage system. *Applied Energy*, 86(2), 202-213.

Liljemark, S., Arvidsson, K., Mc Cann, M. T. P., Tummescheit, H. & Velut, S. (2011) Dynamic simulation of a carbon dioxide transfer pipeline for analysis of normal operation and failure modes. *Energy Procedia*, 4, 3040-3047.

Lin, Y. & Franzke, C. L. (2015) Scale-dependency of the global mean surface temperature trend and its implication for the recent hiatus of global warming. *Scientific reports*, 5.

Littel, R. J., Versteeg, G. F. & Van Swaaij, W. P. M. (1992) Kinetics of $CO_2$ with primary and secondary amines in aqueous solutions-II. Influence of temperature on zwitterion formation and deprotonation rates. *Chemical Engineering Science*, 47(8), 2037-2045.

Liu, Y., Zhang, L. & Watanasiri, S. (1999) Representing Vapor−Liquid Equilibrium for an Aqueous MEA−$CO_2$ System Using the Electrolyte Nonrandom-Two-Liquid Model. *Industrial & Engineering Chemistry Research*, 38(5), 2080-2090.

Lucquiaud, M. & Gibbins, J. (2009) Retrofitting $CO_2$ capture ready fossil plants with post-combustion capture. Part 1: Requirements for supercritical pulverized coal plants using solvent-based flue gas scrubbing. *Proceedings of the Institution of Mechanical Engineers, Part A: Journal of Power and Energy*, 223(3), 213-226.

Mac Dowell, N., Llovell, F., Adjiman, C. S., Jackson, G. & Galindo, A. (2009) Modeling the Fluid Phase Behavior of Carbon Dioxide in Aqueous Solutions of Monoethanolamine Using Transferable Parameters with the SAFT-VR Approach. *Industrial & Engineering Chemistry Research*, 49(4), 1883-1899.

Mac Dowell, N., Pereira, F. E., Llovell, F., Blas, F. J., Adjiman, C. S., Jackson, G. & Galindo, A. (2011) Transferable SAFT-VR Models for the Calculation of the Fluid Phase Equilibria in Reactive Mixtures of Carbon Dioxide, Water, and n-Alkylamines in the Context of Carbon Capture. *The Journal of Physical Chemistry B*, 115(25), 8155-8168.

Mac Dowell, N. & Shah, N. (2013) Identification of the cost-optimal degree of $CO_2$ capture: An optimisation study using dynamic process models. *International Journal of Greenhouse Gas Control*, 13(0), 44-58.

Mahgerefteh, H., Denton, G. & Rykov, Y. (Year) Pressurised $CO_2$ pipeline rupture. *In*, 2008. 869-879.

Mangalapally, H. P. & Hasse, H. (2011) Pilot plant study of post-combustion carbon dioxide capture by reactive absorption: Methodology, comparison of different structured packings, and comprehensive results for monoethanolamine. *Chemical Engineering Research and Design*, 89(8), 1216-1228.

Marchioro Ystad, P. A., Lakew, A. A. & Bolland, O. (2013) Integration of low-temperature transcritical $CO_2$ Rankine cycle in natural gas-fired combined cycle (NGCC) with post-combustion $CO_2$ capture. *International Journal of Greenhouse Gas Control*, 12(0), 213-219.

Mason, J. W. & Dodge, B. F. (1936) Equilibrium absorption of carbon dioxide by solutions of the ethanolamines. *Trans. Am. Inst. Chem. Eng*, 32, 27-48.

McCollum, D. L. & Ogden, J. M. (2006) *Techno-economic models for carbon dioxide compression, transport, and storage & Correlations for estimating carbon dioxide density and viscosity* [Online]. Available: http://www.canadiancleanpowercoalition.com/pdf/CTS1%20-%202006_UCD-ITS-RR-06-14[1].pdf [Accessed 6th 2016 2016].

McCoy, S. & Rubin, E. (2008) An engineering-economic model of pipeline transport of $CO_2$ with application to carbon capture and storage. *International Journal of Greenhouse Gas Control*, 2(2), 219-229.

Merkel, T. C., Lin, H., Wei, X. & Baker, R. (2010) Power plant post-combustion carbon dioxide capture: an opportunity for membranes. *Journal of membrane science*, 359(1), 126-139.

Mores, P., Rodríguez, N., Scenna, N. & Mussati, S. (2012) $CO_2$ capture in power plants: Minimization of the investment and operating cost of the post-combustion process using MEA aqueous solution. *International Journal of Greenhouse Gas Control*, 10(0), 148-163.

Mores, P. L., Godoy, E., Mussati, S. F. & Scenna, N. J. (2014) A NGCC power plant with a $CO_2$ post-combustion capture option. Optimal economics for different generation/capture goals. *Chemical Engineering Research and Design*, 92(7), 1329-1353.

NASA. (2016) *Carbon Dioxide* [Online]. NASA. Available: http://climate.nasa.gov/vital-signs/carbon-dioxide/ [Accessed 6th June 2016].

National Grid. (2014) *Yorkshire and Humber CCS Project* [Online]. Available: http://www.ccshumber.co.uk/ [Accessed 6th June 2016].

NERC. (2014) *Storing carbon dioxide beneath the Moray Firth explored* [Online]. Available: http://www.bgs.ac.uk/research/highlights/2010/scottishCCS.html [Accessed 6th June 2016].

Nimtz, M., Klatt, M., Wiese, B., Kühn, M. & Joachim Krautz, H. (2010) Modelling of the $CO_2$ process- and transport chain in CCS systems—Examination of transport and storage processes. *Chemie der Erde - Geochemistry*, 70, 185-192.

NOAA. (2015) *The Recent Global Surface Warming Hiatus* [Online]. Available: https://www.ncdc.noaa.gov/news/recent-global-surface-warming-hiatus [Accessed 6th June 2016].

Notz, R., Mangalapally, H. P. & Hasse, H. (2012) Post combustion $CO_2$ capture by reactive absorption: Pilot plant description and results of systematic studies with MEA. *International Journal of Greenhouse Gas Control*, 6, 84-112.

Ogden, J. M., Yang, C., Johnson, N., Ni, J. & Johnson, J. (2004) *Conceptual design of optimized fossil energy systems with capture and sequestration of carbon dioxide* [Online]. Available: http://www.osti.gov/scitech/servlets/purl/829538 [Accessed 6th June 2016].

Ong'iro, A. O., Ugursal, V. I., Al Taweel, A. M. & Blamire, D. K. (1995) Simulation of combined cycle power plants using the ASPEN PLUS shell. *Heat Recovery Systems and CHP*, 15(2), 105-113.

Oyenekan, B. A. & Rochelle, G. T. (2007) Alternative stripper configurations for $CO_2$ capture by aqueous amines. *AIChE Journal*, 53(12), 3144-3154.

Pachauri, R. K., Allen, M., Barros, V., Broome, J., Cramer, W., Christ, R., Church, J., Clarke, L., Dahe, Q. & Dasgupta, P. (2014) *Climate Change 2014: Synthesis Report. Contribution of Working Groups I, II and III to the Fifth Assessment Report of the Intergovernmental Panel on Climate Change* [Online]. Available: http://www.ipcc.ch/report/ar5/syr/ [Accessed 6th June 2016].

Panahi, M. & Skogestad, S. (2011) Economically efficient operation of $CO_2$ capturing process part I: Self-optimizing procedure for selecting the best controlled variables. *Chemical Engineering and Processing: Process Intensification*, 50(3), 247-253.

Peng, D. Y. & Robinson, D. B. (1976) A new two-constant equation of state. *Industrial and Engineering Chemistry Fundamentals*, 15(1), 59-64.

Pershad, H., Harland, K., Stewart, A. & Slater, S. (2010) *$CO_2$ pipeline infrastructure: An analysis of global challenges and opportunities* [Online]. Cambridge: Element Energy. [Accessed.

Piessens, K., Laenen, B., Nijs, W., Mathieu, P., Baele, J. M., Hendriks, C., Bertrand, E., Bierkens, J., Brandsma, R., Broothaers, M., De Visser, E., Dreesen, R., Hildenbrand, D., Lagrou, D., Vendeginste, V. & Welkenhuysen, K. (2008) Policy Support System for Carbon Capture and Storage.

POST. (2009) *Postnote 335 – carbon capture and storage*. London, United Kingdom: The Parliamentary Office of Science and Technology.

R.F., S. (1987) *Random packings and packed towers: Design and applications* (Second ed.). Houston: Gulf Publishing Company.

Race, J. M., Wetenhall, B., Seevam, P. N. & Downie, M. J. (2012) Towards a $CO_2$ pipeline specification: defining tolerance limits for impurities. *Journal of Pipeline Engineering*, 11(3), 173-190.

Rao, A. B. & Rubin, E. S. (2002) A technical, economic, and environmental assessment of amine-based CO2 capture technology for power plant greenhouse gas control. *Environmental Science and Technology*, 36(20), 4467-4475.

Rao, A. B. & Rubin, E. S. (2005) Identifying Cost-Effective $CO_2$ Control Levels for Amine-Based $CO_2$ Capture Systems. *Industrial & Engineering Chemistry Research*, 45(8), 2421-2429.

Razi, N., Bolland, O. & Svendsen, H. (2012) Review of design correlations for $CO_2$ absorption into MEA using structured packings. *International Journal of Greenhouse Gas Control*, 9, 193-219.

Razi, N., Svendsen, H. F. & Bolland, O. (2013a) Cost and energy sensitivity analysis of absorber design in $CO_2$ capture with MEA. *International Journal of Greenhouse Gas Control*, 19, 331-339.

Razi, N., Svendsen, H. F. & Bolland, O. (2013b) Validation of mass transfer correlations for $CO_2$ absorption with MEA using pilot data. *International Journal of Greenhouse Gas Control*, 19(0), 478-491.

Reddy, S., Scherffius, J. R., Yonkoski, J., Radgen, P. & Rode, H. (2013) Initial Results from Fluor's $CO_2$ Capture Demonstration Plant Using Econamine FG PlusSM Technology at E.ON Kraftwerke's Wilhelmshaven Power Plant. *Energy Procedia*, 37, 6216-6225.

Rochelle, G. T. (2009) Amine Scrubbing for $CO_2$ Capture. *Science*, 325(5948), 1652-1654.

Rochelle, G. T. (2012) Thermal degradation of amines for $CO_2$ capture. *Current Opinion in Chemical Engineering*, 1(2), 183-190.

Roussanaly, S., Bureau-Cauchois, G. & Husebye, J. (2013) Costs benchmark of $CO_2$ transport technologies for a group of various size industries. *International Journal of Greenhouse Gas Control*, 12(0), 341-350.

Rumpf, B. & Maurer, G. (1992) Solubilities of hydrogen cyanide and sulfur dioxide in water at temperatures from 293.15 to 413.15 K and pressures up to 2.5 MPa. *Fluid Phase Equilibria*, 81(C), 241-260.

Samanta, A., Zhao, A., Shimizu, G. K., Sarkar, P. & Gupta, R. (2011) Post-combustion $CO_2$ capture using solid sorbents: a review. *Industrial & Engineering Chemistry Research*, 51(4), 1438-1463.

SASKPOWER. (2015) *The world's first post-combustion coal-fired CCS facility* [Online]. Available: http://saskpowerccs.com/ [Accessed 6th June 2016].

SCCS. (2016) *CCS-the full chain* [Online]. Scottish Carbon Capture and Storage Research Group. Available: http://www.sccs.org.uk/education-and-training/downloads [Accessed 6th June 2016].

Schach, M.-O., Schneider, R., Schramm, H. & Repke, J.-U. (2013) Control Structure Design for CO2-Absorption Processes with Large Operating Ranges. *Energy Technology*, 1(4), 233-244.

Seevam, P. N., Race, J. M., Downie, M. J. & Hopkins, P. (2008) Transporting the Next Generation of $CO_2$ for Carbon, Capture and Storage: The Impact of Impurities on

Supercritical $CO_2$ Pipelines. *2008 7th International Pipeline Conference*. Calgary, Alberta, Canada: International Petroleum Technology Institute and the Pipeline Division.

Shah, R. K. & Sekulic, D. P. (2003) *Fundamentals of heat exchanger design*: John Wiley & Sons.

SIEMENS. (2016) *Siemens sets new performance and efficiency world record at Düsseldorf power plant* [Online]. Available: http://www.siemens.com/press/en/pressrelease/index.php?content%5B%5D=Corp&search=Irsching&date-1-dd=26&date-1-mm=04&date-1=2015&date-2-dd=26&date-2-mm=04&date-2=2016&intern=1 [Accessed 6th June 2016].

Sime, L. C. (2014) Greenland deglaciation puzzles. *Science*, 345(6201), 1116-1117.

Sinnott, R. & Towler, G. (2009) *Chemical engineering design* (5th ed.). Oxford: Butterworth heinemann.

Sipöcz, N. & Tobiesen, F. A. (2012) Natural gas combined cycle power plants with $CO_2$ capture – Opportunities to reduce cost. *International Journal of Greenhouse Gas Control*, 7(0), 98-106.

Soave, G. (1972) Equilibrium constants for modified Redlich-Kwong equation of state. *Chem. Eng. Sci.*, 27, 1196-1203.

Song, J. H., Yoon, J. H., Lee, H. & Lee, K. H. (1996) Solubility of carbon dioxide in monoethanolamine + ethylene glycol + water and monoethanolamine + poly(ethylene glycol) + water. *Journal of Chemical and Engineering Data*, 41(3), 497-499.

Song, Y. & Chen, C. C. (2009) Symmetric electrolyte nonrandom two-liquid activity coefficient model. *Industrial and Engineering Chemistry Research*, 48(16), 7788-7797.

Span, R. & Wagner, W. (1996) A new equation of state for carbon dioxide covering the fluid region from the triple-point temperature to 1100 K at pressures up to 800 MPa. *Journal of Physical and Chemical Reference Data*, 25(6), 1509-1596.

Stichlmair, J. & Fair, J. R. (1998) *Distillation: principles and practices*: Vch Verlagsgesellschaft Mbh.

Sulzer. (2014) *Putting a chill on global warming* [Online]. Available: http://www.sulzer.com/en/-/media/Documents/Cross_Division/STR/2008/2008_3_4_Sulzer_e.pdf [Accessed 6th June 2016].

Sulzer. (2015) *Structured Packings_Energy-efficient, innovative and profitable* [Online]. Available: http://www.sulzer.com/cs/-/media/Documents/ProductsAndServices/Separation_Technology/Structured_Packings/Brochures/Structured_Packings.pdf [Accessed 6th June 2016].

Svensson, R., Odenberger, M., Johnsson, F. & Strömberg, L. (2004) Transportation systems for $CO_2$—application to carbon capture and storage. *Energy Conversion and Management*, 45(15-16), 2343-2353.

Sweeting, J. (1997) *Project Cost Estimating: Principles and Practice*: IChemE.

Szulczewski, M. L., MacMinn, C. W., Herzog, H. J. & Juanes, R. (2012) Lifetime of carbon capture and storage as a climate-change mitigation technology. *Proceedings of the National Academy of Sciences*, 109(14), 5185-5189.

Tobiesen, F. A., Svendsen, H. F. & Juliussen, O. (2007) Experimental validation of a rigorous absorber model for $CO_2$ postcombustion capture. *AIChE Journal*, 53(4), 846-865.

Tong, D., Trusler, J. P. M., Maitland, G. C., Gibbins, J. & Fennell, P. S. (2012) Solubility of carbon dioxide in aqueous solution of monoethanolamine or 2-amino-2-methyl-1-propanol: Experimental measurements and modelling. *International Journal of Greenhouse Gas Control*, 6, 37-47.

Towler, G. & Sinnott, R. K. (2012) *Chemical engineering design: principles, practice and economics of plant and process design* (2nd ed.). Oxford: Butterworth-Heinemann

Tsai, R. E., Seibert, A. F., Eldridge, R. B. & Rochelle, G. T. (2011) A dimensionless model for predicting the mass-transfer area of structured packing. *AIChE Journal*, 57(5), 1173-1184.

Ulfsnes, R., Karlsen, G., Jordal, K., Bolland, O. & Kvamsdal, H. M. (2003) Investigation of physical properties of $CO_2/H_2O$-mixtures for use in semi-closed $O_2/CO_2$ gas turbine cycle with $CO_2$-capture. *Department of Energy and Process Eng., Norwegian Univ. of Science and Technology* 9.

UNFCCC. (2015) *Historic Paris Agreement on Climate Change* [Online]. Available: http://newsroom.unfccc.int/unfccc-newsroom/finale-cop21/ [Accessed 6th June 2016].

USDOE. (2010a) Energy Market and Economic Impacts of the American Power Act of 2010. Washington, DC, USA.

USDOE. (2010b) *Interagency Task Force on Carbon Capture and Storage*. Washington, DC, USA.

Valdés, M. & Rapún, J. L. (2001) Optimization of heat recovery steam generators for combined cycle gas turbine power plants. *Applied Thermal Engineering*, 21(11), 1149-1159.

Van den Broek, M., Brederode, E., Ramírez, A., Kramers, L., Van der Kuip, M., Wildenborg, T., Turkenburg, W. & Faaij, A. (2010) Designing a cost-effective $CO_2$ storage infrastructure using a GIS based linear optimization energy model. *Environmental Modelling & Software*, 25(12), 1754-1768.

Vargas, J. V. C. & Bejan, A. (2000) Thermodynamic optimization of the match between two streams with phase change. *Energy*, 25(1), 15-33.

Wagner, M., von Harbou, I., Kim, J., Ermatchkova, I., Maurer, G. & Hasse, H. (2013) Solubility of Carbon Dioxide in Aqueous Solutions of Monoethanolamine in the Low and High Gas Loading Regions. *Journal of Chemical & Engineering Data*, 58(4), 883-895.

Wang, M., Lawal, A., Stephenson, P., Sidders, J. & Ramshaw, C. (2011) Post-combustion $CO_2$ capture with chemical absorption: A state-of-the-art review. *Chemical Engineering Research and Design*, 89(9), 1609-1624.

Wegstein, J. H. (1958) Accelerating convergence of iterative processes. *Commun. ACM*, 1(6), 9-13.

Weiland, R. H. (1996) *Carbon dioxide removal by mixtures of amines: Final report*: Gas Research Institute.

Weiland, R. H., Dingman, J. C. & Cronin, D. B. (1997) Heat capacity of aqueous monoethanolamine, diethanolamine, N-methyldiethanolamine, and N-methyldiethanolamine-based blends with carbon dioxide. *Journal of Chemical and Engineering Data*, 42(5), 1004-1006.

Weiland, R. H., Dingman, J. C., Cronin, D. B. & Browning, G. J. (1998) Density and viscosity of some partially carbonated aqueous alkanolamine solutions and their blends. *Journal of Chemical and Engineering Data*, 43(3), 378-382.

Wertheim, M. S. (1984) Fluids with highly directional attractive forces. I. Statistical thermodynamics. *Journal of Statistical Physics*, 35(1-2), 19-34.

Wertheim, M. S. (1986) Fluids with highly directional attractive forces. IV. Equilibrium polymerization. *Journal of Statistical Physics*, 42(3-4), 477-492.

Whitman, W. G. (1962) The two film theory of gas absorption. *International Journal of Heat and Mass Transfer*, 5(5), 429-433.

Wildenborg, T., Holloway, S., Hendriks, C., Kreft, E., Lokhorst, A., Brook, M., Brandsma, R., Egberts, P. & Larsen, M. (2004) Cost curves for $CO_2$ storage. Part 2: European sector.

Witkowski, A. & Majkut, M. (2012) The impact of $CO_2$ compression systems on the compressor power required for a pulverized coal-fired power plant in post-combustion carbon dioxide sequestration. *Archive of Mechanical Engineering*, 59(3), 343-360.

Witkowski, A., Rusin, A., Majkut, M., Rulik, S. & Stolecka, K. (2013) Comprehensive analysis of pipeline transportation systems for $CO_2$ sequestration. Thermodynamics and safety problems. *Energy Conversion and Management*, 76, 665-673.

Wong, S. (2005) *Module 4: $CO_2$ compression and transportation to storage reservoir* [Online]. Asia-Pacific Economic Cooperation (APEC). Available: https://hub.globalccsinstitute.com/publications/building-capacity-co2-capture-and-storage-apec-region-training-manual-policy-makers-and-practitioners/module-4-co2-compression-and-transportation-storage-site [Accessed 6th June 2016].

Xu, Q. & Rochelle, G. (Year) Total pressure and $CO_2$ solubility at high temperature in aqueous amines. *In:* Energy Procedia, 2011. 117-124.

Yan, Y. & Chen, C.-C. (2010) Thermodynamic modeling of $CO_2$ solubility in aqueous solutions of NaCl and $Na_2SO_4$. *The Journal of Supercritical Fluids*, 55(2), 623-634.

Ycharts. (2015) *European Union Natural Gas Import Price* [Online]. Available: http://ycharts.com/indicators/europe_natural_gas_price [Accessed 6th June 2016].

Ying, J. & Eimer, D. A. (2012) Measurements and correlations of diffusivities of nitrous oxide and carbon dioxide in monoethanolamine+ water by laminar liquid jet. *Industrial & Engineering Chemistry Research*, 51(50), 16517-16524.

Zhang, Y. & Chen, C.-C. (2013) Modeling $CO_2$ Absorption and Desorption by Aqueous Monoethanolamine Solution with Aspen Rate-based Model. *Energy Procedia*, 37(0), 1584-1596.

Zhang, Y. & Chen, C. C. (2011) Thermodynamic modeling for $CO_2$ absorption in aqueous MDEA solution with electrolyte NRTL model. *Industrial and Engineering Chemistry Research*, 50(1), 163-175.

Zhang, Y., Chen, H., Chen, C.-C., Plaza, J. M., Dugas, R. & Rochelle, G. T. (2009) Rate-Based Process Modeling Study of $CO_2$ Capture with Aqueous Monoethanolamine Solution. *Industrial & Engineering Chemistry Research*, 48(20), 9233-9246.

Zhang, Y., Que, H. & Chen, C.-C. (2011) Thermodynamic modeling for $CO_2$ absorption in aqueous MEA solution with electrolyte NRTL model. *Fluid Phase Equilibria*, 311, 67-75.

Zhang, Z. X., Wang, G. X., Massarotto, P. & Rudolph, V. (2006) Optimization of pipeline transport for $CO_2$ sequestration. *Energy Conversion and Management*, 47(6), 702-715.